UNIVERSITY OF SOUTHAMPTON
FACULTY OF ENGINEERING AND THE ENVIRONMENT
School of Engineering Science

The use of Conducting Polymer Films for Drug Release Device Applications

by

Badr ALShammary

Thesis for the degree of Doctor of Philosophy

November 2016

UNIVERSITY OF SOUTHAMPTON

ABSTRACT

FACULTY OF ENGINEERING AND THE ENVIRONMENT

SCHOOL OF ENGINEERING SCIENCES

Doctor of Philosophy

THE USE OF CONDUCTING POLYMER FILMS FOR DRUG RELEASE DEVICE APPLICATIONS

by Badr ALshammary

The aim of this project was to develop electrodes that allow drugs to be uploaded and released from conductive polymer films for biomedical applications. A thorough literature review of conducting polymer synthesis, analysis and doping mechanisms was presented and the applications of conducting polymers in the development of drug delivery systems were reviewed.

Electrochemical deposition of polyppyrrole (PPy) was carried out on different susbstrates, including stainless steel (SS), cellulose acetate membranes, AZ31 Mg alloy and hybrid systems. A series colorant and model drugs, such as rhodhamine 6G (Rh-6G), fluorescein sodium salt (FSS), methylene blue (MB), dopamine hydrochloride (DB), ibuprofen sodium salt (IP), were incorporated into PPy films grown on different substrates and the kinetics of drug release were investigated. The AZ31 Mg alloy was used to investigate self-powered systems. The results presented about this topic include the liberation of IP and sodium salicylate from PPy films deposited on AZ31 Mg alloy. The presence of drugs uploaded into the system, such as IP and salicylate affect the nucleation and growth processes. SEM micrographs of PPy films show a less compact, cracked, uneven surface with needle-like structures observed for sodium ibuprofen containing solutions (>5 mmol dm^{-3}). Self-powered IP release experiments in 0.9% wt. NaCl are fitted to Avrami's equation and the rate variations being attributed to uneven corrosion of the underlying alloy. Mechanical properties such as hardness and reduced modulus decreased 54% and 40% respectively for PPy films prepared in salicylate solutions compared with those prepared in solutions containing different ibuprofen concentration (0.5 to 10 mmol dm^{-3}), indicating a more plastic film with IP.

Other results presented include the release of fluorescent dyes and drugs deposited in cellulose membranes covered with magnesium PPy or deposited on SS substrate.

Contents

List of Tables

List of Figures

Acknowledgements

I would like to express my sincere gratitude to my supervisors Dr. Carlos Ponce de Leon Albarran and Professor Frank C. Walsh. My sincere thanks and appreciations to them for their continuous guidance, unlimited support, helpful comments and invaluable advice throughout my PhD. studies. I had the honour to study under their supervision and this project would not have been possible without their support. Dr. Carlos's kindness also extended to my life outside the university. His understanding of the difficulties that my family and I have gone through during my studies, which had a great deep impact on my heart, will remain for my whole life.

I would also like to thank my co-supervisor Dr. Jonathan Swingler from Heriot Watt University who introduced me to this research field after completing my MSc, and specifically helping me with the Inkjet printing technique.

I am extremely thankful to Professor Pilar Herrasti from Universidad Autónoma de Madrid for her assistance and helping me during my studies. Prof. Pilar generously hosted me in her laboratory for three months. Pilar's patience to answers my questions and always maintaining her welcome smile in every meeting was a source of continuous inspiration. Many thanks to Pilar's postgraduates Dr. M.del Rosario Galindo Gonzalez, Gerardo Ivan Lozano Gutierrez and Claudia Lopez Aguilar. Their presence made my stay in Madrid enjoyable and unforgettable.

My sincere thanks and heartfelt gratitude goes to the visiting Professor Norberto Casillas from the Universidad de Guadalajara for his support during the critical last six months, and coauthoring our second paper. I was lucky of having him as office mate and as a neighbour at home. Thanks to the universty for placing him near me, I was privilaged seeing him and working with him more too often.

Many thanks to Dr. Richard Cook for his help with the nanoindentations experiments and to Dr. Dmitry Bavykin for providing me titanate nanotubes.

My sincere appreciation also is to the University of Southampton and the Engineering Sciences Unit for offering all the valuable facilities and resources useful for my research.

Special thanks for all my friends that I have met in the laboratory: Dr. Irene Merino, Dr. Rachel Mckerracher, Christian Harito, Fernando Arenas, Muthu Krishna, Horacio Figueredo, Dr. Rooben Truncheons, Chao Wang, Hannah Goode, Abdulaziz Abahussain and to many others both MSc and visiting students.

I am pleased to acknowledge my employee, the Ministry of Health for granting me this scholarship and a special thanks to the Ministry of Higher Education and the Saudi Cultural Bureau in London for their support and help during my studies in the United Kingdom.

I am very grateful to all the members of the Saudi Students Society in Southampton particularly my loyal friends: Dr. Khaled AL-Othman, Dr. Khaled AL-Fahad, Dr. Abdulelah Alwabel, Ibrahem Al-Mansour, Dr. Mohammed ALShadouki, Dr. Abdullah ALjohani, Dr. Musaab Alnaim, Dr. Ibrahem Alasmary, Salman Alamri and Mabkhoot Alsaiari.

My brother and sister in-law, Nawaf and Dr.Abeer AlShammari, you made my life in the UK more enjoyable and pleasant, I was lucky having a close family near my wife, children and myself.

I am entirety grateful to my beloved parents, my sisters and brothers for all their love and continuous encouragements and for all they have done to me. Last, but not least, I hereby express my deep sense of gratitude and indebtedness to wife (Ferihah), my son (Rakan), my daughters (Hour) and (Deema) for their understanding, patience, support, encouragement and endless love through the duration of my studies.

DEDICATION

This work is dedicated to:

My beautiful daughter (Wãrd) who witnessed the beginning of this project and whom I wished had stayed until this moment. I will never forget you. May Allah make your place close to mine in heaven.

Dr. Ali Al-Anazi, words cannot express my deepest love, appreciation and gratitude.

DECLARATION OF AUTHORSHIP

I, Badr Alshammary, declare that this thesis entitled

Electrodeposited Conducting Polymer Films for Drug Release Applications

And the work presented in the thesis are both my own, and have been generated by me as a result of my own original research. I confirm that:

- this work was done wholly or mainly while in candidature for a research degree at this University;
- where any part of this thesis has previously been submitted for a degree or any other qualification at this University or any other institution, this has been clearly stated;
- where I have consulted the published work of others, this is always clearly attributed;
- where I have quoted from the work of others, the source is always given. With the exception of such quotations, this thesis is entirely my own work;
- I have acknowledged all main sources of help;
- where the thesis is based on work done by myself jointly with others; I have made clear exactly what was done by others and what I have contributed myself;
- parts of this work have been published as:

(*Papers Published in Peer-Reviewed Journals*)

1. B Alshammary, F. C Walsh, P Herrasti, C Ponce de Leon, (2015). Electrodeposited conductive polymers for controlled drug release: polypyrrole. *Journal of Solid State Electrochemistry*, 20(11), 839-859.

2. B Alshammary, N. Casillas, R.B. Cook, C. Ponce de León, F.C. Walsh, (2016). The importance of film structure during self-propelled Ibuprofen salicylate drug release from polypyrrole electrodeposited on AZ31 Mg. *Journal of Solid State Electrochemistry*, 1-29.

(*Papers to be Submitted to Peer-Reviewed Journals*)

3. B Alshammary, N. Casillas, H. Figueredo, C. Ponce de León, F.C. Walsh. Numerical modelling of Self-powered Ibuprofen Salicylate drug release from Polypyrrole Electrodeposited on AZ31 Mg in preparation for *Electrochimica Acta*, expected submission date March (2017).
4. B Alshammary, N. Casillas, C. Ponce de León, F.C. Walsh, Surface modification of implantable Magnesium alloy to improve both biodegradability and corrosion resistance in preparation for *Synthetic Metals*, expected submission date May (2017).

Conferences

5. B Alshammary, C. Ponce de León, P Herrasti, J.Swingler, D.V. Bavykin and F.C. Walsh, Towards Polypyrrole Self-Powered Drug Delivery System, *Electrochem 2013*, Southampton, September 2013.

Signed: Badr Alshammary

Date: Friday, 18 November 2016

Aims and objectives

In this thesis, the main objective was to investigate the uses of conducting polymers and their role in the fabrication of components for medical devices. The following were particular goals:

1. To design a self-powered drug delivery system based on the uses of a AZ31 Mg alloy as a sacrificial anode and a conducting PPy film as a cathode. The galvanic coupling between the Mg layer and the PPy film provides the driving force for the drug release.

2. To improve the capacity of PPy by incorporating nanostructures material to the PPy polymer film, such as titanate nanotubes.

3. To investigate the drug release profile for a variety of different drugs and fluorescent dyes: rhodhamine 6G (Rh-6G), fluorescein sodium salt (FSS), methylene blue (MB), dopamine hydrochloride (DB), ibuprofene sodium salt (IP).

4. To investigate the effect of the substrate materials on the properties of the conducting polymer film properties and processing characteristics.

5. To characterise conducting polymer films being produced in different substrates by using traditional electrochemical techniques: cyclic voltammetry (CV), chronoamperometry and surface characterisation techniques, such as, scanning electron microscopy (SEM) and energy dispersive analysis (EDS) and FTIR spectroscopy.

6. Characterise the mechanical properties of PPy film incorporated with drugs by using nanoindentation techniques.

Thesis outline

This thesis was divided in eight chapters. Chapter 1 provides an insight into the main types of conducting polymers, particularly PPy; polymer doping and the polymerisation mechanism are described. The use of conducting polymers in drug delivery systems is also introduced and a brief review of the challenges and limitations of using conducting polymers in a drug delivery system are presented. Progress in the use of conducting polymers in drug delivery systems is reviewed, including aspects such as nanostructured conducting polymers, biodegradable conducting polymers and self-powered drug delivery systems. The biomedical application of conducting polymers is examined. In chapter 2, the materials and cells used for the experiments are discussed. In chapter 3, a general experiment for electropolymerisation of PPy and the influence of polymerisation conditions on the polymer characteristics is described. In chapter 4, self-powered drug delivery system based on a galvanic couple between a biodegradable AZ31 Mg alloy and a PPy film is described. The system rely on the dissolution of the Mg substrate to reduce the polymer film and release the incorporated drug. In chapter 5 and 6, the synthesis of PPy films for absorbing and releasing different molecules including methylene blue, fluorescence sodium salt, dopamine and ibuprofen were described. The effect of the incorporation of titanate nanotubes on the absorption and release of these model drugs from the PPy films is examined and the release of the incorporated model drug molecules with or without electrical stimulation is discussed. In chapter 7, the chemical deposition of PPy on the cellulose acetate membrane during molecule delivery, the synthesis of a self-powered PPy drug delivery system based on a galvanic cell and drug release from these composite films were described. In chapter 8, the results and conclusion of the study are presented; planned future research was also discussed. Figure 1 shows the thesis outline.

Figure 1: Thesis outline.

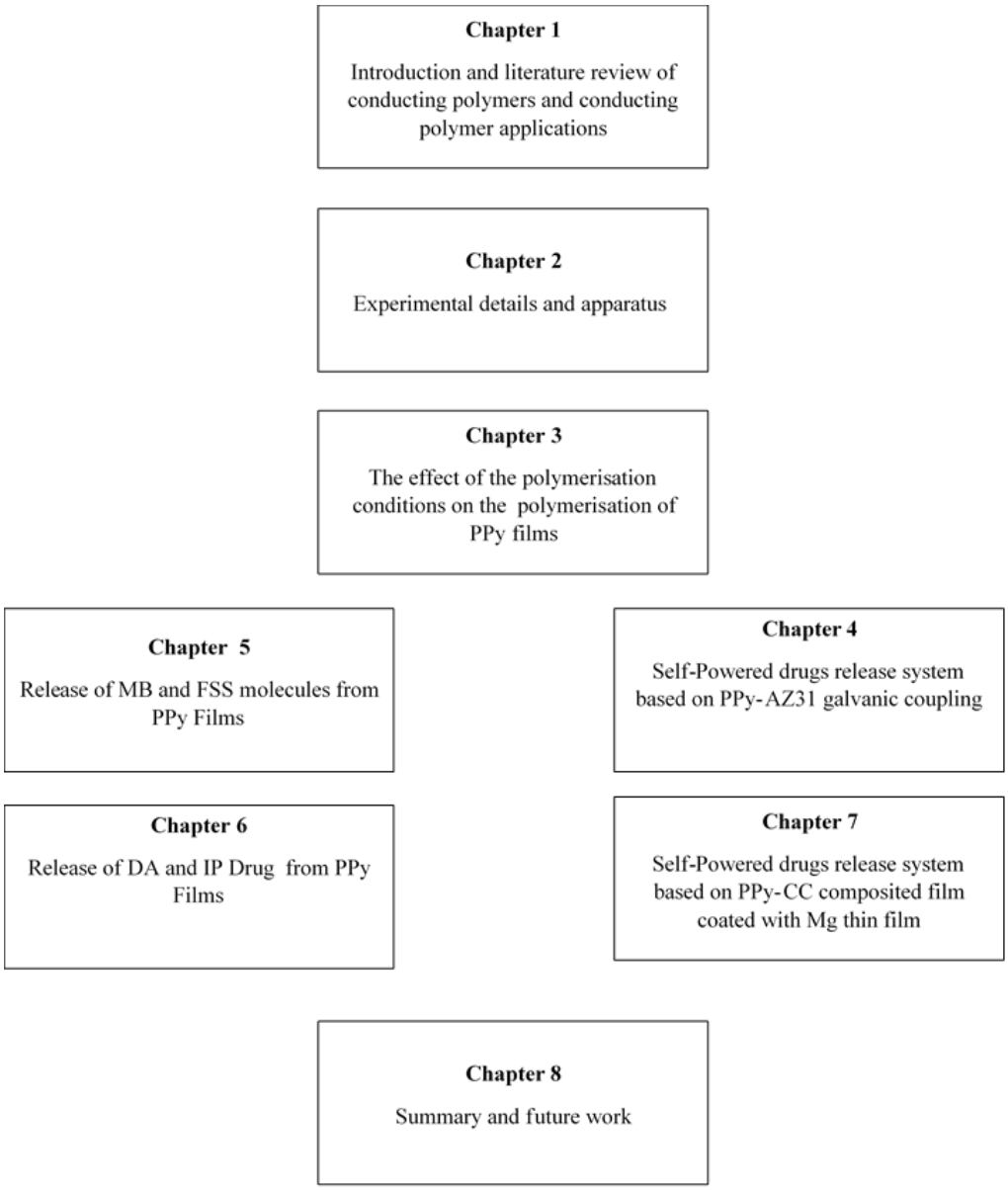

List of Abbreviations

AA	Ascorbic acid
AFM	Atomic force microscopy
ATP	adenosine triphosphate
CAM	Cell-adhesion molecule
CC	Celluose acetate membrane
CPC/PPy	Chitosan-g-polycaprolactone/ Polypyrrole
CPY	Cetylpyridinium
CPZ	Chlorpromazine
CSA	Camphorsulfonic acid
CV	Cyclic voltammetry
DA	Dopamine hydrochloride
DBS	Dodecylbenzenesulfonate
DCE	1, 2-dichloroethane
DET	Direct electron transfer biofuel cell
DEX	Dexamethasone sodium
DM	Durapol membranes
DMFe	1,1'-Dimethylferrocene mediator
DMSO	Dimethyl sulfoxide
DNA	Deoxyribonucleic acid
DRG	Dorsal roots ganglia
DSI	Depth-sensing indentation
EDOT	Ethylenedioxythiophene
EDS	Energy-dispersive X-ray spectroscopy
E_r	Reduced modulus
FAD	Flavin-adenin-dinucleotide
Fe(III) pTS	Iron (III) p-toluenesulfonate

FSS	Fluorescein sodium salt
FT-IR	Fourier transform infrared spectroscopy
GC	Glassy carbon
Ge	Germanium
GEE	Glycine ethyl ester
GOD	Glucose oxidase
H	Average hardness
H-NMR	Proton nuclear magnetic resonance spectroscopy
HOMO	Higest occupied molecular orbital
IP	Ibuprofen
ITO	Indium tin oxide
k	Release constant
LUMO	lowest unoccupied molecular orbital
MB	Methylene blue
MTT assay	(3-(4,5-Dimethylthiazol-2-yl)-2,5-Diphenyltetrazolium bromide) assay
MTX	Methotrexate
MWCNT	Multiwall carbon nanotubes
n	Avrami's parameter
NAD^+	Nicotinamide adenine dinucleotide
NapTs	Sodium *p*-toluenesulfonate
NPs	Nanoparticles
OCP	Open circuit potential
OLED	Organic light-emitting diode
P3-BTSNa	Sodium poly (3-thiophene-δ-butanesulfonate)
P3-ETSNa	Sodium poly (3-thiophene-β-ethanesulfonate)
PAMPSA	Polypropylamidopropanesulfonic acid
PANI	Polyaniline

PBDTT-DPP	poly {2,6- 4,8-di (5-ethylhexylthienyl) benzo [1,2-b;3,4b'] dithiophene-alt-5-dibutyloctyl-3,6 bis (5-bromothiophen-2-yl) pyrrolo [3,4-c] pyrrole-1,4-dione}v
PBS	Phosphate buffer saline
PC	propylene carbonate
PCL	Polycaprolactone
PDLLA	Polypyrrole blended with poly(dl-lactic acid)
PECA	Poly(z-ethyl cyanoacrylate)
PEDOT	Poly (3,4-ethylenedioxythiophene)
PEM	Polymer electrolyte membrane fuel cells
PGAP	Poly [(glycine ethyl ester) (aniline pentamer) phosphazene] copolymer
PLA:PLGA	Poly(D-lactide-co-glycolide) copolymer
PLED	Polymer light emitting diode
PLGA	Poly(lactic-co-glycolic acid)
PLLA	Polylactide
PPy	Polypyrrole
PR	Phenol red salt
PS	Polystyrene
PTFE	Polytetrafluoroethylene
PTh	Polythiophene
pTS	*para*-Toluene sulphonic acid sodium salt
PVA	Poly(vinylalcohol)
QCM	Quartz crystal microbalance
RP HPLC	Reversed-phase chromatography
SDS	Sodium dodecyl sulphate
SEM	Scanning electron microscope
Si	Silicon
SS	stainless steel
St	Styrene sulfonate

SWCNT	Single-walled carbon nanotubes
TBA-PF6	Tetrabutylammonium hexafluorophosphate
TCPs	Tissue culture polystyrene
THF	Tetrahydrofuran
TiNT	Titanate nanotubes
TiO_2	Nanotubular titania
TMAH	Tetramethyl ammonium hydroxide
UA	Uric acid
WHO	World Health Organisation

Chapter 1: Conducting polymers: background

This chapter provides a critical review of the common types of intrinsic conducting polymers including their synthesis, properties and characterisation. It aims to review and summarise the modification and challenges of the previous and current use of conducting polymers in biomedical application such as biosensors. The fundamentals of conducting polymers drug delivery system, synthesis, properties, characterisation and limitations of this system are highlighted. Furthermore, it gives an overview of degradable conducting polymers synthesis and fabrication methods. A summary of self-powered drug delivery system based on conducting polymers and active metal anode in recent works published before April 2016 is provided for the purpose of building an understanding of the theme and background of the current research, and contribute to the general aims of the thesis.

1.1 Introduction

Since the discovery of doped polymers for electronic conduction in the 1970s, many efforts have been made to develop the conductivity of these materials and improve the product durability and manufacture [1, 2]**.** Conducting polymers have been obtained with properties that are comparable to those of traditional semiconductors, such as Si and Ge, and occasionally even exceeding their flexibility and malleability**.** Cost effectiveness has been achieved in terms of cheap raw materials, manufacturing process and power consumption, easy processability, light weight, ability to be used in wet and harsh environments, and good optoelectronic properties. In addition, highly conductive polymers with conductivities comparable to some metals and with narrow band gaps have been developed [3-5]. For example, Dou et al. [6] demonstrated a low-band conducting

polymer poly {2,6- 4,8-di (5-ethylhexylthienyl) benzo [1,2-b;3,4b'] dithiophene-alt-5-dibutyloctyl-3,6 bis (5-bromothiophen-2-yl) pyrrolo [3,4-c] pyrrole-1,4-dione}v (PBDTT-DPP) with a band gap of 1.44 eV for application in solar cells, noting that the band gap of crystalline silicon is about 1.1 eV. In addition, Kim et al. [5] prepared a highly conductive poly (3,4-ethylenedioxythiophene) (PEDOT) nanofilm doped with Fe (III) tosylate with pyridine, using the vapour phase polymerisation technique. The obtained film has a conductivity of up to 4500 S cm^{-1}, compared to the conductivity of the crystalline silicon which is in the order of 1 μS cm^{-1}.

Among devices based on conducting and semiconducting polymers, the first field effect transistor was created by a research group from Cambridge University in 1988, followed by the first polymer light-emitting diode (PLED) in 1990 by the same group [7]. In 2000, the first full-colour inkjet-printed PLED display was announced [8]. The development of conducting and semiconducting polymers led to their use in a wide range of applications that include, but are not limited to, the following categories:

- Electrochromic devices such as smart windows, smart membranes, antiglare mirror displays etc. [9, 10].
- Energy applications, for example, solar cells [11, 12], quantum dots for photovoltaics [13], capacitors [14] and flexible and bendable batteries [15-17].
- Biomedical applications, for example, tissue engineering [18] and smart drug delivery systems [19-24].
- Sensing applications, such as pH sensors, ion-selective sensors, humidity sensors and biosensors [25].

- Artificial and smart devices, for example, memories [26, 27], active and semi-active radio frequency identification tags (RFID), integrated circuit smart cards, [28-33] and smart textiles [34].
- Actuators and artificial muscles [35, 36].
- Coating applications, such as corrosion inhibitors [37, 38].
- Electrocatalysis [39].
- Interface device, display, power source and complete electronic circuits for inexpensive equipment such as games and remote controls [40-42].
- Lab-on-a-chip applications, for example, a full polymeric microfluidic device for electrophoresis [43].

This evolution has continued and many products available in the market are now based on conducting and semiconducting polymers, including smartphone displays and organic light-emitting diodes (OLED) in laptop and television (TV) screens [44, 45].

Several strategies have been developed to manufacture conducting polymers that can be divided into two groups: the first group include those techniques that use polymer ink directly, such as inkjet printing techniques, screen printing, micro-contact printing, probe-based deposition, roll-to-roll processes such as gravure and flexographic printing, soft lithography, photolithography, dip-pen nanolithography and spin coating [46, 47]. The second group includes those techniques that use monomers, such as chemical and electrochemical deposition, chemical vapour deposition, vacuum deposition, physical vapour deposition and plasma techniques [48].

Inkjet printing is a fairly simple technique, fast and easy to use and does not require expensive equipment, such as masks or a clean room, for processing. The technique has been successfully employed to manufacture electronic devices based on polymers. The method can be applied to deposit layers of various conducting polymers onto flexible substrates in a well-defined configuration. In addition, complicated structures can be patterned precisely at desired positions without losing printing materials or influencing their properties. Moreover, it may be possible to fabricate electronic polymer devices together using different ink materials, avoiding the cost of additional assembly procedures [47, 49, 50].

Despite the development of conducting polymers in terms of active materials and manufacturing techniques, many limitations and challenges still exist. For example, viscosity and surface tension are both key parameters of the polymer solution used in inkjet printing and it is necessary to use additives to improve processability. However, additives can reduce the polymer conductivity [47]. In addition, some polymers are not stable and are sensitive to the air and certain specific environments. Additives are used to improve their stability, but these additives can change the polymer conductivity, as well as the viscosity and surface tension of the polymeric solution. This makes it difficult to deposit the polymers using an inkjet printer and affects the surface morphology of the polymeric films. Moreover, the polymeric films that are obtained using chemical polymerisation usually have lower conductivity than those films obtained by electrochemical polymerisation techniques [51].

1.2 Bonding in Conducting Polymers

Intrinsic conducting polymers are characterised by the presence of carbon atoms in their backbone, where each carbon atom is covalently bonded to its neighbour by alternating single and double bonds. A single strong bond, σ, between neighbouring carbon atoms which is formed from the localised sp^2 hybrid wave has the function of binding the polymer structure. The double bonds comprise the σ bond and a weaker π orthogonal bond to the plane of the σ bonds. The overlap between the Pz orbitals leads to π electron delocalization along the carbon chain. This electronic delocalisation permits the charge to be transported through the polymer chain and it is the reason behind the semiconductor properties that are attributed to conjugated polymers [52].

1.3 Polymer doping

The injection of a charged species onto the conjugated polymers backbone is usually called doping. The doping process is reversible such that the doped polymers can be returned to their original state with little or no degradation of the polymer backbone. This reversibility provides the ability to control the conducting properties of polymers that can vary from that of an insulator up to the high values as those of a metal. There are different doping methods that can be used including chemical, electrochemical and interfacial doping [53]. These methods are briefly described in the following sections.

1.3.1 Chemical doping

Chemical doping involves introducing charge carriers into the electronic structure of polymers using an acid-base reaction in the presence of counter ions to maintain charge neutrality. Shirakaw et al. [54] successfully conducted polyacetylene film doping for the first time with halogen vapour, chlorine, bromine or iodine. Their discovery lead to an

increase in the conductivity of the resultant polymer film up to 10^5 S cm^{-1}, which is more than 10^9 times that of undoped polyacetylene. Chemical doping is easy and efficient, although it is difficult to control the level of the dopant; however, inhomogeneous or incomplete doping levels are common [54].

1.3.2 Electrochemical doping

The electrochemical doping process involves either an oxidation or a reduction reaction. This process is conducted in an electrochemical cell in the presence of doping ions such as SO_4^{2-}, BF_4^- and Et_4N^+. The doping level can be precisely controlled by the potential between the working electrode (where the polymer is deposited) and the reference electrode. The doping ions which are dissolved in the electrolyte solution diffused in or out of the conducting polymer structure when a redox potential is applied to the electrode to compensate the charge on the polymer backbone. The electrochemical doping using a Li^+ (BF_4^-) electrolyte can be described by the following reactions at the working electrode surface [53]:

Oxidation (p-doping)

$$(\pi - polymer)_{n,neutral\,chain} + [Li^+(BF_4^-)]_{aq,n}$$

$$\rightarrow [(\pi - polymer)^{x+}(BF_4^-)_x]_n + Li_{electrode} + xe^- \quad (1.1)$$

Reduction (n-doping)

$$(\pi - polymer)_{n,neutral\,chain} + Li_{electrode} + xe^-$$

$$\rightarrow [(\pi - polymer)^{x-}(Li^+)_x]_n + [Li^+(BF_4^-)]_{aq,n}\,. \quad (1.2)$$

1.3.3 Interfacial doping

In this method, the conducting polymer film is located between two electrodes. The charge carriers are injected into the polymer from the metal contacts without the need for an ion dopant. With an adequate redox potential, the polymer is oxidised by removing electrons from the highest occupied molecular orbital (HOMO) or reduced by adding electrons to the lowest unoccupied molecular orbital (LUMO). The doping phenomena can be described by the following mechanisms [53]:

Hole injection (p-doping)

The positive charge carriers (holes) are injected from the anode to the polymer layer:

$$(\pi - \text{polymer})_{\text{n,neutral chain}} - \text{ne}^- \rightarrow [(\pi - \text{polymer})^{x+}]. \quad (1.3)$$

Electron injection (n-doping)

The electrons are injected from the cathode to the polymer layer:

$$(\pi - \text{polymer})_{\text{n,neutral chain}} + \text{ne}^- \rightarrow [(\pi - \text{polymer})^{x-}]. \quad (1.4)$$

This type of doping is used in light-emitting devices such as an organic light emitting diode (OLED). Figure 1.1 illustrates the simple configuration of OLED. In such a

configuration, the conducting polymer layers are sandwiched between two metal electrodes, a cathode from a low work function metal such as aluminium (Al) to match the polymer LUMO and an anode from a high work function metal that matches the polymer HOMO (see Figure 1.2). To allow light to escape, one of the two electrodes should be transparent or semi-transparent with good transmissive properties such as an indium tin oxide film (ITO) on a polymer or glass substrate.

By applying a suitable potential, the electrons are injected from the cathode and the holes are injected from the anode to the polymer layer. The electrons and the holes meet in the polymer bulk and recombine. The light is emitted from the polymer film as a result of the recombination of the charge carriers.

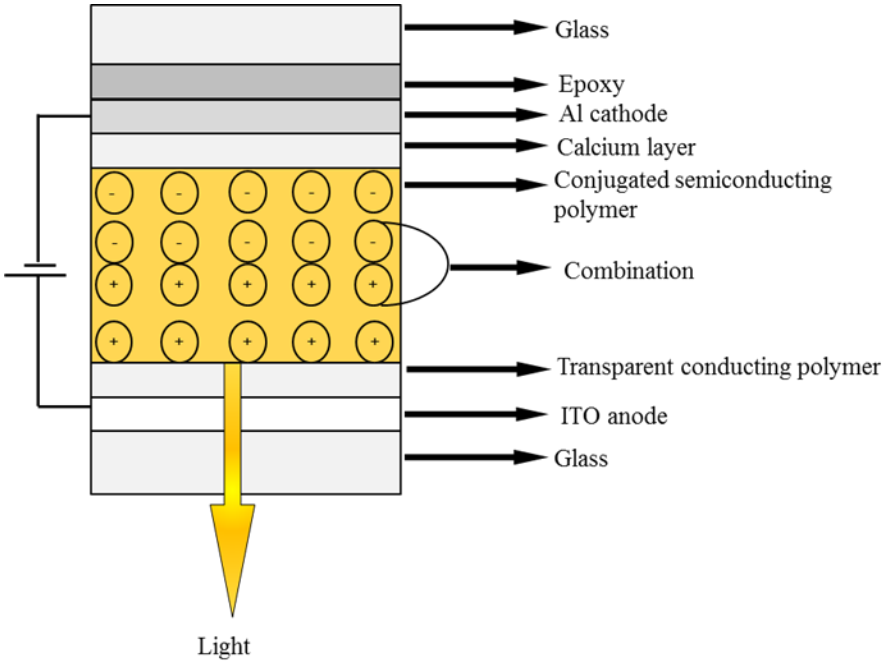

Figure 1-1:A basic schematic of an OLED [54].

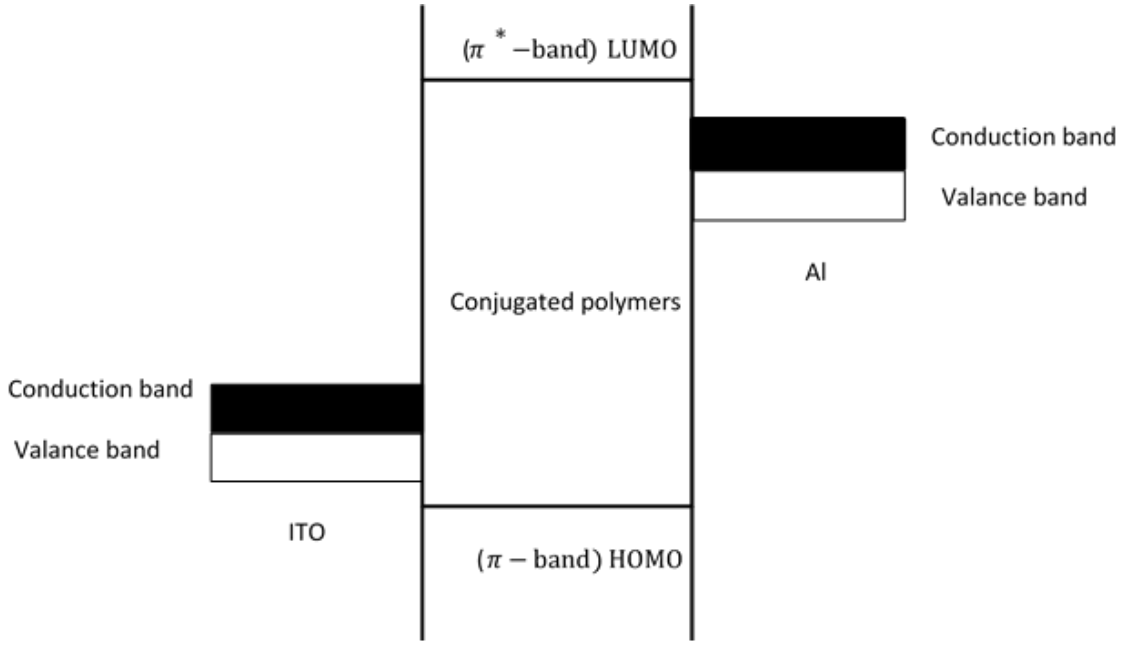

Figure 1-2: Schematic energy-level diagram for an OLED device [55].

1.3.4 Photo doping

In this process, polymers are exposed to electromagnetic spectra with higher energy than the polymer band gap. This leads the electrons in the polymer HOMO band to be excited by photons; thereby enabling them to jump to the conducting band. The promotion of electrons from the HOMO energy band to the LUMO energy level leads to the production of mobile carrier charges, holes in the π-band and electrons in the $\pi^* - \text{band}$ as shown in Figure 1.3. This type of doping is used in polymers used for photovoltaic devices and does not involve dopant ions [52, 53]. The following example illustrates the doping mechanism [53]:

$$(\pi-\text{polymer})_{\text{n,neutral chain}} + h\gamma \rightarrow [(\pi-\text{polymer})^{x+} + (\pi-\text{polymer})^{x-}]_n. \quad (1.5)$$

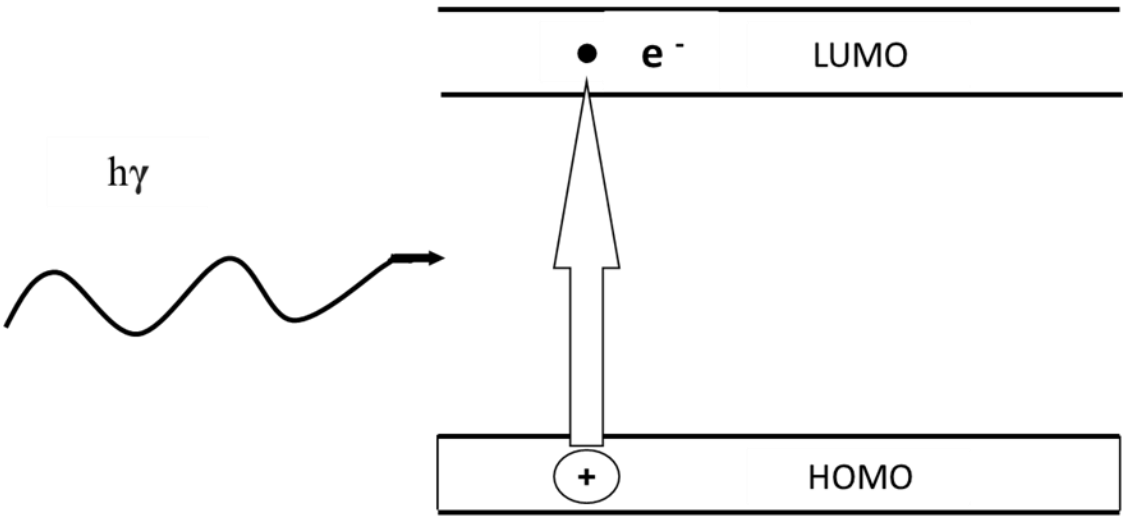

Figure 1-3: Interband transitions in semiconducting polymers and the resultant charge carriers in the photo doping process of conjugated polymers [52].

1.4 Classes of Conducting Polymers

Polyacetylene is the first discovered intrinsic conducting polymers. The simplest conjugated chain structure of polyacetylene make it widely used as a model for the conjugated conducting polymers. However, the poor stability of of polyacytelene in air and difficult processability shifted the attention to other conducting polymers. The following sections focus on the more stable and most studied hetrerocyclic conducting polymers: polyaniline, polythiophine, polypyrrole and their derivatives. Figure 1.4 shows the chemical structures of the main heterocyclic coduting polymers.

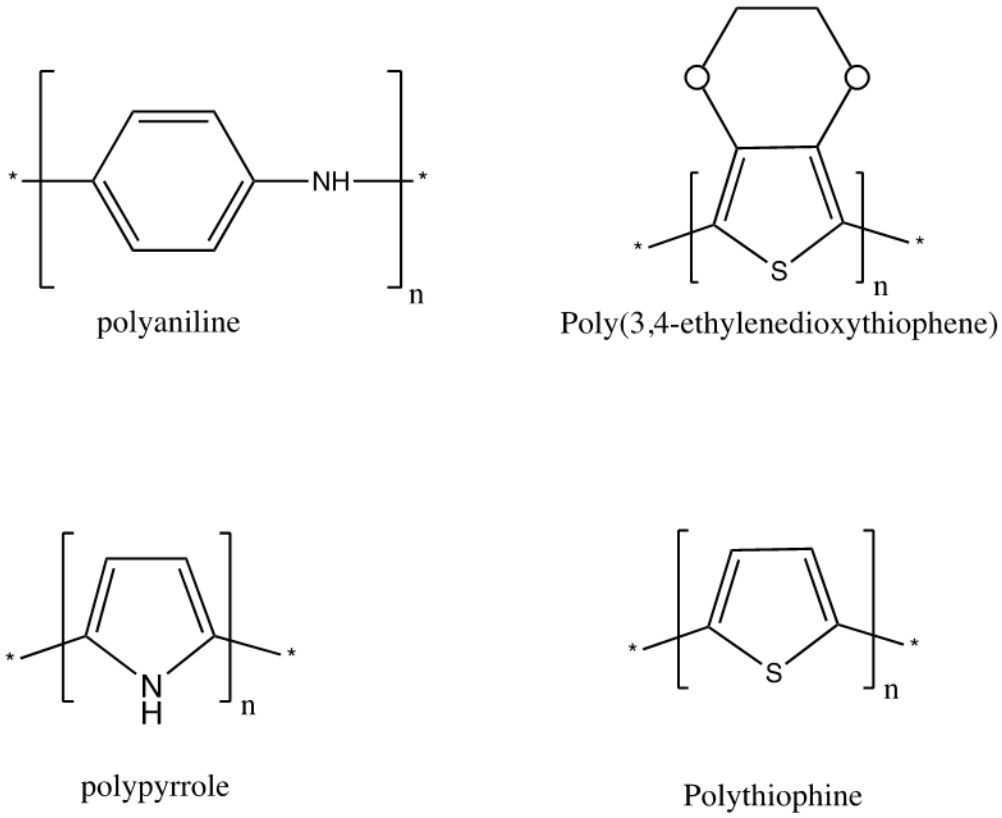

Figure 1-4: Scheme showing the chemical structures of main hetrerocyclic conducting polymers.

1.4.1 Polyaniline

Polyaniline (PANI) belongs to a family of semi-flexible polymers and was discovered in 1862 as black aniline during the oxidation of aniline [56]. MacDiarmid et al. brought PANI to the attention of scientists after its rediscovery in 1978, which changed the concept (i.e. the polymer as not being able to conduct electricity) and introduced the possibility of changing this polymer from an insulator to a semiconductor or a high conductive by a simple protonic doping process involving an acid/base reaction.

PANI is like other conducting polymers in that it can be synthesised by both chemical and electrochemical methods in aqueous solutions containing aniline monomers [57]. These monomers are less expensive than the monomers of the other conducting polymers [56]. PANI can be formed into the following types: leucoemeraldine, emeraldine and pernigraniline. However, only protonated emeraldine (emeraldine salt) is electrically conductive [57], while doped leucoemeraldine and doped pernigraniline have poor conductivity. PANI is thermally, electrochemically and environmentally stable in solution and air [56-58]. This polymer has many interesting properties resulting from the flexible –NH group in its backbone [57]. These electrochemical, electronic, optical and electro-optical properties make it a suitable material to be used for various applications [56]. The polymer is transparent yellow at reduced state and gradually changes from green to blue with the increase of the oxidation potential. PANI, for example, has been used for providing corrosion protection to metals, forming an antistatic coating and in electromagnetic shielding [56, 58, 59]. The optical and electro-optical properties of PANI enable it to be used in electro-optic and electrochromic devices, OLED, electrochromic displays, and smart windows [56]. PANI is also used for energy storage, such as the electrodes zinc-PANI and lithium-PANI used in secondary batteries [7, 60]. Further, PANI is biocompatible and has biomedical applications. For example, it can be used in tissue engineering as a tissue scaffold [59] and biosensor [8, 56, 61, 62]. PANI can also function as a membrane in gas liquid separation processes [57, 58]. In addition, PANI can be used for effective filters for water decontamination from micropathogens and in biotechnology for isolation and purification of antibiotics- polypeptides from culture liquids [63].

1.4.2 Polythiophene

One of the most commonly studied polymers is polythiophene (PTh) and its derivatives [64]. These conjugated polymers have excellent environmental and thermal stability in both neutral and doped states [65-67]. In addition, they exhibit optical properties (blue in its oxidised form and red in its undoped state) and high conductivity up to 600 S cm^{-1} in the doped form [68]. In spite of these interesting properties, the use of these polymers has been hampered due to poor solubility in most organic solvents, except in certain mixtures such as arsenic trifluoride/pentafluoride. However, much progress over the past two decades has permitted to overcome this problem by incorporating a long flexible alkyl side chain on the 3-position of the thiophene ring. This produces a soluble polymer in common organic solvents without altering the chemical and physical properties of the polymer [66, 69].

Pati et al. [70] synthesised two polymers: sodium poly (3-thiophene-β-ethanesulfonate) (P3-ETSNa) and sodium poly (3-thiophene-δ-butanesulfonate) (P3-BTSNa). The resulting polymers and their respective conjugate acids are soluble in water in both doped and undoped states.

Poly (3,4-ethylenedioxythiophene) (PEDOT) was developed in the late 1980s at the Bayer AG research laboratories in Germany [68]. PEDOT can be synthesised by oxidative chemical polymerisation, electrochemical polymerisation and transition-mediated coupling using EDOT monomers. Moreover, PEDOT thin films are optically transparent in the reduction state and turn light blue colour with high stability and conductivity in the

oxidised state [68]. Polystyrene sulfonate (PSS) is the most common dopant for PEDOT and makes it soluble in water [68].

1.5 Polymerisation Mechanism

In general, polymerisation begins with the initiation step where the monomer oxidises to form a radical cation. This is followed by a dimer formation from the reaction between two radical cations. The polymer chain propagation continues when the dimer oxidises to a radical cation and undergoes a coupling reaction with another radical cation to form a trimer. The polymer chain growth process continues until the termination step when the final products are formed [71, 72].

The PPy polymerisation mechanism is used as a model to explain the polymerisation mechanism of the heterocyclic conducting polymers.

1.5.1 The pyrrole polymerisation mechanism

Although PPy is one of the most conductive polymers that has been studied and synthesised, the polymerisation mechanism is a complicated process and has not been fully understood thus far, thereby remaining an interesting research topic [73, 74]. There are a number of polymerisation mechanisms that have been widely accepted and proposed by different researchers. Sadki et al. [74] intensely reviewed the PPy polymerisation mechanism. They reported that the polymerisation mechanism reported by Diaz et al. [75] was acceptable and was the most commonly used mechanism by researchers in scientific papers. This mechanism has been confirmed theoretically by studies conducted by

Waltman and Bargan. However, other mechanisms have been proposed by other researchers such as Kim, Pletcher and Reynold which are also acceptable in the literature [74]. The following section is a brief description of the polymerisation mechanism:

Step One:

Polymerisation begins with the initiation step where the pyrrole (Py) monomer is oxidised at a suitable positive potential (generally 0.65 V *vs.* SCE on the electrode surface). The monomer loses an electron at the anode surface, and different radical cation resonances are formed as shown in scheme 1 (Figure 1.5). Since the oxidation of the monomer to the radical cation ($R^{+\cdot}$) at the electrode surface is faster than the diffusion of the monomers from the electrode surface to the electrolyte solution, there is an increase in the radical cation concentration at the electrode surface, which is maintained by conserving the polymerisation condition. Then, the radical cation can be involved in different coupling reactions depending on its activity. It can react with the solution substance and generate non-conducting oligomers, which may deposit on the electrode, or diffuse into the solution and produce a soluble brown cloud if the radical cation is extremely active (very unstable) or extremely inactive (relatively stable). The stable radical cation can also undergo further coupling reactions to form dimers and then lead to a proton release, as shown in scheme 2 [74, 76].

Step Two:

Among the resonance forms of the radical cation, the resonance form (3) is predominant. This form is more active at position α- α'(2, 5) because it has a great density of unpaired electrons at this position. The propagation of the polymer chain begins with the generation

of a dihydromer dication resulting from the reaction coupling between two stable radical cations at the alpha position. The dihydro-dimer loses two protons to give a neutral stable species (see scheme 2). In addition, Diaz explained the coupling mechanism as π-radical coupling [74]. The reaction coupling between two π-radical cation monomers leads to the formation of a dimer precursor. Then, the dimer precursor deprotonates by eliminating two protons to form a dimer, as shown in scheme 2 [74].

Step Three:

The dimer radical cation is more stable and oxidises more easily than the monomer at the existing anode applied potential because the unpaired electron is delocalized over the rings of the dimer radical. The predominant dimer radical resonance form (9) is oxidised into a cation radical and undergoes further coupling reactions at β or β' with monomer radical cation 3 at α or α' positions, which produces trimer dication (11) (see scheme 3). The trimer dication then loses two protons to form the neutral trimer 12 (see scheme 2,3) [74].

Step Four:

The neutral trimer 12 is oxidised at the anode surface and produces a trimer radical cation (13) (see scheme 3), which further reacts with the monomer to form a tetramer. The polymer chain continues growing via the same sequence of oxidation, coupling and deprotonation until the chain growth terminates and the final polymer product is obtained. Reaction with water could be one of the steps that terminate the polymerisation. Although the α-α' position is the most active and predominant coupling, the β coupling occurs and increases as chain length increases. It has been found in previous research that there is a structural disorder in one Py unit out of every three. This structural disorder that forms the β coupling is responsible for the poor crystallinity in PPy [74, 76]. This has been

confirmed by blocking both the β position of the Py ring using methyl groups and the Cl atoms in the poly (β-β'-dimethylpyrrole) and poly (β-β'-dichloropyrrole), which are shown to increase the crystalline order because of the elimination of β coupling [77, 78].

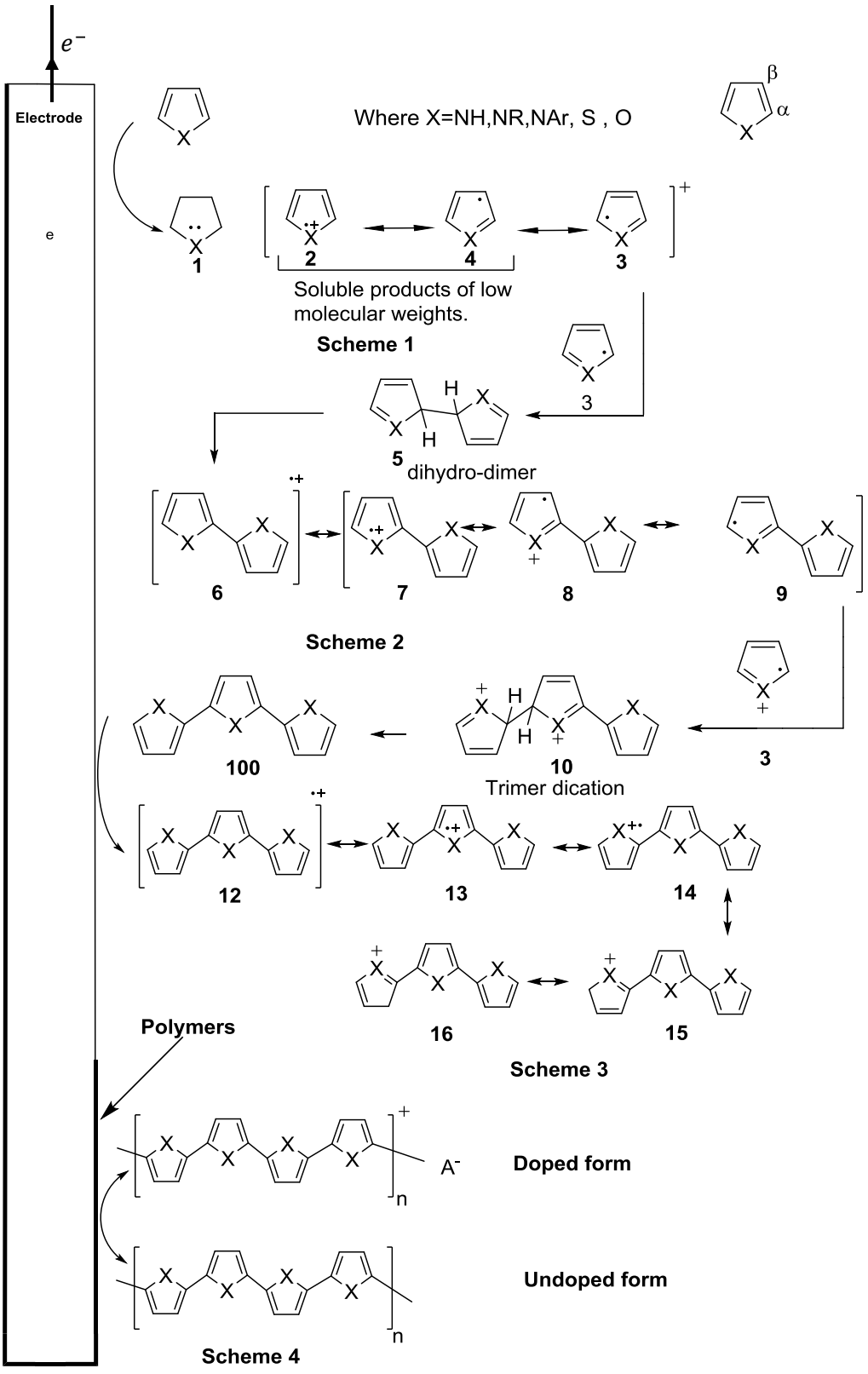

Figure 1-5: The accepted mechanism for electropolymerisation of Py and other aromatic heterocyclic monomers [73, 74].

1.5.2 Parameters affecting the PPy polymerisation mechanism

a) Temperature effects

The synthesis temperature is an important condition affecting the structure of conducting polymers and their properties. The increase in the temperature of the polymerisation solution may increase the interaction among monomers themselves or those between the monomers and the formed film, and may also activate unwanted reactions. Thus, there is an increase in the possibility of the occurrence of α-β and β-β' coupling instead of a free polymer defect-chain via α-α' bonding. When the α-α' bonding dominates, the film surface becomes smoother and the length of the conjugation chain increases. When the β-β' bonding dominates, the film exhibits a shorter conjugation length and rough surface. Teshima et al, [79] have found that there is an inverse relationship between the synthesis temperature and the surface roughness of the polymer film when the synthesis temperature decreases, the film's surface gradually changes from rough to smooth and becomes more compact. The produced films are coherent and mechanically strong. This relationship is also applicable to the conjugation chain length where a long conjugation chain with a less defective structure is formed at a low preparation temperature. In addition, the doping level increases as the synthesis temperature decreases, and the film's conductivity increases as the preparation temperature decreases. However, a relatively low synthesis temperature leads to an increase in the required electrochemical potential for polymerisation. Yoon et al, [80] found that there is a decrease in polymer conductivity when the polymers synthesise at a temperature below -40 ^{o}C, using a solution containing 0.1 mol dm^{-3} of pyrrole monomer, 0.1 mol dm^{-3} of tetrabutylammonium hexafluorophosphate (TBA-PF6) and 1 vol% of water in propylene carbonate (PC). Similarly, Teshima et al, [79] reported that the conductivity of polyaniline

increases with decreasing electropolymerisation temperature when the polymer film was synthesised in a non-aqueous solution of 1, 2-dichloroethane (DCE) without a protic acid at temperature varying from 248 K to 298 K. Further, the morphology of the films deposited at low temperature is smoother and denser and is composed of smaller and more uniform grains than that prepared at higher temperature.

b) Effect of pH

The solution pH level is a very important variable that strongly influences the PPy polymerisation and its properties. The effect of the pH level is associated with parameters such as synthesis method, nature of the doping anions and the substrate material. A medium with a low pH level produces a smooth good film quality without cracks, in contrast to an alkaline medium which may produce a brittle and non-uniform film. In general, the PPy polymerisation potential in an acidic medium is lower than the PPy polymerisation potential in a medium with a higher pH level. Hence, this may affect the quality of the synthesis of PPy films in an alkaline medium.

Shimoda et al, [81] has reported that the growth rate of PPy doped with immobile large anions, such as the large aromatic surfactant anion dodecylbenzenesulfonate (DBS), is higher at a pH between 1 and 11 when a potentiostatic method is used. In addition, the PPy deposition does not occur in a medium with pH equal to or greater than 11 when a lower deposition potential is used, such as 0.65 V *vs.* SCE. When the deposition potential is increased, spots and a non-uniform layer are formed. If the potentiodynamic method is used, the polymers' growth rate increased with an increase in the electrolyte pH level between 3.2 and 10. When the medium pH is increased to 11.2, PPy deposition does not

occur and when PPy film deposited at a lower pH (pH 1), it becomes non-conductive [81]. The conductivity of the PPy film increases when the polymer synthesis is conducted in a highly acidic solution, and the film which is polymerised in basic or alkaline solution may become less conductive or an insulator. The irreversible overoxidation potential is decreased with the increase in the pH level of the synthesis medium. This was also true for the electrode potential required for the water decomposition to produce oxygen, which reduces as the alkalinity of the solution increases. Therefore, the produced oxygen may be the cause of the overoxidation of the PPy film, thereby destroying the conjugated structure of the polymer. However, in metals where oxygen evolution is prevented by a passive layer on the reactive metal surface such as aluminium, the overoxidation of PPy was independent of the pH of the electrolyte.

Bhattacharya et al. [82] stated that the conductivity of PPy films doped with vinyl sulphonate PPy-V and synthesised in an acidic medium had a much higher conductivity (13 S cm^{-1}) than the films synthesised in a neutral or high pH solution (6.2 S cm^{-1}). The decrease of the films' conductivity is probably caused by the presence of a carboxyl group which reacts with the produced oligomer radical, thereby reducing the length of the conjugated polymers. In addition, the decrease of the films' conductivity may also be due to the migration of the dopant within the polymers to OH^- ions. Bhattacharya et al. [82] also found that the conductivity of PPy films doped with styrene sulfonate (St) is much higher than that of the PPy-V films and not affected by the increase in the pH level of the synthesised solution. Further, the surface morphology of the PPy films are affected by the variation of the synthesised solution pH. When a solution with a high pH of 10 or more is used, the PPy-V and PPy-St films showed a similar globular surface containing small

spherical bubbles. When the pH is reduced to 3.1, the PPy-V films showed a similar surface morphology with more surface regularity. Further, the PPy-St films showed a nodular-shaped growth for the films synthesised at a low pH of 4.

Saidman et al. [83] studied the effect of the pH variation of the PPy growth in nitrate solutions. They found that the change in the pH level strongly influences the PPy growth on a reactive metal substrate such as aluminium (Al). This material is characterised by the present of a passive oxide layer which protects and inhibits the oxidation of the monomer and thus film deposition. The increase in solution pH leads to partial dissolution of the passive layer and defects in the oxide layer, which caused the PPy deposition. However, the increase in the pH level may have lead to a high dissolution of the metal by OH^- ions and thus prevented the PPy deposition. They obtained homogeneous and adherent PPy films, which perfectly covered the substrate surface when they applied a constant potential between 0.7 to 1.15 V at pH 12. They did not observe any growth of the PPy on the substrate at a pH level between 4 to 11 and more than 13.

In addition, Saidman et al, observed good deposition of the PPy films on the Al substrate using the potentiodynamic method at pH 12 in the presence of a high concentration of NO_3^-. Moreover, they observed a decrease in the PPy deposition rate with the decrease in the concentration of NO_3^- and found that in the absence of NO_3^-, the Al substrate was not covered with PPy, which gives an indication that the polymerisation rate of Py decreases at low NO_3^- concentration [83].

1.6 Drug Delivery Systems

There is a number of conventional methods for drug delivery, which depend on the drug type and treatment requirements. Conventional routes used for drug delivery include: peroral and gastrointestinal, rectal, ocular, intravaginal, transdermal, vascular injection, nasal and pulmonary routes [84]. While some methods are suitable to deliver certain drugs, the same method might not be appropriate for others. For example, intravenous or intramuscular injections are used to deliver drugs but they are not suitable for drugs based on peptides and proteins, such as insulin for patient with type 1 diabetes. Although taking drugs through the peroral route is probably less expensive and more convenient for patients, particularly patients suffering from chronic diseases that prevent them from using injections to avoid pain and tissue trauma, this route is currently unsuitable for some drugs. Drugs administrated through peroral route can break down through the destructive acid medium in the stomach and by the intestine enzymes. The absorption of drugs in the digestive system is difficult; and almost all macromolecules cannot be absorbed, which limits the drug's effectiveness before reaching its target location.

Numerous attempts have been made to improve the currently existing drug delivery systems. One common strategy is to encapsulate the drugs with a protective layer while they pass through a destructive environment. The protective layer dissolves at the targeted location, and increases the drugs' susceptibility to be absorbed in the right part of the body. Other examples include, the develop of an insulin injection through the skin using a needle-less injector and constant infusion pump [85].

Despite the fact that these traditional methods are used to deliver drugs, they cannot provide the optimum level and ensure sustained drug release. The concentration of the drugs in the body fluctuates, initially increasing after being introduced and decreasing over a period of time. In the case of insulin, for example the best way to provide it is to ensure that the release profile mimics the body's physiology and conforms with the pancreatic islet release profile, in response to changes of the concentration of sugar in the blood. This cannot be done by traditional methods. In addition, a drug delivery system can also be used to locally deliver neuro-growth factors in the brain to treat neurodegenerative diseases such as Parkinson, Alzheimer and Huntington and to overcome the blood-brain barrier that prevents the drug from entering the brain. Moreover, in order to understand the processes that take place in the brain and to address the loss of functionality of the nerve cells, such as the eyesight and hearing, electrodes can be implanted. These electrodes collapse and lose functionality shortly after implantation, due to the inflammation generated in the surrounding tissue and, consequently, the body rejects the implant. Drug delivery systems can provide anti-inflammatory medicaments and growth factors directly into the local vicinity of the implant, forcing the body to accept the implant [86]. Another application of the drug delivery system is in bone tissue engineering where growth factors can be delivered locally at high concentrations with precise control.

Some drugs are unstable and strongly influenced by their administration time; they require rapid and accurate delivery to target a certain location within the body in order to be effective. This includes DNA-based drugs, which must be delivered to the host genome precisely where existent drug delivery systems are unable to do so [85]. The use of traditional methods to deliver drugs often require repeated and high dosages with toxic

effects, such as cancer drugs that exposes the entire body to toxicity. Therefore, doctors must carefully control the delivery of these drugs to the target location with the precise concentration, so the drugs will work effectively and efficiently with minimal toxicity.

Controllable drug delivery systems provide advantages that outweigh those offered by the traditional methods. These systems can deliver drugs with the effective concentrations required for a long time, without the need to take repeated doses at frequent intervals. Therefore, they are very useful for patients with chronic diseases, especially those who have difficulties to adhere to their treatment regimes.

The main objective of drug delivery systems is to provide intact drugs specifically to targeted locations using an intermediary system that can control drug administration by chemical, electrical, electrochemical, thermal or physiological release circuits, or by a combination of the above [87]. In addition, these systems can decrease drug toxicity and side effects providing protection and preservation of the drugs until they reach their target resulting in an improvement in the drugs' absorption rates.

1.6.1 Drug delivery system based on conducting polymers

1.6.1.1 Introduction

There are many interesting properties of conducting polymers, which make them suitable materials to be used in drug delivery systems. These polymers can be formed easily either chemically or electrochemically from an aqueous solution containing monomers. A drug

can be incorporated during the polymerization process without the need for additional procedures or equipment. Polymerization offers the possibility of incorporating various types of drugs and molecules whether anions, cations or neutral molecules into the polymers. Moreover, two or more drugs can be combined in the same film [88]. The possibility of controlling the conditions of the polymer synthesis to obtain the desired type of surface and composition or to improve its mechanical and electrical characteristics is advantageous. In addition, integrating conducting polymers with other materials and nanostructures, such as titanium and carbon nanotubes [89, 90], yields high surface areas where drugs and molecules can be stored. Further, the miniaturisation of polymer devices and the diversity of methods that can be used to incorporate drugs into polymers films are also beneficial.

Conducting polymers have the ability to undergo a reversible redox reaction involving ion transport into and out of the polymer bulk at low electrical power, typically less than 1 V depending on the environmental conditions. They are usually operated in an electrolyte solution and in a broad range of temperatures. In addition, the natural biological compatibility of these polymers with various living body tissues and fluids without causing any toxicity or immune problems for long periods makes them suitable for use *in vivo* and *in vitro* [91, 92].

Conducting polymers are characterised by their ability to undergo reversible redox reactions by the application of a potential difference. When the conducting polymer films oxidise, they are positively charged and are associated with counter ion movement from the solution into the polymer to compensate for the charge, thereby resulting in an

increase in the film's volume. In the reduction state, the counter ions are expelled from the film and cause the film to shrink. These properties can be used for drug delivery systems, where the drugs are incorporated into the polymer film during oxidation and released when the film is reduced [93].

1.6.1.2 History

The first attempts to use conducting polymers to store and release molecules began in the 1980s, shortly after the discovery of their ability to conduct electricity by Shirakawa et al. at the end of the 1970s [94]. In 1982, Miller et al. [95] developed the first controlled release system to deliver a small amount of the neurotransmitter dopamine, which is cathodically cleave-bonded to the conducting polymer using CV. In 1984, this was followed by the use of ferrocyanide and glutamate drug as dopants using PPy as the conducting polymer. Zinger et al. [96] were the first to report the possibility of using repetitive electrical pulses to trigger controllable small amounts of ferrocyanide ion to be released gradually from the polymer. Despite this, the amount of incorporated molecules in the polymer was very small, estimated to be 3.2 $x10^{-8}$ mol cm^{-2}, thereby making the released ferrocyanide very impractical. However, this achievement was significant because it demonstrated the principle of the controllable release of molecules. Since then, many researchers have sought to develop and improve the use of conducting polymers as a controlled delivery and release system for drugs and other molecules. In this chapter, the properties that make conducting polymers suitable for drug delivery systems will be discussed. This will include the types of drug delivery systems that can be based on conducting polymers, types of drugs that have been incorporated, the conditions that must be present for the drugs to be incorporated, the release methods and how these methods

have been developed. The future of polymers for use in drug delivery systems and the methods used to increase the amount of drugs that can be loaded within the polymers will also be discussed. There are several reviews and studies on the use of conducting polymer on drug release applications. Table 2.1 gives an example of these papers and a summary of these papers' scope.

Table 1-1: Examples of published review papers of conducting polymers drug release applications.

Authors	**Year**	**Topic**	**Scope**	**Ref.**
Ravichandran R., Sundarrajan S. Venugopal J., Mukherjee S. and Ramakrishna S.	2010	Applications of conducting polymers and their issues in biomedical engineering	Conducting polymers biomedical application and various methods modulate their properties for such application.	[97]
Guimard N., Gomez N. , and Schmidt C.	2007	Conducting polymers for biomedical applications	An overview of common type conducting polymers including their properties modification and challenges in biomedical application.	[98]
Svirskis D.,[2] Travas-Sejdic J. Rodgers A.,[2] and Garg S.	2010	Conducting polymer drug delivery system	Fundamentals of intrinsic conducting polymer drug delivery system, synthesis, properties, characterisation and limitation of this system.	[94]
Vallejo-Giraldo C., Kelly A. and J.P. Biggs M.	2014	Conducting polymers for neural applications	An overview of the use of PPy and PEDOT in biomedical applications specifically as neural biomaterials.	[99]

Authors	Year	Topic	Scope	Ref.
Pillay V, Tsai T., Choonara Y., Toit L., Kumar P., Modi G., Naidoo D., Tomar L., Tyagi C. and Ndesendo V.	2014	Conducting polymers and conducting polymers hydrogel for drug delivery system.	A critical review of commonly used conducting polymers and conducting polymers hydrogel including: polymerization, doping and actuation mechanism, and their redox reaction characterization techniques, applications as drug delivery systems and related challenges are discussed.	[105]
Yue Z., E. Moulton S., Cook M., O'Leary S. and Wallace G.	2013	Conducting polymers for neuro-bionics applications.	An overview of conducting polymer drug delivery neuro-bionic devices to improve the biocompatibility, stability, the neuroactivity and the electrical properties of the implanted electrodes.	[106]
Asplund M., Boehler C., and Stieglitz T.	2014	Conducting polymer electrodes for neurons drug delivery.	A review of the incorporation and release of neurons drug from conducting polymers. The mechanism and efficiency of the various release strategies along with their possible risks and challenges *in vivo* applications has been summarised.	[107]

Authors	Year	Topic	Scope	Ref.
Otero T. , Martinez J., and Arias-Pardilla J.	2012	Soft and biomimetic reactive devices	A clear summary of soft and biomimetic reactive devices based on conducting polymers including a view of the characterisation in such application, the emerging and start-up companies, patents and scientific challenges	[100]
Guo B., Glavas L., and Albertsson A.	2013	Biodegradable conducting polymers	A critical review of degradable conducting polymers synthesis and fabrication methods. The developments and the challenges of these methods are also discussed. Application to tissue engineering is highlighted.	[101]
Llorens E., Armelin E., Pérez-Madrigal M., Valle L., Alemán C. and Puiggalí J.	2013	Biodegradable nanofibers and nanomembranes based on conducting polymers	Progress review of the preparation of biodegradable nanofibers and nanomembranes based on conducting polymers focused on electrospinning and spin coating technique. Their potential in biomedical applications are highlighted specially in drug delivery and tissue engineering.	[102]
Smith J., and Lamprou D.,	2014	Conducting polymers for biomedical applications	A summary of conducting polymers recent works published between 2011 and mid 2013 on biomedical applications; including: drug delivery, biosensors, cardiovascular stents, tissue engineering, orthopaedic and antibacterial materials.	[103]
Long Y., Li M., Gu C., Wan M., Duvail Jm. , Liu Z., and Fan Z.	2011	Nanostructured conducting polymers	Synthesis methods, physical properties, promising application and consistent challenges.	[104]

1.6.1.3 Drug incorporation and release

Anionic, cationic, or neutral drug molecules can be incorporated into a polymer film during or following the polymerisation process [94]. Drug anions can be added to a suitable electrolyte solution containing the monomer. When the monomer oxidises, forming the polymer, the drug ion is incorporated to compensate for the positive charge of the polymer backbone due to the loss of electrons. The incorporated drug can then be released upon the reduction of the polymer film due to the electrostatic repulsion force. Cationic drug molecules also can be incorporated during the polymerisation process. For example, Svirskis et al. [108] incorporated the cationic drug risperidone into a polypyrrole film doped with Para-toluene sulfonate (pTS) anions during the polymerisation process using a galvanostatic method. The freshly prepared PPy films released 1.1±0.2 μg s^{-1} when ±0.6 V *vs*. Ag/AgCl at 0.5 Hz was applied. In addition, the cationic neurotrophine-3 (NT-3) has been incorporated in a PPy-pTS film during the galvanostatic polymerisation process. The mechanism of NT-3 incorporation into the polymer is not fully understood. The incorporation process may include electrostatic interaction between the NT-3 and the doping anion pTS, hydrophobic interaction between the NT-3 and pTS ions or pyrrole monomer, or the NT-3 molecules may be physically trapped inside the polymer bulk [88].

To incorporate a cationic drug after the polymerisation process, the polymer needs to be doped with immobile anions during the polymerisation process. When the polymer film is doped with large immobile anions, the anions are trapped in the polymer bulk. The reduction of the film by incorporated cations leads the film to swell during the process. Therefore, the cationic drug can be incorporate by reducing the film using a suitable

potential and electrolyte solution containing the cationic drug. When the film oxidises, the incorporated cationic drug is ejected by the electrostatic repulsion force and the film shrinks [109]. The actuation of the film between the polymer redox state may cause cracks and holes in the film, which may lead to an increase in the release rate of the incorporated molecules [94].

An anionic drug can be absorbed in a polymer film doped with small anions, which oxidise by anion incorporation and are reduced by anion ejection. Both cation incorporation and counter ion expulsion simultaneously occur when a mobile ion is used. Figures 1.6 and 1.7 illustrate the mechanism of drug incorporation and release from a conducting polymer film [94, 109].

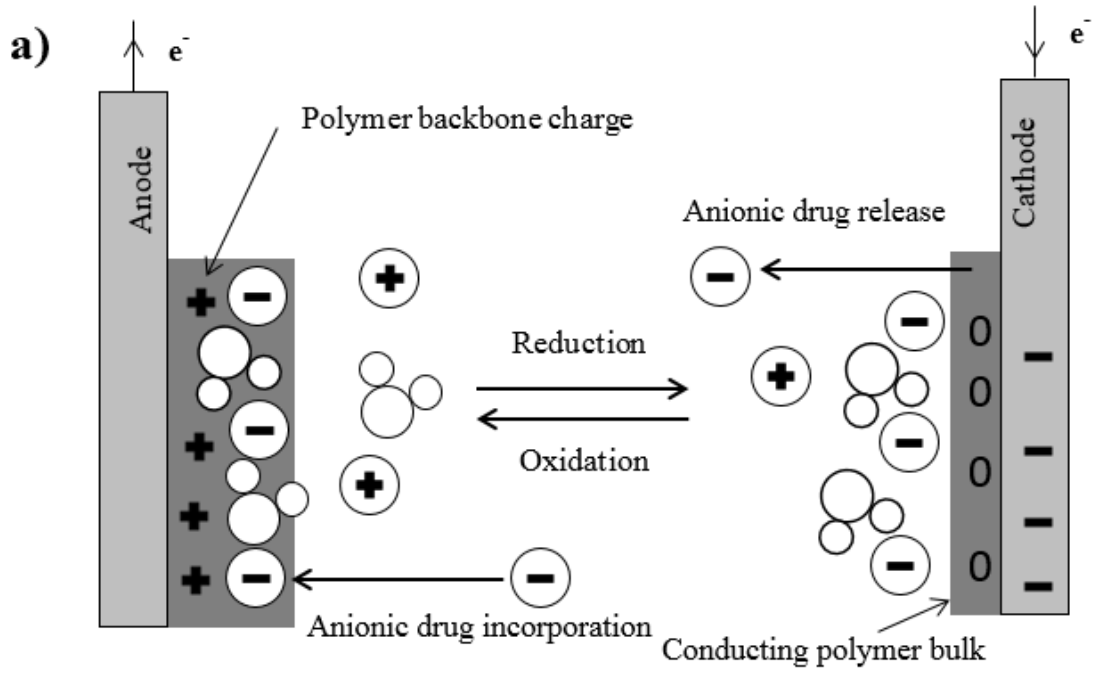

Figure 1-6: Schematic for the incorporation and the release of an anionic drug.

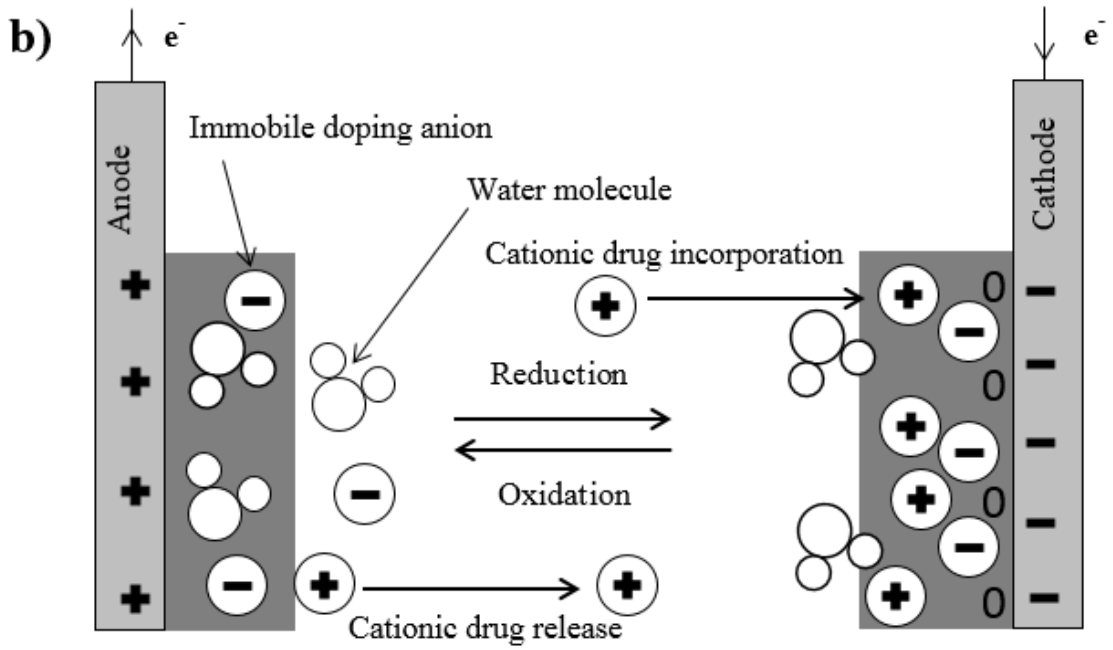

Figure 1-7: Schematic for the incorporation and the release of a cationic drug.

1.6.1.4 Limitations

Despite the interesting specifications that characterise conducting polymers as suitable drug delivery matrices and the ongoing efforts made to develop them, this field of research still suffers from an obstacle that prevent their extensive use in release systems. These limitations are still under study and can be summarised in the five main points listed below:

a. The amount of storage and release

The capacity of conducting polymer films to store a drug is limited, and the amount of drug being released is very small. Recently, the surface area of conducting polymer films

has been increased by modifying the polymer structures using nanoporous materials and by incorporating the polymers into nanotubes such as carbon nanotubes, thereby increasing the storage and release amount of the drugs using nanostructures such as nanopores.

b. Power source

The drug is released from the conducting polymer film by applying an electrical potential to reduce it. However, using an external power source restricts its use *in vivo,* although some drug delivery systems do not need external power sources and use temperature increase to release the drug, but such systems still have some shortcomings because the change of human body temperature is limited.

c. Operational stability

The long-term stability of conducting polymer films constitutes one of the problems that challenge the drug delivery system. It has been highlighted that the failure of conductive polymer films is because they are separated into many layers as a result of physical stresses and are exposed to oxidation and reduction reactions over a period of time [110].

d. Control

The release of incorporated drug molecules into the framework of conducting polymers is triggered and controlled by an electrical stimulus. Consequently, the rate of release could be constant and non-dynamic and will not necessarily interact with changes in response to the reactions of a living body. This makes them unsuitable for use in certain drugs, which require variable dosage rates that depend on the patient's clinical response. It can only be used for drugs that require constant dosage rates. There have been attempts to overcome these shortcomings and to take advantage of the influence of conducting polymers by physical and chemical factors, such as changes in temperature and pH, and to combine them with electric stimulus to control drug release. In addition, some scientists

have sought to take advantage of the ability of conducting polymers to function as sensors, thereby attempting to integrate them into the drug delivery system to monitor the release rate [111].

e. Biodegradability

Despite the attractive specifications of conducting polymers, which include biocompatibility, these polymers are not biodegradable. Therefore, these polymers must be expelled as waste from the living body or removed surgically after having been used in drug delivery systems or as implanted scaffolds and devices *in vivo*.

1.6.2 Towards a self-powered PPy drug delivery system

A self-powered drug delivery system based on the galvanic cell mechanism was demonstrated recently [112]. This system eliminates the need of an external power source and wiring. There are three techniques used to prepare the self-powered drug delivery system based on a galvanic cell, which have been demonstrated in the literature.

In the first technique, the polymer film is connected to a separate anode electrode such as zinc (Zn) and magnesium (Mg) based alloys [113]. In the second technique, the conducting polymer film (CP) is electrodeposited in a metal substrate such as titanium foil. The substrate is used as an anode electrode to reduce the deposited polymer film [112]. In the third technique, the CP film cathode is coated with a thin layer of active metal, such as Mg and Zn, which serve as the anodes, as shown in Figure 1.8 [112]. The galvanic coupling between the Mg layer and the CP film provides the driving force for the drug release.

All these techniques are based on galvanic coupling where the conducting polymer electrode is employed as a cathode and coupled with a metal electrode as an anode. Immediately, in the presence of electrolytes, the soluble metal electrode oxidises and begins dissolution, thereby reducing the CP which causes the expulsion of the incorporated molecules via the following electrochemical reactions:

1- The anode reactions involve the oxidation of Mg metals [114]:

$$Mg\ (s) \rightarrow Mg^{+}_{(aq)} + e^{-} \qquad 1.5$$

$$Mg^{+}_{(aq)} + H_2O \rightarrow Mg^{2+}_{(aq)} + OH^{-}_{(aq)} + \frac{1}{2} H_{2\,(g)} \qquad 1.6$$

The produced metastable Mg^{+} ion can be easily oxidised to Mg^{2+} with associated hydrogen gas evolution:

$$2Mg\ (s) + 2H_2O \rightarrow 2Mg^{2+}_{(aq)} + \frac{1}{2} H_{2\,(g)} + OH^{-}_{(aq)} + e^{-} \qquad 1.7$$

2- The cathode reactions involve the following conducting polymer (PPy) reduction:

$$PPy^{+}.D^{-} + ne^{-} \rightarrow PPy^{0} + nD^{-} \qquad 1.8$$

Where D^{-} is the drug anion.

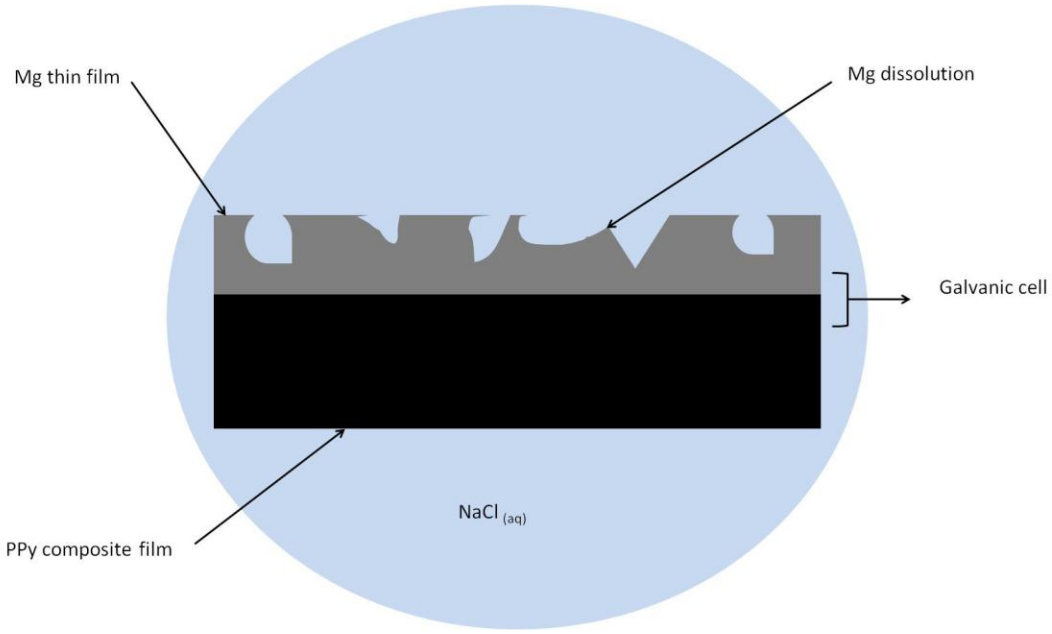

Figure 1-8: Self-powered drug delivery system based on a galvanic cell.

A limited number of studies have demonstrated a self-powered, controllable drug delivery system. Such systems can release a drug without the need of an external power source. This simplifies the manufacturing process and may reduce production costs. In addition, these systems do not need power wiring, which may limit the application of drug delivery systems, particularly for implant systems. Although most reported studies used self-powered systems to release dye molecules or model drugs (less than 10 studies used actual drugs), all relied on the same galvanic principle to generate power.

Ge et al. [112] constructed a self-powered drug delivery system based on a galvanic cell mechanism. The model drug, adenosine triphosphate (ATP), was incorporated into the polymer matrix during the electrochemical polymerisation of PPy, depositing the polymer

on pure polished titanium foil. The system released 62% of the ATP drug within 12 hours at room temperature. In addition, the researchers reported that by coating the naked side of the titanium foil with a thin eicosane-poly (L-lactide) blend film, they reduced the released amount of the drug to 14% under the same conditions. The amount of the drug released increased by 82% within the same period of time, when the temperature rose to human body temperature (37.5 ^{o}C). This is because the melting point of eicosane is 36 ^{o}C, which is close to human body temperature. This can help to protect the system at room temperature and may provide an on-demand drug delivery system.

Ge et al. [112] also described a self-powered drug delivery system based on a cellulose-PPy composite film. They incorporated the model drug ATP during the polymerisation process and then sputtered a thin layer of Mg or Zn of varying thickness onto one side of the composite film. They reported that the drug release rate into 10 ml NaCl solution was slightly increased when the Mg layer grew from 450 to 500 μm. In addition, the driving force of drug release was higher when a Mg anode was used rather than a Zn anode, thereby increasing the release rate of the drug. This is because the Zn electrode potential is less negative than that of Mg. Moreover, the concentration of the released Mg ion is very small, approximately 14 ppm, which is safe for the human body.

Moulten et al. [113] incorporated the glucocorticoid dexamethasone sodium anti-inflammatory drug salt, dexamethasone sodium (DEX), into PPy films. The drug was used as a dopant during the galvanostatic polymerisation of PPy onto a gold-coated mylar or gold-coated quartz crystal microbalance (QCM) crystal electrode. The PPy/DEX electrode was coupled galvanically with the magnesium alloy in the phosphate buffer

saline. This led to Mg dissolution; the conducting polymer matrix was reduced, and the DEX drug was released. The initial release profile was high after the galvanic coupling. Although the final concentration of released DEX was low, it is sufficient as a treatment dosage. The Mg alloy electrode benefits from its ability to degrade and its non-toxicity. In addition, Mg has good mechanical properties and presents a low density and a high strength to weight ratio.

Wang et al. [113] incorporated phenol red salt (PR) into a PPy matrix (PPy) during its electropolymerisation. The PPy-PR cathode was galvanically coupled with the Zn counter electrode in a sodium dodecyl sulphate (SDS) solution. This action leads to the oxidisation of the counter electrode and reduction of the polymer matrix, thereby resulting in the release of phenol red from the polymer and the dissolution of Zn^{2+}. The initial release of dye was high, being 55% in 740 s. The release rate declined with time and 67% of the dye was expelled in 60 min. The use of phenol red salt as a doping ion can be observed with the naked eye during the release process.

Jensen and Clark [115] used a chemical method to incorporate sodium sulphate or phenol red and another class of sulfonephthalein dye into PPy conducting polymers. In the first method, they dissolved the dye in water: ethanol (50:50 w/w) and then mixed with pyridine. The mixture was incorporated into an oxidant solution of iron (III) para-toluenesulfonate (Fe(III)) pTS in butan-1-ol.The mixture was printed on a range of substrates either directly using a pipette or using a Dimatic Materials Inkjet printer Model 2811 facilitated with a DMC-11610 cartridge (10 pL nominal rate). The printer was set so

that the space between each drop was 15 μm and the reservoir temperature was at 40 °C to optimize uniformity and edge resolution. After the substrate dried, it was used as a polymerization template where it was exposed to monomer vapour to form a conducting polymer film. In the second experiment, the polymerisation inhibitor factor pyridine and the monomer were added into the dye-oxidant mixture and then they were applied to the substrate. The substrate was then heated for 20 minutes at 70 °C to evaporate the inhibitor factor and complete the polymerization process. The dye molecules were successfully released in 0.1 mol dm^{-3} NaCl solution using Zn anode and the PPy containing the dye as a cathode on a paper coated with conducting polymer PEDOT. They also used the PPy containing the dye on indium tin oxide (ITO)-coated glass and ITO-coated polyethylene naphthalate (ITO-PEN) film electrodes.

Despite the attractive features of these systems, they still have some shortcomings. The initial release of molecules is high, and their final concentration in solution is low. A number of attempts have been made to improve the release profile to increase the concentration. It has been reported that the deposition of PPy-DEX films on a polythiophene-conducting layer provides a large active surface area and increases the release rate of the DEX drug. In addition, the presence of a physical barrier on the metal anode, either naturally from the metal oxide on the surface or by coating the anode with an insulating biodegradable material, provides an advantage for controlling the release profile and metal dissolution.

Coating the magnesium with a bioresorbable polymer poly(vinyl alcohol) (PVA) and biodegradble polymer poly(lactic-co-glycolic acid) (PLGA) decreased the release rate of

the DEX from PPy matrix and Mg dissolution. However, this coating decreased the final released concentration to 1.3 mg cm^{-2} for Mg-PVA and 0.2 mg cm^{-2} for Mg-PLGA, compared with 3 mg cm^{-2} for the Mg anode without coating [113]. Moreover, it has been reported that the incorporated molecules diffuse into the solution after the electrode is soaked in an electrolyte for more than 30 minutes before the galvanic coupling. The deposition of the conducting polymers' bilayer of PPy-polystyrene sulfonate on the main PPy phenol red layer prevented the release of the dye while it was being soaked in electrolyte for four hours [116]. The galvanic coupling between the Zn anode anodic (potential -0.7 V reference electrode not mentioned in the reference paper) with PEDOT dye composites (reduction potential -0.782 V) did not lead to the release of the incorporated dye molecules. Therefore, the potential of the employed metal anode must be lower than the conducting polymer cathode to reduce the polymers and release the molecules [115]. It has been reported that the use of chemical polymerisation methods to incorporate the chemical compounds into the polymer matrix might decompose some types of molecules, such as anionic dyes, that contain the azo and quinone groups. Furthermore, the incorporation of large highly charged molecules with hydroxyl groups into the conducting polymers matrix might lead to a reduced rate of release or might even eliminate it. For example, there was no release for pyrocatechol violet dye, which contains three hydroxy groups; this might be due to strong bounding to the Fe (II) within the PPy [115]. Moreover, a detailed understanding of the toxicity of the metal anode, corrosion process and amount of ion dissolution is required before the process can be used in an implant system [113].

1.6.3 Biodegradable conducting polymers

Using conducting polymers with controlled biodegradable characteristics and the matrix with nanoparticles attached to non-conducting biodegradable polymers may eliminate the need for surgery, thereby reducing the risk of infection and contributing to patient healing and comfort [117].

Boutrs et al. [117] synthesised polymer matrixes from PPy nanoparticles and the biodegradable conducting polymers polylactide (PLLA) or polycaprolactone (PCL). They suggested that by using Matlab modelling and HFSS simulation, the synthesised polymers could be used in the manufacture of biodegradable all-polymer RF-driven RLC resonators for use *in vivo* sensors. They synthesised PLLA/PPy and PCL/PPy composites by emulsion polymerization of PPy in PLLA or PCL and then precipitated it. The precipitation was redissolved and treated with ultrasound and then cast in a PTFE plate. The resultant membranes were compressed using a hot hydraulic press between silanized silicon wafer templates to increase the homogeneity of the films. The samples were cut into clover shapes and gold was deposited as an electrode by e-beam evaporation for conductivity measurements. The resistance of the polymer films was measured as a function of the weight ratio of the PPy content in the PLLA/PPy and PCL/PPy films using the four point's resistance and Van der Paum measurements methods to achieve the least resistance with the lowest percentage of PPy in the films. The lowest measured resistivity was 0.0043 and 0.0016 Ω m for the PLLA/PPy and the PCL/PPy, respectively, in the films that contained 39% PPy. In addition, the less resistant films were those that were polymerised under nitrogen at 0 ºC for the PCL/PPy films and at 50 ºC for the PLLA/PPy films.

Two different models of the RLC resonator circuit were designed and investigated using Matlab modelling and HFSS simulations, using the properties of the synthesised polymers, which have been measured and compared with the characteristics of copper as a reference model. Good agreement was found between the obtained results from the Matlab models and HFSS simulation. The results also proved that all-polymer RLC resonators can be manufactured from PLLA/PPy and PCL/PPy films. Although the highest quality factor was 6.6, using the properties of the PCL/PPy film (39% PPy), this may be sufficient for use in certain medical applications such as in implantable, biodegradable sensor.

Zhang et al. [118] produced biocompatible biodegradable electrically conductive polymers. Initially, they synthesised poly (dichlorophosphazene) and parent aniline pentamer, and then they synthesised poly [(glycine ethyl ester) (aniline pentamer) phosphazene] copolymer (PGAP). The dissolved parent aniline pentamer monomers in tetrahydrofuran (THF) were added into a poly (dichorophosphazene) solution drop-wise by stirring under dry nitrogen conditions. The mixture was refluxed for two days at 60 ^{o}C and then cooled to 0 ^{o}C. A glycine ethyl ester hydrochloride and triethylamine suspension was whisked in boiling THF for 10 hours and then cooled to 0 ^{o}C. The triethylamine hydrochloride was removed by filtering the mixture in a dry nitrogen atmosphere. The resultant mixture was added and stirred with the above polyphosphazene solution for 6 hours at 0 ^{o}C and was permitted to reach room temperature for 24 hours and refluxed for another 2 days. Then, the mixture was poured into 400 ml of water and filtered. The resultant solid mixture was cleaned with water and dried with air. The dried mixture was dissolved in THF and then filtered to remove undissolved material. The bulk of THF was

removed by evaporation, and the remaining solid was purified by using the soxhlet extraction method with ethanol solvent and finally vacuum dried at 40 ^{o}C.

The FT-IR and H-NMR spectra showed that polyphosphazene had been successfully grafted with parent aniline pentamer and glycine ethyl ester (GEE) group as side groups by grafting the parent aniline pentamer for its electrical activity and glycine ethyl ester for its biodegradability, as well as to increase the biocompatibility as a side group on the polyphosphazene by nucleophilic replacement reaction.

The results of the resistance measurements showed a decline in the conductivity of the synthesised polymer to approximately 2 x 10^{-5} S cm^{-1}, but this conductivity may be sufficient for cell stimulation applications. The decrease in the polymer conductivity is due to the decrease in the number of aniline pentamers in the polymers and also because of the –NH- bond in the amide that resulted from the interaction of the chlorine atoms, which consumed the end group (-NH_2) in the amine oligomer but did not involve conjugation with the other aniline oligomer.

The *in vitro* biodegradable study was conducted in phosphate buffer saline (PBS) solution at 37 ºC and pH 7.4. The results revealed that the poly(glycine ethyl ester) phosphazene (PGEP) lost approximately 60% of its weight after 840 hours, while the PGAP lost approximately 30%. Since these biodegradable polymers can be used as a conduit for neuron regeneration in peripheral and spinal cord injuries, the biocompatibility of these polymers was examined with Schwann cells, which play an important role in nerve

functional recovery and repair. They stimulate nerve regeneration and provide guidance and structural support for the regenerating axons [119, 120]. To examine biocompatibility, Schwann cells RSC96 were cultured on the PGAP, PGAP doped with CSA, Polypyrrole blended with poly(dl-lactic acid) (PDLLA) and tissue culture polystyrene (TCPs) films [118].

The cell proliferation test was conducted using (3-(4,5-Dimethylthiazol-2-yl)-2,5-Diphenyltetrazolium Bromide) (MTT) test assay. The SEM images after five days of culture revealed that the cells showed long filopodia in all groups, as well as faster growth and good attachment of the cells on the PGAP and the PGAP doped with CSA films. In particular, the PGAP/CSA showed the fastest growth rate and had an elongated shape. Many cells showed a single filopodia oriented in the migration direction of cells on the PDLLA film. The statistical findings of the total cell density showed the greatest density on the PGAP and the PGAP with the CSA films compared to the PDLLA and TCPs [118].

1.6.4 Conducting polymers utilising nanoporous surfaces and nanostructures

Although an increase in the thickness of the conducting polymer films increases the amount of drug that can be incorporated, the resistance of the films increases and the electroactivity decreases [121]. It has also been reported that thin films released a larger proportion of the incorporated drug than thicker films, although more molecules may also be released by thicker films by determining the appropriate electrode potential with or without longer release time [88, 122]. For example, Thompson et al [88], reported that when using a 3.6 µm PPy/pTS/NT-3 film, 5.6 ng cm^{-2} and 3.4 ng cm^{-2} of a neurotrophic

factor were released when the film was stimulated (Pulsed current ± 0.5 mA cm^2 at 5 Hz) and unstimulated over 7 days, respectively. This amount is lower when compared with 8.8 ng cm^{-2} and 5.3 ng cm^{-2} from a thicker film 26 µm using the same release protocol and shows the importance of film thickness. The efficiency of the polymer films in releasing the drug from its surface is higher than from the polymer bulk [123]. This may help to overcome the shortcomings of traditional conducting polymer films, which includes low capacity to load the drug associated with limited surface area. In addition, the amounts of the drug released from these films by electrical stimulation are low and not stable or sustainable, which leads to restricted application of these systems. Researchers are attempting to develop and manufacture materials with well-controlled structures at the nanometer-scale for various applications, including that in biosensors. In the area of controlled drug-delivery systems that are based on conducting polymer films, the construction of conducting polymer nanostructures is an effective way to increase the surface area of polymer films and thus increase the efficiency of the integration and release of a drug.

In general, the construction of conductive polymer films with nanoporous surfaces and conducting polymer nanotubes has led to an improvement in conducting polymer drug-delivery systems.

1.6.4.1 Nanoporous surfaces

Open nanopores on conducting polymer films surfaces significantly increases the surface area of these films and, consequently, increases the capacity of the loaded drug molecules and the amount of released molecules. They also facilitate the diffusion of the dopants

and enhance the possibility of accessibility in multilayer constructions. Furthermore, they permit the efficient transport of large molecules when compared with traditional flat surfaces. The conductive polymer films with a porous surface can be obtained in several ways.

1.6.4.2 Porous membranes

Nanoporous membranes are used as a template where one side of the membrane is coated with conducting material to serve as a working electrode and then the conducting polymer is electrodeposited into the pores of the other side. After attaining the required thickness by controlling the total charges passing through the polymerization process, the nanoporous membrane template is dissolved with an appropriate material. A drug delivery system, designed by Leprince et al. [110], used this methodology. The system was electrically controlled to deliver and release the anti-inflammatory drug dexamethasone (DEX). This drug has been shown to reduce tissue interaction around implants but may cause muscle myopathy and diabetes. Therefore, conducting polymer local drug delivery system could eliminate these side effects.

The synthesis drug delivery system uses a hard template method to produce nanostructure PPy electrodes with DEX. In the beginning, gold was evaporated into one side of a nanoporous polycarbonate template to form a layer of 21 μm thickness to serve as a working electrode. Then, platinum was electrochemically deposited into the pores of the other side of the polycarbonate template. After removing the polycarbonate template, the

PPy/DEX was potentiostatically deposited on the resulting platinum nanopillar brush that resulted from dissolving the polycarbonate template [110].

The PPy/DEX nanostructured electrode was cycled in 20 x 10^{-3} mol dm^{-3} PBS with 150 x 10^{-3} mol dm^{-3} NaCl at room temperature and pH 7, cycled between -0.8 V to 0.9 V *vs*. Ag/AgCl at scan rate of 100 mV s^{-1}. The reduction and oxidation peak of PPy/DEX film on the nanostructured electrodes appeared at -0.2 and 0.15 V *vs*. Ag/AgCl respectively, which is significantly lower compared to oxidation potential peaks when planar electrodes were used. This decrease in the operating potential for the drug release is due to the increase in the surface area. The positive adhesion between the polymer and the electrode metal substrate improved the mechanical stability of the PPy film, where there were no cracks or delamination on the nanostructured PPy/DEX film after 150 CV stimulation cycles to release the drug. Conversely, the flat PPy films did show cracks and delamination after several cycles, thereby suggesting that this nanostructured design may improve the efficiency of the polymer electrodes in the long term [110].

Increasing the film thickness could enhance the amount of drug released without affecting the release profile [88, 96, 110]. For example, Leprince et al. [110] reported the manufacture of two conducting polymer, a thin film that consumed 27 μC cm^{-2} and a thick film consuming 700 μC cm^{-2} during the electropolymerisation process. Cyclic voltammetry stimulation of these films between -0.8 V to 0.8 V *vs*. Ag/AgCl released 39 and 105 μg from the thin and thick films, respectively after 150 cycles. This amount is three times more for an increase in film thickness 25 times which although not proportional, is sufficient amount to alleviate the inflammatory reactions surrounding body implants. In addition, this result confirms that the release rate does not cope with

the amount of increase of film thickness and the films released molecules more efficiently from their surfaces compared to releasing drugs from the polymer's bulk. This might have been resulted from the fact that the thicker film are less electroactive and have less diffusion rate.

The authors also reported that the stimulation scan rate affects the rate of drug release and the film properties. In the case of using a high scan rate, the drug ions remain and oscillate in the polymers' bulk, and thus they are not released and incorporated once again before they have time to diffuse into the buffer solution when the film is oxidised as a result of the high speed potential switching. The use of a low scan rate also causes some problems: if a negative potential is applied for a long time, the film becomes an electrical insulator because it loses the incorporated doping ions and the recovery of the film's conductivity upon reverse oxidation becomes more difficult. Therefore, the scan rate should be optimised to obtain an effective drug release without the affecting films' conductivity. The authors report that 100 mV s^{-1} is an optimal scan rate to release DEX and maintain of the characteristics of the film [110]. Furthermore, Jiang et al [124], found that the scan rate affects considerably the release of ATP drug from a PPy nanowire network coated by a PPy film. The percent of ATP released increased significantly from 57% to 89% and 95% when the system was stimulated at 50, 100, and 200 mV s^{-1}, respectively within 10 h. This suggests that the amount of drug released is not directly proportional to the thickness of the film and that the film releases molecules more efficiently from their surfaces rather than from the bulk of the polymer. This might have resulted from the fact that the thicker films are less electroactive and allow a lower diffusion rate of the drug molecules.

1.6.4.3 Closed packed colloid crystal array templates

Self-assembled polystyrene (PS) templates are used to fabricate porous materials. The synthesis of these templates involves several steps to obtain a uniform deposited PS nanoparticle template where a conducting polymer can be electrochemically deposited [125, 126]. The first step involves synthesising a PS colloid sphere using an emulsifier-free emulsion polymerization technique. The second step involves the ordered assembly of the sphere using different methods such as vertical deposition, gravity sedimentation and dip-drawing [125, 126]. The resultant polystyrene colloid sphere aqueous suspension is diluted with an appropriate amount of ethanol. Thereafter, a substrate such as ITO is dipped into the PS emulsion to induce the self-assembly of the PS nanospheres in uniform three dimensional layers. The assembly continues by slow evaporation of ethanol over approximately five days at room temperature. Thus, in this manner, a uniform deposited PS nanoparticle template is obtained. The conducting polymer is electrochemically deposited on the obtained template [125, 126]. After deposition, the colloidal crystals template can be dissolved by incubation in tetrahydrofuran for 24 hours, yielding porous conducting polymer films. The driving forces for the formation of close-packed PS crystals involve electrostatic interaction and lateral capillary force, and the ion diffusion during the evaporation is considered to be an important factor for the successful assembly of ordered structure on the latex surface [127].

Chao et al. [128] developed an electrically controlled nanoparticles release system based on nanoporous conductive films which incorporated biotin (molecular probes) during the electrochemical deposition. The authors used an aqueous solution of 0.1 mol dm^{-3} Py monomers, 9 x 10^{-3} mol dm^{-3} biotin and 0.01 mol dm^{-3} sodium dodecylbenzenesulfonate on an indium tin oxide (ITO) electrode modified with polystyrene spherical template

(spherical diameter 1 μm) using a cathode potential of 0.7 V *vs*. Ag/AgCl. After dissolving the polystyrene template, the film was immobilized with streptavidin-coated gold (Au) NPs (Nanocs) with a diameter of 1.4 or 5 nm at a concentration of 0.1 mg cm^{-3}. Cyclic voltammetry from -1 to 1 V *vs.* SCE in 0.1 mol dm^{-3} phosphate-buffered saline (PBS) containing 5 x 10^{-3} mol dm^{-3} mixture of $K_4Fe(CN)_6$/ $K_3Fe(CN)_6$ was used to observe the electrochemical properties of the films surface by sweeping the films at a scan rate of 50 mV s^{-1}. The release of biotin was stimulated between -2 to 2 V *vs.* Ag/AgCl for the Au-NPs for different time intervals.

The results show that the porous biotinalited PPy films along with the electrical stimulation permits a controllable release of the gold nanoparticles by changing the strength of the chemical bonds between the PPy and biotin. The SEM images showed that a cleaned defined porous surface with clear spherical voids are interrelated and arranged in a substantially similar manner to the arrangement of polystyrene pellets used in a template [128].

The conductivity test using a four-point method showed a reduction in the conductivity from 7.62 S cm^{-1} for PPy/Biotin flat films to 3.02 S cm^{-1} for PPy/Biotin porous films with a thickness of 2.7–4.4 μm. The conductivity increased to 47.62 S cm^{-1} for PPy-Biotin/SA-Au NPs (thickness 3.2 - 5.1 μm) due to the increase of the gold nanoparticle concentration in the film.

The contact angle measurement was used to evaluate the wetting of the surface. The measured high contact angle of 88±5^{o} for the porous film indicated that the biotin had been incorporated in the porous PPy where the natural hydrophobicity of biotin lead to the increase of the contact angle. The contact angle decreased to 27.3±3.6 ^{o} for the porous PPy-Biotin/SA-Au-Nps due to the exposure of hydrophilic moieties from streptavidin. When an electrical potential -1 V *vs*. Ag/AgCl was applied for 20 s on the PPy-Biotin/SA-Au-Nps film, the biotin linked with the nanoparticles was released; therefore, the contact angle increased to 54 ^{o} and the conductivity of the film decreased.

The recorded high-resolution XPS spectra of the films clearly showed the Au 4f peak, which returns to the gold in the PPy film incorporated with 1.4 nm SA-Au NPs. This indicates the successful combination of gold nanoparticles in the porous PPy film. In addition, the emergence of S2p signal at 161.0 eV, which belongs to the sulphur, proves the existence of the Biotin-Streptavidin in the film via their sulphur atoms. The application of a constant potential of -1 V *vs*. Ag/AgCl for 60 s resulted in a weakening in the S2p peak, and the Au 4f peak was not directly observed possibly because of the released nanoparticles. There have been slight peaks in the flat PPy film incorporated with Biotin-Strapataridin in the location of the Au 4f peak, which confirms that the film porosity promotes and provides useful sites to incorporate and release nanoparticles. Note: S2p and 4f are assign for electron energy configuration.

Luo et al. [123] designed a system to release a model drug, fluorescein, based on porous PPy. They pre-treated 3 mm-diameter GC electrodes rods by dropping 5 ml of a 1% (w/v) PS nanobead suspension (mean diameter 46 ± 2 nm) using a micropipette. The electrodes

were placed vertically until the suspension dried over several hours. The template solidified by heat treatment at 60 °C for approximately 15 min. The PPy film incorporated with fluorescein was potentiostatically deposited on the GC electrode at 0.9 V *vs*. Ag/AgCl for 200 s in a solution containing 0.02 mol dm^{-3} Py and 0.01 mol dm^{-3} fluorescein sodium salt. Then, the polystyrene template was removed by steeping the electrode in toluene for 12 hours. The film was stimulated to release the drug by applying -2 V *vs*. Ag/AgCl for 10 s in a cell containing 1.6 ml 0.1 mol dm^{-3} PBS (pH 7.4). The amount of released fluorescein was measured using a fluorimeter.

The results revealed that the amount of released fluorescein from the porous PPy film was approximately 10 times more than the released amount from the non-porous PPy film that was synthesised at the same conditions. This suggests that the porous surface increased the surface area of the film and, thus, increased the amount of the incorporated fluorescein and enhanced drug release effectiveness. In addition, the amount of the released fluorescein from the nanoporous film without electrical stimulation (pure diffusion) is negligible (3%) compared to the control released using electrical stimulation. This indicates that the drug release system based on nanoporous PPy is a true controlled system [123].

Luo et al. [123] studied the effect of the increase in the value of the negative applied potential on the amount of released drug. It was observed that a gradual increase in the released drug amount will occur when a fixed potential between 0 V and -2 V *vs*. Ag/AgCl is applied. Potentials higher than - 2 V have not been tested because it may produce

bubbles as a result of the electrical decomposition of water, which may affect the release efficiency. It is interesting that some released amount of drug was observed when a positive potential 0.5 V *vs.* Ag/AgCl was applied. The release of the drug at a positive potential may have been caused by the negative capacitive current that surged at the end of the positive potential pulse or due to film actuation.

Sharma et al. [129], reported the electropolymerisation of PPy on a 3-dimensionally macroporous poly-(methyl methacrylate) (PMMA) colloidal crystal template of approximately 430 nm diameter supported on stainless steel. The colloidal template PMMA was removed by chemical etching and a cationic drug, risperidone, was physically entrapped inside the macroporous PPy film (6–7 μm thick) by dropping 20 μL of methanol containing 0.1 mol dm^{-3} risperidone. After the drug was entrapped in second layer of PPy thin film, a PPy layer (<0.5 μm), was polymerised on top of the macroporous film to avoid spontaneous release. The macroporous film released a considerable amount of risperidone drug, 162.69 ± 3.6 μg under the application of ± 0.6 V *vs.* Ag/AgCl at 0.5 Hz over 1 h . When the film was not stimulated, the release over an hour was 119.8 ± 2.5 μg. This compares well with the amount released from a non-porous PPy film which is 42.5± 0.737 μg and 31.3 ± 0.4 μg for stimulated (± 0.6 V *vs.* Ag/AgCl at 0.5 Hz) and non-stimulated films, respectively. The increase of the drug release from the macrostructure can be ascribed to the higher amount of the incorporated drug within the high surface area of the modified film. The authors reported that the macroporus polypyrrole film has a higher surface area of 19.2 m^2 g^{-1} compared to that of the plain polypyrrole film, 4.8 m^2 g^{-1}.

1.6.4.4 Nanotubular structures

The interesting unique advantages of carbon nanotubes such as high electrical conductivity, high surface area relative to size and other ones based on the scale [130] and ability to be dispersed in water, have made them suitable for many areas of research. Researchers are attempting to use carbon nanotubes in many applications, either independently or in combination with other materials and chemical compounds. For example, carbon nanotubes have been used in many different applications including sensors [131], field effect transistors [132], biological materials [133], AFM probe tips for high resolution imaging of nanostructures and biological materials [134], as well as in sustainable energy applications such as hydrogen storage [135], solar cells [136], and fuel cells [137].

In the field of medical applications, it has been reported that carbon nanotubes are compatible with biological fluids and can be excreted through the renal route. In the area of controlled drug delivery systems, the efficacy of the use of carbon nanotubes to deliver a variety of drugs ranging from small molecules to peptides and proteins has been demonstrated. Carbon nanotubes can have different mechanisms to transport drug molecules. The drug molecules can form covalent or non-covalent bonds with the surface of the carbon nanotube; moreover, the nanotube cavities can be filled by different drugs by opening their ends. However, the surface tension of the liquid inside the tubes reduces the effectiveness of the filling. In addition, leaving the tube end open after filling it with a drug is problematic because the drug tends to diffuse out from the open end in an uncontrolled manner. A possible solution to this problem is to close the ends of the filled

nanotubes by depositing a conducting polymer to control the drug release when necessary [138].

There are many reports of the toxicity caused by single-walled carbon nanotubes (SWCNT) and multiwall carbon nanotubes (MWCNT) such as oxidative stress of human keratinocyte cells [139, 140], inflammatory and fibrotic reactions in rats' lungs [141], and inhibition of human HEK293 cells [142].

Shedova et al. [139] and Mana et al. [140] reported that SWCNT initiate toxicity in human cells. When human keratinocyte cells are exposed to SWCNT, it induces oxidative stress which inhibits cell proliferation. Muller et al. [141] found that MWCNT and ground carbon nanotubes induce inflammatory and fibrotic reactions in rats' lungs; they suggest using a system to reduce human exposure during the manipulation of carbon nanotubes. Cui et al. [142] showed that SWCNT inhibit the proliferation of human HEK293 cells by inducing cell apoptosis. In addition, they found the treatment of human HEK293 cells with SWNTs results in reduced viability of cell adhesion and that this decrease is inversely proportional to the increase in the concentration of SWCNT and culture time.

Ivanova et al. [63] synthesised an antibiotic and a virus control system based on MWCNT/polyaniline composite. The polyaniline was chemically synthesised by the oxidation of 0.1 mol dm^{-3} aniline by 0.1 mol dm^{-3} ammonium persulphate in 0.5 mol dm^{-3} HCl aqueous solution at room temperature with or without the presence of MWCNT. The MWCNT diameter ranged between 40–80 nm and attained a length of 10 μm. The

specific conductivity and the specific surface area of the carbon nanotubes were 40 S cm^{-1} and 60-80 nm, respectively, and the porosity was more than 70%.

The PANI salts were treated with 0.5 mol dm^{-3} of NH_3 aqueous solution to form a polyaniline base. Polyaniline interpolymer complexes with polypropylamidopropanesulfonic acid (PAMPSA) syntheses were formed using the same method in the absence of the MWCNT. The isolated influenza virus strain A/11V-Moscow/01/2009 (H1N1) SWL was grown in 9–10 embryonated egg strains and the mixer (virus and sorption) was then centrifuged at 2000 rpm. The hemagglutination test with human erythrocytes was used to determined viruses in the solutions. The results revealed that PANI is a better sorbent for influenza viruses, followed by MWCNT coated with PANI and the absorption of viruses by carbon nanotubes was the least. The viruses' titre before sorption was 64, and was reduced after sorption to 16 in MWCNT, 8 in MWCNT/PANI, and 4 in PANI base. These results indicate that the absorption of the viruses strongly depends on the absorbent materials.

The same authors investigated the sorption of the following antibiotics: Gramicidin S, Teicoplanin AZ, Bleomycetin, and Polymyxin B in MWCNT coated with polyaniline. A solution of 600 µl containing a concentration 0.2 mg ml^{-1} of the antibiotics added to different amounts of carbon nanotubes 1.25, 2.5 and 5 mg and incubated for periods of different time: 15 min, 1 hour and 18 hours at 22 ^{o}C. This was followed by separation of the antibiotics solution from the absorbent (carbon and viruses) by a centrifuge at 5600–8850 rpm for 5–7 min. The amount of antibiotics in solution had been calculated and

analysed before and after the absorption using reversed-phase chromatography (RP HPLC) on microcolumn liquid chromatograph using a multichrome-spectrum programme. The results showed that the hydrophobic antibodies Gramicidin S and teicoplanin A2 were removed within 1 hour, while the removal of the plymyxin B and bleomycetic, the hydrophilic antibodies, took 18 hours. This indicates that the absorption of antibiotics depends on the hydrophobic properties of the sorption materials and the antibiotics structures.

Metal oxide nanotubes, such as nanotubular titania (TiO_2), which were discovered in 1990s, are potentially useful materials for many applications, including biomedical ones [143-145]. These TiO_2 nanotubes have the same advantages associated with scale that are found in carbon nanotubes, such as high specific surface area and controllable dimensions. For example, the diameter of the nanotubes can be varied from 12 nm to more than 180 nm and the tube length can be varied from 200 nm to 360 μm. In addition, these materials are both chemically, physically and thermally stable and corrosion resistant [146-148]. Moreover, these nanotubes exceed the properties of carbon nanotubes in other characteristics, including photoelectric and photocatalytic properties [145] and can be manufactured at a cost less expensive than that of carbon nanotubes [149, 150]. They can be fabricated using simple manufacturing processes such as hydrothermal, electrochemical and surfactant template techniques, unlike carbon nanotubes [147, 149, 150]. It has been proven that the titania nanotubes are nontoxic, biocompatible, and good candidates for various biomedical applications including drug delivery systems [146, 150]. The wetting behaviour of these materials depends on the diameter and can be controlled from super hydrophilic to hydrophobic and super hydrophobic by varying their

diameters. However, TiO_2 have a high band gap and can be considered semiconductor materials [151, 152].

Noh et al. [153] designed a drug delivery system using aluminium oxide nanotubes. A model drug, amoxicillin, was loaded onto the internal nanotube structure and subsequently permitted to diffuse in a phosphate buffer saline solution (PBS) at a defined rate. The system showed a high release rate in the first 6 hours, and the highest released drug amount was 13 μg in the first hour. A relatively steady release profile was achieved after 7 days. The system demonstrated sustained drug release over 35 days, and the amount of drug released was proportional to the square root of time. However, anodic aluminium oxide is an electrical insulator, therefore it is considered as a passive system. Therefore the drug release is only controlled by diffusion.

Other nanomaterials such as palygorskite clay which consist of fibrillar single crystals of 20-30 nm diameters can also be used to construct a nanostructure conducting polymer. For example, Kong et al [154], used palygorskite clay to construct a nanocomposite film to absorb and release aspirin. The film was deposited at 0.80 V *vs.* SCE for 500 s, onto an indium doped tin oxide glass (ITO) working electrode from an electrolyte consisting of 0.56 g palygorskite clay, 75 mg of aspirin and 0.34 ml Py in 25 ml PBS at pH 3.5. The natural nanostructure palygroskite helps to increase the specific surface area of the PPy film and enhance the drug incorporation and release due to the high specific surface area, high adsorption and good stability. Although the authors reported that the incorporation of the non-conductive clay had reduced the electrochemical activity of the film, the

electrochemical effective surface area increased significantly from 0.72 cm^2 to 4.04 cm^2 for conventional and nanostructured films, respectively. The amount of aspirin released increased due to the large surface area but also due to other processes including doping, adsorption and ion dipole interactions between the carbonyl groups of aspirin anions and hydrated palygorskite cations (Mg^{2+}, Al^{3+} and Fe^{3+}). The result indicates that the aspirin released from the nanostructured polymer after 160 minutes increased from 720 µg to 1527.5 µg from unstimulated and electrically stimulated films at -0.6 V *vs.* SCE, respectively. This is higher than the amount released from the conventional PPy film which was 320 µg and 870 µg when the same procedure was used.

Playgroskite with conducting polymers could enhance the incorporation and release of other drugs and eliminate the problem associated with some hard templates such as anodised aluminium oxide (AAO) and colloid frameworks where the templates need to be removed which increases the synthesis time or cause degradation of the drug.

1.6.4.5 The use of catalytic nanomotors for self-powered drug delivery systems

The next generation of intelligent drug delivery system is based on autonomous self-propelled nano- and micro-scale robotics that are able to *catalytically convert* chemical energy from their environment to mechanical energy [115, 155-157]. These miniaturised systems can be allocated, subject to their motion and actuation into two main categories: micro/nano motors and micro/nano pumps [155, 156, 158].

The first catalytic nanomotors were invented by Paxton et al. in 2004 [159]. The device made up of two metal segments: Au and Pt. The bimetallic segments are each 1 µm long

and 370 nm in diameter. The device used hydrogen peroxide fuel and rely on a self-electrophoresis mechanism. The fuel is oxidised to oxygen at the surface of the Pt portion, thus causing the released electrons to be transferred through the metallic nanorods to the Au part, where the hydrogen peroxide is reduced to water. This makes nanorods in the two segments behave as a short-circuited electrochemical cell that provides a path for electrical current to flow. The electron transfer is compensated by the formation and consumption of protons on the surface of Pt and Au segments, respectively. The movements of positively charged ions creates an electroosmotic flow on the nanorods/ liquid interface and drags the electrolyte solution by viscosity forces, resulting in the movement of nanorods in the opposite direction by speeds that are up to 40 $\mu m\ s^{-1}$ [156, 158]. In addition, other proposed catalytic nanomotors have used different propulsion methods, such as self-diffusiophoresis (spontaneous motion of dispersed particles in a fluid induced by a concentration gradient) [160] and bubble ejection [161]. Moreover, these miniature devices can be propelled and controlled by external stimulation, such as magnetic fields [162, 163], external electric fields [164], visible light [165], ultraviolet light (UV) [166] and ultrasonic energy [167, 168]. Catalytic nanomotors are capable of perform sophisticated actions and tasks; the tiny machines are able to communicate with each other and navigate autonomously in a complex microfluidic channel, finding the channel entrance and climb vertically following the fuel concentration gradient, changing their velocity depending on the pH of the medium [155, 156, 169-173].

Sundararajan et al. [174] electrodeposited conducting polymer PPy segments on the side of the Au segments of Pt-Au catalytic motors. The nanomotors selectively pick up a positively charged polystyrene-amidine microsphere on the side of the negatively charged

PPy segment at one end of the rods since the PPy segment has a more negative zeta potential than the metal segments. The presented nanomotors can transport the attached microsphere model cargo and the motor translational motions decrease with the increase of microsphere radius. The nanorods start to move in a translational motion when the nanosphere radius increases to 1.65 µm. Ni segments were incorporated into the motor to add more control on the motion by using an external magnetic field. The segments sequence of the modified motors is Pt-Ni-Au-Ni-Au-PPy. Using a few-hundred-gauss electromagnetic field made it possible to control the direction of the movement and reduced the rotational diffusion of the rod, though the applied magnetic field decreases the motor linear movement.

It was proved that the incorporated molecules can be released by using chemical stimuli [175] and the pH change of surrounding media [158, 175] or by using an external stimulation factor, such as UV light [176] and magnetic fields [177]. Theoretically, it could be possible to electrodeposit a PPy-containing drug on the nanomotor side that is then coated with Mg. The nanomotors transport the PPy cargo, which is the desired target, and the galvanic coupling between the Mg and the conducting polymer films release the drug as shown in Figure 1.9.

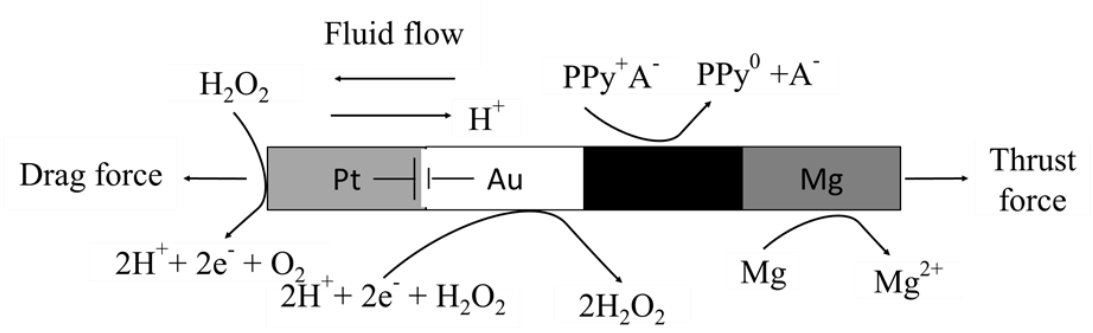

Figure 1-9: Catalytic nanomotors for a self-powered drug delivery system. After M. Pumera [70] and S. Sundararajan et al. [88]

The concept of transportation and the release of an incorporated drug by using nanomachines has been demonstrated by a number of studies. However, several problems and challenges remain and need to be resolved in order to use these machines in biomedical applications [156]. For instance, the biocompatibility of these systems and their influence *in vivo* application must be investigated [156]. Other areas of research ought to include the effect of the physiological environment on the nanomachine's operation and performance and the interaction between the nanomotors and the surrounding medium such as electrostatic interaction with surrounding walls [156]. The precise speed control of the nanomotors and the provision of steady movement in the real 3D environment should be considered before these tiny machines can be used *in vivo* [178, 179]. The circulation path management of the nanomotors in the living body and their safe disposal is not clear and further studies are needed. In addition, these machines commonly use toxic fuels such as hydrogen peroxide or hydrazine which may obstruct their use in biomedical application [156]. The use of a physiologically available biological fuel such as glucose [180] or other biocompatible fuel may be an alternative solution for this problem. Mano et al. [180] demonstrated a self-propelled bioelectrochemical motor

powered by the glucose-oxygen reaction. The proposed motor is made of carbon fibres and divided into three segments. A hydrophobic segment at the middle ranging between 6-10 mm and a hydrophilic, 1 mm anode and cathode at the end sides of the motor. The anode and the cathode are modified with bioelectrocatalyst redox polymer wired glucose oxide and redox polymer wired bilirubin oxidase respectively, for the oxidation of fuel glucose and oxygen reduction. The catalytic oxidation of glucose at the anode induces electrons to move from the anode to the cathode side where oxygen is reduced. The electrons stream is compensated with proton stream through the solution from the anode to the cathode causing the motor movement. The hydrophobic segment caused the motor to float at the gas/air interface which reduces the drag force and allow the motor movement. However, the drag force increases when the segment becomes hydrophilic preventing the motor movements. Moreover, Zhang et al. [157] designed a self-propelled motor driven by a rapid polymerisation reaction of an FDA approved polymer, poly(z-ethyl cyanoacrylate) (PECA). The motor consists of hydroxide anion exchange resin beads (Amberlite IRA-400) soaked in PECA/ acetone solution. One side of the beads was coated with PMMA to direct the propulsion and allow the motor to float in the electrolyte. When the motors floated in an ionic electrolyte, the hydroxide ions released from the beads surface trigger the PECA depolymerisation, causing the motor to move by 160 mm s^{-1} in 1 M NaCl solution. However, the motor speed significantly decreased to 10 mm s^{-1} when the experiment performed in relatively higher pH 7.4, in phosphate buffer saline. This may reduce the efficiency of the motor *in vivo*. The drug can be incorporated in the motor fuel (PECA polymer) and released with the non-toxic products of the PECA depolymerisation. In addition, other researchers have proposed a fuel-free motor. However, such a motor is nonautonomous and requires an external power force to drive it, such as an external magnetic field, which may complicate its use *in vivo*, to drive it. In

addition, these machines are usually designed from a nondegradable material having the potential to generate toxic species such as nickel, chromium and silver ions [162, 181, 182].

Biocompatible and biodegradable materials instead of the non-degradable metals such as Pt are commonly used to fabricate these motors have been investigated. The chemical and electrochemical reaction between the nanomachine segments such as the likelihood of galvanic corrosion of the segments should be understood before the use of these machines in real applications. Other aspects needed to evaluate the performance of the nanomachines include size and the shape design, effect of biological substances such as ascorbic acid and other ions on the motor operations. In addition, the effect of the physical parameters of the physiological environment such as temperature, pH, pressure, flow rate of the body fluid and tissue type on the motor movement [156].

1.6.4.6 The use of implantable biofuel cells for a self-powered drug delivery system

Biofuel cells, also known as biological fuel cells, are a kind of fuel cells that can directly convert chemical energy to electricity by using biocatalyst redox reactions. The cell structure includes two electrodes, and at least one of them is coated with biological electrocatalyst materials, such as proteins, enzymes, or whole living cell organisms to catalyse the oxidation of the biofuels onto the anode electrode and/or catalyse the reduction at the cathode [183-185]. The field of biofuel cells has been intensively reviewed by Bullen et al. [186], Osman et al. [184, 187] and recently by Cracknell et al. [188] and Neto et al. [185].

As in a conventional fuel cell, the oxidation of the biofuel cell results in the release of electrons which are forced from the anode to the cathode through an external electrical circuit coupling both electrodes. The electron flow is propeled by an electromotive force emanating due to the potential differences between the two electrodes. The electrical circuit is completed by the electrolytes' and ions' movement to maintain the charge's balance inside the system [184, 185]. Unlike conventional fuel cells, such as polymer electrolyte membrane fuel cells (PEM) that ordinarily function at relatively high temperature around 80–100 ^{o}C using an acidic or alkaline electrolyte, the biofuel cell is usually operated at a pressure and temperature close to the ambient in electrolytes with a relatively narrow pH range close to the neutral pH. The operation temperature is between 20–50 ^{o}C and a pH between 4 and 8 [188].

The majority of the enzymatic biofuel cells employ a reversible redox active electron transfer mediator to shuttle the electrons between the enzyme reactive site and the electrode. This type of fuel cell is identified as an indirect biofuel cell or mediated electron transfer (MET) [185, 187].

There is another type of biofuel cell used as an enzyme to electronically couple well to the electrode in a manner that facilitates a pathway for the fast and efficient direct electron transfer between the enzyme reaction site and the electrode surface. This type is a direct electron transfer biofuel cell (DET) [188]. The biofuel cell can harvest its fuel from its physiological surrounding electrolytes, such as cerebrospinal fluid, serum and blood [189, 190].

Unlike the PEM fuel cell, the selectivity of the enzyme enables the cell to work in an electrolyte containing a mixture of the fuel and the oxidant without the need to separate the cell electrode into different compartments and using a selective membrane. This simplifies the biofuel cell design and enables the miniaturised of the biofuel cell for bioimplantable applications [188]. A membrane may be necessary, in some cases, to prevent the diffusion of the immobilised mediator from moving from the electrode to the electrolyte.

This energy conversion technology is a promising sustainable implantable electrical energy source to power several biomedical devices, such as pacemakers, neuromorphic circuits, artificial organs, implantable sensor and monitoring devices and drug delivery systems [186, 191-193]. Zhou et al. [193] proved the concept of the use of biofuel cells to power drug delivery systems. They demonstrated a biocomputing, logic-based, autonomous detection and self-powered controlled-release drug delivery system based on an enzymatic biofuel cell. The system, "sense-act-treat', is made of a glassy carbon electrode modified with a carbon nanotube and Meldola's blue. The cathode is Au coated with poly(3,4-ethylenedioxythiophene)–(PEDOT) containing the acetaminophen drug (APAP). The cell operated in a 0.1 mol dm^{-3} PBS electrolyte (pH 7.4) containing nicotinamide adenine dinucleotide (NAD^{+}) as the cofactor. The biomarkers for abdominal trauma lactic acid (LAC) and lactate dehydrogenase (LDH) are selected as signal inputs. The results show that there is no drug release detected in the absence of one input signals ((LAC, LDH) = (0,0), (0,1) and (1,0)). In the presence of both biomarker signals ((LAC, LDH) = (1,1), the NADH was oxidised at the anode, which with the reduction of PEDOT

at the cathode caused the drug's release. The designed biofuel cell can produce a maximum power output density of 33.8 $\mu W\ cm^{-2}$ at 0.40 V.

Other alternatives to increase the amount of drug contained in the polymer structure have been suggested. These strategies consist in increasing the surface area by incorporating nanoporous structures within the polymer or by nanostructuring the polymer itself. The next section explains the most common techniques used to obtain nanoporous surface structures and their advantages for drug release.

1.7 Biomedical Applications of Conducting Polymers

1.7.1 Biomedical sensors

Conducting polymers have been widely used as the active layers for different types of sensors and biosensors since a few years after the discovery of the conducting polymers approximately four decades ago. This is due to the attractive properties of these materials such as their ease of processing and synthesis, chemical stability in harsh environment, high sensitivity and selectivity towards various molecules [194]. Pirsa et al. [194] used PPy as chemiresistor sensor for various organic compound vapours including, acetone, methanol, benzene, chloroform, benzaldehyde, benzyl alcohol, acetonitrile, pyridine, dimethylformamide and dimethyl sulfoxide gas (DMSO). The results show good abilities and reproducibility for the proposed sensors to detect organic gasses. For example, the polypyrrole sensor shows a fast response time <1 s and a lower detection limit 30 ng for DMSO vapour [194]. The mechanical robustness and the ability to tailor and extend the properties of surface films make it possible to use conducting polymers as mechanical sensors such as strain sensor [195, 196] and resistive pressure sensors based on hollow-

sphere microstructure polypyrrole hydrogel [197]. In addition, other types of sensors have been proposed for example, humidity sensors based on PANI [198, 199], and pH sensor [200]. Furthermore, most of intrinsic conducting polymers feature by their biocompatibility and non-toxoid that they are a suitable sensor materials for biomedical and food applications. For example, conducting polymers have been used as a food analysis sensor such as conducting polymer sensor for olive oil characterisation [201]. Moreover, conducting polymers have been used widely in biomedical applications such as body movement like polypyrrole/ nylon-lycra fabric sensor to monitor breast motion [202]. Conducting polymers label-free sensors are also used in gene analysis for routine and clinical applications to detect specific DNA fragments [203-205]. Also, conducting polymer sensors have been used to selectively detect protein such as immunoglobulin G antigen [206] and ciprofloxacin antibiotic [207], viruses and bacteria such as gram-negative and gram-positive bacteria [208]. Considering the importance of the use of biomedical sensors in our lives and the need for continuous research and development as well as the economic opportunities that are offered by the field of biomedical sensors. For example, the appraised global market of biomedical sensor is foreseeable to attain US$ 12 billion by 2016 and predicted to grow annually by 11% to achieve US$ 16.8 billion by 2018 [209, 210]. Several reviews and studies on the use of conducting polymer sensors on health care, food industries and environments can be found in the literature [25, 56, 204, 205, 211-213]. The most well-known and widely used biosensor, glucose biosensors will be briefly reviewed and used as an example of a biosensor and the use of conducting polymers in such applications [214].

1.7.1.1 Glucose Sensors

The World Health Organisation (WHO) announced that approximately more than 346 million people in the world have diabetes. The number of patients is increasing and is expected to reach twice that number. The death toll from complications related to diabetes has reached 3.4 million in 2004, and predicts this number will double by 2030 [215, 216].

Diabetes is a chronic disease that can lead to diseases such as blood vessels damage, failure of various organs, and tissue problems, including renal, retinal and neural complications. Diabetes and other related illnesses are a great drain on the national incomes of countries worldwide. For example, the American Diabetes Association reported that the total cost of diagnosed diabetes has increased from $174 billion to $245 billion between 2007 and 2012, in the USA [217, 218].

This well-known disease is the result of an increased blood glucose concentration caused by a lack of insulin produced by the pancreas or by the body's inability to use the produced insulin effectively [219]. The glucose concentration in normal human blood ranges from 4 to 8 mmol dm^{-3} approximately and fluctuates before and after meals. This range expands from 2 to 30 mmol dm^{-3} for people with diabetes [220, 221]. Therefore, to diagnose and manage this very large fluctuation, blood tests are commonly used to measure and monitor blood glucose concentration. The glucose blood test is an invasive method and may be painful for patients. In addition, a urea sensor is commonly used in routine health examinations as an indirect and non-invasive method for testing glucose. Moreover, the use of other invasive sensors based on body fluids, such as tears, seurm and saliva have been proposed. Unfortunately, these fluids contain low glucose concentrations. For

example, the glucose concentration in saliva ranges between 8–210 μmol dm^{-3} and that in tears ranges between 128–166 μmol dm^{-3}. Therefore, glucose sensors based on these fluids should be sensitive for a micromoles concentration [222-224]. However, sensors based on these fluids are not in clinical use yet and there are some problems related to the correlation between blood glucose concentration and the glucose concentration in saliva since it is complicated due to the presence of bacteria, epithelial cells and leukocytes [222, 225, 226]. In addition, other non-invasive methods based on transdermal and optical still have shortcomings that prevent them from becoming reliable glucose measuring methods. For example, the glucose sensor based on the transdermal method (Gluco Watch Biographer) was withdrawn from the market in 2008. This device needs a long time to warm up, may cause skin irritation and is not accurate; moreover, it cannot be used to detect and prevent hypoglycemia. Electrochemical methods to measure glucose are the most common [191, 227].

These electrochemical methods include amperometry [228], potentiometry [229], chronoamperometry [230], chronopotentiometry, impedimetric and conductometric sensors [231]. Among these sensors, amperometric sensors function effectively and extensively and are used *in vivo* and *in vitro* for glucose detection.

In glucose enzymatic biosensors, the enzyme usually glucose oxidase (GOD) is immobilised on the electrode surface. The active part of the enzyme, the flavin-adenin-dinucleotide (FAD) radical, selectively oxidises the glucose into gluconolactone, and the enzyme is reduced to GO-FADH2 (as shown in equation 1.9) [231-233]:

$$C_6H_{12}O_6(\text{glucose}) + GO(FAD) \rightarrow C_6H_{10}O_6(\text{gluconolactone}) + GO(FADH2). \quad (1.9)$$

There are three generations of glucose biosensors that depend on the oxidation reaction of biosensors [231, 232, 234] as described in the following bellow:

1. Oxygen electrode-based sensors

Following reaction (1.9), the reduced GOD can be oxidised by oxygen to produce hydrogen peroxide in accordance with the following reaction:

$$GO(FADH2) + O_2 \rightarrow GO(FAD) + H_2O_2. \quad (1.10)$$

The glucose concentration then can be determined amperometrically, from the increase of hydrogen peroxide concentration or the decrease of oxygen concentration, due to the existence of a linear proportional relationship between them and the glucose concentration [227, 231, 232]. In addition, the glucose concentration can be measured using potentiometric glucose biosensors by measuring the change of the pH level, which results from the oxidation of glucose to gluconic acid, as indicated by the following reaction [234]:

$$C_6H_{12}O_6 \text{ (glucose)} + O_2 \xrightarrow{GOD} C_6H_{12}O_7(\text{gluconic acid}) + H_2O_2 \quad (1.11)$$

2 Mediator -based sensors

The first generation biosensors operated at a relatively high potential of ≈ 0.6 V *vs.* SCE. This potential has led to the activation of unwanted interfering reactions for some substances commonly presented in the blood, such as ascorbic acid, uric acid and

electroactive drugs. In addition, the first generation amperometric biosensors employed oxygen to transfer the electrons from the GOD to the electrode, making it an oxygen-dependent process. Thus, these sensors suffer from oxygen deficit, which may be caused by a drop in the partial pressure of oxygen due to the restricted oxygen dissolution in biological fluids [227, 232, 234].

Various non-physiological mediators have been used to overcome these problems and improve the sensors' performance. These mediators eliminate the effect of oxygen fluctuations. Instead of oxygen, the mediator function is to transfer the electrons from the enzyme GOD to the electrode. Glucose is oxidised by GOD (FAD), which is reduced to GOD (FADH2). The latter is reoxidised by the mediator into GOD (FAD). The mediator reoxidises at the electrode surface, and the resultant current flows through the electrode, which is proportional to the glucose concentration. The oxidised mediators are reduced by the oxidisation of the reduced glucose and recycled to its oxidised state at the electrode surface, as shown in the reactions below [231, 232, 234]:

$$C_6H_{12}O_6(\text{glucose}) + GO(FAD) \rightarrow C_6H_{10}O_6(\text{gluconolactone}) + GO(FADH2) + 2H^+ \quad (1.12)$$

$$GO(FADH2) + M_{ox.} \rightarrow GO(FAD) + M_{red.} \quad (1.13)$$

$$M_{red.} - e^- \rightarrow M_{ox.} \quad (1.14)$$

The use of these mediators which do not react with oxygen in glucose biosensors lead to the elimination of oxygen interference. In addition, they increase the transfer rate of

electrons between the enzyme and the electrode surface. Further, they also reduce the operational potential, which leads to a reduction in unwanted interfering reactions, thereby improving the sensors' performance [227, 231].

3. Directly coupled enzyme electrodes

The development of non-porous and nanostructured material provides the structure of electrode materials with a high specific area, good stability and biocompatibility. Moreover, this structure permits access to the redox active centre of the enzyme, which is not possible at a traditional planar electrode. Thus, permitting the GOD to couple directly with the electrode provides direct transfer of the electron between the GOD and the electrode, as shown in Equation 1.15. The glucose concentration can be measured from the resulting amperometric signal [231, 232].

$$C_6H_{12}O_6(\text{glucose}) + \text{GO(FAD)} \rightarrow C_6H_{10}O_6(\text{gluconolactone}) + \text{GO(FADH2)} \quad (1.15)$$

$$\text{GO(FADH2)} \rightarrow \text{GO(FAD)}. \quad (1.16)$$

Tamiya et al. [235] designed a three-micro planar GOD/PPy electrode without the 1,1'-Dimethylferrocene mediator (DMFe) for glucose sensing. The GOD/PPy sensors without DMFe mediator are insufficient to monitor glucose in human blood directly based on the detection of H_2O_2. The current response of the sensor saturated at 15 x 10^{-3} mol dm^{-3} glucose concentration. The high potential of the sensor operation at 0.7 V *vs.* SCE and the reaction with hydrogen peroxide caused damage to the PPy films. However, the uses

of DMFe mediator in DMFe/GOD/PPy sensors reduce the sensor operation potential to 0.1 V *vs.* SCE. Moreover, this sensor shows a large detection range at more than 30 x 10^{-3} mol dm^{-3} of glucose with high response time of 30 s. Tamiya et al. [235] also studied the effect of the polymerisation electrolyte on the sensor response and reported that the surface of PPy films which was the synthesis with acetonitrile-solution was flat and smooth and this reduced the adsorption of GOD. Thus, this sensor did not respond to the addition of glucose. On the other hand, the PPy sensor which was prepared with aqueous solution using pTS-Na, TFAC-Na and KCl showed a high response to glucose. The latter showed the roughest surface structure and the highest response. Therefore, these PPy electrodes seemed to exhibit a much better adsorption of GOD because of their large surface area [235].

Tech and Lin [236] designed PPy multiwall carbon nanotube (PPy-MWNT) nanocomposite glucose sensors. First, they sputter-deposited and patterned Ti/Pt line electrode on silicon nitride covered with a P-type Si substrate. Then, they deposited and patterned a low temperature oxide (LTO) mask at 200 nm and plasma etch to open a window for PPy deposition. Thereafter, they used a stable colloid electrolyte of 0.1 mol dm^{-3} of each Py monomer and the dopant anion sodium-dodecylbenzenesulfonate and 0.1% (wt) of well-dispersed MWNT to conduct the deposition of PPy-MWNT potentiostatically using 0.6 V *vs.* (Ag/AgCl). Then, the 1.94 U/ml glucose oxidase was physically adsorbed onto the PPy-MWNT film. They found that the MWNT increased the roughness of the film's surface. They tested the sensor with bita-D glucose in a concentration ranging from 0 to 20 mmol dm^{-3} and found that the PPy-MWNT functioned from 0 to 20 mmol dm^{-3} of glucose, while the PPy sensors prepared without MWNT had

a lower detection range and functioned up to 10 mmol dm^{-3} of glucose. They reported that the MWNT prevented the PPy backbone from overoxidation caused by hydrogen peroxide since MWNT has a high specific capacitance that stores excess redox changes. In contrast, the PPy sensors without MWNT were overoxidised by hydrogen peroxide and, thus, had decreased conductivity [236].

Ozyilmaz et al, [237] prepared amperometric glucose biosensors based on GOD/PPy electrode using cyclic linear voltammetry technique. An electrolyte solution of 0.2 mol dm^{-3} *p*-toluenesulfonic acid (pTS) or sodium *p*-toluenesulfonate (NapTS) containing 0.1 mol dm^{-3} Py and 2.5 mg/ml GOD was used to carry out the polymerisation in three electrode single compartment cell. The 0.18 cm^2 Pt sheet working electrode was cycled on the potential range of 0.1 to 1 V and 0.1 to 0.75 V *vs.* Ag/AgCl (3 M KCl) for NapTs and pTS solution, respectively. The scan rate was 50 mV s^{-1} for a period of 50 cycles. They reported the optimum pH for the highest response at pH 4.5 and 7 for PTs and NapTs supporting electrolyte, respectively. The two sensors showed a linear response for glucose concentration up to 1 mmol dm^{-3}, though Pt/PPy-GOD_{NapTs} has a more sensitive and better biosensor response than Pt/PPy-GOD_{PTS}. In addition, they reported that the acidic solution pTS improves the conductivity of PPy compared to the use of neutral NapTS as an electrolyte solution for electropolymerization of PPy, although partial denaturation of GOD enzyme in PTS was observed [237].

However, they concluded that the NapTS sensor showed better response, as well as better operational and storage stability as compared to pTS. Moreover, they tested both sensors in five commercial drinks a malt drink, a fizzy drink, fresh grape juice, honey and wine.

They found that the measurement results using the Pt/PPy-GOD_{NapTS} sensor are close to the results obtained by using a glucose assay kit [237].

The development of nano-porous and nanostructured material provides the structure of electrode materials with a high specific area, much higher conductivity, good stability, enhanced sensors sensitivity, decreased response time and extend the detection range. Moreover, this structure permits access to the redox active centre of the enzyme, which is not possible at a traditional planar electrode. Thus, permitting the GOD to couple directly with the electrode provides direct transfer of the electron between the GOD and the electrode. Tech and Lin [236] designed PPy-MWNT nanocomposite glucose sensors. The MWNT increased the roughness of the film's surface. The PPy-MWNT functioned from 0 to 20 mmol dm^{-3} of glucose, while the PPy sensors prepared without MWNT had a lower detection range and functioned up to 10 mmol dm^{-3} of glucose. They reported that the MWNT prevented the PPy backbone from overoxidation caused by hydrogen peroxide since MWNT has a high specific capacitance that stores excess redox changes. In contrast, the PPy sensors without MWNT were overoxidised by hydrogen peroxide and, thus, had decreased conductivity [236]. In addition, Palod et al. [238] synthesised PPy nanootubes glucose sensor using alumina membranes template assisted electrochemical polymerisation. Despite the low detection limit and the wide range of linear operation (0.25- 20 mmol dm^{-3}), this sensor are unable to detect glucose in human saliva. The sensitivity of the conducting polymer sensors can be improved further by using an organic microelectrochemical transistors (OECT). The OECT sensors can be fabricated using a relatively simple and inexpensive method such as inkjet printing techniques [239]. Shim et al. [240] developed PEDOT/PSS/GOD glucose sensor based

on OECT using a one-layer patterning process. The demonstrated sensor is able to detect the glucose concentration down to the micromolar range (1-200 μmol dm^{-3}) when a ferrocene mediator was used to shuttle electrons between the GOD enzyme and PEDOT/PSS gate's electrode. This makes it suitable for measuring glucose in human saliva. Kanakamedala et al. [241] demonstrated a PEDOT/PSS/GOD glucose sensor based on OECT using a simple and an inexpensive xurography and spin-coating technique. The sensor functions from 1 to 10 μmol dm^{-3} without using any external mediators, adequate to use it as a non-invasive glucose sensor.

Although the common commercially available glucose sensors are an enzymatic biosensor, there are still short comings due to the nature of the enzyme. For example, the enzyme essential instability, complex immobilization process, and the operating sensitivity to the ambient factors are disadvantages. In the other hands, the poor selectivity of the non-enzymatic sensors limit their use due to the present of the interference substances in the human body fluid [242]. However the use of the over oxidised polypyrrole film (OPPy) as a selective membrane increase sensor selectivity and eliminate the effect of the interference substances. For example, Shi et al. [242] designed a non-enzymatic glucose sensor based on OPPy modified palladium/silicon micro channel plate electrode OPPy/Pd/Si MCP. The pores size of the micro channel was 5 × 5 μm with a 200 μm depth and the thickness of the channel's side wall was ≈ 1 μm. The outer and inner surfaces of the MCP were coated with a Ni-Pd thin film by electroless deposition technique. The MCP was cycled on the potential range of - 0.1– 0.7 V *vs.* SCE with a scanning rate of 100 mV s^{-1} over five cycles in an electrolytic solution of 0.05 mol dm^{-3} Py, 0.02 M $K_3Fe(CN)_6$ and 0.02 mol dm^{-3} H_2SO_4. The deposited film was then cycled in a 0.1 mol dm^{-3} Na_2HPO_4 electrolyte solution at a potential scanned ranging from

-0.3 to 0.95 V with a scan rate of 30 mV s^{-1} for a period of seven cycles to overoxidise the PPy films. They reported that the proposed sensor has higher sensitivity and wider linear range compared with other non-enzymatic glucose sensors. The estimated detection limit was 2.06 μmol dm^{-3} and was linear with the glucose concentration up to 24 μmol dm^{-3}. The sensor response time was 5 s and the sensor reading was in agreement with the commercial monitor reading in actual biological samples. In addition, the proposed sensor succeeded to eliminate the uric acid and ascorbic acid (UA, AA) interferents. The OPPy films improved sensor selectivity and succeeded to eliminate the interference of common species such as UA and AA. After storage for one month at room temperature, the sensors retained 92% of their original response to glucose [242].

1.7.2 Conducting polymers for application in the nervous system

The diseases, disorders, and disruptions of the nervous system such as Alzheimer's disease, Parkinson's disease, epilepsy, head trauma, cancer, and stroke might lead to impairment in the daily lives of patients and may include loss of voluntary muscle movements, memory or speech, and might even lead to death. The disease, wounds and injuries in the spinal cord and peripheral nervous system caused by diseases, accidents, falls or sports injuries could lead to loss of normal function, permanent disability or paralysis [243, 244]. Such an injury might also occur at birth when the child is surgically extracted in an obstructed labour process, which might lead to disruption in the peripheral nerves [245].

These illnesses, diseases and injuries affect a large number of people and the cost of care and treatment is rather high [244]. In addition, disorders, injuries and diseases of the central nervous system and peripheral nervous system constitute challenges for researchers because of the physiological nature of these systems. Among these challenges is the presence of blood-brain barrier, which could prevent access of some therapeutic molecules to the central nervous system [243, 244]. Further, it is possible that fully differentiated neurons do not divide [245]. An additional challenge is the use of drugs that have serious side effects.

The chronic response characterised by the presence of both activated microglial cells and interactive astrocytes cells eventually surround the electrode to a certain extent, thereby increasing the electrode resistance in addition to the high initial resistance of the microelectrode. These interactive responses have been associated with a gradual increase in the resistance of the electrode/tissue interface [89, 110].

The development of neural prosthetic implants has led to the treatment of many patients; for example, the use of cochlear implants to stimulate nerve cells in the inner ear for those with loss of hearing. In addition, the use of deep brain stimulators helps patients with Parkinson's disease, and the use of a spinal cord stimulator is used to treat patients suffering from incontinence and chronic pain. Additional systems in the development process include retinal prostheses for blind people [246]. However, the incidence of immune inflammation that occurs in the vicinity of the neural prosthetic implant and the record and activation electrodes may lead to unexpected failure, with glial scar tissue

forming between the electrode and the nerve, thereby reducing or preventing the transfer of a signal between the electrode and the nerve [247].

There are certain important requirements for materials to be used in neural implants. These generally include being biocompatible and biostable because they are used in a harsh environment for periods that range from days to decades. The materials must achieve a very low resistance to the electrode/tissue interface to improve the signal quality and reduce noise. The basic functional requirements for these interfaces include the recording or/and stimulation, requiring that the electrode have a high selectivity 'possibly up to a one nerve cell', thereby requiring minimal electrode size. This leads to increased interface impedance, thereby causing reduced sensitivity and quality of the signal transfer [246-248]. Traditional noble metal electrodes such as iridium, tungsten, platinum, and gold have limited options to significantly improve their impedance [247].

The transportation of signals between the ionically conductive living tissue and the electronically conductive metal electrode at the electrode/tissue interface is mainly through capacitive or faradic current due to redox reactions at the surface of the electrode [247]. Conductive polymers have the advantage of being electrically and ionically conductive as well as being biocompatible and, as such, can be used to control cell behaviour for different types of cells, including osteoblasts, muscle cells, bone marrow cells, neurons cells, endothelial cells and fibroblast cells using an external stimulator [247, 248].

The coating of the metal electrodes used in neural prosthetic devices has led to a reduction in the electrode's impedance, increased the capacity of charge and decreased the mismatch of mechanical properties at the electrode/tissue interface, thereby enabling increased implant life [248].

Conducting polymers show that they are suitable scaffolds to promote nerve regeneration and provide guidance for the neurite outgrowth (regenerating axons). Quigley et al. [249] created hybrid tubes from the conducting polymer PPy doped with para-toluenesulfonate (pTS) and biodegradable fibres of poly(D-lactide-co-glycolide) copolymer (PLA:PLGA (75:25)). The biodegradable fibres of PLA:PLGA with a diameter of 30 μm were synthesised by wet-span onto gold coated Mylar coiled on reel collector spools with the gaps between the fibres ranging between 20–200 μm. These resulting scaffolds were laid flat and then the PPy doped with pTS galvanostatically deposited between biodegradable fibres. The composite films are then removed from the gold-Mylar layer and shaped into 3D structures. Two chambers made of polystyrene are fastened to the scaffold surface and coated with polyornithine and laminin to facilitate cell culture. Dorsal roots ganglia (DRG) isolated from rat pups were permitted to adhere to the chamber surface for 4.5 days. Electrical stimulation was applied through PPy/TPS strips. The DRG growing on scaffolds coated with the cell-adhesion molecule (CAM) showed strong growth compared with the one growing on the non-coated scaffold, which showed limited adhesion, limited axonal elongation and limited Schwann cell migration. The DRG growing on the hybrid scaffolds, with or without electrical stimulation, showed that the growth of the axons and the migration of the Schwann cells followed the path of the biodegradable fibres. On the contrary, the DRG growing on the PPy/pTS plain films with and without electrical stimulation showed growth of the axons and migration of Schwann cells in radial forms.

The rate of the axon growth with electrical stimulation exceeded the one without electrical stimulation where the maximum length of the axonal growth with electrical stimulation reached 9750 ± 1430 μm during 8.5 days compared with 6040 ± 510 μm without the electrical stimulation during the same period. In addition, the mean maximal migratory distance of Schwann cells was 3450 ± 220 μm during 8.5 days compared with 2780 ± 220 μm without electrical stimulation during the same period of time. In addition, the mean maximal migratory distance of Schwann cells with and without electrical stimulation were 3450 ± 220 μm and 2780 ± 220 μm with and without electrical stimulation, respectively, during the same period of 8.5 days.

Wan et al. [250] synthesised conduits to bridge nerve gaps in nerve repair applications from chitosan-g-polycaprolactone/PPy (CPC)/(PPy) composite and chitosan/PPy composite where the PPy nanoparticles caused the conduits to become conductive, and the polycaprolactone biodegradable polymer improved the mechanical properties of the chitosan. These conduits can be used to bridge a nerve gap with a length of almost 30 mm where the internal and external diameters of these conduits are approximately 2 mm and 2.7 mm, respectively, and the length is approximately 40 mm. The results of conductivity measurements showed that the CPC/PPy conduits incorporated with 5% PPy have a conductivity of approximately 2 x 10^{-2} S cm^{-1} and when the PPy content increased, there was no observed significant increase in the conduits' conductivity. This percentage of the PPy contents (5%) in the conduits was selected because it provides sufficient conductivity for the transfer of electrical stimulation with the least amount of PPy contents, where the PPy is a non-biodegradable material. The mechanical tests showed that the wet CPC/PPy conduits have a tensile strength and lateral compression resistance better than those of the

chitosan/PPy conduits, thereby making them suitable to resist the tissue pressure around the implant (graft) resulting from the movement and weight, and maintain its cavity until the nerve growth is completed. The low biodegradation of the CPC/PPy conduits compared with the chitosan/PPy conduits might be due to the hydrophilic properties of chitosan and the hydrophobic properties of the CPC and PCL.

The biodegradable test was done *in vitro* by immersion in a solution of PBS and *in vivo* by implant in rabbits for 10 weeks. The results of the tests showed that the biodegradation CPC/PPy conduits were lower than the biodegradation of the Chitosan/PPy conduits; moreover, the Chitosan/PPy conduits were biodegraded partially or completely after eight weeks and lost most of their conductivity. Some CPC/PPy conduits maintained suitable mechanical strength, thereby making them suitable conduits to bridge a nerve gap. The weight loss rate and the maintenance of the mechanical properties were dependent on the percentage of the incorporated polycaprolactone (PCL), where the higher the incorporated percentage of PCL, the lower the percentage of the weight loss, thereby sustaining more mechanical strength. In addition, the CPC/PPy showed sufficient electrical conductivity for electrical stimulation in biomedical applications. However, this conductivity is low and there are few conduits with conductivity higher than 10^{-3} S cm^{-1} after degradation *in vivo* for eight weeks.

1.8 Summary and Conclusions

1. Polymerisation potential and polymerisation at low temperature conditions, significantly affect the formation and film properties of conducting polymers. Therefore, these factors need to be optimised for the desired application. For example, low-temperature conditions with low current density result in the preparation of films with high apparent density, long conjugation chains with a less defective structure, high doping levels, high conductivity and high electrochemical stability; however, it may increase the synthesis cost. Polymerisation using a relatively higher oxidation potential and current brings about the formation of a porous and more open film structure, which facilitates ingress and release of drugs. In contrast, a tightly compact polymer structure can impede the motion of drug molecules inside and outside the conducting film. The augmentation of oxidation potential and current needs to be fully considered because the increase may activate an undesirable secondary reaction or over-oxidation of the polymer. The use of a lower polymerisation potential and current may produce low-quality polymer films.

2. The development of neural prosthetic implants has helped patients with neuro and brain defects such as Parkinson's disease. However, immune inflammation can occur in the vicinity of the neural prosthetic implant, which may lead to unexpected failure, and this may reduce or prevent the transfer of a signal between the electrode and the nerve. The coating of metal electrodes used in neural prosthetic devices with a conducting polymer has led to a reduction in electrode impedance,

increased the capacity of charge, and decreased the mismatch of mechanical properties at the electrode/tissue interface, enabling an increased implant life. Intrinsic conducting polymers have proven to be suitable scaffolds to promote tissue regeneration and provide guidance for injured nervous tissue.

3. Traditional methods of drug administration cannot provide an optimum level or ensure sustained drug release; repeated and high dosages having toxic and serious side effects can be involved, such as cancer drugs that expose the entire body to toxicity. Drug delivery systems based on conducting polymers can be used to deliver drugs locally with the effective concentration required for a long time, without the need for repeated doses at frequent intervals. These systems can lower drug toxicity and side effects, providing protection and preservation of the drugs until they reach their target, resulting in an improvement in drug absorption rates. For example, they are useful for delivering growth factors and drugs into the brain to treat neurodegenerative diseases such as Parkinsons and to overcome the blood-brain barrier that prevents some therapeutic molecules from entering the brain.

4. The development of nanoporous and nanostructured conducting polymers provides the structure of electrode materials with good electrical conductivity, low operation potential and a high surface area relative to size. The use of nanostructured polymers may help to overcome the shortcomings of traditional conducting polymer films, which includes low capacity for loading the drug, associated with limited surface area. They facilitate the diffusion of the dopants and enhance the possibility of accessibility in multilayer constructions. They also

permit the efficient transport of large molecules when compared with traditional flat surfaces. Unstructured PPy films showed cracks and delamination after several stimulation cycles. Conversely, there were no cracks or delamination on the nanostructured PPy film after 150 CV stimulation cycles to release the drug, thereby indicating improvements in the efficiency of the polymer electrodes in the long term.

5. The drug is released from the conducting polymer film by applying an electrical potential to reduce it. However, using an external power source restricts its use *in vivo,* although the incorporated drug can be released by reducing the conducting film using a reducing agent. However, the release rate of the pH-stimulation is faster and the release efficiency is lower than the efficiency of the electrochemical stimulation release, and even with the use of a strong redox agent, the release efficiency does not improve remarkably.

6. Galvanic coupling between a biocompatible reactive anode, such as Mg and the conducting polymer film cathode could be used as an autonomous, self-powered source and controller for a long term implant drug delivery system. The potential of the employed metal anode must be lower than the conducting polymer cathode to reduce the polymer film and release the drug molecules. These systems do not need power wiring, which may, therefore, simplify the manufacturing process, reduce production costs and facilitate their use in implant drug delivery systems.

7. The initial spontaneous drug release from the conducting polymers can be eliminated by using multilayers of conducting polymer films with a different redox potential. The conducting polymer layer in contact with the electrolyte, acts as a protective layer between the release medium and other polymer layers, thereby preventing spontaneous drug release from the system. In addition, the conducting polymer layers can be doped with other drugs which cause the system to accept a dual-drug delivery system.

8. Cyclic voltammetry is effective and able to cause a higher drug release rate compared with alternatives. The sweep rate affects the amount of drug released and the film properties. In addition, the film can be exposed to physical stress as a result of swelling and de-swelling during the stimulus cyclic potential, causing the film to delaminate from the electrode surface and cracks appearing. The scan rate should be optimised to obtain effective drug release without unduly affecting film properties.

9. Despite the attractive features of self-powered drug delivery systems, shortcomings remain. The initial release of molecules after the galvanic coupling is high, and their final concentration in solution is low. The presence of a physical barrier on the metal anode, either naturally from the metal oxide on the surface, or by coating the anode with an insulating biodegradable material, provides an advantage for controlling the release profile and metal dissolution.

10. The polymerisation of conducting polymers on a surface of reactive metals such as Mg is a difficult and challenging task due to the competition between fast dissolution of the metal surface and the electrodeposition of the polymer. Coating Mg with a less active metal and the use of sodium salicylate salt during the polymerisation process may passivate the metal surface and enhance the polymerisation process.

11. A wide range of conducting polymer drug delivery systems have been studied, but the amount of incorporated and released drug is not always mentioned, and a considerable number of these studies express the released drugs as a percentage of the incorporated drugs, which makes it difficult to compare the performance of these systems.

Chapter 2: Experimental Methodology

This chapter describes in detail the chemical reactants, material and experimental procedures used in this thesis. Since there is a competition between the polymer deposition and the anode substrate dissolution, two types of experiments have been conducted to deposite self-powered PPy films: chemically and electrochemically methods, with different substrates. In addition, there is a brief description of the experimental techniques used to characterise the polymer films including measuring the OCP and the amount of drug release using Ultraviolet-visible (UV-vis) spectroscopy. Also, since, the morphology and structure of the PPy films are sensitive to the polymerisation condition and may cause an effect on the amount of the incorporated and released drug, the film structure and morphology were analysed by SEM, DIS, and FTIR spectroscopy.

2.1 Materials and Chemicals

The following chemicals were used as received, without any additional purification: potassium sulphate (K_2SO_4; Fisher Scientific), potassium chloride (KCl; Fisher Scientific), acetonitrile (CH_3CN; Fisher Scientific) and tetraethylammonium tetrafluoroborate ($C_8H_{20}BF_4N$; Alfa Aesar), sodium chloride (NaCl; Panreac quimica S.A.U.), ammonium persulfate [$(NH)_4S_2O_8$; Carlo erba], sulphuric acid (H_2SO_4), oxalic acid ($C_2H_2O_4$), *p*-toluene sulfonic acid sodium salt (pTS), a model drug dye fluorescence rhodamine 6G (Rh-6G), methylene blue (MB), fluorescein sodium salt(FSS), dopamine hydrochloride (DA), ibuprofen sodium salt (IP); Sigma-Aldrich. The Py monomer (98%) was supplied by Sigma-Aldrich and was double-distilled under a vacuum and kept under

a nitrogen atmosphere in a darked flask at low temperature. A celluose acetate membrane (CC) with a pore diameter of 0.8 μm and durapol membranes (DM) with a pore diameter of 0.22 μm were used as substrates to hold the PPy. Sodium ibuprofen, (Fluka), sodium salicylate (Aldrich) and acetone (Fisher Scientific) were analytical grade and used as received. Sodium ibuprofen and salicylate solutions for calibration curves were prepared with 18 mΩ cm (O Purite) deionized water. A 250 μm thick AZ31 Mg alloy foil (Goodfellow) was used in all experiments. Figure 2.1 shows the chemical structures of the used drug in release experiments.

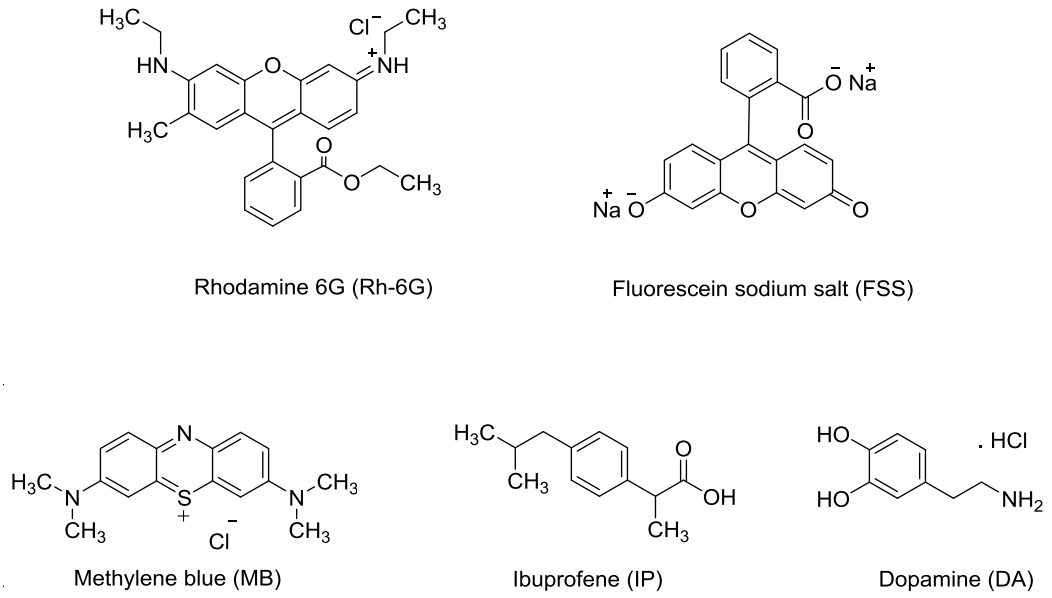

Figure 2-1: Scheme showing the chemical structures of the used drug in release experiments.

2.2 Electrochemical cell with three electrodes

The electrochemical deposition and characterisation of PPy films were conducted with a three-electrode glass cell with a capacity of 100 ml. A platinum mesh electrode of 0.5 × 0.5 cm was used as the counter electrode. A saturated calomel electrode (SCE) was used

as the reference electrode for the majority of the experiments, with some exceptions (which are mentioned in the relevant section). Various working electrodes were used, including stainless steel and platinum electrodes, described here. The reference electrode was positioned in the middle of the cell between the other two electrodes, which were positioned on opposite sides of the cell facing each other, as shown in the cell sketch of the Figure 2.2 below. The same cell configuration was used to measure the open circuit potential and drug release except that the volume of the cell was 20 ml.

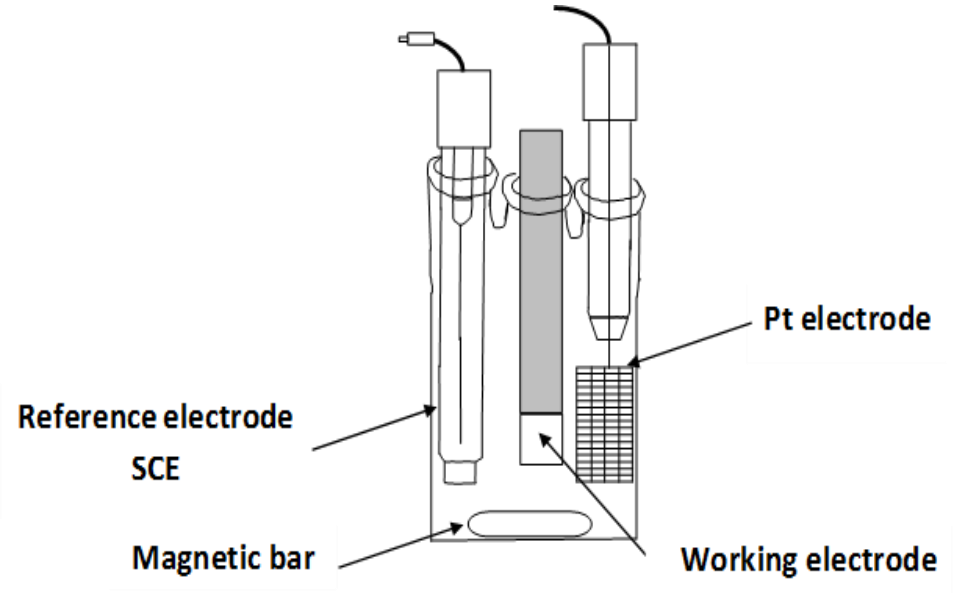

Figure 2-2: Three-electrode electrochemical cell used for electrochemical experiments and drug release.

2.3 Preparation of working electrodes

Three types of anode electrodes were used: a platinum disc electrode measuring 0.6 cm^2 and tow stainless steel disc electrodes measuring 1.2 and 2.27 cm^2 .The platinum electrode was

mechanically polished with 0.05 μm aluminium oxide (Al_2O_3), very carefully cleaned with multi purpose detergent (Teepol), rinsed with plenty of distilled water, and cleaned in an ultrasonic bath before beginning every experiment. The stainless steel electrodes were mechanically polished with 6 μm and 1 μm Al_2O_3 for five min each, very carefully cleaned with detergent, rinsed with plenty of distilled water and cleaned in an ultrasonic bath for five min before beginning every experiment. For the release experiments, a disposable stainless steel electrode was cut from a stainless steel sheet and covered with a tape; 1 cm^2 was left open for exposure to the synthesis solution.

2.4 Free-standing PPy membranes

Free-standing conducting polymer films can be used as ion exchange membranes for biomedical applications such as drug delivery device and biosensor. This section described the synthesis of stand-alone PPy films. The PPy film were deposited from a 0.5 mol dm^{-3} Py monomer doped with 0.1 mol dm^{-3} $EtNBF_4$ or K_2SO_4 on a 2.27 cm^2 stainless steel disc electrode. The polymerisation solution was stirred at 400 rpm. The films were potentiostatically deposited at 0.6 V *vs.* SCE until the accumulated charges applied reaches 27.2 coulomb, which resulted in the growth of a PPy film with a thickness of approximately 27.8 μm [250]. The film was detached from the electrode, cleaned with deionised water, and then left to dry for two hours before measuring the film's resistance.

2.5 Four-electrode electrochemical cell

The conductivity of the conducting polymer film can be measured using different techniques. For example, by measuring the film resistance using the four probe technique or by measuring the film resistivity using electrochemical method. Since the conducting polymer drug delvery systems operated in aqueous environment, the electrochemical

technique was employed to measure the conducting polymer films conductivity. Figure 2.3 depicts a schematic diagram of a four-electrode glass cell which was used to measure the resistivity of the films. The cell comprises similar parts, and the films' resistivity is measured by placing them between these parts. The films were surrounded by two mercury-oxide reference electrodes Hg/Hg_2O. These reference electrodes were used to measure the films potential difference when a galvanostatic current was applied using two-platinum mesh electrodes positioned on the outer sides of the cell across the mounted membrane.

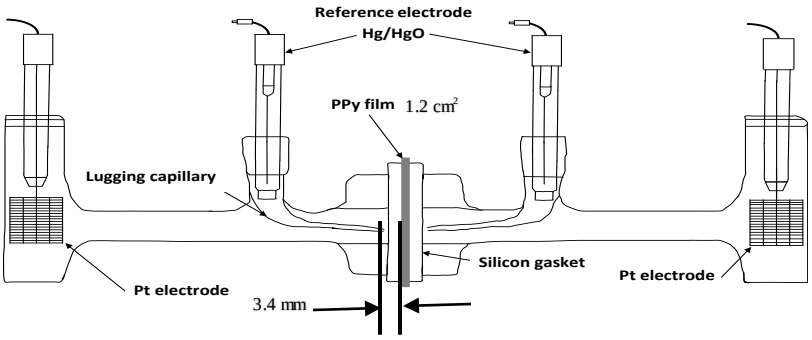

Figure 2-3: Four-electrode electrochemical cell used to measure the membranes' resistivity.

2.6 Two-compartments divided membrane cell

The electrodeposition of PPy film on active metals such as Mg is a challenge task due to the dissolution of the metal substrate which is preventing the film formation. The use of the high concentrated doping ion salicylate may help to passivate the metal dissolution but it may reduces the rate of the drug being release. Therefore, in order to avoid the metal dissolution, the PPy film containing a model drug was chemically deposited using a two-compartment cell, as shown in Figure 2-4. The cell compartments are separated by a CC

or DM membrane, where the PPy containing the model drug is formed. One of the cell compartments contains the Py monomer with the model drug in the absence and presence of TiNT and the other contains the oxidant solution, ammonium persulfate. The cell, filled with the two solutions, was kept at room temperature (295 K) for four hours. The solution was stirred with a magnetic stirring bar to disperse the TiNT. The two solutions diffused into each other through the membrane and the Py gradually oxidised, thereby forming the PPy film containing the model drug on the outer and inner surfaces of the membrane. The obtained composite film was coated with Mg thin film as described in the following section.

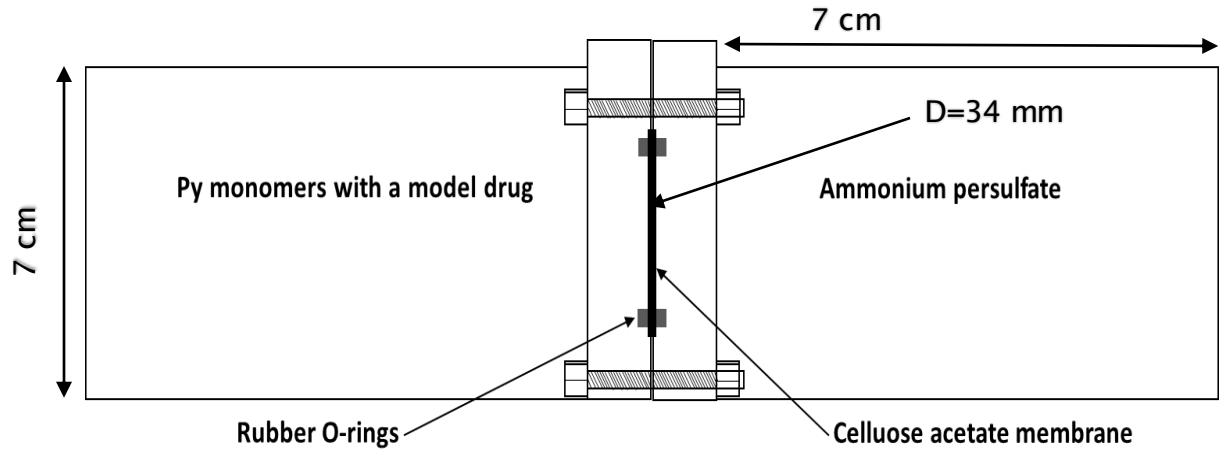

Figure 2-4: Two-compartment divided membrane cell used for the chemical polymerisation of Py.

2.7 Magnesium coating for self-powered release system

The obtained PPy cellulose acetate composite film was cleaned with 0.01 mol dm^{-3} NaCl solution for five minutes and dried under vacuum at 40 ^{o}C. Thereafter, a thin layer of Mg

(0.5 μm approximately) was sputtered on one side of the film using a hanmade sputtering system. The sputtering process was carried out under vacuum pressure ≈ 10^{-6} bar.

2.8 Open circuit electrode potential measurements

The open circuit potential (OCP) of the working electrode is measured when no external current flows. An awareness of the OCP provides denotation for the change of the polymer oxidation level during unstimulated release of incorporated molecules. Thus, it is important to comprehend the relationship between the change of the polymer oxidation state and the detected release profile for unstimulated films. An Autolab potentiostat/galvanostat was used to monitor the OCP of PPy films. The experiments were conducted with a three-electrode glass cell that contained 20 ml of 9% NaCl aqueous solution. The PPy films were used as the working electrode, a platinum mesh electrode was used as the counter electrode and a saturated calomel electrode (SCE) as the reference electrode. A similar cell setup was used for the release experiments. The open circuit potential of the PPy film was recorded over a five-hour period [252].

2.9 Surface characterization (SEM) and (FTIR)

Scanning electron micrographs were obtained with a JEOL JSM-6500F FEG-SEM instrument operating under a vacuum of >9 x 10^{-4} Torr and an acceleration voltage of 5 keV, equipped with an EDS x-ray analyser. A Nicolet 360 FTIR was used to characterise the film.

2.10 Drug release

Ultraviolet-visible (UV-vis) spectroscopy is a relatively inexpensive and easy-to-use technique that is frequently used to measure the amount of organic molecules released from the polymer. This technique is usually based on the Beer-Lambert law, according to which the absorption of the solution is proportional to the concentration of the solution. A model drug solution in distilled water at various concentrations (Table 2.1) was prepared and the absorbance of these solutions at the wavelength of maximum absorption (λ_{max}) was measured using UV-vis spectroscopy to obtain a calibration curve. A calibration curve was obtained by plotting the absorbances alongside the concentration for all the model drugs used in this project. The slope of the obtained calibration line used with the measured absorbances of the released drug to calculate the concentration of the model drugs being released from the PPy films.

The samples of the released drugs were analysed using a Lambda 35 UV/VIS spectrometer to determine the concentration of the model drug being released. The obtained PPy films were washed with 0.01 mol dm^{-3} NaCl for five minutes, and then immersed in a cell containing 20 ml of 0.9% NaCl aqueous solution at room temperature (295 K), with and without the application of electrical potential to stimulate the films. The release solution was stirred using a magnetic bar at low rotation during the release experiments to mix the released molecules with the release solution. Samples of 5 ml were taken at regular intervals of time from the release medium and replaced with an equal volume from the original NaCl solution to maintain the volume of the release medium.

Table 2-1: Identification of the λ_{max}, the concentration ranges, the slope of absorption calibration curves for the use substances.

Model drug	**Absorption λ_{max} / nm**	**Concentration range / mol dm^{-3}**	**Slope of absorption calibration curve Abs./ μmol dm^{-3}**
Rhodamine 6G (Rh-6G)	526.5	25 x 10^{-6} to 25 x 10 $^{-5}$	111.25
Fluorescein sodium salt (FSS)	485	25 x 10^{-6} to 25 x 10 $^{-5}$	54.51
Methylene blue (MB)	664	25 x 10^{-6} to 25 x 10 $^{-5}$	11720
Dopamine hydrochloride (DB)	280	25 x 10^{-6} to 25 x 10 $^{-5}$	3053
Ibuprofen sodium salt (IP)	222	25 x 10^{-6} to 25 x 10 $^{-5}$	7793

2.11 Self-powered electrochemical experiments

Although the chemical technique can be used for the deposition of different types of self-powerd drugs delivery systems, some drugs may react with the oxidant solution during the polymerisation process. This section described the electrochemical deposition of PPy film on AZ31 Mg substrate for self-powerd drug delivery system application. A three-electrode glass electrochemical cell connected to a potentiostat/galvanostat PGSTAT30 (EcoChemie, Netherlands) was used. The AZ31 Mg alloy was used as a working electrode, a 1 cm^2 platinum mesh as a counter electrode and a saturated calomel electrode (SCE) reference electrode. Prior to electrochemical experiments, the AZ31 Mg alloy foil was wet ground with a series of SiC papers down to 2000 grit. All AZ31 Mg alloy samples were tape masked to expose a constant 1 cm^2 area. Polished samples were degreased with acetone, rinsed with deionized water and sonicated for 10 minutes. Samples were

transferred to the electrochemical cell and positioned vertically with a 2 cm separation from a platinum mesh auxiliary electrode then used immediately. The polymerization solution consisted of a mixture of 0.5 mol dm^{-3} pyrrole (Py), 0.5 mol dm^{-3} sodium salicylate (SA) and sodium ibuprofen (IP) with concentrations, i.e., 0.5, 1, 10 and 50 x 10^{-3} mol dm^{-3}. (Hereafter named: SA, SA-Py and SA-Py-xIP, x: represents different concentration values). A rest time of 10 minutes was routinely applied to all the samples prior to each electrochemical studiy and the open-circuit potential was monitored. PPy films were grown potentiodynamically with a continuous N_2 stream bubbling through the solution to remove traces of dissolved O_2. The linear potential sweep started from -0.5 V to 1.0 V *vs.* SCE towards more positive potentials at a scan rate of 20 mV s^{-1} for 20 cycles until reaching a film thickness of ca. 20 ± 5 μm, as determined by SEM and optical imaging. All measurements were made at room temperature (295 K).

2.12 Self-powered drug release electrochemical experiments

PPy films prepared on the AZ31 Mg alloy loaded with sodium ibuprofen (IP) and sodium salicylate (SA) with 1 cm^2 area were released in 20 cm^3, 0.9 wt% NaCl. 5 cm^3 aliquots were collected at intervals, replenished by equal volume of fresh NaCl solution and analysed in a Neosys-2000, UV-VISIBLE Spectrophotometer, Scinco Co. Ltd. The concentrations of IP and SA were determined spectrophotometrically at 222 and 295 nm wavelengths. The latter was selected to quantify the concentration of SA via a calibration curve prepared at this wavelength from a stock solution and a series of volumetric dilutions. The 222 nm wavelength was used to determine the concentration of IP. It is worth noting that both IP and SA absorb UV light at a wavelength of 222 nm, thus it was necessary to subtract the absorbance for SA at this wavelength to determine the IP

concentration. Firstly, the SA concentration was determined at 295 nm where there is not IP absorption. Once this concentration was known, the estimated absorbance expected at 222 nm for SA was subtracted from the experimental value read in the spectra at 222 nm. The difference between both absorbances at this wavelength accounted for the concentration of IP using a calibration curve.

2.13 Depth-sensing indentation (DSI)

The DSI technique was used to characterise the mechanical properties of the PPy film electrodeposited on the AZ31 Mg alloy operating at the 3 mN load control mode with a 0.66 mN s^{-1} loading rate. A round indenter (radius <100 nm) was used and a total of 20 indents were produced for each sample.

Chapter 3: Preparation and characterization of PPy films on different substrates

This chapter presents a series of experimental results focused on the deposition of PPy films on the surface of different substrates. The effect of different polymerisation conditions were examined, including the influence of the number of deposition cycles, electrolyte solution, potential sweep rate, effect of the dopant anions and the monomer concentration on polymer electroactivity. In addition, the resistivity of different membranes was measured using a four-electrode cell. Whilst this work is not novel in itself, it is necessary at this stage for the method development before incorporating drugs in the conducting polymer films.

3.1 The effect of the number of deposition cycles

The oxidation of 0.05 mol dm^{-3} Py in aqueous 0.5 mol dm^{-3} K_2SO_4 solution at a stainless steel disc electrode (1.2 cm^2) using a potential sweep rate of 0.1 V s^{-1} is depicted in Figure 3.1. The cyclic voltammogram of a stainless steel electrode in the absent of Py monomer curve (a) showed that an oxidation peak began around 0.56 V and reached a maximum peak current of 3.8 mA at 0.69 V *vs.* SCE. The current density then decreased to between 0.69 V and 1.2 V *vs.* SCE, thereby indicating a formation of a passive layer on the stainless steel electrode surface [253, 254]. The slight increase in the anodic current at a potential greater than 1.2 V *vs.* SCE may be attributed to the decomposition of the passive layer or the beginning of oxygen evolution [254]. The first cycle in the presence of Py monomer curve (b) showed a relatively symmetrical oxidation peak at approximately 1.01 V *vs.* SCE, with a current peak of 28 mA attributed to the Py oxidation. The presence of the Py monomers caused the modification of the corrosion process of the stainless steel electrode, and the oxidation peak of the electrode

disappeared [255]. A second cycle at the same electrode, without cleaning (c), showed that the Py oxidation process began at an earlier potential of around 0.625 V *vs.* SCE, indicating that the previous deposited PPy layer stimulated a catalytic effect on the PPy deposition reaction, the monomer oxidation potential decreased during the following cycle [256]. In addition, the Py oxidation wave was observed beginning at approximately 0.65 V *vs.* SCE, with a peak potential of approximately 1.1 V *vs.* SCE. The peak current reduced to approximately 50% of the first cycle peak. The peak current decrease is due to the formation of the partially passive layer on the electrode surface, which may consist of Fe(II) and less active Fe(III) that may prevent the interaction between the electrode surface and the monomers. In addition, the decrease in the oxidation peak current may have been because the conductivity of the growing polymer film is low [253].

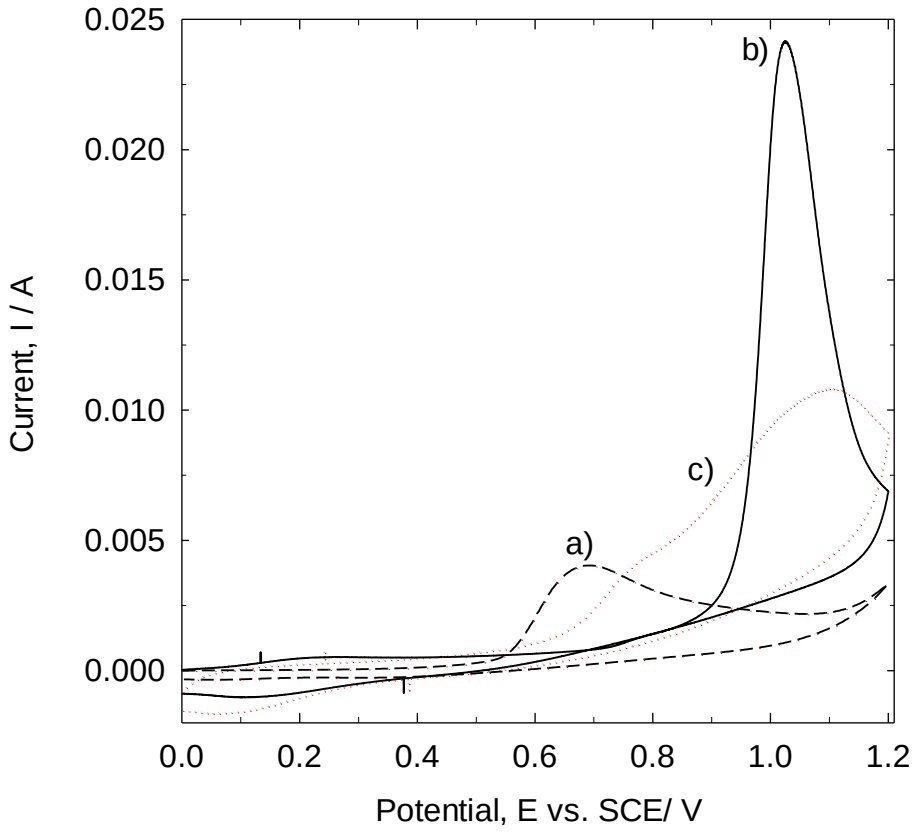

Figure 3-1: Cyclic voltammogram of 0.05 mol dm^{-3} Py in aqueous 0.2 M K_2SO_4 at a potential sweep rate of 0.1 V s^{-1} on stainless steel (1.2 cm^2 area) a) background, b) first cycle and c) second cycle.

3.2 The effect of the electrolyte solution

Figure 3.2 shows the oxidation of Py at a stainless steel electrode in a) anhydrous acetonitrile, b) 1% water and c) acetonitrile with 2% (v/v) water. The Py oxidation peak was positively shifted from approximately 1.45 V to approximately 1.65 V *vs.* SCE. Other peaks appeared after adding water. These two peaks may be attributed to the oxidation of PPy with different chain length [257]. The increase of the water percentage to 2% (v/v) lowered the peak current by 15%, as compared with the anhydrous acetonitrile peak current. This indicated that the amount of water added led to a reduction in the rate of polymerisation. However, the use of a small amount of water with acetonitrile led to improved PPy conductivity and reduced

formation of the partial variation of conjugated PPy. This is because water is a stronger acid than the Py monomers; therefore, the addition of water led to the elimination of the protons released during the polymerisation reaction and hindered extra protonation of the Py. It has been reported that a water content of approximately 1% (wt) in acetonitrile is the optimal content to effectively eliminate the protons released during the reaction. Although the use of acetonitrile as an electrolyte in the PPy polymerisation might lead to electrode passivation, the presence of a small amount of water in the acetonitrile improved the mechanical properties and the adherence of the film [251]. Acetonitrile is, however, a toxic substance; traces must be removed before any relevant medical application.

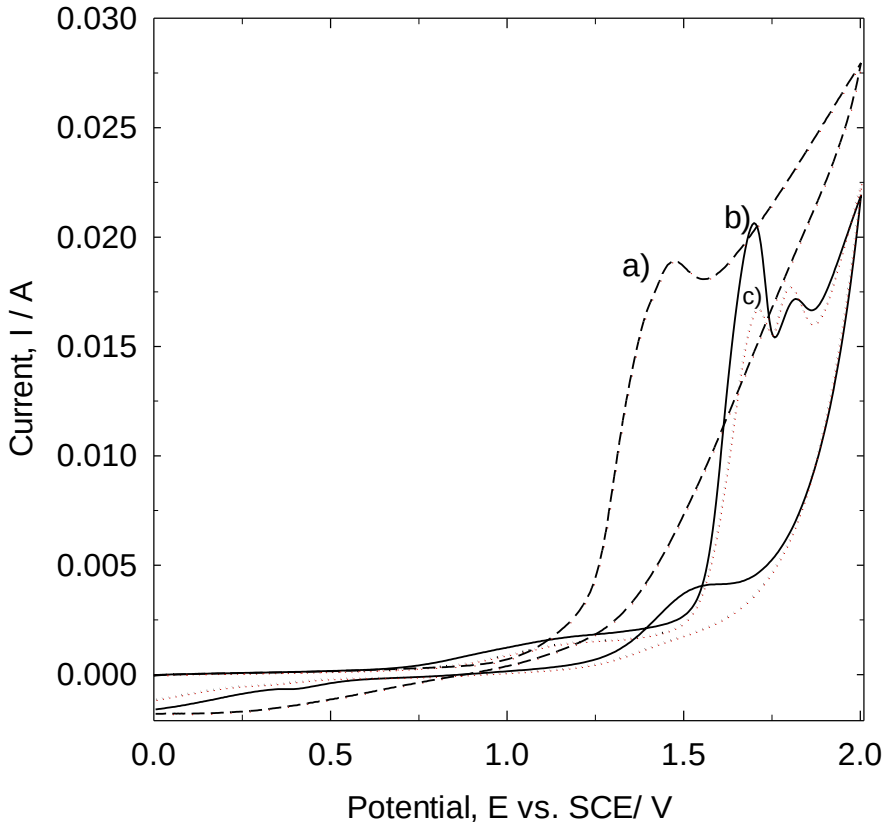

Figure 3-2: Cyclic voltammogram of a stainless steel electrode (1.2 cm^2 area) in 0.01 mol dm^{-3} Py and CH_3CN with 0.1 Et_4NBF_4 at a potential sweep rate 0.1 V s^{-1}. a) Anhydrous CH_3CN, b) 1% (v/v) H_2O and c) 2% (v/v) H_2O.

3.3 The effect of potential sweep rate

Figure 3.3 illustrates the CV of 0.02 mol dm^{-3} Py in anhydrous acetonitrile containing 0.1 mol dm^{-3} $EtNBF_4$ at a platinum disc electrode (0.6 cm^2) at different sweep rates. Two oxidation features are evident at a low sweep rate. These two features are positively shifted by approximately 0.1 V with the increased sweep rate. The two oxidation peaks tend to become a broad single peak when the sweep rate is increased to more than 0.2 Vs^{-1}.

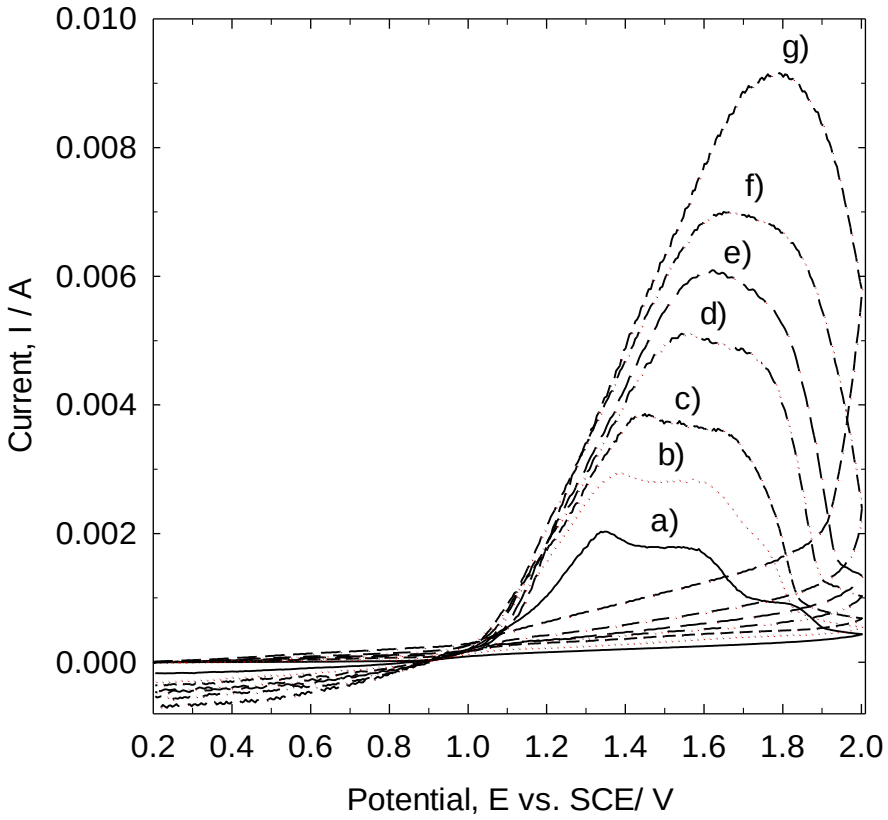

Figure 3-3: Cyclic voltammogram of a platinum disc electrode (0.6 cm^2) in 0.02 mol dm^{-3} Py and anhydrous CH_3CN with 0.1M $EtNBF_4$. Potential sweep rates: a) 0.025, b) 0.05, c) 0.1, d) 0.2, e) 0.3, f) 0.4 and g) 0.8 V s^{-1}.

Figure 3.4 shows the curve peak current *vs.* the square root of the potential sweep rate. The peak current was taken from the curves in Figure 3.3 at 1.35, 1.38, 1.45, 1.55, 1.61, 1.68 and 1.78 V *vs.* SCE. An approximately linear relationship between the peak current and the square

root of the potential sweep rate can be observed up to a potential scan rate equal to 0.1 V s^{-1}. Therefore, the rate of reaction was controlled by rate of diffusion of pyrrole monomer at diffuse layer and the Randless-Sevick equation can be applied in this linear region to calculate the diffusion coefficient, D.

$$I_p = (\ 2.69 * \ 10^5)\ Z^{\frac{3}{2}}\ A\ D^{\frac{1}{2}}\ C\ v^{\frac{1}{2}}, \qquad (3.1)$$

Where I_p is the oxidation peak current, z is the number of electrons involved in the reaction, c is the Py concentration and v is the potential sweep rate. The slope value of the curve in figure 3.4 is $0.01206\ \frac{A}{(Vs-1)^{\frac{1}{2}}}$, which yields the value of $\frac{\Delta I_p}{\Delta v^{\frac{1}{2}}}$.

Therefore, The diffusion coefficient is $D = 1.12 \text{ x } 10^{-6}\ \text{cm}^2\ \text{s}^{-1}$. This value is smaller than the value reported by Girault ($1.3 \pm 0.2 \text{ x } 10^{-5}\ \text{cm}^2\ \text{s}^{-1}$) [251]. This difference may have occurred due to the influence of the experiment conditions such as temperature variation. Different values have also been reported for pyrrole diffusion coefficient ranged between $1\ x\ 10^{-6}$ and $1.5 \text{ x } 10^{-9}\ \text{cm}^2\ \text{s}^{-1}$) [258].

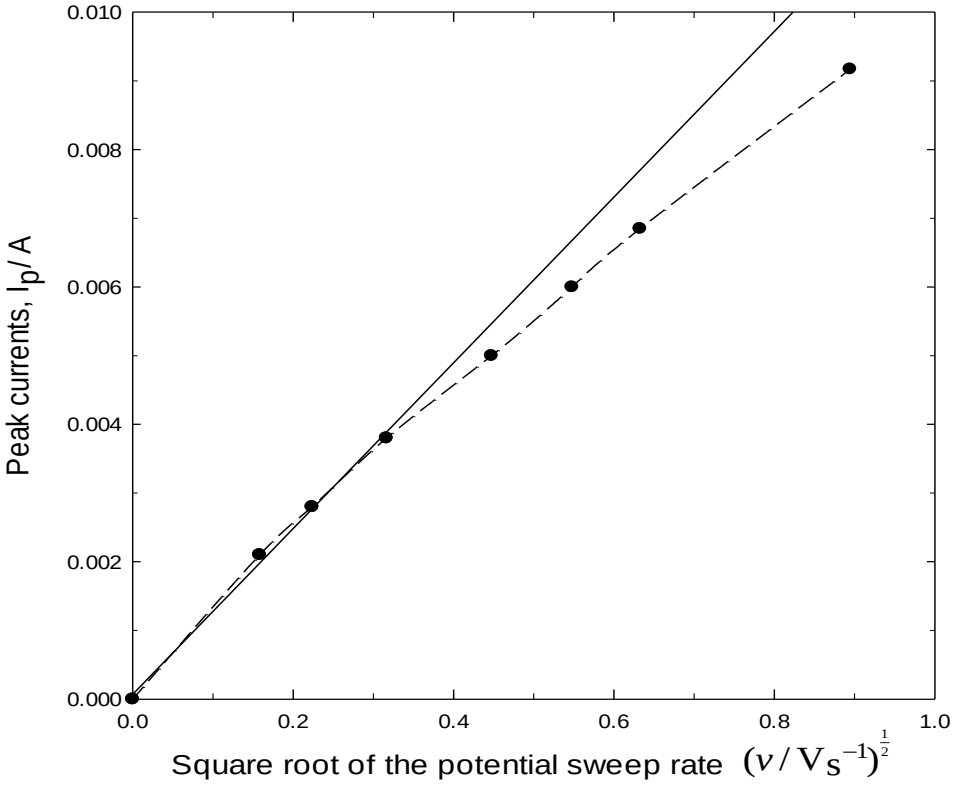

Figure 3-4: Peak current I_p *vs.* square root of the potential sweep rate $\nu^{0.5}$

3.4 The effect of the dopant anions

The effects of the dopant on the polymerisation of PPy in the presence of two different anions were examined. Figure 3.5 shows cyclic voltammograms for the oxidation of 0.02 mol dm^{-3} Py in a) 0.1 mol dm^{-3} Et_4NBF_4 and b) 0.1 mol dm^{-3} K_2SO_4. The peak current of the oxidation of Py doped with K_2SO_4 is approximately 60% higher than the oxidation of Py doped with Et_4NBF_4. Thus, the polymerisation rate is slightly higher with the use of K_2SO_4 compared with the use of $EtNBF_4$ as a dopant.

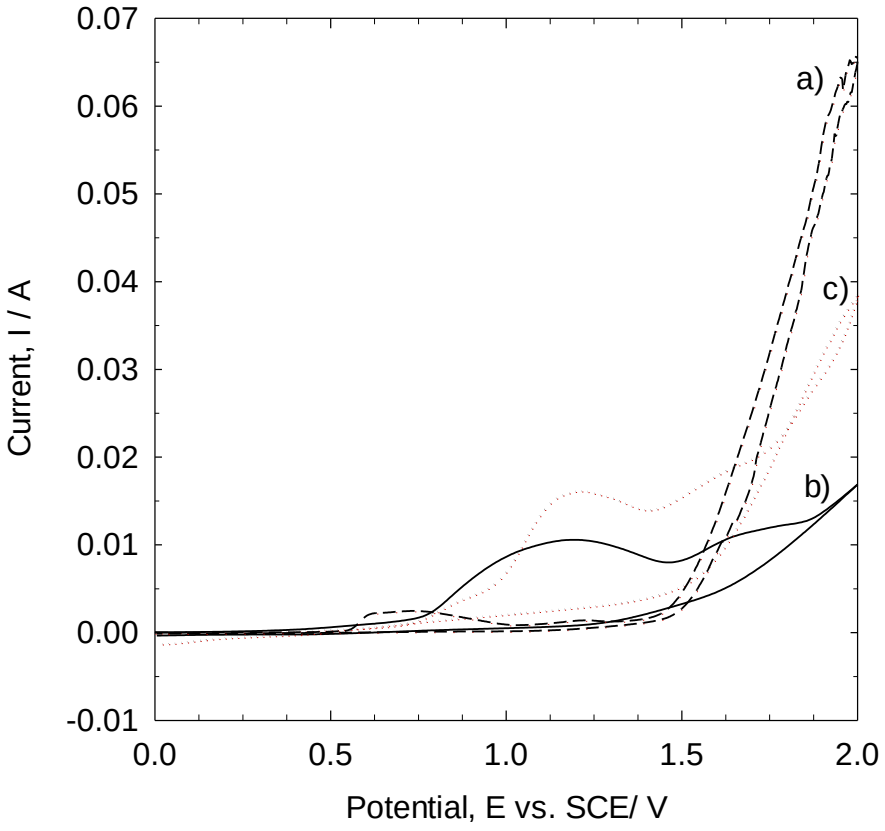

Figure 3-5: Cyclic voltammogram of a stainless steel electrode (1.2 cm^2 area) in an aqueous solution of 0.02 mol dm^{-3} Py and a) background, b) 0.1 mol dm^{-3} Et_4NBF_4 and c) 0.1 mol dm^{-3} K_2SO_4.

3.5 The effect of monomer concentration

Figure 3-6 depicts the effect of the increase of the Py monomer concentration on the polymerisation rate of polypyrrole with 0.01 mol dm^{-3} Et_4NBF_4. A broad oxidation wave was observed with a peak potential of around 1.4 V *vs.* SCE at a monomer concentration of 0.01 mol dm^{-3}. The increase of the monomer concentration to 0.02 mol dm^{-3} led to increased oxidation current and no oxidation peak observed up to a potential of 2 V *vs.* SCE, thereby indicating an unlimited growth of polymer films. Girault et al. [251] reported that the main oxidation peak shifted positively by 100 mV, corresponding to the incremental increase of Py monomers by 0.01 mol dm^{-3} from 0.01 mol dm^{-3} to 0.04 mol dm^{-3}. They found that at a

monomer concentration of 0.045 mol dm^{-3}, the oxidation current rose and no oxidation peak was observed up to a potential of 2.1 V *vs.* SCE.

Iroh et al. [259] reported that the increase of the Py monomer concentration led to an increased electropolymerisation rate. They found that the electropolymerisation potential exponentially decreased with the increase of monomer concentration. The increase of monomer concentration by approximately 800% from 0.1 to 0.8 mol dm^{-3} led to a reduction in the electropolymerisation potential by approximately 11%.

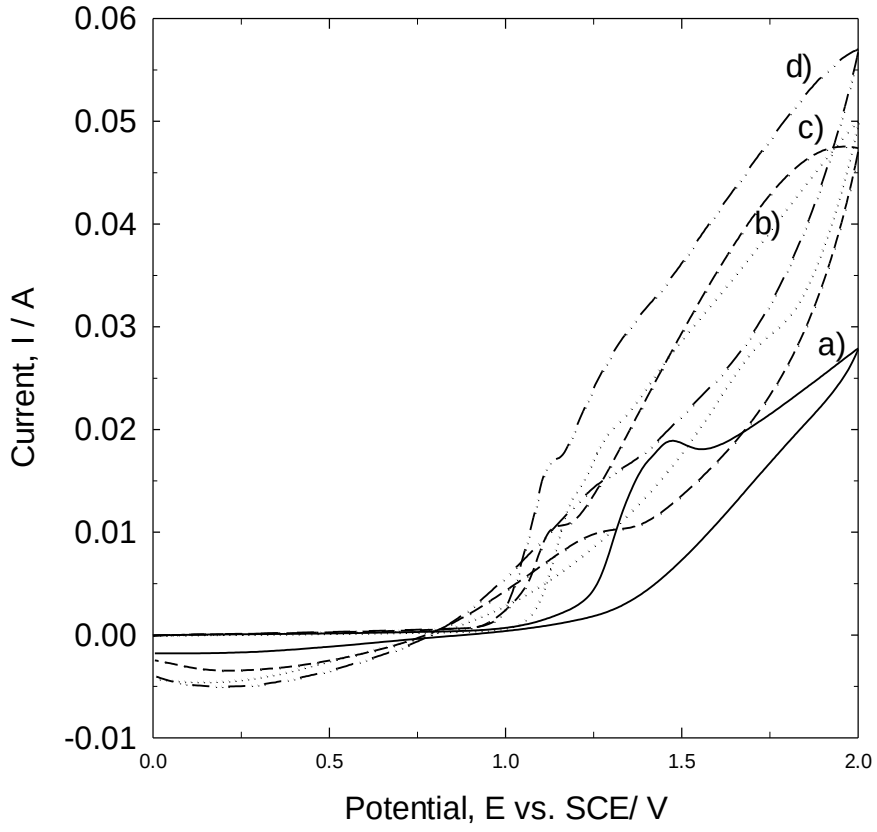

Figure 3-6: Cyclic voltammogram of a stainless steel electrode (1.2 cm^2 area) in aqueous solution of 0.01 mol dm^{-3} $EtNBF_4$ and a) 0.01 mol dm^{-3} Py , b) 0.02 mol dm^{-3} Py , c) 0.03 mol dm^{-3} Py and d) 0.04 mol dm^{-3} Py.

3.6 CV of a PPy film at different potential scan rates

A PPy film was first grown potentiostatically at 0.9 V *vs.* SCE from an aqueous solution of 0.05 mol dm^{-3} Py in 0.2 mol dm^{-3} K_2SO_4 in a three-electrode chemical cell with a platinum mesh and SCE as counter and reference electrodes, respectively. The film was permitted to grow to a thickness of 331 nm corresponding to the charge density of 143 mC cm^{-2} [251]. The film was washed with deionised water before it was placed in a fresh electrolyte solution of 0.2 mol dm^{-3} K_2SO_4. Figure 3.7 illustrates the behaviour of 331 nm PPy film at various potential sweep rates.

3.7 Film thickness calculations

The polymer thickness can be calculated based on the consumed charges obtained during the film synthesis process using Faraday's law with the following assumptions:

1. Efficiency of the polymerisation current is 100%.
2. Two electrons are involved in each monomer molecule oxidation.
3. Pyrrole monomer molar mass, M = 67.09 g mol^{-1}.
4. PPy density equals 1.5 g cm^{-3} [251]
5. Faraday's constant equals 96485 C mol^{-1} [260].
6. Electrode surface area, A = 1.2 cm^2.

Thus, the film thickness x

$$x = \frac{Q_{deposition} * M}{\rho * A * z * F}. \quad (3.2)$$

Thus, $t = 331\ nm.$

The oxidation peaks of the PPy films in 0.2 mol dm^{-3} K_2SO_4 aqueous solution can be observed clearly, while the reduction peaks are not well defined in figure 3.7. The oxidation peaks currents rise with the increase in the potential sweep rates and the peak potentials are positively shifted. At a lower scan rate (scan rate 0.01 V s^{-1}), the oxidation peak appeared at a potential of approximately -0.32 V *vs.* SCE and the peak current was approximately 0.001 A. The oxidation peak are positively shifted by approximately 100 mV to approximately -0.21 V *vs.* SCE, when the sweep rate increased to 0.3 V s^{-1} and the current peak increased to 0.004 A. On the other hand, the reduction peak appeared at around -0.85 *vs.* SCE (for v = 0.01 V s^{-1}). The reduction peaks became broad waves with increased sweep rates and shifted to more negative potentials.

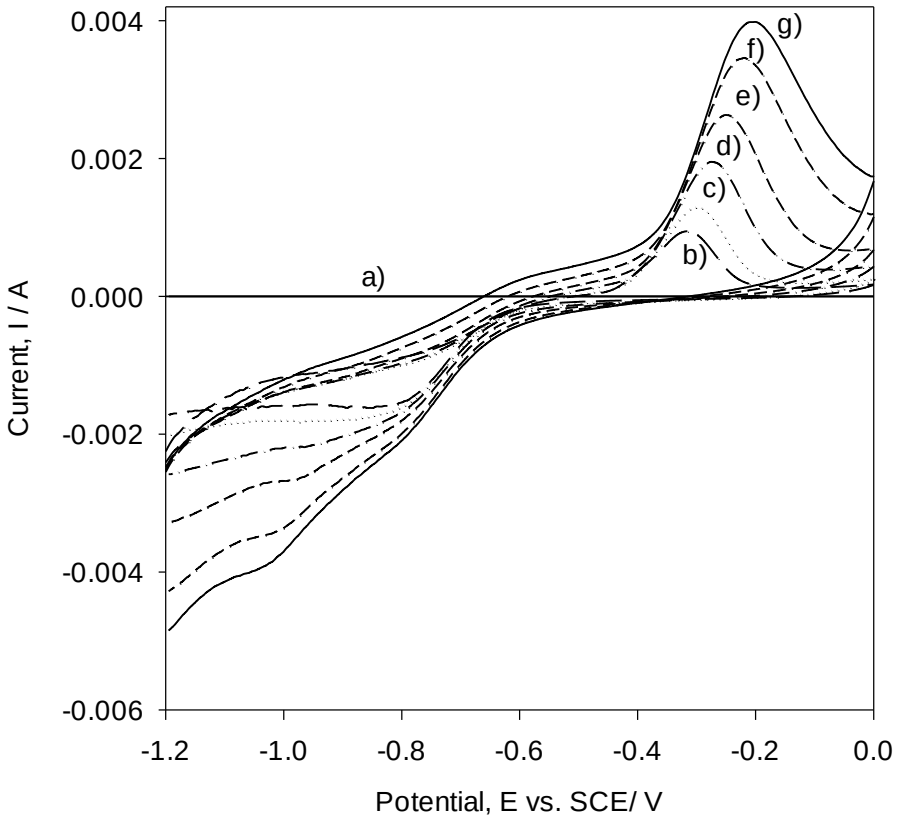

Figure 3-7: Behaviour of a 360 nm PPy film at various potential sweep rates in 0.2 mol dm^{-3} K_2SO_4 aqueous solution. The film was grown from 0.05 mol dm^{-3} Py in aqueous 0.2 mol dm^{-3} K_2SO_4 on a stainless steel electrode (1.2 cm^2 area) at a constant potential of 0.95 V *vs.* SCE. a) Background electrolyte and samples at potential sweep rates of: b) 0.01, c) 0.02, d) 0.05, e) 0.1, f) 0.2 and g) 0.3 V s^{-1}

3.7.1 Resistance measurements

Resistance measurements for different films including N550, ICI CHEMICAL, IONIC MA-3 and N430 membranes were conducted. The films were cleaned with distilled water and soaked in a 0.5 mol dm^{-3} KCl aqueous solution for 24 h prior to the resistance measurements process. The resistivities of the films were measured in a four electrode cell, as shown in Figures 2.3. Two platinum mesh electrodes were used to apply a glavanostatic current across the mounted membrane, between -30 and 30 mA. The corresponding potential was measured via two Hg/HgO reference electrodes. Figure 3.8 and 3.9 show the relation between the applied current through the membrane and the resultant potential drop across it. The resistance measurements of the films were calculated according to Ohm's law, Equation (3.3), where the value of the line slope is equal to the membrane resistance.

$$R_{total} = \frac{V}{I} \tag{3.3}$$

where

$$\mathrm{R_{total}} = \mathrm{R_{membrane}} + \mathrm{R_{solution}}. \tag{3.4}$$

The membranes' specific resistivities were calculated using the following equation:

$$\rho_e = \frac{R_{membrane} * A_{membrane}}{t_{membrane}}, \tag{3.5}$$

where

ρ_e is the membrane resistivity, $R_{membrane}$ is the resistance across the membrane, $A_{membrane}$ is the membrane surface area and equal to 1.2 cm^2, x, is the membrane thickness is 27.8 μm, $R_{solution}$ is the solution resistance, considering that the distance between each luggin capillary tip and the membrane is equal to 3.4 mm.

Table 3.1 presents the obtained results of the measured resistance. The specific resistivity of the 0.5 mol dm^{-3} KCl aqueous solution is 18.4 Ω cm, which is higher than the previous value in the literature, which is 15.6 Ω cm. This difference may be due to the differences in the experimental conditions and the purity of the materials. However, the obtained resistivity of PPy/$EtNBF_4$ films, 2720 Ω cm, was close to the result obtained by Girault et al. [251], which was 2700 Ω cm for the oxidised film. The obtained results are in the range of previously reported resistance measurements of some semiconductor materials. The specific resistance of the PPy/K_2SO_4 membrane was 4320 Ω cm. The increase in the resistivity value may be due to several reasons. For example, the difficulty in expelling the dopant ions SO_4^- from the polymer membrane may have impeded the migration of chloride ions into and across the PPy membrane. On the contrary, the migration of chloride ions across the PPy/$EtNBF_4$ would be easier. Moreover, the deposition rate of PPy/K_2SO_4 is faster than the deposition rate of PPy/$EtNBF_4$ and, thus, the PPy/K_2SO_4 is thicker and has higher resistance compared with PPy/$EtNBF_4$ may be because it is more compact. In addition, film characteristics such as film thickness, surface morphology, film smoothness, and uniformity may influence film resistivity but were not measured.

Table 3-1: Resistivity and resistance for free-standing membranes mounted in a 4-electrode cell with aqueous 0.5 mol dm^{-3} KCl on each side

Membrane	R_{total} / Ω	$R_{membrane}$ / Ω	ρ_e / Ω cm
N550	20.5	8	3200
ICI chemical	21	8.5	3400
Ionic MA-3	42	29.5	11800
N430	30	17.5	7000
0.5 M KCl	12.5	--	18.4
PPy/$EtBF_4$	19.3	6.8	2720
PPy/K_2SO_4	23.3	10.8	4320

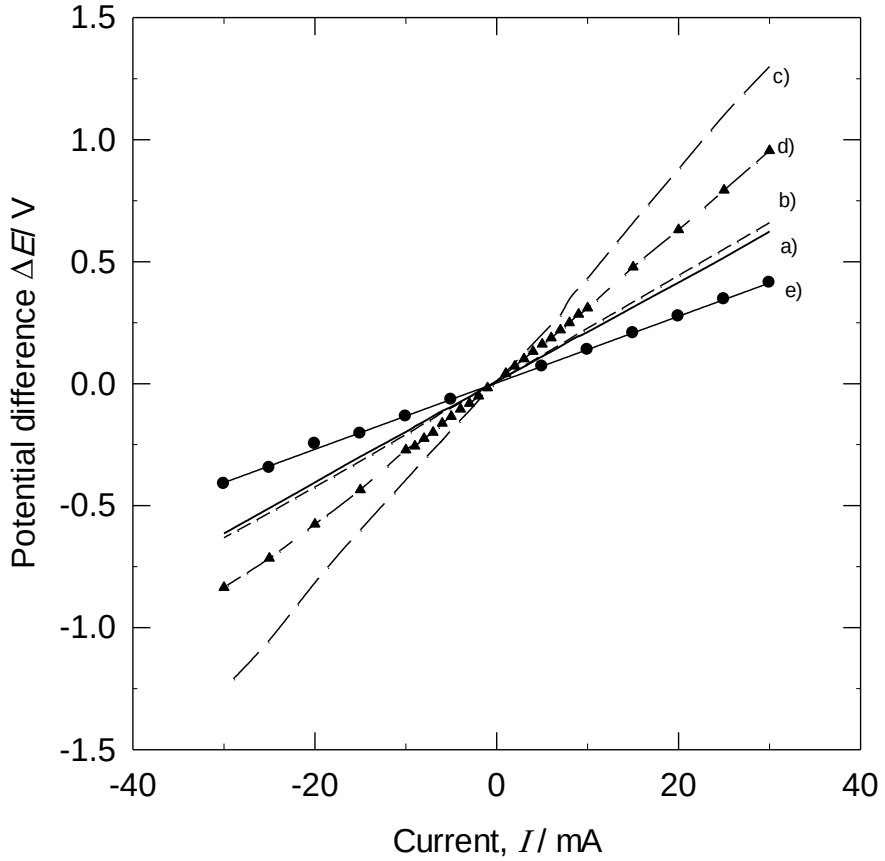

Figure 3-8: Current compared with potential curve for a) N 550 membrane, b) ICI chemical membrane, c) Ionic MA-3475CAPM, d) N430 membrane and e) cell without membrane. The membranes were mounted on a 4-electrode cell with aqueous 0.5 mol dm^{-3} KCl on each side. A maximum current through the membrane of -30 to 30 mA was applied via two platinum electrodes and the potential difference was recorded using two identical Hg/HgO reference electrodes.

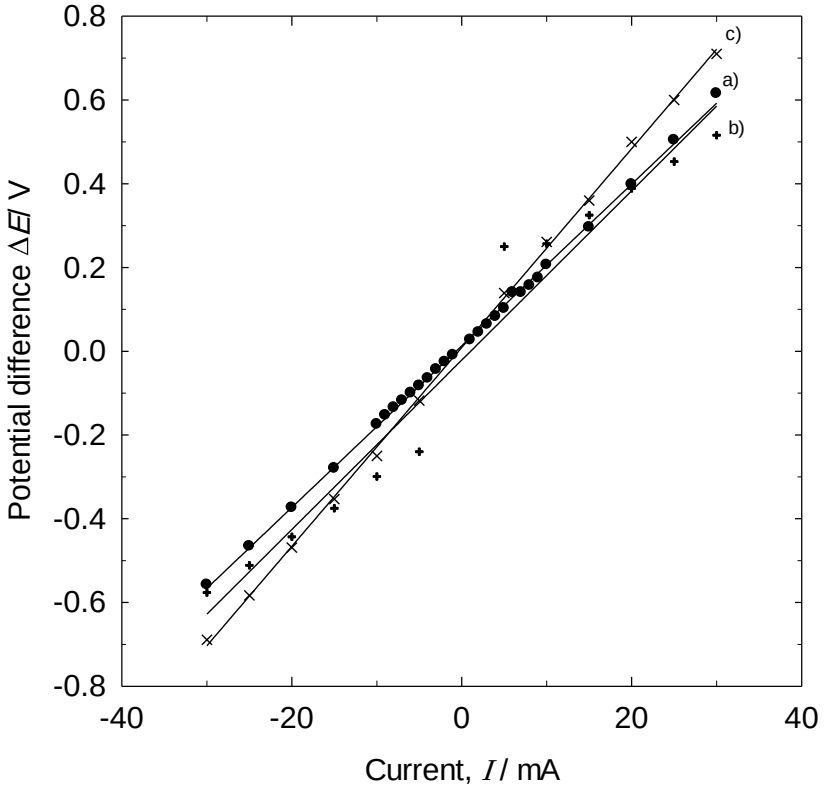

Figure 3-9: Current *vs.* potential curve for a 40 μm thick PPy membrane doped with a) BF^-_4, b) SO_4^- /C and c) SO_4^-. The membranes were mounted on a four-electrode cell with aqueous 0.5 mol dm^{-3} KCl on each side. A maximum current across the membrane of -30 to 30 mA was applied via two platinum electrodes and the potential difference was recorded using two identical Hg/HgO reference electrodes.

3.8 Summary and Conclusions

Polymerisation conditions such as electrolyte type, pH, monomer concentration and doping nature, significantly affect the formation and film properties of conducting polymers. Therefore, these factors need to be optimised for the desired application. For example, the nature of the doping ions affects the polymerisation rate and the properties of the polymer film. The peak current of the oxidation of Py doped with K_2SO_4 is approximately 60% higher than

the oxidation of Py doped with $EtNBF_4$. Thus, the polymerisation rate is slightly higher with the use of K_2SO_4 as compared to with the use of $EtNBF_4$ as a dopant.

The presence of Py monomers in the electrolyte solution have modified the corrosion process of the stainless steel electrode, and the stainless steel oxidation peak disappeared when it was immersed in an electrolyte containing 0.5 mol dm^{-3} K_2SO_4 and 0.05 mol dm^{-3} Py due to the formation of the PPy film on the electrode surface, which lead to the passivation of the electrode surface. In the second cycle, the Py oxidation process began at an earlier potential of roughly 0.625 V *vs.* SCE, where the oxidation potential began at approximately 0.65 V *vs.* SCE in the first cycle; this indicates that the previous deposited PPy layer stimulated a catalytic effect on the PPy deposition reaction, and the growth of PPy on PPy film is higher than its growth on the stainless steel electrode surface.

The polymerisation electrolyte solution has a significant effect on Py polymerisation. The Py oxidation peak was positively shifted from approximately 1.45 V *vs.* SCE in anhydrous acetonitrile electrolyte to approximately 1.65 V *vs.* SCE, when 1% (v/v) water was added to the solution. In addition, other oxidation peaks appeared after adding water. These two peaks may be attributed to the oxidation of PPy with different chain lengths. The increase of the water percentage to 2% (v/v) lowered the peak current by 15% as compared to the anhydrous acetonitrile peak current. This indicated that the amount of water added reduced the rate of polymerisation. However, it has been reported that the use of a small amount of water with acetonitrile led to improved PPy conductivity and reduced formation of the partial variation of conjugated PPy. This is because water is a stronger acid than Py monomers; therefore, the

addition of water led to the elimination of released protons during the polymerisation reaction and hindered extra protonation of the Py [251].

The use of a high concentration monomer leads to a less positive polymerisation potential and an increase in the polymerisation rate. This feature can be useful in drug delivery and biosensor applications, where the increase of monomer concentration may prevent chemically active drug and enzyme oxidation during polymer synthesis.

Chapter 4: Self-powered drug release system

4.1 Introduction

Polypyrrole films electrodeposited on active Mg alloys and the film incorporated with various ionic drugs are the subject of current investigation. It was encouraged by the development of self-propelled drug release systems, whose mechanism relies on galvanic coupling between a conducting polymer film and the active metal alloy underneath. In corrosive environments, such as the ones encountered inside a human body or on the surface of skin, implanted active Mg alloys undergo corrosion, releasing electrons into the PPy film and releasing the uploaded therapeutic drug [261]. These Mg alloy corrosion properties contribute in one side to the development of biodegradable implants, but in the other side provide the alternative to locally release different types of drugs, e.g., risperidone, dexametasona, pain relievers or antibiotics [113]. There are reports in the literature of self-powered drug releasers, that employ a number of active magnesium alloys including the alloy (97% Mg, 2% Al, 1% Zn) Mg alloy [113], pure Mg (99.9% purity) [262], sputtered Mg thin film [263, 264], AZ91 and AZ31 [265, 266]. These Mg alloys are particularlly attractive since their mechanical properties match those of the human bones and posessess a high strength/density ratio. For instance, Mg has an approximate density of 1.74-2.00 g cm^{-3}, an elastic modulus of 41-45 GPa and a compressive yield strength of 65-100 GPa which is similar to the mechanical properties of human bone with a density of 1.8-2.1 g cm^{-3}, elastic modulus of 3-20 GPa and compressive yield strength of 130-180 GPa [267]. One concern with the use of active Mg alloys containing Al as drug delivey systems, is that their corrosion can release undesireable metals such as Al, limiting their use inside the human body [268]. Thus, magnesium alloys with minimal Al content such as AZ31 Mg alloy are disarable for biomedical applications.

One of the most common, readily prepared, biocompatible, mechanically robust conductive polymers (CPs) is polypyrrole (PPy). This polymer has been used as a passive layer for corrosion protection of metals and Mg alloys [269] and as a model system for local drug delivery induced by an electrical stimulus [270]. CPs undergo oxidation while growing, attracting counterions to balance the charge, which allows therapeutic drugs to be uploaded or downloaded as dopants into and from the film [271]. The size and chemical structure of the uploaded drug into the film may affect the polymer nucleation and growth processes, as well as affecting other properties such as the mechanics of the film [269]. There are some reports in the literature aimed at the effect that uploaded dopants or thermal treatments may play on the mechanical properties of PPy [272-274]. One of the tools used to investigate these properties is depth-sensing indentation (DSI). This technique uses the relationship between the load and depth of penetration of an indenter to determine the average hardness (H) and reduced modulus (E_r) of the film [272, 273, 275].

Although the incorporation of a therapeutic drug into CPs is adequate for treatment of acute or chronic diseases upon delivery, it does not necessarily contribute favourably to the polymer structure. Some reports in the literature have identified difficulties to prepare adherent, compact, PPy films under specific experimental conditions [276]. So, it becomes evident that the chemical structure, steric effects, functional groups and charge of the dopant drug affect both the preparation of the film and its final properties [277, 278]. In addition, some therapeutics drugs can be absorbed on the alloy surface breaking down the passivity and affecting the CPs deposition. This is a critical issue for self-propelled drug release processes based on the uses of active Mg alloys. Two competitive processes may arise involving a competition between the underlayer metal dissolution and the nucleation and growth processes of the polymer film. This

has encouraged the use of polymer dopants that also passivate the metal surface, such as salicylate and oxalate ions [279].

The amount of drug incorporated into CPs needs to be optimized [278]. Usually, it is required that the amount of drug uploaded into the polymer film increases in order to ensure a long-acting time therapeutic action. While uploading a large amount of a dopant, the polymer matrix and consequently its mechanical properties modify [272]. To increase the amount of the drug, several alternatives have been undertaken; for instance, CPs can be nanostructured, or two-layer CPs can be deposited to produce a continuous PPy film, releasing a higher drug loading [278]. In other instances, an additional chemical agent is added, such as a cationic surfactant, that modifies the hydrophobicity of the polymer [280]. An alternative is the addition of a large, multi-charged anionic heparin molecule that can act as a high-capacity cation exchanger [280]. This chapter aims at investigating the effects that sodium ibuprofen, a well-known anti-inflammatory drug, has on the electrochemistry, structure, kinetics of release and mechanical properties of PPy films electrodeposited on an active AZ31 Mg alloy in an aqueous 0.5 mol dm^{-3} sodium salicylate solution. The aims of this chapter are to synthesis novel self-powered ibuprofen release sytem and study the effects of ibuprofen concentrations on the polymerisation process, the morphological structure and mechanical properties of the deposited PPy film.

4.2 Electrochemical characterisation

Open-circuit potential (OCP) measurements of the AZ31 Mg alloy in SA-Py, and SA-Py xIP solutions obtained during the 10 min rest period are illustrated in Figure 4.1. Although Mg and AZ31 Mg alloys are naturally active metals in aqueous media and possess extremely high negative redox potentials, the presence in solution of species capable of forming a stable protective layer contributes to the displacement of the OCPs to nobler values. According to the

experimental conditions used, the AZ31 Mg alloy in SA-Py solution displays an OCP of -1.75±0.022 V *vs.* SCE and rapidly changes to a less negative OCP value of -1.619±0.002 V *vs.* SCE as is seen in curve (a) of Figure 4.1. It is worth noting an overlap between Figure 4.1a) and Figure 4.1b) after 100 s. A similar trend can be observed for an AZ31 Mg alloy immersed in SA-(0.5–50 × 10^{-3} mol dm^{-3}) IP containing solutions (Figure 4.1b-4.1f)). For solutions with low IP content (<0.5 × 10^{-3} mol dm^{-3}) the OCP is similar to that in SA-Py solutions, but for concentrations above 50 × 10^{-3} mol dm^{-3} IP, the OCP becomes much more noble reaching -1.26 V *vs.* SCE after 10 minutes as shown in Figure 4.1f). The formation of a passive hydroxide/oxide Mg film layer on the metal alloy would be expected, in fact the formation of a salicylate magnesium chelate film has also been reported, which can further diminish the magnesium dissolution and contribute to the equilibrium at the alloy/solution interface [279]. No oscillations, indicating breakdown and reconstruction of the passive layer, were seen during the OCP measurements. The increase of the OCP with increasing concentration of the IP suggests that the IP is contributing to the passivation of the magnesium surface. It was confirmed that before attempting to growth a stable compact PPy film on the surface of an AZ31 Mg alloy, it was critical to leave the sample at the open-circuit for at least 10 minutes in the SA solution to passivate the surface. Failure to do so risk forming an incomplete PPy film.

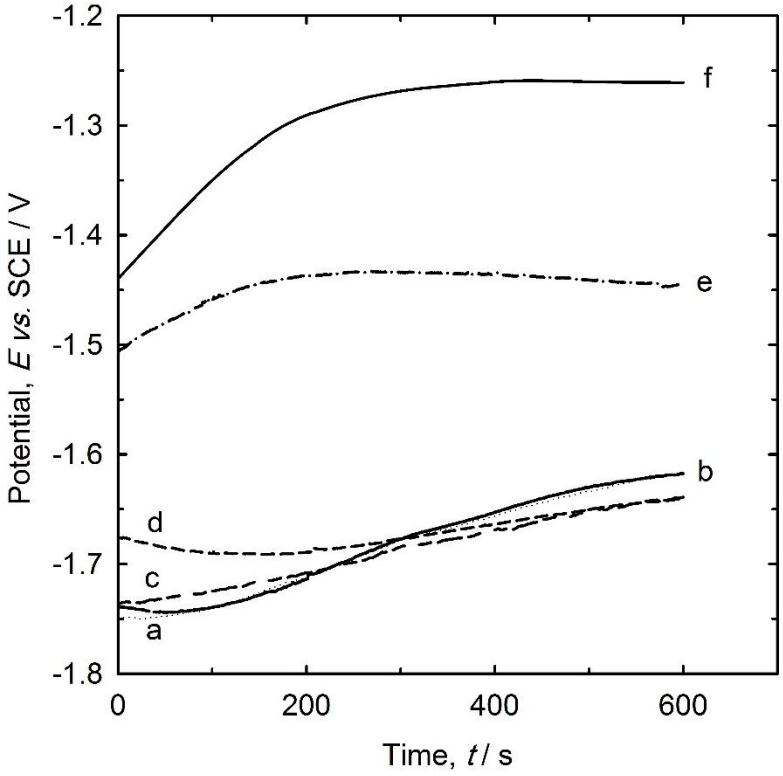

Figure 4-1: OCP *vs.* time for an AZ31 Mg alloy in 0.5 mol dm^{-3} Py, 0.5 mol dm^{-3} SA with different sodium IP concentrations a) 0, b) 0.5, c) 1, d) 5, e) 10 and f) 50 × 10^{-3} mol dm^{-3} monitored over 10 minutes.

The CVs of an AZ31 Mg alloy in three different SA containing media is shown in Figure 4.2. A freshly prepared AZ31 Mg alloy, with a 10 minutes rest time in the SA solution, case (a), shows a large oxidation peak at a potential of *ca.* -0.35 V *vs.* SCE. In this case the potential was scanned from -0.5 V *vs.* SCE, which is far away from the OCP and toward less negative potentials, but near to the oxidation of salicylate to passivate the Mg alloy. A large Mg alloy dissolution was expected, which would react with the SA in solution to form a protective magnesium salicylate film [279, 281, 282]. Previous studies based on FT-Raman spectrometry for similar systems, investigated the reaction of salicylate with other transition metals and suggested the formation of a salicylate metal chelate complex with high molecular weight and low solubility that precipitates on the metal surface [283]. Accordingly, two overall reactions describe the

formation of the magnesium salicylate ad layer on the surface of the AZ31 Mg alloy, i.e., two electron oxidation irreversible process, followed by coupled chemical equilibrium reaction:

$$Mg \xrightarrow{k_f} Mg^{2+} + 2e^- \tag{4.1}$$

$$Mg^{2+} + 2SA^- \xrightarrow{k_c} MgSA_2 \tag{4.2}$$

Where k_f and k_c are formation constant of Mg^{2+} and $MgSA_2$, respectively.Inspection of the CVs at more positive potentials reveal a less defined and extended oxidation peak at *ca*. +0.8 V *vs*. SCE, attributable to the anodic oxidation and polymerization of salicylate [279, 282, 284].

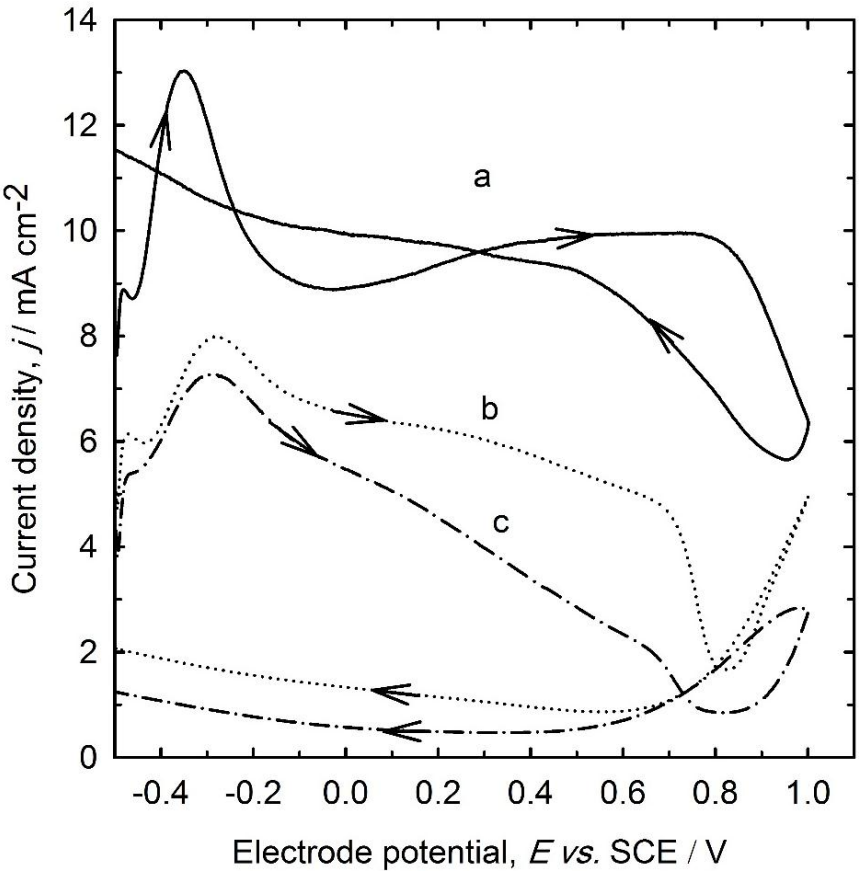

Figure 4-2: First cycle voltammogram of an AZ31 Mg alloy in: a) 0.5 mol dm^{-3} SA, b) 0.5 mol dm^{-3} SA and 0.5 mol dm^{-3} Py, c) 0.5 mol dm^{-3} SA, 0.5 mol dm^{-3} Py and 0.5 × 10^{-3} mol dm^{-3} IP. Potential scan rate of 20 mV s^{-1}.

The CVs responses recorded for SA-Py and SA-Py-0.5 IP solutions appear as cases b) and c), respectively. As in the previous SA plain solution, both new solutions exhibit a similar broad oxidation peak at a potential *ca.* -0.3 V slightly shifted to more positive potentials than for the SA solution. This can be explained in terms of the salicylate chelate layer, whose complexation constant, k_c, shifts the potential. In these new solutions, nucleation and growth of the PPy film at a potential at *ca.* 0.8 V *vs.* SCE also takes place [284, 285]. The nucleation and growth processes for PPy are evidenced by the crossing potentials at 0.8 V and 0.73 V *vs.* SCE for SA-Py and SA-Py-0.5 IP, respectively [284]. When the potential is shifted to more positive values than the PPy nucleation and growth crossing potentials, there is a rapid increase in the current due to the oxidation of the polymer and the dissolution of the underlying AZ31 Mg alloy and a sudden increase of the current at 1.0 V *vs.* SCE is reached. The two solutions seem to follow a similar trend, but a higher current density was observed for SA-Py and a more blunt reversal current wave for SA-Py-0.5 IP, indicating that less PPy film on the electrode was formed from SA-Py-0.5 IP solutions.

To further characterise the broad oxidation peak at *ca.* -0.35 V *vs.* SCE a series of cycles were recorded for the 0.5 mol dm^{-3} SA solution after a 10 minutes rest time; this is shown in Figure 4.3. The oxidation peak is now shifted to a much more negative potential, i.e., -0.75 V *vs.* SCE in comparison to the sample that did not have the 10 minutes equilibration time and does not seem to displaying any additional dependence on the number of cycles. It is likely that a gradual build-up of the passive chelate salicylate ad layer with a lower resistance at the electrode surface causes a lower potential drop resulting in the potential shift. Moreover, the CVs do not show any reduction peak during the reverse potential direction, indicating an irreversible electrochemical reaction [285].

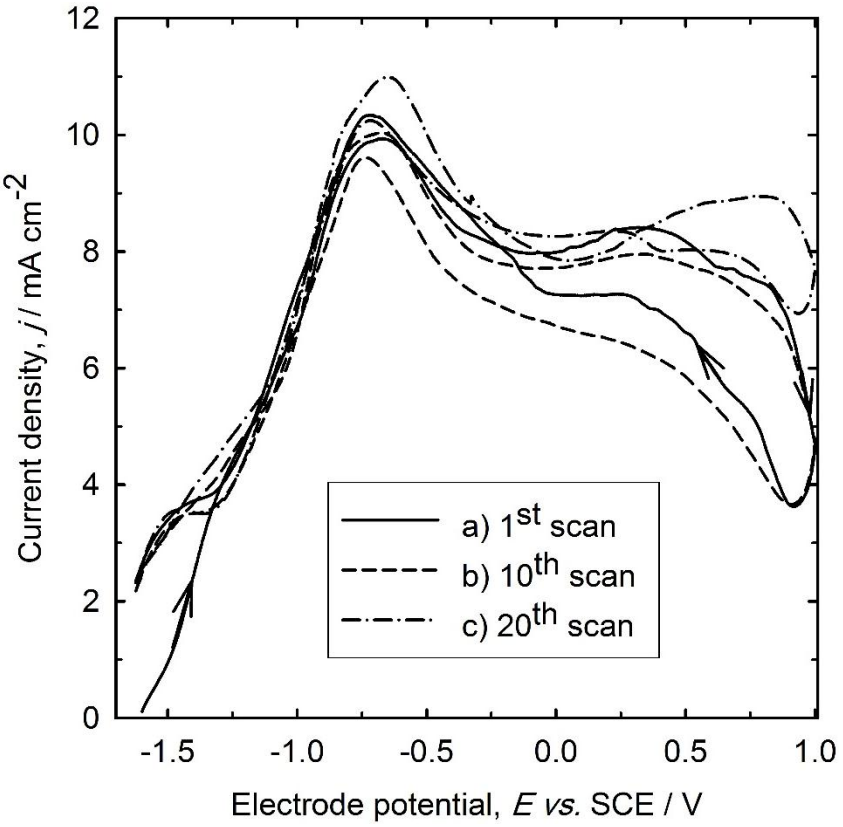

Figure 4-3: Cyclic voltammograms for an AZ31 Mg alloy in a 0.5 mol dm^{-3} SA. The potential scan starts from OCP toward positive potentials at a sweep rate of 20 mV s^{-1}. The samples were equilibrated for 10 minutes.

A series of CV for the SA solution was run at controlled potential sweep rates in Figure 4.4a. The oxidation currents peaks do not follow a linear relationship when plotted either against the square root of the scan rate or the scan rate in the range of 10-70 mV s^{-1} in Figure 4.4b. The oxidation is neither a diffusion-controlled process nor adsorption, instead, the formation of the passivating chelate layer on the alloy limits diffusion of the out coming magnesium ions and forms a stable magnesium chelate complex. The shift in the peak potentials as the scan rate increases, is consistent with a completely irreversible process [285]. One small current shoulder at 0.45 V *vs.* SCE for high potential sweep rates (>50 mV s^{-1}) can be attributed to an augmented double layer capacitance of the system.

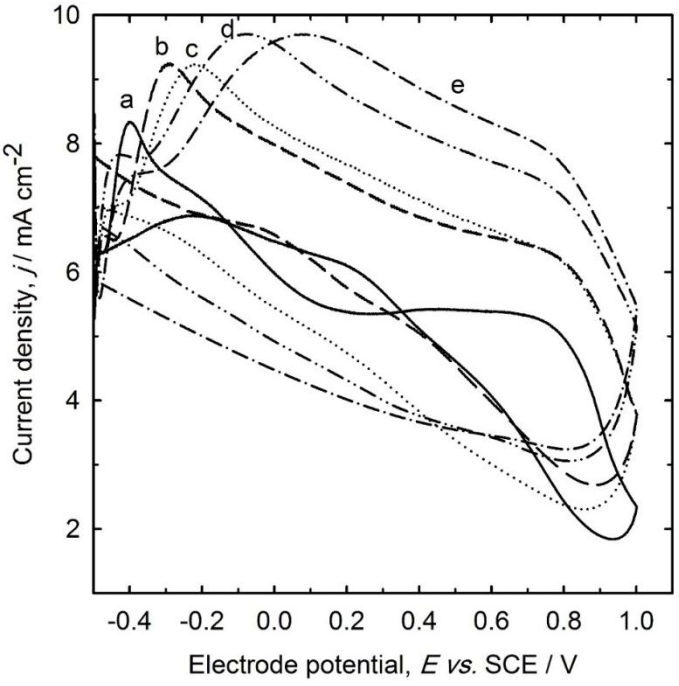

a

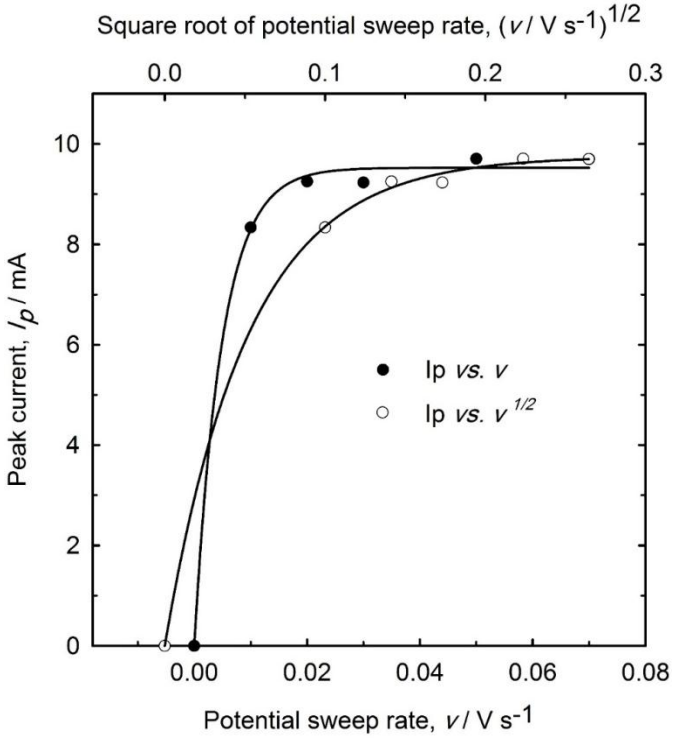

b

Figure 4-4: a) Cyclic voltammograms of an AZ31 Mg alloy in a 0.5 mol dm^{-3} SA solution obtained at different potential sweep rates: a) 10, b) 20, c) 30, d) 50 e) 70 mV s^{-1}. b) Peak current dependence on the scan rate: j_p *vs.* $v^{1/2}$ and j_p *vs.* v.

Figure 4.5a) and 5b) show a collection of CVs for SA-Py and SA-Py-0.5 IP solutions at different number of cycles. All the curves exhibit a potential crossover near +0.8 V *vs.* SCE in Figure 4.5a) and +0.7 V *vs.* SCE in Figure 4.5b). In general terms, the electrochemical behaviour detected in these solutions resembles the technique already reported in the literature for similar systems [282, 284], however with a major difference used in the current work which is the use of ibuprofine drug. Immediately after the first scan was completed, the current rapidly decreases and the subsequent potentiodynamic ongoing-waves become elliptical-like shaped. They account for the PPy growth and thickening of the polymer film. Furthermore, there is the oxidation of the AZ31 Mg alloy substrate by crevice and pitting corrosion mechanisms, that strongly increases at very positive potentials >1 V *vs.* SCE [284]. The thicknesses of the PPy films formed potentiodynamically after 20 cycles, determined by SEM and optical stereoscope measurements for SA-Py solution are *ca*. 20±5 μm, consistent with results published by other authors [284], howerer, none of the previous studies have used drug in their research papers. The current study was the first study to incorporate ibuprofen drug during the electrdeposition of PPy on AZ31 substrates from aqueous solution.

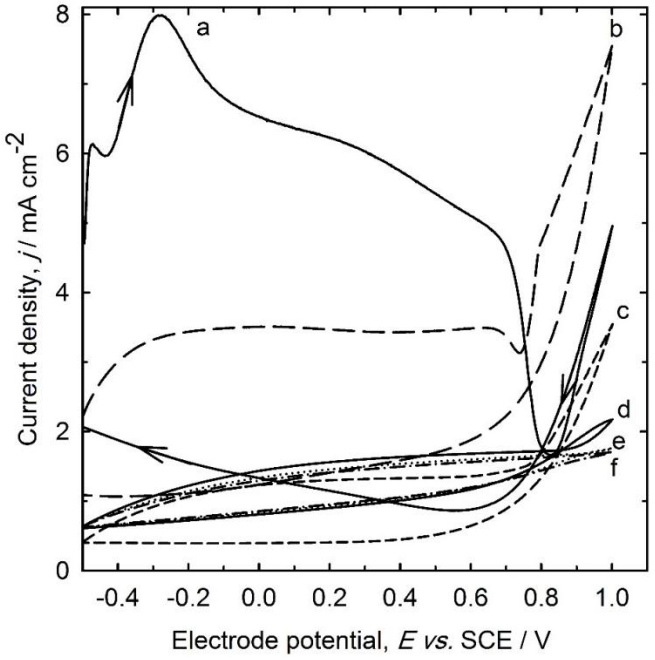

a

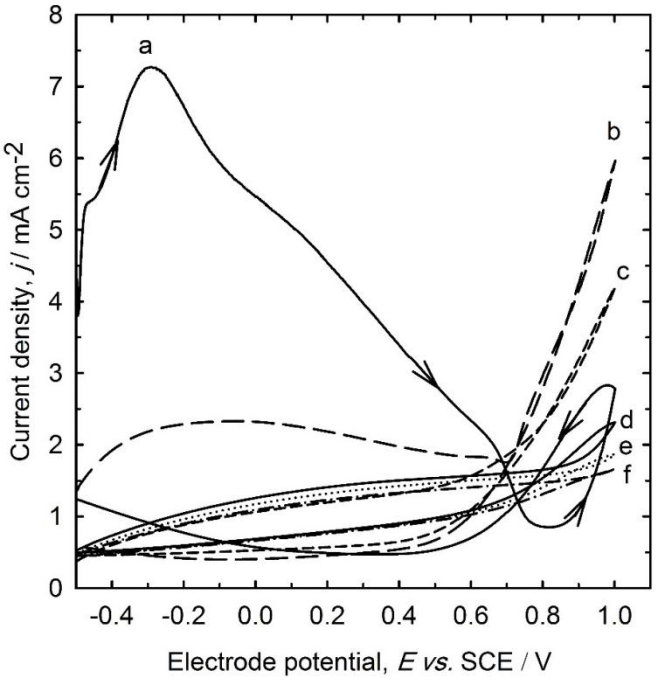

b

Figure 4-5: a) Cyclic voltammetry of an AZ31 Mg alloy in a 0.5 mol dm^{-3} SA solution over 20 cycles. b) Cyclic voltammetry for an AZ31 Mg alloy in 0.5 mol dm^{-3} SA + 0.5 mol dm^{-3} Py with 0.5×10^{-3} mol dm^{-3} IP solution over 20 cycles. In both cases the potential sweep rate is 20 mV s^{-1}.

To gain more insight on the first cycle of the CVs for SA-Py and SA-Py-0.5 IP, a series of current-transients for different applied potential steps are reported in Figure 4.6a) and 6b), respectively. Initially, all current-transients display a sharp current peak with a local minimum produced by charging of the double layer and a well-defined oxidation peak at *ca*. 20 s elapsed time. As above mentioned, the oxidation peak is due to the formation of a stable magnesium salicylate chelate film which slightly shifts to higher potentials consistent with a thickening of the film at the electrode surface.

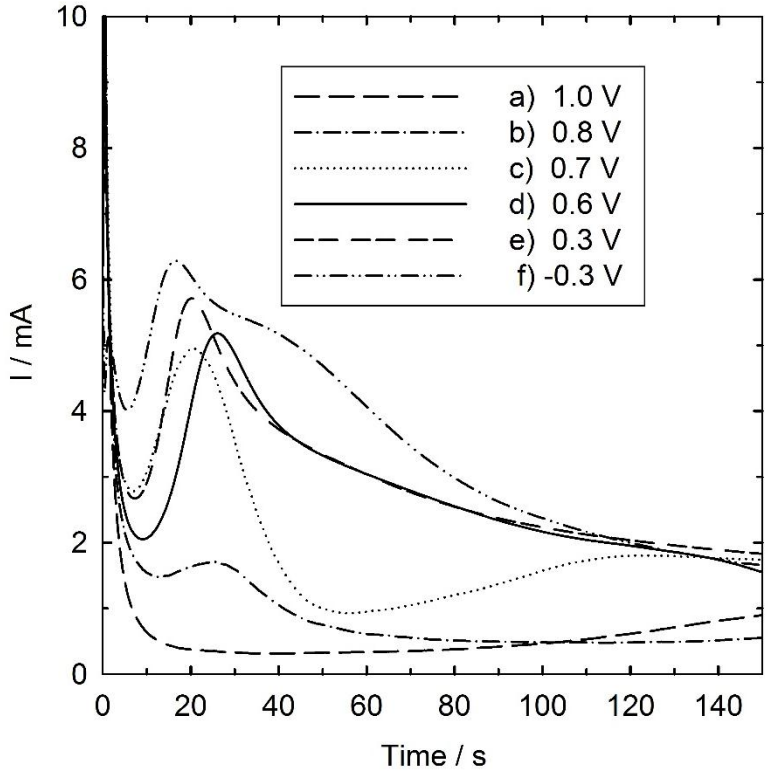

Figure 4-6a: Chronoamperometric response for an AZ31 Mg alloy in 0.5 mol dm^{-3} SA solution, a) +1.0, b) +0.8, c) +0.7, d) +0.6, e) +0.3 and f) -0.3 V *vs.* SCE.

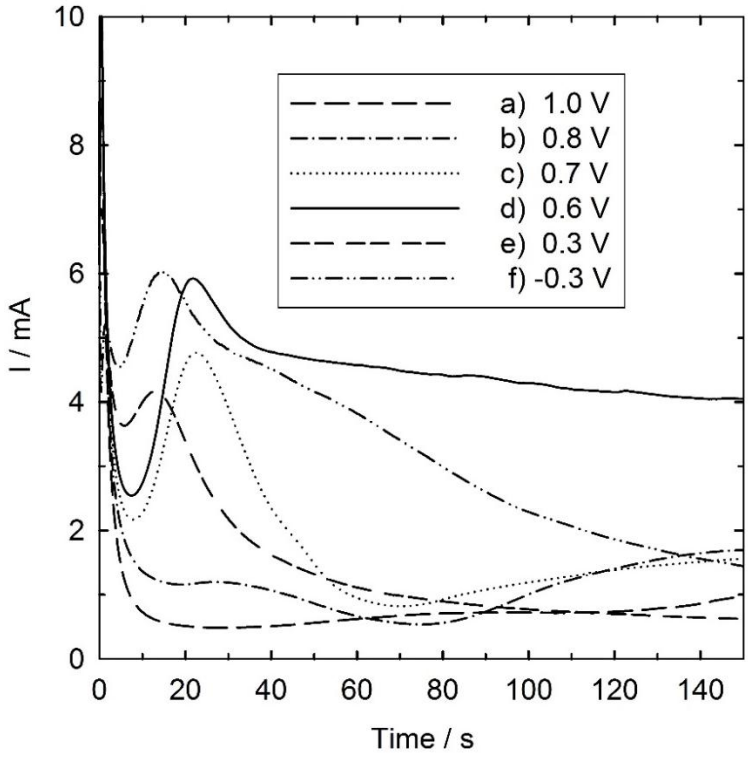

Figure 4-6b: Chronoamperometric response for an AZ31 Mg alloy in 0.5 mol dm^{-3} SA solution containing 0.5 × 10^{-3} mol dm^{-3} IP, a) +1.0, b) +0.8, c) +0.7, d) +0.6, e) +0.3 and f) -0.3 V *vs.* SCE.

For this set of potential steps, the PPy film only started to form when the potential was stepped to +0.7 V *vs.* SCE in SA-Py solution and the transient encompasses the nucleation and growth of the PPy film after 70-80 seconds in Figure 4.6a). This conclusion is drawn from the direct observation of the electrode surface by SEM micrographs and EDS analysis of each of the samples.

Figure 4.7a) shows a SEM micrograph of a sample stepped at 0.7 V *vs.* SCE in SA-Py solution displaying an incipient, globular PPy film with some worm-like decorations formed on the surface of the AZ31 Mg alloy. EDS analysis on the top of these decorations showed the presence of carbon and nitrogen expected for PPy, that further supports its formation in Figure 4.7b).

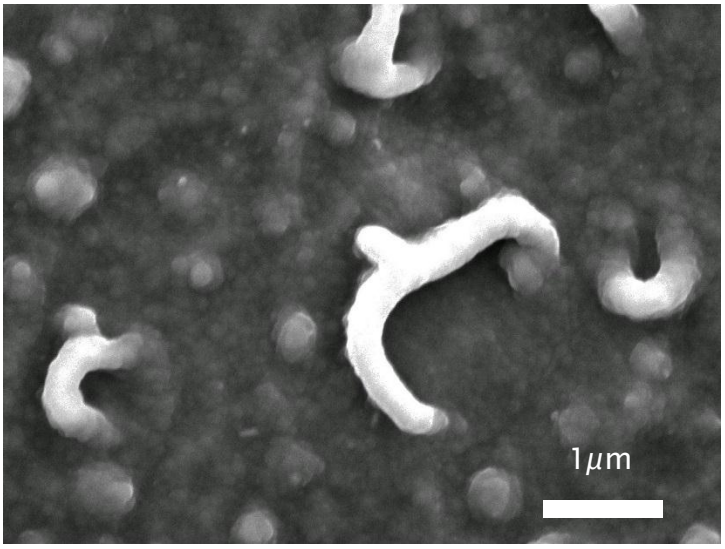

Fig. 7 (a)

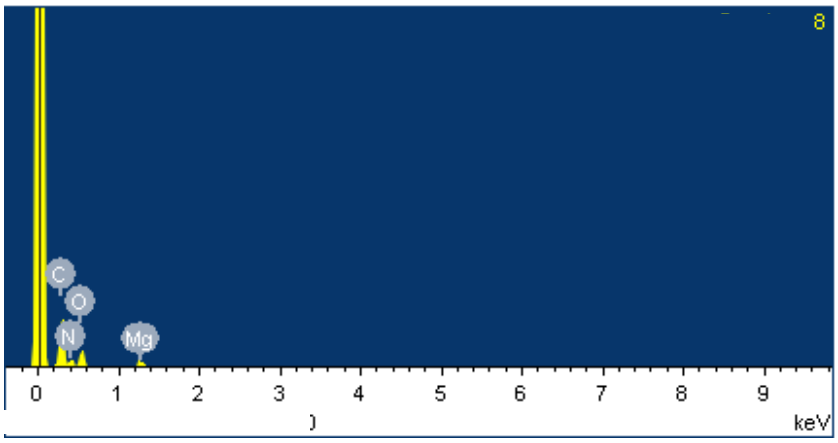

Fig. 7 (b)

Figure 4-7: a) SEM micrographs showing the globular structure and worm-like decorations for the formation of the PPy film on an AZ31 Mg alloy in 0.5 mol dm^{-3} SA and 0.5 mol dm^{-3} Py at a potential step of +0.7 V *vs.* SCE, b) EDS analysis of the sample.

From the analysis of the current transients it was not possible to separate the PPy nucleation and growth from the dissolution of the AZ31 Mg alloy substrate corrosion. Furthermore, the current transient at a +0.7 V *vs.* SCE denoted an extended oxidation peak which reached a maximum at *ca.* 120 s which was associated with the nucleation and growth of PPy on the

AZ31 Mg alloy under potentiostatic conditions in Figure 4.6a). Similar results were consistently seen in repeat trials. The oxidation peak for the salicylate layer formation vanished completely, given a feature less current *vs.* time transient for the samples stepped at potentials above +1.0 V *vs.* SCE for both solutions. These transients show a sharp increase in the current initially followed by a rapid decay which is due to the passivation of the AZ31 Alloy Mg surface [286].

4.3 Electrochemical characterisation at different concentrations of IP

The addition of IP into the solution affects the electrochemical response, structure and mechanical properties of the PPy films. Figure 4.8) and 4.9) shows a series of CVs acquired in solutions with different IP concentrations, i.e., 10 and 50 × 10^{-3} mol dm^{-3}, respectively. For PPy films prepared in solutions containing IP at 10 × 10^{-3} mol dm^{-3} concentration (Figure 4.8), the initial cycle in the CV that represents the formation of the Mg salicylate film (see Figure 4.5b)), does not appear. Therefore, it becomes evident that IP not only affects the formation of the passive salicylate adsorbed layer, but also the nucleation and growth of the PPy film. Under these conditions, the PPy films could not uniformly be coating the AZ31 Mg alloy surface. Instead, a series of randomly distributed black PPy spots with poor adherence and several cracks were formed, which readily detached from the surface revealing underlying corrosion products.

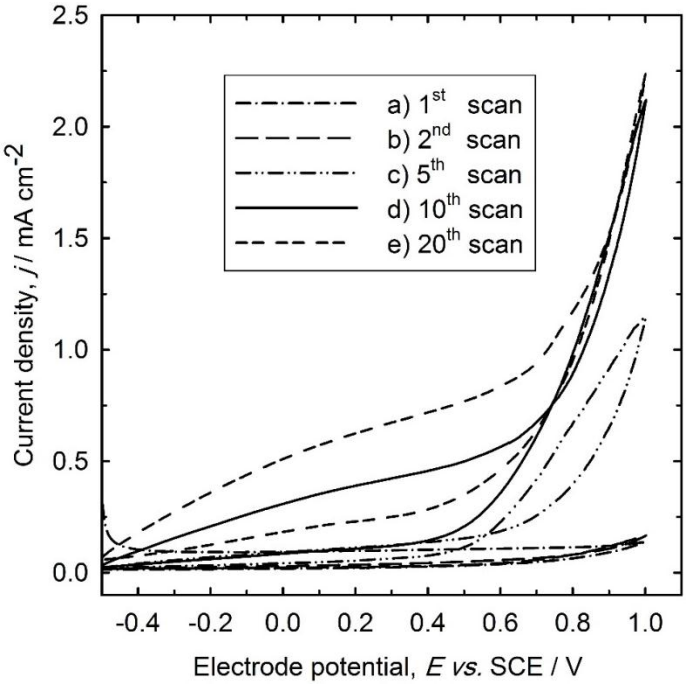

Figure 4-8: Cyclic voltammetry for an AZ31 Mg alloy in a solution containing 0.5 mol dm^{-3} SA, 0.5 mol dm^{-3} Py with 10×10^{-3} mol dm^{-3} IP solution for 20 cycles at a potential sweep rate of 20 mV s^{-1}.

Additional increase in the IP concentration up to 50×10^{-3} mol dm^{-3} in Figure 4.9) completely inhibited the formation of the PPy film. The salicylate layer was absent and the current density was substantially reduced (>10%) without any potential crossings that denote the PPy nucleation and growth in Figure 4.9).

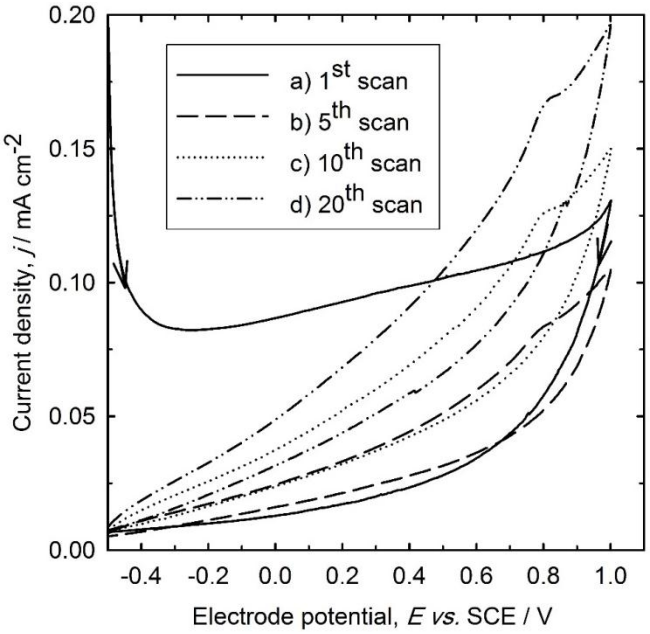

Figure 4-9: Cyclic voltammetry of an AZ31 Mg alloy in a 0.5 mol dm^{-3} SA with 0.5 mol dm^{-3} Py and 50×10^{-3} mol dm^{-3} IP solution over 20 cycles at a potential sweep rate of 20 mV s^{-1}. In both cases the electrode was immersed in the solution for 10 minutes before starting.

SEM micrographs of PPy films prepared in SA-Py and SA-Py-0.5 IP solutions at low and high magnifications are shown in Figure 4.10a-d). At low magnification, films prepared in SA-Py solutions are black, compact, crack-free and adherent in Figure 4.10a). At high magnification, Figure 4.10b), the SEM micrographs reveal a globular surface morphology characteristic for PPy films [284]. After the addition of ibuprofen to the solution, low magnification SEM micrograph in Figure 4.10c) shows an uneven surface with some scattered pits and cracks usually formed after rinsing the sample in sodium chloride solutions and drying in air. In some cases, the PPy films rinsed in a NaCl solution cracked and detached from the surface. This is probably due to the interchange of uploaded ions (IP and SA) with chloride ions that causes volume shrinkage, generating stresses which tear the film. Higher magnification SEM images of PPy films uploaded with IP films displayed a needle-like structure with sizes in the order of 3 µm randomly distributed on the surface in contrast to the globular structure observed for ibuprofen-free solutions in Figure 4.10b). The average film thickness reached for the samples after 20

cycles was *ca*. 20±5 μm for the films formed in SA-Py and SA-Py-IP solutions measured by SEM and optical microscope for cross sectioned samples.

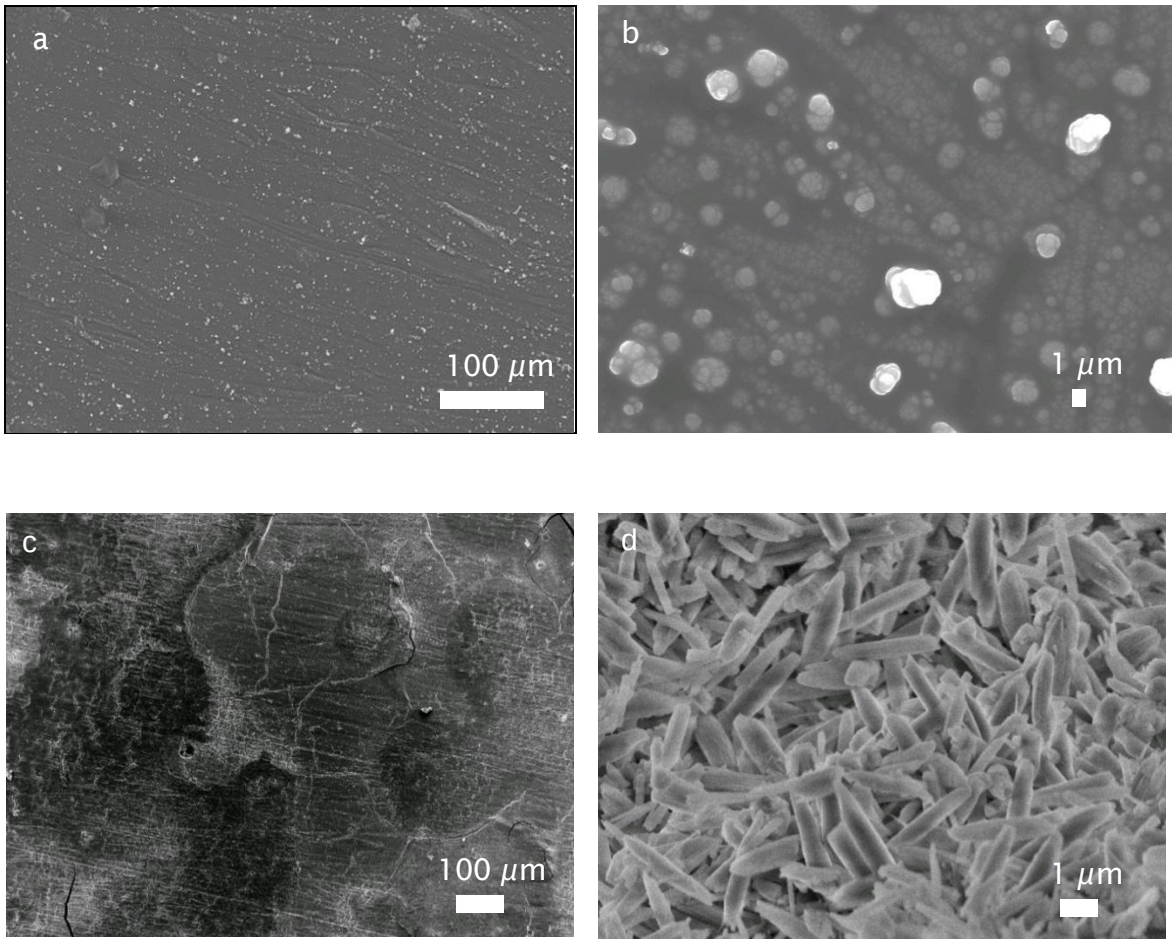

Figure 4-10: SEM micrographs of the surface of the PPy film formed electrochemically on an AZ31 Mg alloy in 0.5 mol dm^{-3} SA and 0.5 mol dm^{-3} Py (a)-(b) and 0.5 mol dm^{-3} SA, 0.5 mol dm^{-3} Py and 0.5 × 10^{-3} mol dm^{-3} IP (c)-(d) by cyclic voltammetry in a potential range of −0.5 to 1 V *vs.* SCE at a scan rate of 20 mV s^{-1} for 20 cycles.

Additional optical photographs taken of a PPy film prepared at higher IP concentrations (>5 × 10^{-3} mol dm^{-3}) are shown in Figures 4.11a)-d). A pitted surface with round pieces of polymer film delaminated from the surface with the remains of corrosion products underneath can be seen in Figure 4.11a). Some scattered pits show an optically reflective AZ31 Mg alloy substrate

in Figure 4.11b) and volcano-like craters with expelled material are also visible and are assumed to be salicylate magnesium chelate coming from the substrate alloy in Figure 4.11c). Some large cracks across the film with the presence of some salicylate chelate adsorbed layer underneath the PPy film were also observed in Figure 4.11d).

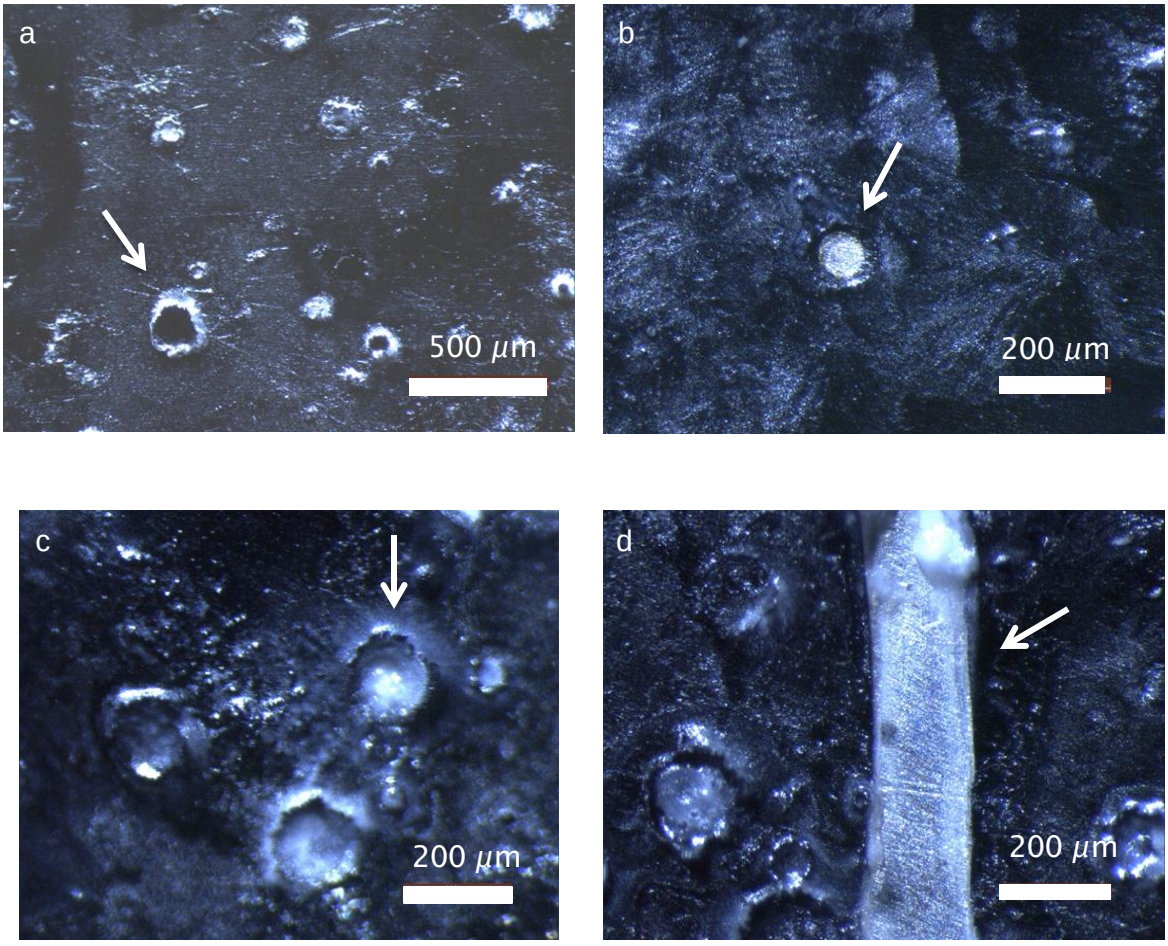

Figure 4-11: Optical images of a PPy film on an AZ31 Mg alloy prepared in 0.5 mol dm^{-3} SA, 0.5 mol dm^{-3} Py and 10×10^{-3} mol dm^{-3} IP by cyclic voltammetry in the range of -0.5 V to 1 V *vs.* SCE at a potential sweep rate of 20 mV s^{-1} for 20 cycles. Arrows show pits and salicylate magnesium chelate.

4.4 IR characterization

FTIR spectra of the AZ31 Mg alloy surface and the PPy films with and without IP are presented in Figure 4-12. The AZ31 Mg alloy surface showed two broad small peaks in the range of 1300-1700 cm^{-1}. For the PPy coated films, the FTIR spectra has characteristic peaks at 1300 cm^{-1}, 1185 cm^{-1} and 1035 cm^{-1} [265]. A comparison with the FTIR spectra with the presence of SA shows little difference, likely since IP becomes undetected at this concentration level [287].

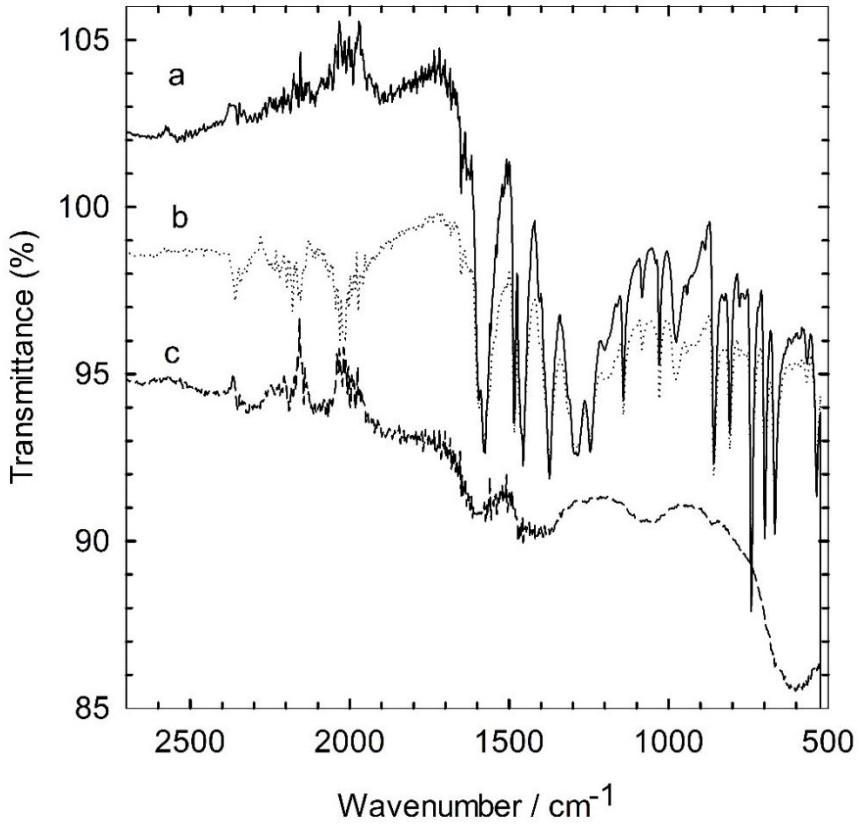

Figure 4-12: FTIR spectra of a) PPy film electrodeposited on an AZ31 Mg alloy by cyclic voltammetry in a solution 0.5 mol dm^{-3} Py, 0.5 mol dm^{-3} SA and 0.5 x 10^{-3} mol dm^{-3} IP, (b) in the absence of IP and (c) an AZ31 Mg alloy surface.

4.5 Drug uploading and release

As previously mentioned, both SA and IP are uploaded into the PPy film during its nucleation and growth to balance the charge of the PPy backbone. The amount of PPy deposited potentiodynamically on 1 cm^2 area of the AZ31 Mg alloy was 3.0×10^{-3} g [251]. One of the variables investigated in this work is the IP loading capacity without inhibiting the nucleation and growth processes or greatly affecting the mechanical properties of the PPy film. PPy films deposited potentiodynamically (as mentioned earlier in the section 4.2) on 1 cm^2 AZ31 substrate. The polymerization electrolyte consisted of a mixture of 0.5 mol dm^{-3} Py, 0.5 mol dm^{-3} SA and IP with concentrations, i.e., 0.0, 0.5, 1.0 and 5.0×10^{-3} mol dm^{-3}. Figure 4.13 shows a horizontal bar plot illustrating the experimental results of the liberation of the IP when the PPy film was synthetized in the presence of different concentrations of IP. The left hand side shows the concentrations of IP (i.e., 0.0, 0.5, 1.0 and 5.0×10^{-3} mol dm^{-3}) in the solution used to prepare the films in the presence of SA-Py. On the right hand side, the figure is shown the total amount of IP released in 0.9 wt. % NaCl after 200 hours. These amounts vary from 0 to 414×10^{-6} g for each of the IP concentrations investigated, which correspond to 0 and 138×10^{-3} g g^{-1} (IP/PPy) respectively. Representative values for the amount of dopant in PPy films range from a few $\times$ 10^{-9} g to several $\times$ 10^{-3} g, either for nanostructured or chemically assisted drug uploading in PPy films [113, 280]. One example is the anticancer drug neurotrophin-3, which can be successfully incorporated in PPy films by the so called two-layered approach on gold coated Mylar at a level of 25×10^{-9} g cm^{-2}, for thin films ranging from (3.6 to 26) $\times$ 10^{-6} m thick [278]. Another example is the uploading of methotrexate (MTX), a major chemotherapeutic agent to treat different types of cancer, on the hydrophobic PPy film by adding cetylpyridinium (CPY), a cationic surfactant, which modifies the hydrophobicity of the PPy and improves the efficiency of MTX doping, with a loading capacity of 24.5×10^{-3} g g^{-1} of PPy [280]. A similar procedure

has been applied to enhance the loading capacity of chlorpromazine (CPZ) by the use of heparin, a large molecule, which enables the incorporation of 191 ± 7 × 10^{-3} g on a Pt disc of 0.126 cm^2 coated with an 8 ± 2 × 10^{-6} m thick PPy film [280]. The electrochemical synthesis methods that have been employed, e.g., galvanostatic, potentiostatic or potentiodynamic, as well as the polymer morphology, dopant chemical properties or the incorporation of other additives contribute significantly to the loading capacity of the PPy film [271].

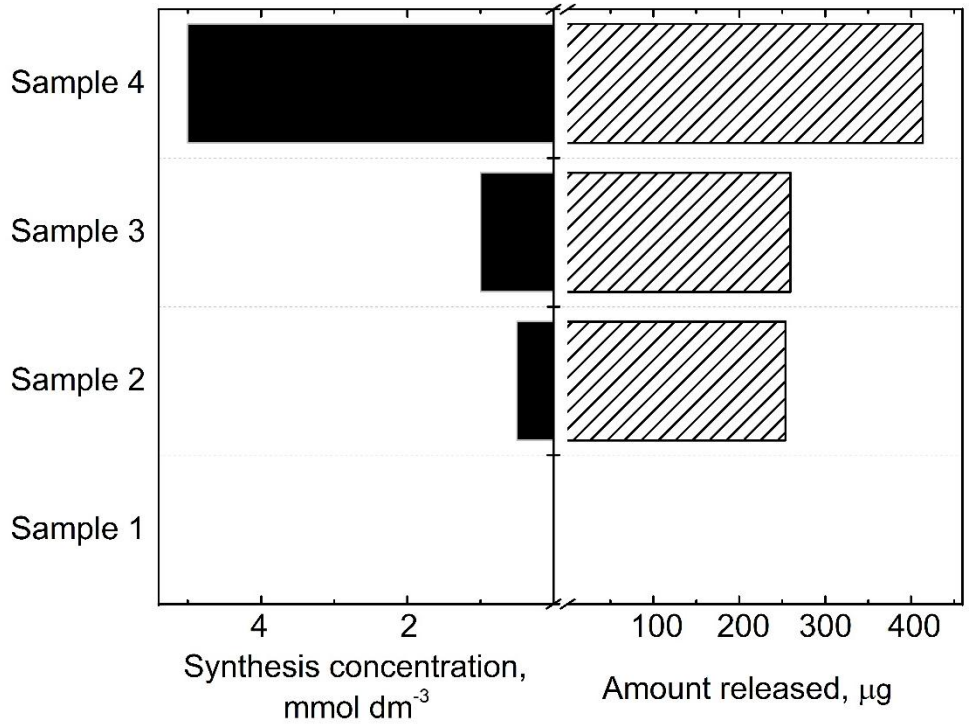

Figure 4-13: Left hand side identification number *vs.* concentration used to prepare the PPy film and right hand side total amount of IP released for the film for a period of 200 h in 0.9% wt. NaCl solution.

In one set of experiments as mention earlier, the rate of IP release from PPy films was studied. IP is released from the PPy film on the AZ31 Mg alloy by galvanic coupling immersed in a 0.9% NaCl solution. For these experiments, 1 cm^2 of the 250 × 10^{-6} m thick AZ31 Mg alloy front section was coated with the 20 ± 5 μm PPy film and the bare back of the sample was

exposed to the NaCl solution. Figure 4.14 shows a release profile curve of mass fraction of drug released, defined as the ratio between the mass released at each time and the total amount released for a large period of time, as a function of time. For short periods of time (<50 minutes), the rate of release was high and tends to level off with time. This result is consistent with previous reports in the literature denoting a rapid release at the initial stages for the drug dexamethasone (DEX) in higher 10% wt. NaCl solutions [113]. The morphological characteristics of the polymer, e.g., globular or needle-like obtained can also lead to a different active area affecting the amount of drug released and the mechanical actuation of the film and other conformational changes in the polymer structure [270]. Furthermore, the triggering signal, which in this case i) largely dependent of the galvanic coupling, is determined by the corrosion processes in the NaCl solution [113]. Self-propelled systems rely on the dissolution of the substrate metal to reduce the polymer film and release the incorporated drug. Any through porosity or cracks in the PPy film can also provide a pathway for chloride ions to diffuse through to the substrate metal and promote crevice and pitting corrosion in the PPy/AZ31 Mg alloy interface. This increases the corroding area above the fixed area at the back of the sample. Moreover, it also accounts for a large scattering in the data for the release fraction at larger periods of time, where the error bars enlarge substantially likely due to the unpredictable corrosion rate (see Figure. 4.14 for t >250 min). This is consistent with previous results reported in the literature which shows large scattering at longer times, for self-propelled systems [113].

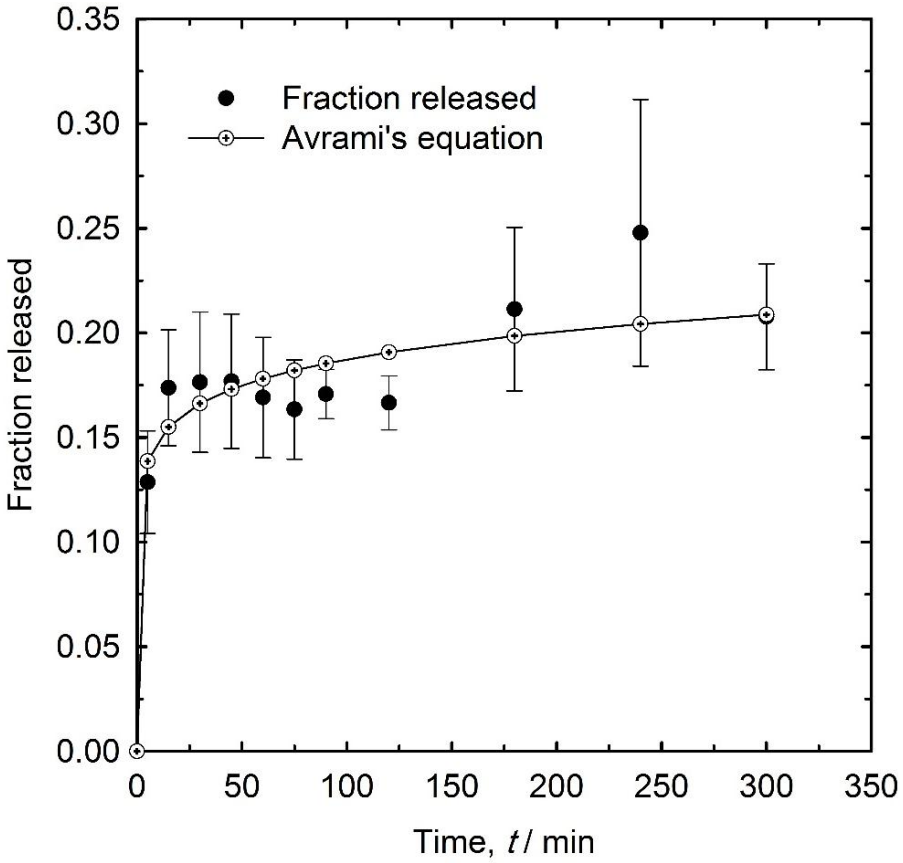

Figure 4-14: Mass fraction of IP released from a 1 cm^2, ≈ 20 x10^{-6} m thick PPy film grown in 0.5 mol dm^{-3} SA, 0.5 mol dm^{-3} Py and 0.5 × 10^{-3} mol dm^{-3} IP. Drug delivery was performed in a 0.9% wt. NaCl solution at room temperature (295 K).

For samples grown at concentrations of 0.5 × 10^{-3} mol dm^{-3} IP, Avrami's equation (4.3), is used as a model to represent the release profile. Avrami's equation was initially proposed to analyse and predict crystallization processes, but it can also fit well to diffusion controlled and potential-assisted drug release data, particularly for PPy in salicylate media and different types of drugs [280, 288, 289]. Both Avrami's parameter, *n*, and the release constant, *k*, are obtained from the slope and intercept of the Avrami plot of ln[-ln(1-*X*)] *vs.* ln *t*.

$$X = 1 - k\exp(-t^n) \tag{4.3}$$

According to the literature, for diffuse controlled drug release systems, the Avrami parameter, *n*, varies from 0.54 to 1 (first order), depending on the contribution of diffusion to the drug release [280, 288, 289]. For a self-propelled release, the release constant, *k*, is equal to 0.125, which is within the reported values for potential-assisted release processes of ionic drugs, but the Avrami parameter, *n*, kinetic order parameter, is equal to 0.11, much smaller than values reported in the literature [280, 289]. Besides these differences, Avrami's equation describes the trend of the experimental data obtained for the self-propelled IP release from PPy films. For self-propelled release systems the contribution of both potential and diffusion in the release processes can be expected due to potential variations across the film [270].

4.6 Depth-sensing indentation (DSI)

The mechanical properties of the PPy films are dependent on the chemical structure (or related to electrosynthetic condition), molecular size, dopant ion concentration and related electrosynthetic conditions [272, 273]. To determine the effect of IP in the PPy film, a series of 20 indentations along randomly selected sampling lines were performed on IP-free and IP-loaded PPy films. Figure 4.15 shows load-displacement curves obtained from PPy films uploaded with different amounts of IP. For each sample, the 3 mN load resulted in a different depths of penetration, with the maximum depth of the indents in the 5 x 10^{-3} mol dm^{-3} doped sample being less than 1 µm, the indentation interaction volume being confined to the PPy film and not influenced by the substrate.

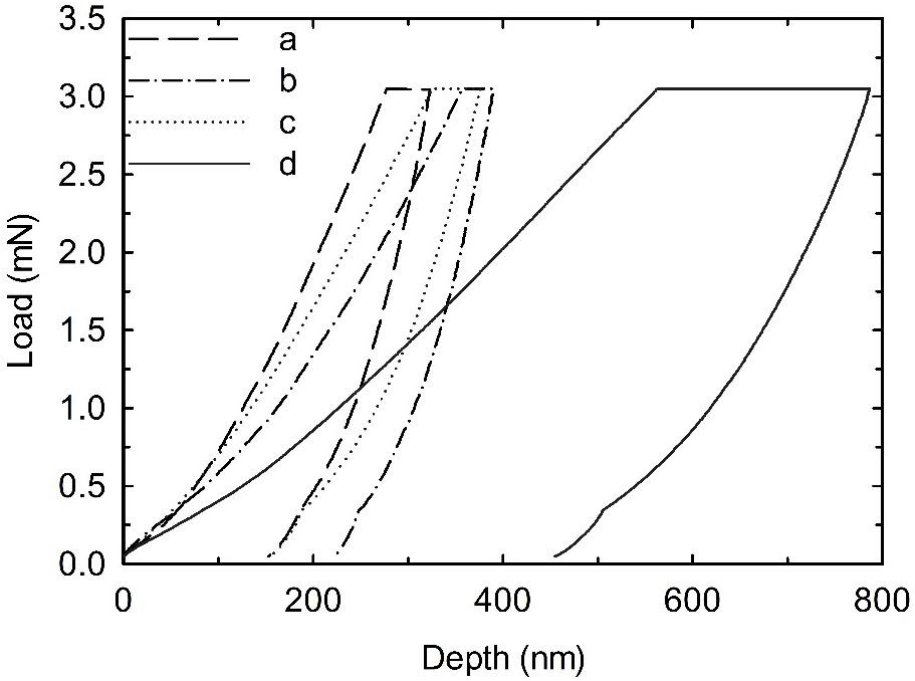

Figure 4-15: Load-displacement curves for PPy films prepared at different IP concentrations: a) 0, b) 0.5, c) 1.0 and d) 5 x 10^{-3} mol dm^{-3} at a constant load of 3 mN.

Table 4.1 summarizes the average hardness (H), reduced modulus (E_r) and the ratio between H and E_r of the films investigated, as well as the concentration of IP in solution and contained in the PPy film. Comparison of the mechanical properties of IP-free PPy films with those containing large amounts of IP (414 × 10^{-6} g), showed a decrease in the H and E_r ratio of 54%, 40% respectively and an H/E_r increase of 66%, denoting a softer more elastic material. Theoretically, the addition of IP into the PPy film increases the free space in the polymer matrix and modifies the structure of the PPy film [272, 273]. Sodium ibuprofen is a large molecule with a single charge, when added into the PPy matrix it acts as an additional ion dopant along with the sodium salicylate ions to balance the polymer charge. The size of the ibuprofen molecule however results in an increase in the gap between the polymer chains, reducing the strength of the attractive forces between them making polymer chain motion and deformation easier than IP-free polymer films [272, 273].

Table 4-1: Mechanical properties of PPy films electrodeposited on AZ31 Mg substrate.

Concentration of IP, $\times 10^3$ mol dm^{-3}	**Release of IP, $\times 10^6$ g**	**Hardness (H), GPa**	**Reduced modulus (E_r), GPa**	**H/E_r ratio**
0	0	0.37 ± 0.09	10.2 ± 1.72	0.03
0.5	254	0.29 ± 0.07	9.4 ± 2.14	0.03
1	260	0.32 ± 0.04	7.8 ± 0.76	0.04
5	414	0.20 ± 0.02	4.1 ± 0.36	0.05

As previously shown *vide supra*, in the absence of IP, PPy films in SA media developed a uniform, compact, adherent, globular-like structure (Fig. 4.10a)-b)). In contrast, the addition of ibuprofen into the PPy film produces a less compact, less adherent, needle-like structure in Fig. 4.10c)-d). There are reports in the literature concerning the role that dopant ions play in PPy in terms of their effects on molecular conformations, charge location and structural defects in the polymer chain [277, 290]. Usually, ion dopants induce changes in the polymer conformation that result in either a better alignment or increased misalignment of the polymer chains and contribute to additional packaging or unpacking of the polymer matrix [290]. The mechanical properties of the PPy films can be also modified by the electrosynthesis method used to prepare the film or by additional heat treatments [274, 280]. This provides the opportunity to prepare films which are optimized in terms of their elasticity for specific purposes, such as a more corrosion protective films or more reliable drug delivery systems.

4.7 Summary and Conclusions

The IP loading capacity in the PPy film is tunable for a specific therapeutic or other application. Here, the amount of IP incorporated into the PPy film was higher than that reported in the literature for other drugs. By adding IP to the polymerisation solution, both the passivation of the AZ31 Mg alloy and the properties of the obtained PPy film are altered. The AZ31 Mg alloy displaces to more noble potentials and the structure and morphology of the PPy film is affected when the IP is added. A transition from a globular to needle-like surface morphology is observed by increasing the amount of IP in the PPy film. This also affects the IP release and increases the possibility of crevice and pitting corrosion at the PPy/AZ31 Mg alloy interface. For even higher IP loadings, an upper limit is reached where a continuous, adherent PPy film cannot be prepared; instead, a series of randomly distributed black, soft, poorly adherent, patches are produced. An effect that cannot be attributed to the rapid dissolution of the AZ31 Mg alloy, is the modification of nucleation and growth of the PPy film.

The amount of IP released from PPy uploaded films is high at quaite short times; consistent with reported data in the literature for other drugs in self-propelled systems. For a longer time, a large scattering in the release data appears to result from the breakdown of the polymer film and the occurrence of crevice and pitting corrosion processes at the PPy/AZ31 Mg alloy interface. Avrami's equation provides an approximate fit to the experimental release data, but the values for the release constant and the exponent of Avrami's equation deviated from the values commonly reported for processes dominated either by diffusion or potential-controlled. Most of the IP incorporated in the film produces substantial changes in the mechanical properties of the PPy when compared with IP-free PPy films. Up to 54% reduction in H, 40% reduction in, E_r, and an increase of 66% for its ratio was observed. An increment of the polymer free volume is the major cause for diminishing the mechanical properties of the PPy film.

Chapter 5: Release of MB and FSS Molecules from PPy Films

The aim of this chapter is to investigate the use of PPy films as a delivery system for methylene blue (MB) and fluorescein sodium salt (FSS) dyes. The two dyes has been particularly chosen for the following reasons; they can be traced easily in the release solution; they have different charges which makes it easy to compare with the release of different cationic and anionic drugs.The PPy films are synthesised electrochemically using CV and galvanostatic methods. In addition, the influence of the presence of the titanate nanotubes (TiNT) on the polymerisation solution on the uptake and release of the dye molecules from the polymer films as well as the effect of the variations of the doping anions is investigated. The effect of the use of stimulation potentials on the molecule's release rate is also examined.

5.1 Polymer synthesis using a galvanostatic method for methylene blue release

PPy-MB films were synthesised from an electrolyte containing 0.1 mol dm^{-3} Py, 0.025 mol dm^{-3} oxalic acid as dopant, and 0.5 x 10^{-3} mol dm^{-3} MB in the presence and absence of 1 mg mol^{-1} TiNT. The films were electro-synthesised galvanostatically at various current densities (0.2, 0.3, 0.4, and 0.7 mA cm^{-2}) for 10 min. Figure 5.1 illustrates the potential *vs.* time curves during the electropolymerisation of the PPy-MB film on stainless steel electrodes (surface area 1 cm^2) at different galvanostatic current densities. The galvanostatic polymerisation of Py on stainless steel electrode can be divided into two stages, as shown in Figure 5.1. In the initial stage (I), there is a passivation and formation of insoluble crystalline ferrous-oxalate layer on the electrode surface, as described by equation (5.1) [259, 291], followed by the deposition of PPy.

$$Fe^{2+} + C_2O_4^{2-} + 2H_2O \leftrightarrow FeC_2O_4\ [2H_2O]. \quad (5.1)$$

The observed potential peaks at short times, indicated the initial nucleation of PPy as polymerisation begins. The electrode materials have a great effect in the first stage. For example, a decomposition of the ferrite from the substrate surface occurs before the formation of the passive layer in case of using a carbon steel working electrode. The polymerisation process continued in Stage II and the polymerisation potential decreased because the Py oxidised more easily on the PPy surface than the electrode surface reaching a constant value at each applied current [291] reaching a constant value at each applied current.

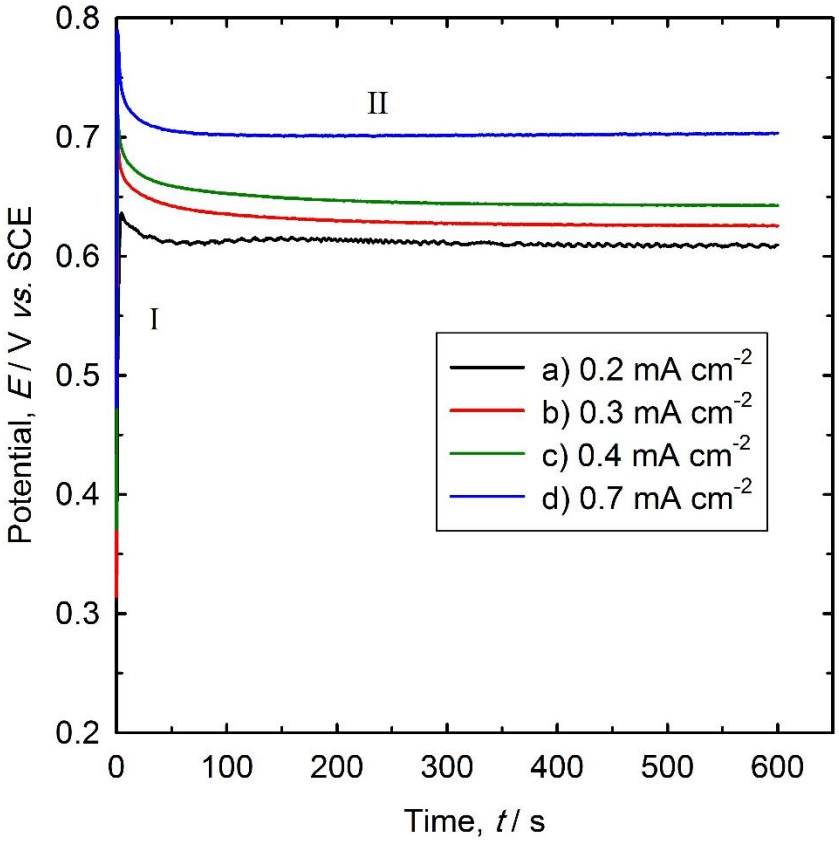

Figure 5-1: Chronopotentiogram for the galvanostatic polymerisation of PPy-MB films grown from a solution containing 0.1 mol dm^{-3} Py, 0.5 x 10^{-3} mol dm^{-3} MB, and 0.025 mol dm^{-3} oxalic acid at current densities of (a) 0.7, (b) 0.4, (c) 0.3 and (d) 0.2 mA cm^{-2} for 600 s on 1 cm^2 stainless steel substrate.

At a deposition current density of 0.2 mA cm^{-2}, the evolved potential rapidly peaked at 0.64 V *vs.* SCE, thereby indicating that nucleation initiation (the effect of double layer charging colud also be contributed), and then the potential stabilised quickly to 0.61 V *vs*. SCE, where it remained for the duration of the polymerisation. The observed peak indicated the initial nucleation of Py monomers as polymerisation began. As the deposition current increased, the working electrode potential also increased, as expected. When the applied current density was 0.3 mA cm^{-2}, the potential rose sharply to 0.71 V *vs*. SCE and then took approximately 100 s to reach a stable potential of approximately 0.63 V. The electrode potential reached a maximum value of 0.73 V *vs*. SCE and eventually reached a steady-state value of approximately 0.64 V *vs*. SCE when the current density of 0.4 mA cm^{-2} was used. When the current was further increased to 0.7 mA cm^{-2}, the potential increased to approximately 0.79 V *vs*. SCE after a short time and then stabilized at approximately 0.7 V *vs.* SCE. The potential increased with the increase in the applied current density, because more electrons are released from the electrode surface and could not be compensated immediately due to the slow reaction of the monomer oxidation. The obtained polymerisation potentials were matched with those reported in the literature, which start at more than 0.5 V *vs.* SCE approximately [292]. It should be noted, however the polymerisation potential is influenced by certain parameters, including the pH of the polymerisation solution, the applied current density, the concentration of Py monomer, the nature of the doping anions and the electrode materials.

CV analysis of the deposited PPy-MB films was conducted in 20 ml (0.9 wt%) NaCl solution to observe the electrochemical response for the obtained films in the medium that would be used for releasing the MB. The obtained CVs of the PPy films deposited at different current densities was conducted at a sweep potential scan rate of 50 mV s^{-1}, between -0.28 and 1.2 V *vs.* SCE (Figure. 5.2). The films are characterised by wide oxidation and reduction waves, with

no clear reduction or oxidation peaks. The positive currents rose without reaching a peak up to a potential of 1.2 V *vs.* SCE, and there was a slight difference observed in the films' electroactivity. The film that electrodeposited at an intermediate current density of 0.3 mA cm^{-2} shows the best electroactivity as compared with the other films. Therefore, the current density of 0.3 mA cm^{-2} was chosen to conduct the next experiment. The use of higher current densities may cause overoxidation of the conducting polymer, and overoxidation has unfavourable irreversible effects on the polymer structure and properties. Overoxidation causes defects along the polymer chain and breaks the electronic conjugation owing to the hydroxyl or carbonyl group introduced into the Py unit at high potential [293-296]. This influences the electroactivity of the polymer. In addition, it has been reported that a brittle polymer film and could be easily peeled off from the substrate at a higher current [293-296].

A current density of 0.3 mA cm^{-2} was passed during 1600 s polymerisation of Py in an aqueous solution containing 0.1 mol dm^{-3} Py in 0.025 mol dm^{-3} oxalic acid, and 0.5 x 10^{-3} mol dm^{-3} MB. Given that the area of the electrode is 1 cm^2; the total charge passed was 480 mC. The theoretical thickness of the obtained films would be 2 μm, considering that a charge of 24 mC cm^{-2} corresponds to form a 0.1 μm film based on the findings in existing literature that the PPy density equals 1.5 g cm^{-3} [251, 297]. A homogenous black PPy film was formed over the working electrode. The obtained film was cleaned with 0.1 x 10^{-3} mol dm^{-3} NaCl solutions for five minutes to eliminate any loosely bonded MB and Py monomer before the release experiments were conducted.

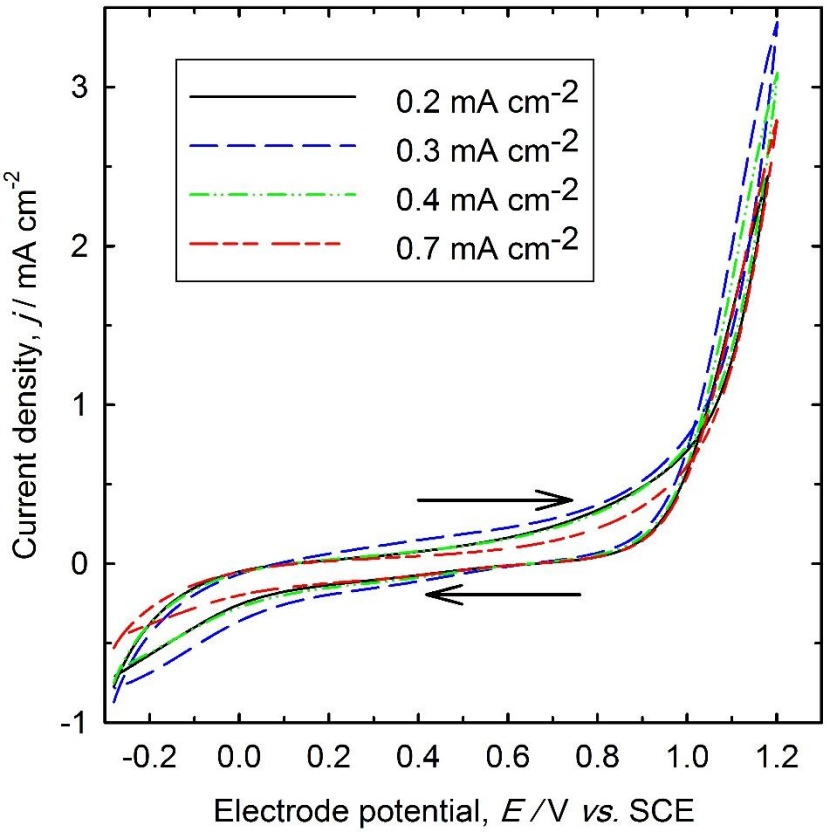

Figure 5-2: CV of PPy-MB films grown for 900 s at 0.2 mA cm^{-2}, 0.3 mA cm^{-2}, 0.4 mA cm^{-2} and 0.7 mA cm^{-2} in 0.9 wt% NaCl at a scan rate of 50 mV s^{-1} *vs.* SCE on 1 cm^2 stainless steel electrode. The direction of the potential sweep is indicated by arrows, and the fifth scan is plotted for each film.

5.2 Methylene blue open circuit potential measurements

A CV analysis of the obtained PPy-MB films was conducted in 0.9% NaCl aqueous solution to observe the oxidation and reduction potential of the polymer film in a medium that would be used for the MB release. The PPy-MB film was swept between -0.3 and 1.2 V *vs.* SCE at a sweep rate of 50 mV s^{-1}. The CV curve shows wide oxidation and reduction waves with no clear reduction or oxidation peaks (Figure 5.3), which may indicate low electroactivity of the formed films [298]. The anodic currents begins rising at a potential of 0.5 V *vs.* SCE, indicating the oxidation of the PPy-MB film. The current density started to decline at a potential of 0.45 V *vs.* SCE during the backward cycle due to the reduction of the polymer film. The decrease of

the film electroactivity may have been caused by the structure and the surface roughness of the formed film. It has been reported that the use of oxalic acid leads to the formation of a strong non-porous adherent PPy film with low surface roughness, as compared to other PPy salts [299]. Saidman [300] reported that the tight morphology of PPy doped with SO_4^{2-} restricts the transfer of SO_4^{2-} and the solvated cation. Moreover, the ionic resistance of the film doped with a divalent anion is much larger than that doped with monovalent anions due to the strong ion-ion interaction between the polymer chains and the divalent ion [301]. Further, the characteristics of the conducting polymers such as the structure, conductivity and redox switching is heavily influenced by the dopant anion [298]. In addition, the electronic interaction between the doping anions and conducting polymer chain is affected by the cation which is incorporated during the polymerisation results in changing the polymer structure and morphology [302]. A limited number of studies consider the ion transfer from PPy doped with a divalent anion system [303], and to the best of our knowledge, the ion transfer from the PPy-MB film doped with oxalic acid is not reported in the literature and it appears that there is no sufficiently similar data for comparison.

The open circuit potential obtained for PPy-MB film was monitored over five hours in an electrochemical cell identical to that used in MB release. Figure 5.4 shows the open circuit potential for the PPy-MB film. The potential started at 0.13 V *vs.* SCE, then decreased quite rapidly over the initial 40 min, from 0.13 to 0.103 V *vs.* SCE. The decrease in the potential may be due to the release of the MB cations that occurs immediately after the film is immersed in the solution. The potential increased slightly until it stabilised at 0.11 V *vs.* SCE after 200 min. The OCP which is between 0.13 V to 0.102 V *vs.* SCE indicated that the polymer film would be partially reduced, corresponding to the CV analysis of the film (Figure 5.3), which indicates that at a potential lower than 0.45 V *vs.* SCE, the polymer film would begin reducing.

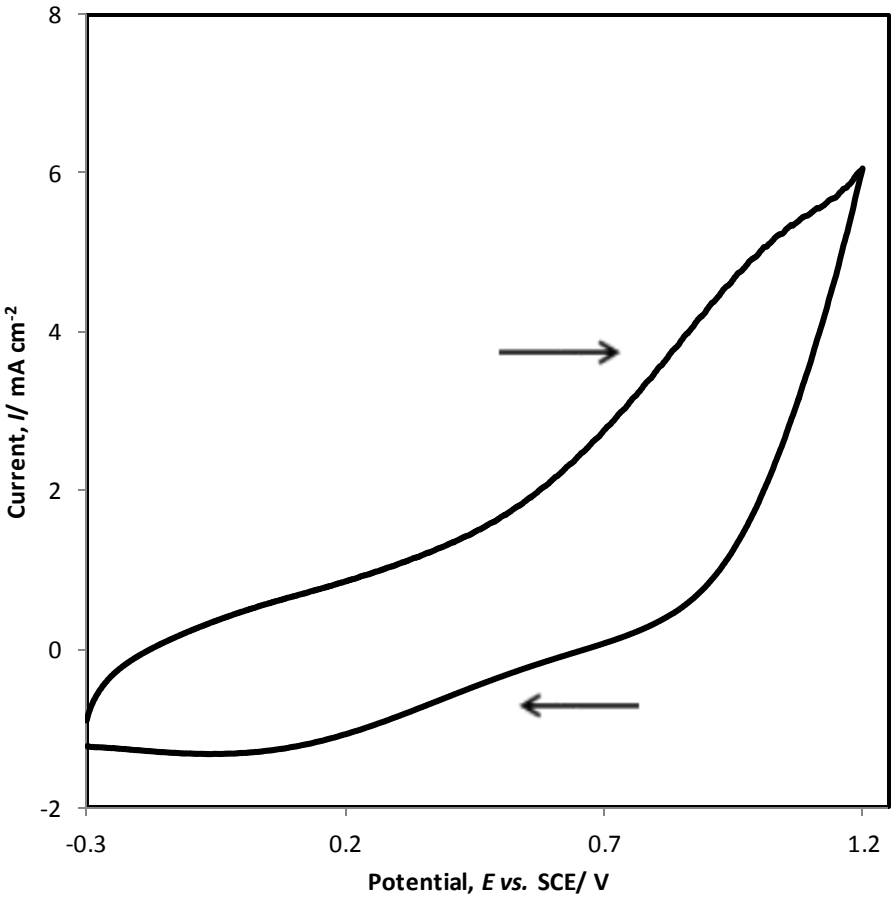

Figure 5-3: CV of PPy-MB films in 0.9% NaCl, at a potential sweep rate of 50 mV s^{-1} for the PPy-MB film grown galvanostatically for 1600 s at 0.3 mA on a 1 cm^2 stainless steel electrode.

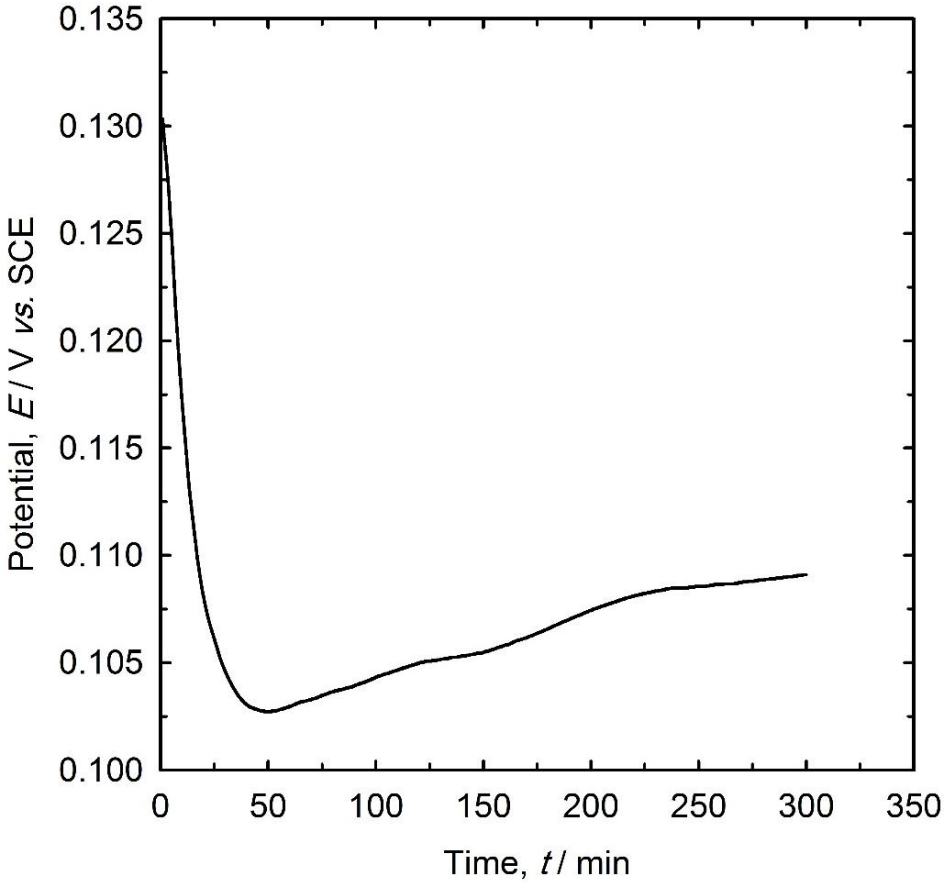

Figure 5-4: Open circuit potential for PPy-MB film deposited on a stainless steel electrode at 0.3 mA cm^{-2} for 1600 s on a 1 cm^2 stainless steel substrate. The potential was observed in 0.9% NaCl aqueous solution *vs.* SCE reference electrode, over five hours.

5.3 Release of methylene blue from PPy-MB films

The release of MB from PPy films prepared galvanostatically at charge density 0.3 mA cm^{-2} for 1600 s was investigated under electrochemical unstimulated (passive release) and stimulation conditions in 0.9% NaCl solution. The electrochemical controlled release was performed using a constant potential of +0.6 V, 0.95 V *vs.* SCE and a pulsed potential of ± 0.6 V at 0.05 Hz *vs.* SCE. The release of MB from PPy-MB under these conditions is illustrated in Figure 5.5. The highest release of MB was observed when the oxidation potential of +0.6 V *vs.* SCE was applied to the PPy films. The maximum concentration of MB in the release solution reached 60 x 10^{-9} mol dm^{-3} after approximately 30 minutes. When the film is oxidised, the PPy

backbone was positively charged, which resulted in the expulsion of MB from the polymer matrix to maintain the charge neutrality. A large initial concentration of MB was detected from these oxidised films within the first 30 minutes. However, the release rate of MB decreased when the oxidation potential increased to 0.95 V *vs.* SCE. This might have occurred because the higher potential led to overoxidation of the films and a corresponding decrease in film electroactivity. When the film was unstimulated, there was a period of large concentration of MB where the release was observed, although the release rate under this condition was lower than that observed at + 0.6 V *vs.* SCE stimulation. However, the MB was released even after the initial burst, although at a lower rate. The lowest amount of MB release was observed when the films were exposed to ± 0.6 V *vs.* SCE at 0.05 Hz. This may be because there was not enough time for the MB to diffuse outside the polymer matrix during the short oxidation periods, so it was attracted to the polymer matrix during the reduction period. The release of MB appears to depend on the charge of the polymer backbone. Although the MB was successfully released from the PPy films, the amount of MB released was very low. This may have occurred because a small amount of MB was incorporated into the polymer matrix, thereby indicating physical entrapment of the MB into the polymer film during the polymerisation process rather than electrostatic interactions. Previously published studies state that the maximum release for cationic molecules occurs when the polymer oxidises [94, 109]. However, different release behaviour for large cationic molecules, such as risperidone, has been reported. The greatest amount of risperidone release was observed when the film was in the reduced state. It was found that the risperidone released more depending on the morphology and the change in the film volume rather than electrostatic forces. The PPy film became swollen when the reduction potential was applied, and the risperidone diffused to the release solution [304].

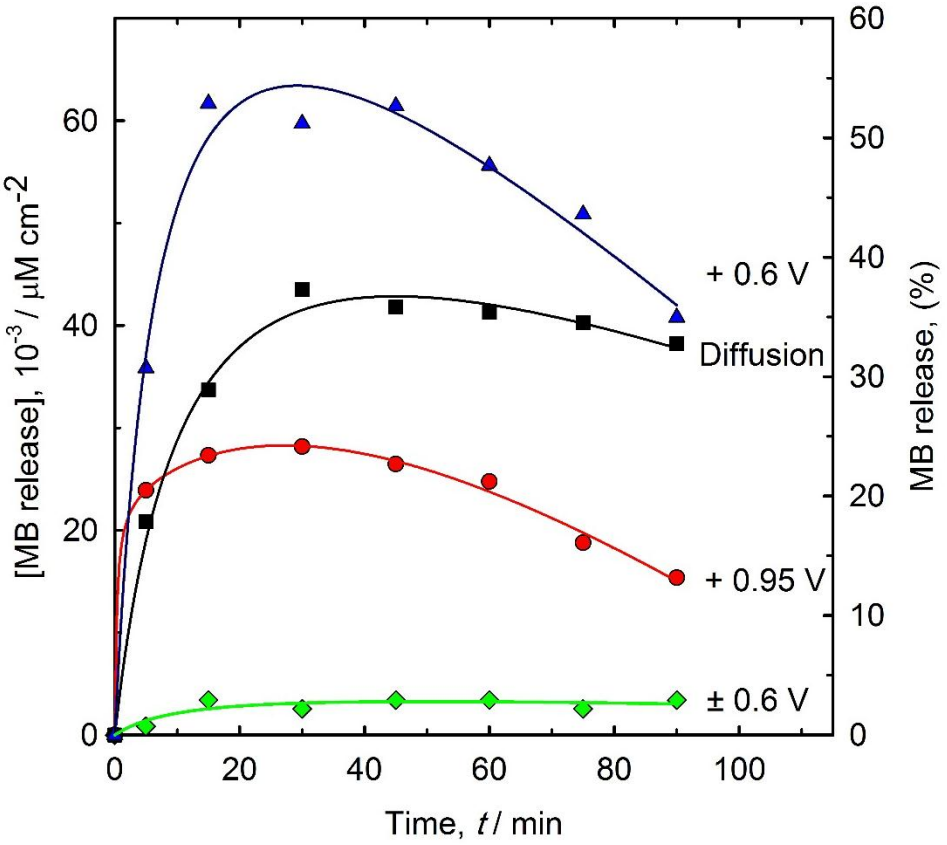

Figure 5-5: MB release from PPy films grown for 1600 s at 0.3 mA cm^{-2} from a solution of 0.1 mol dm^{-3} Py, 0.5 x 10^{-3} mol dm^{-3} MB, and 0.025 mol dm^{-3} oxalic acid. The films were stimulated with (a) + 0.6 V *vs.* SCE constant potential, (b) no stimulation, (c) + 0.95 V *vs.* SCE constant potential and (d) pulsed potential ± 0.6 V at a frequency of 0.05 Hz *vs.* SCE over 90 min.

5.4 Polymerisation methods for increasing dye loading

An attempt was made to use CV as a polymerisation technique to increase the loading concentration of the dye into the PPy films. MB is a cationic dye assumed to be incorporated during the reduction of the polymer. When a positive oxidation potential was applied, PPy was formed in its oxidised state, and simultaneously the oxalate ions were incorporated into the PPy film to maintain charge neutrality of the polymer backbone, as described in equation 5.2.

$$PPy^{+} + n(C_2O_4^{2-}) \rightarrow PPy^{+}.n(C_2O_4^{2-}) + ne^{-} \qquad (5.2)$$

During the PPy reduction, the cationic charge carriers of the PPy backbone neutralised and the electrostatic attractive force between the polymer backbone and the oxalate doping anions was eliminated. Therefore, there is no force holding the oxalate anions in the polymer matrix, instead the applied reduction potential led to the expulsion of the doping anions from the film. It was expected that the oxalate divalent anions is immobile and trapped within the PPy matrix. Consequently, the presence of the MB cations in the medium solution results in ingress of the MB into the polymer matrix to balance out the excess of the negative charge of the entrapped anions, as described in reaction (5.3).

$$PPy^{+} + n(C_2O_4^{2-}) + mMB^{+} - ne^{-} \rightarrow PPy^{o}.n(C_2O_4^{2-}).mMB^{+} \quad (5.3)$$

5.4.1 Cyclic Voltammetry of PPy-MB

CV was used to deposit the PPy film containing MB from an aqueous solution comprising 0.1 mol dm^{-3} Py in 0.025 mol dm^{-3} oxalic acid, and 0.5 x 10^{-3} mol dm^{-3} MB in both the presence and absence of 1 mg mol^{-1} TiNT, which is the same electrolyte used in the experiments described in Section 5.1, at a linear potential sweep rate of 50 mV s^{-1} between 0.25 and 1 V *vs.* SCE during 10 cycles. The solutions were stirred at approximately 500 rpm with a magnetic stirring bar to disperse the TiNT. A platinum mesh and stainless steel (SS) sheet that was 0.1 mm thick and with a surface area of 1 cm^2 were used as counter and working electrodes, respectively, while the potentials were measured against an SCE reference. The working electrodes were polished with 600-grade SiC paper, cleaned with a reagent, and then degreased with deionised water in an ultrasonic bath for 10 min. Vacuum-distilled Py was kept in cooled dark storage before use.

Figure 5.6 depicts the 1st and 10th CV cycles for the PPy synthesis. On the first positive scan, the curve shows a sharp increase in the oxidation current due to the polymerisation of Py, starting at approximately 0.7 V *vs.* SCE and reaching a maximum current of 5 mA at 1.1 V *vs.* SCE.

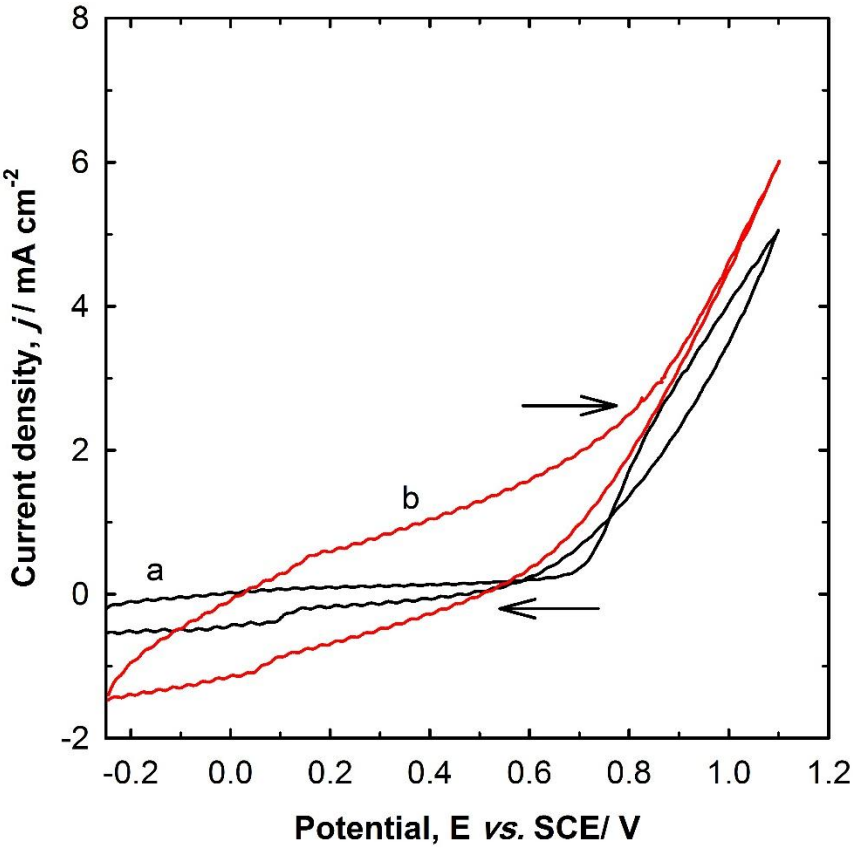

Figure 5-6: CV at a stainless steel electrode (1 cm^2) in 0.1 mol dm^{-3} Py, 0.025 mol dm^{-3} oxalic acid and 0.5 x 10^{-3} mol dm^{-3} MB at a potential sweep rate of 50 mV s^{-1} in a) the first cycle and b) the 10th cycle. The solutions were stirred at approximately 500 rpm.

The slight increase in the current on subsequent scans can be explained in the following manner: in the first cycle, the electropolymerisation reaction occurs and PPy is deposited on the electrode's surface. This reaction involves approximately two electrons per molecule of Py incorporated in the polymer chain. On account of the re-oxidation of PPy formed on previous scans, the monomer oxidation potential decreased during the subsequent cycle. The 10th cycle

curve (b) showed that the Py oxidation process began at an earlier potential (approximately 0.15 V *vs.* SCE), thereby indicating that the previously deposited PPy layer stimulated a catalytic effect on the Py deposition reaction and showed an oxidation current of approximately 6 mA at approximately 1.1 V *vs.* SCE [256]. No oxidation peaks were observed up to a potential of 1.1 V *vs.* SCE during the film's deposition, thereby indicating an unlimited growth of polymer film.

The analysis of the of PPy-MB films synthesised from a solution comprising 0.1 mol dm^{-3} Py in 0.025 mol dm^{-3} oxalic acid and 0.5 x 10^{-3} mol dm^{-3} MB using galvanostatic and CV methods, as described in Sections 5.1 and 5.4.1, respectively, was done using CV methods. The CV was conducted in 0.9% NaCl aqueous solution to observe the effect of the synthesis method on the electroactivity of the polymer films in a medium that would be used for the MB release. Figure 5.7 shows the CV curves for the PPy-MB synthesis, using CV and galvanostatic methods in 0.9% NaCl aqueous solution.

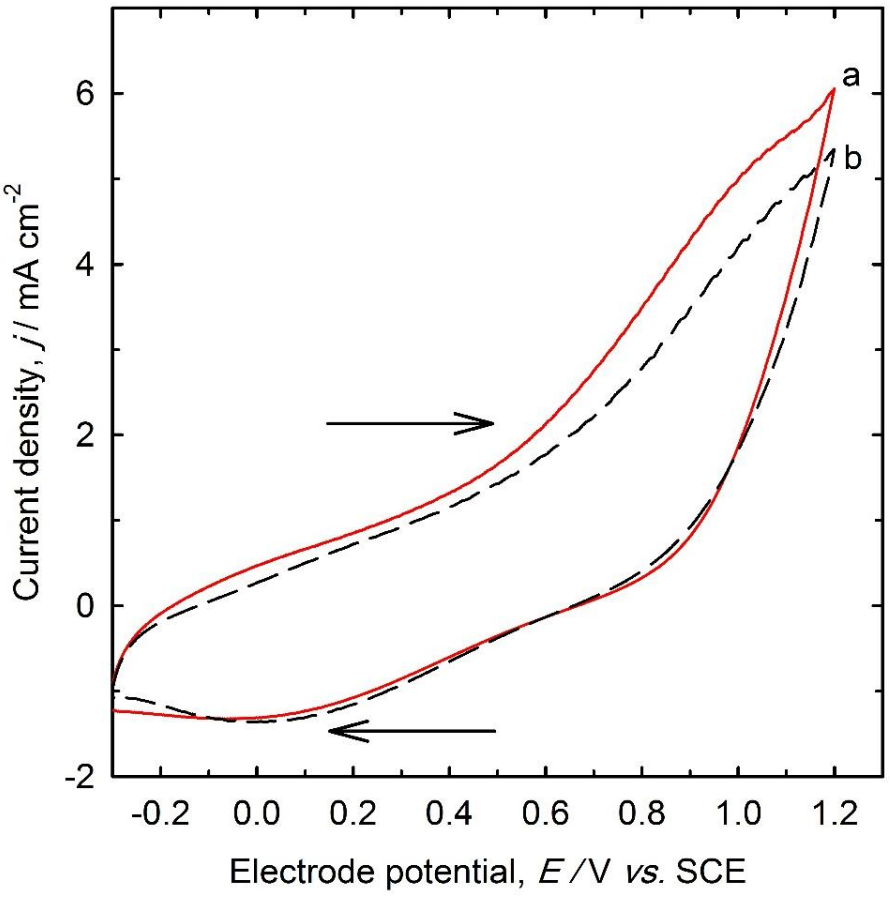

Figure 5-7: CV of PPy-MB films in (0.9%) NaCl at a potential sweep rate of 50 mV s^{-1} a) PPy-MB film synthesis using CV at a potential sweep rate of 50 mV s^{-1} for 10 cycles and b) PPy-MB film grown galvanostatically for 1600 s at 0.3 mA.

Curve a in Figure 5.7 shows wide oxidation and reduction waves, but no reduction or oxidation peaks for the PPy-MB films' synthesis using CV. The oxidation current density of the film is 6 mA cm^{-2} at 1.2 V *vs.* SCE. Curve b represents the PPy-MB synthesis using the galvanostatic method with an oxidation current of 5.26 mA cm^{-2} at 1.2 V *vs.* SCE. These CV curves indicate an insignificant increase in the electroactivity of the PPy-MB synthesis using CV.

5.4.2 MB release from PPy films synthesis using CV

The release profile of MB from PPy films synthesised using CV after 10 cycles is depicted in Figure 5.8. The release profile for all used protocol (electrical stimulation and passive release) is similar to that observed for films prepared by galvanostatic deposition. However, the amount of MB release was lower than expected; the difference in the concentration of released MB was not significant. The decrease in the MB release rate may have occurred because less MB was incorporated into the PPy films during the CV, which is for a shorter duration than with the galvanostatic method. This is because the negative charge of the PPy backbone was compensated by the entry of small, highly mobile cations and the release of a doping anions oxalate ($C_2O_4^{2-}$) rather than the incorporation of large MB molecules, which have a molecular weight of 319.85 g mol^{-1}. In addition, some amount of the entrapped MB may also be released when the polymer oxidises during the CV synthesis. To avoid this limitation, large immobilised and partially mobile anions such as melanin, polystyrene sulfonate, or β-cyclodextrins were used to dope the PPy film [304]. These anions had a limited ability to move out of the PPy films, thereby permitting the cation molecules to become incorporated into the polymer matrix through electrostatic forces and increasing the intake and release of cations from the PPy film. Moreover, the bonding of the molecules in the PPy matrix via electrostatic forces provided more control over the release of molecules using electrical stimulation.

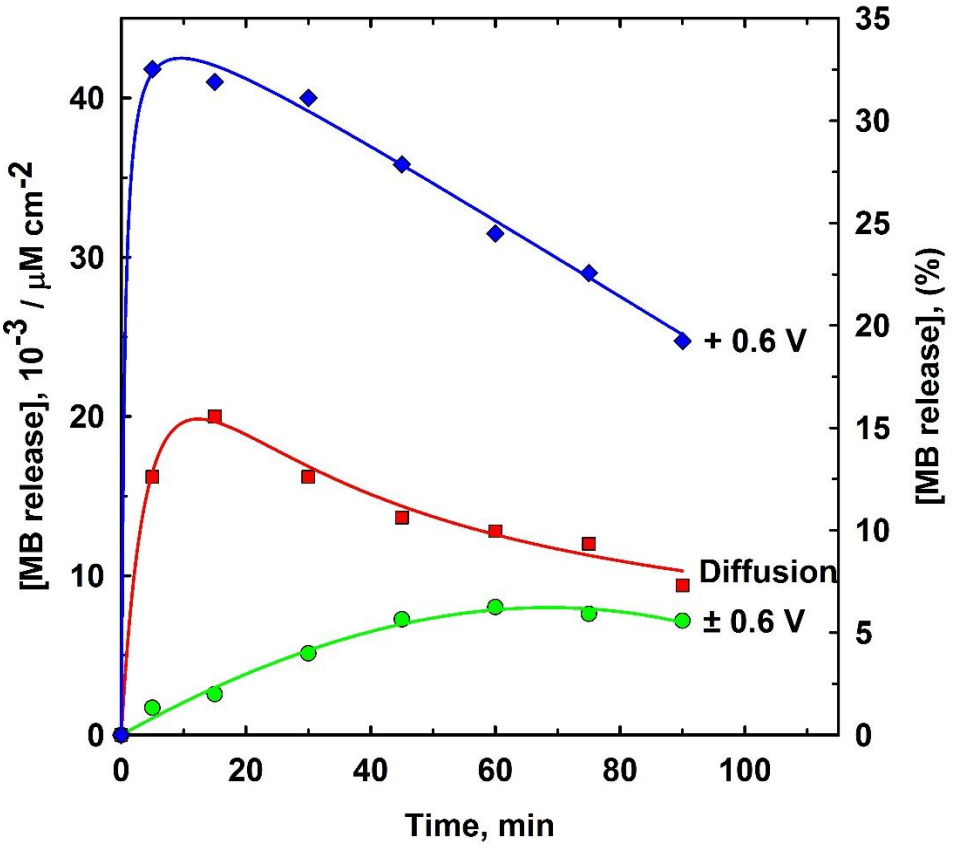

Figure 5-8: MB release from PPy films grown for 10 CV cycles from a solution containing 0.1 mol dm^{-3} Py, 0.5 x 10^{-3} mol dm^{-3} MB, and 0.025 mol dm^{-3} oxalic acid. The films were stimulated with (a) + 0.6 V *vs.* SCE constant potential, (b) no stimulation and (c) pulsed potential ± 0.6 *vs.* SCE at a frequency of 0.05 Hz *vs.* SCE over 90 min.

5.5 Influence of using titanate nanotubes (TiNT) on the MB release

The integration of conducting polymers with nanostructured materials, such as titanate and carbon nanotubes [89, 90], may increase the capacity of the polymer to absorb and release molecules. Titanate nanotubes can be produced using an alkaline hydrothermal process at low cost. The advantages of titanate nanotubes, such as a high surface area, nontoxicity, and biocompatibility, make them a good candidate for various applications, including drug delivery systems [146, 150]. This section describes the influence of using titanate nanotubes on the release of MB from the PPy film.

5.5.1 Electrodeposition of the PPy film with TiNT

Titanate nanotubes powder (2g) was dispersed in 0.5 dm^3 distilled water and stirred with a magnetic follower for 2 weeks. The solution was then kept for four days until a stable titanate nanotubes suspension was formed. The concentration of the suspended TiNT was evaluated by measuring the optical absorbance, A, at 280 nm, using the Lambert-Beer law.

$$A = \varepsilon \; x \; C \; x \; L, \tag{5.4}$$

where ε is the molar extinction coefficient of TiNT = 5900 dm^{-3} mol^{-1} cm^{-1} and L is the optical path length (1 cm) [305].

The PPy-MB film was electrodeposited using CV and the galvanostatic method from an aqueous solution containing 0.1 mol dm^{-3} Py in 0.025 mol dm^{-3} oxalic acid, and 0.5 x 10^{-3} mol dm^{-3} MB in the presence of 1 mg mol^{-1} TiNT, as outlined in Section 5.1 and 5.4.1. The solutions were stirred at approximately 500 rpm with a magnetic stirring bar (2 cm length) to disperse the TiNT.

Figure 5.9 illustrates the chronopotentiogram for the polymerisation of PPy-MB films using the galvanostatic method. The polymerisation potential in the absence of TiNT rapidly peaked at 0.68 V *vs.* SCE, and then reduced quickly to approximately 0.65 V *vs.* SCE, where it stabilised for the duration of polymerisation process. When the TiNT was present, the evolved potential instantly peaked at 0.73 V *vs.* SCE and then stabilised at approximately 0.66 V *vs.* SCE for the remaining polymerisation time.

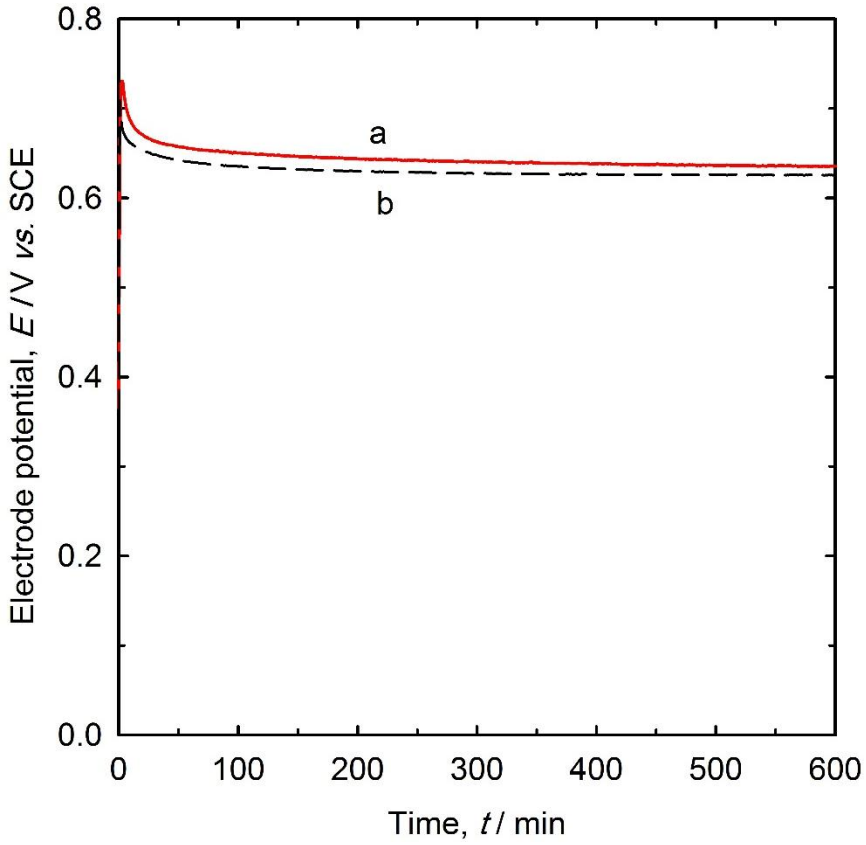

Figure 5-9: Chronopotentiogram for the galvanostatic polymerisation of PPy-MB films at current densities of 0.3 mA cm^{-2} for 1600 s from a solution comprising 0.1 mol dm^{-3} Py in 0.025 mol dm^{-3} oxalic acid, and 0.5 x 10^{-3} mol dm^{-3} MB, in the presence (red), and in the absence (black), of 1 mg mol^{-1} TiNT. For better clarity, only the first 600 s is shown.

This slight increase in potential observed in the presence of TiNT indicates that the conductivity of PPy-TiNT-MB is lower than the conductivity of the PPy-MB film. A decrease in the film's conductivity may occur because the TiNT catalysed the Py polymerisation, which leads to an increase in the film's thickness, thereby increasing the film's resistance. The other possible explanation for the increase in the film's resistance is that it occurs due to the high electrical resistance caused by the incorporation TiNT.

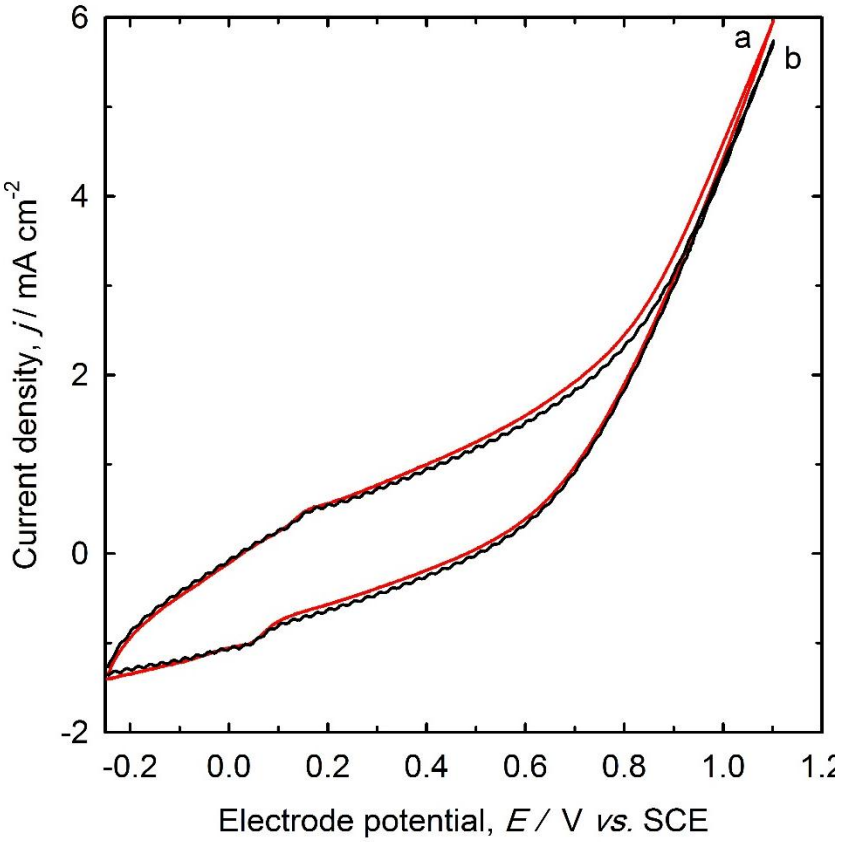

Figure 5-10: CV at a stainless steel electrode (1 cm^2) in 0.1 mol dm^{-3}, 0.025 mol dm^{-3} oxalic acid and 0.5 x 10^{-3} mol dm^{-3} MB at a potential sweep rate of 50 mV s^{-1} in a) the presence and b) absence of TiNT . The 10^{th} cycle is shown and the solutions were stirred at approximately 500 rpm.

The CVs during the synthesis of the PPy films in a) the presence and b) the absence of TiNT are depicted in Figure 5.10. Their CV curve indicates that there is an insignificant difference between the electroactivity of the two films, although it seems that the PPy-TiNT-MB film is slightly more active than the PPy-TiNT-MB.

5.5.2 Release of methylene blue from PPy-TiNT-MB films

The release of MB from PPy films was investigated under electrochemical stimulation and unstimulated conditions (passive release) in 0.9% NaCl solution. The controlled electrochemical release was performed using a constant potential of + 0.6 V and a pulsed potential of ± 0.6 V at 0.05 Hz *vs.* SCE. The release of MB from PPy-TiNT-MB films, deposited using galvanostatic and CV methods, are illustrated in Figures 5.11 and Figure 5.12, respectively.

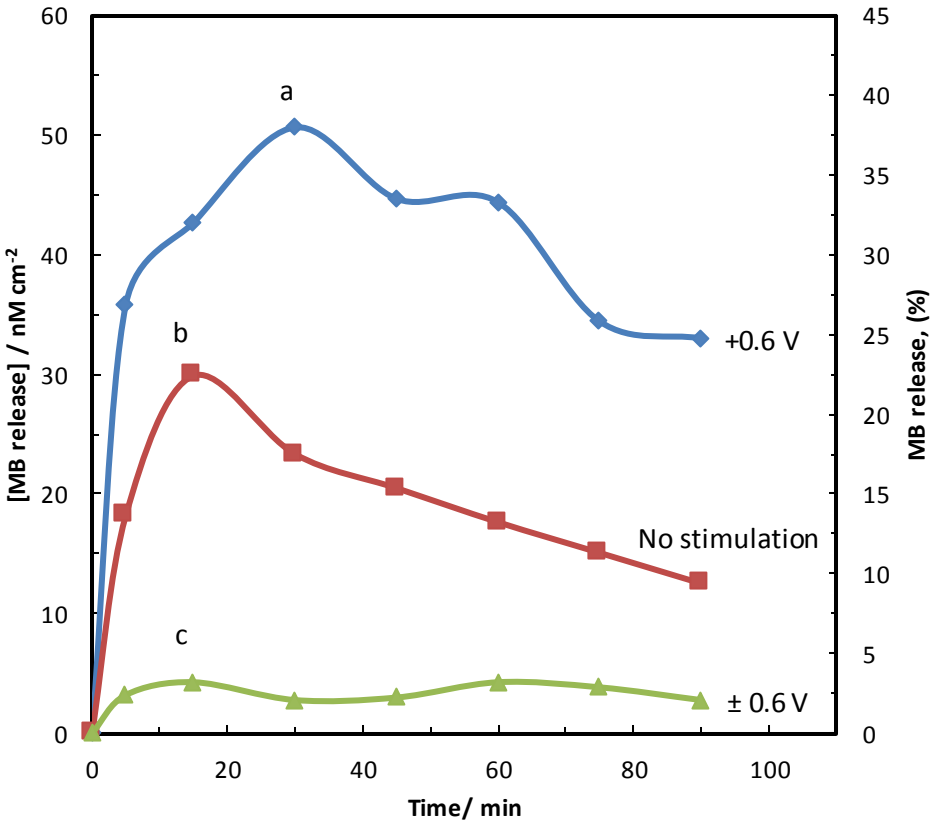

Figure 5-11: Release of MB from PPy films grown galvanostatically for 1600 s at 0.3 mA cm^{-2} from a solution of 0.1 mol dm^{-3} Py, 0.5 x 10^{-3} mol dm^{-3} MB and 0.025 mol dm^{-3} oxalic acid with 1 mg mol^{-1} TiNT. The films were stimulated with (a) + 0.6 V *vs.* SCE constant potential, (b) no stimulation, (c) pulsed potential ± 0.6 *vs.* SCE at a frequency of 0.05 Hz *vs.* SCE over 90 min.

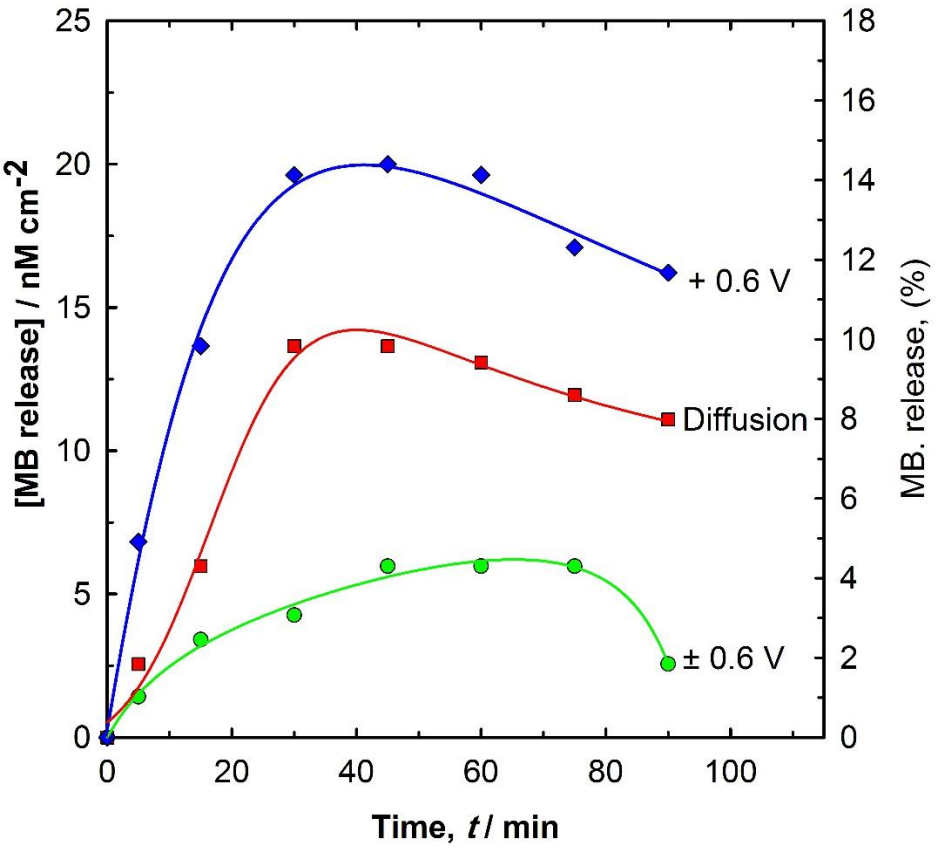

Figure 5-12: Release of MB from PPy films grown using CV for the 10th cycle from a solution of 0.1 mol dm^{-3} Py, 0.5 x 10^{-3} mol dm^{-3} MB and 0.025 mol dm^{-3} oxalic acid with 1 mg mol^{-1} TiNT. The films were stimulated with (a) + 0.6 V *vs.* SCE constant potential, (b) no stimulation and (c) pulsed potential ± 0.6 V *vs.* SCE at a frequency of 0.05 Hz *vs.* SCE over 90 min.

It is evident from the concentration profile graphs that the release patterns for MB from PPy-TiNT-MB films are similar to those from PPy-MB films, discussed in Sections 5.3 and 5.4.2.

However, there was a slightly lower level of concentration released from the PPy-TiNT-MB films. The highest amount of MB released from the PPy-TiNT-MB synthesised using the galvanostatic method occurred when the film was oxidised with the application of a constant potential + 0.6 V *vs.* SCE. The concentration of MB in the release medium reached 50 x 10^{-9}

mol dm^{-3} cm^{-2} after 30 min, which is slightly lower than that released from PPy-MB films when the same release protocol was applied (figure 5.5). The amount of released MB decreased when the polymer film was unstimulated.

The decrease of MB release from PPy-TiNT-MB film may occur because the adsorption of Py in the TiNT is 240 mg g^{-1}, which is higher than the adsorption of MB in TiNT (133 mg g^{-1}) [90]. Therefore, the surface of TiNT is occupied by the positively charged Py monomers, which may lead to reduced adsorption of MB. In addition, the incorporation of TiNT in the polymer matrix may change the film's morphology, thereby reducing the MB release.

The release rate of MB from the PPy films is low and highly variable (figure 5.11). This takes place because the large cationic ion MB is physically entrapped in the polymer film during the polymerization process instead of interacting electrostatically (section 5.3). The use of large doping ions instead of oxalic acid may increase the absorption and release of MB from the PPy film.

5.6 The effect of varying film thickness on the release of methylene blue

The film thickness was varied by holding the current density constant at 0.3 mA cm^{-2} and increasing the deposition time. PPy-MB films (without TiNT) with an estimated thickness of 2, 4, 8, 12, 24 and 32 μm were prepared, assuming that 240 mC cm^{-2} forms a PPy film of 1 μm thickness. The film thickness was estimated theoretically from the consumed charge during the film synthesis to provide the results in Table 5.1.

Table 5-1: Time and charge required to synthesise PPy-MB with different thicknesses

Polymerisation time /s	Consumed charge density / mC cm^{-2}	Film thickness /μm
1600	480	2
3200	960	4
6400	1920	8
9600	2880	12
19200	5760	24
25600	7680	32

Figure 5.13 depicts the effect of varying the PPy film thickness on the release of MB. The increase in the films' thickness from 2 to 4 μm does not appear to influence the amount of MB released. This is due to the fact that most of the MB was released from the film's surface. Thicker films of 8, 12, 24 and 32 μm exhibited a powder-like appearance. Further, PPy particles split up from these films, as observed in the release solution. The concentration of MB in the release medium increased by approximately 30% when the film thicknes, increased by a factor of 4. The increase in the amount of MB released can be attributed to the contribution of the MB from the polymer bulk in addition to that released from the polymer surface due to the change in the film structure and morphology.

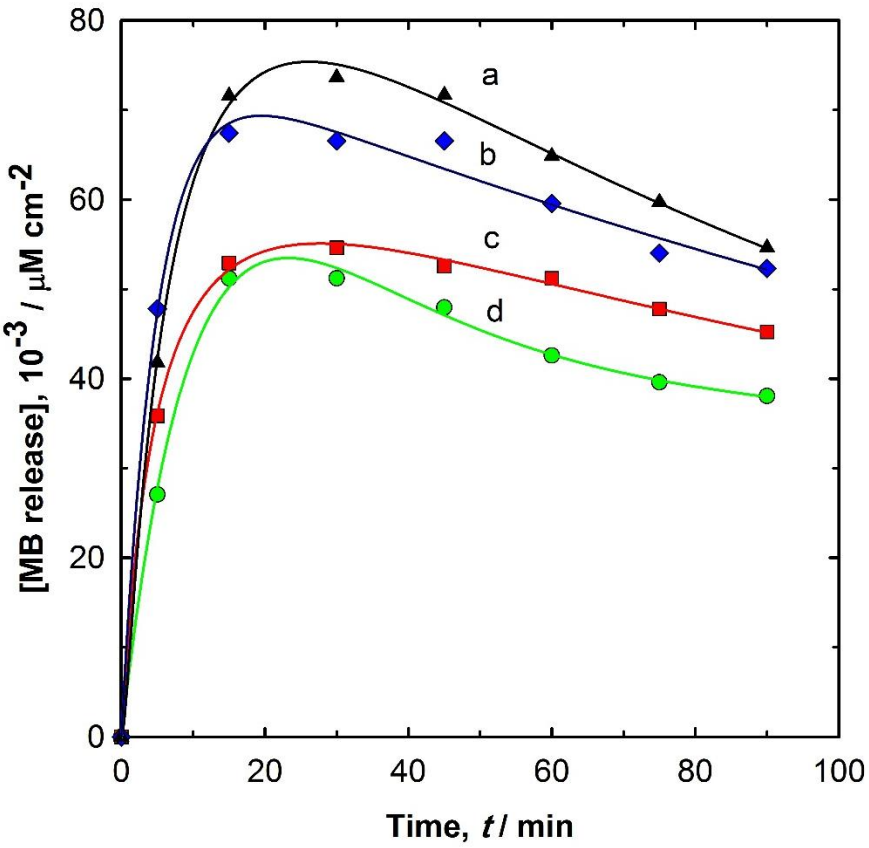

Figure 5-13: Release of MB from PPy films with different thicknesses of 2, 4, 8 and 12 μm grown galvanostatically for 1600 s at 0.3 mA cm^{-2} from a solution of 0.1 mol dm^{-3} Py, 0.5 x 10^{-3} mol dm^{-3} MB and 0.025 mol dm^{-3} oxalic acid. The films were stimulated with a constant potential of + 0.6 V *vs.* SCE from PPy films with thicknesses of (a) 12 μm, (b) 8 μm, (c) 4 μm and (d) 2 μm.

When the film thickness increased from 8 to 12 μm, the release rate of MB only increased by 10%. The release of MB from the thicker films was excluded because the thicker films formed a powder-like structure and some PPy particles were released from the films during the experiment, which made it difficult to control the amount of MB being released and affected the reproducibility of the films.

5.7 The effect of loading MB after the polymerisation process using different potentials

The effect of loading MB after the polymer is synthesised was investigated using different negative potentials to incorporate the MB. First, PPy films were prepared from a solution comprising 0.1 mol dm^{-3} Py and 0.025 mol dm^{-3} oxalic acid in the absence of MB by applying a current density of 0.3 mA cm^{-2} for 1600 s, as described in Section 5.1. Thereafter, the polymer-film-covered working electrode was moved to an identical electrochemical cell arrangement, containing 0.025 mol dm^{-3} oxalic acid and 0.5 x 10^{-3} mol dm^{-3} MB; a reduction potential of -0.2, -0.4, and -0.6 V *vs.* SCE was applied to the PPy film for 1600 s to incorporate the cationic dye MB in the PPy film. Due to charge repulsion, the incorporated doping oxalic anions are expelled from the PPy film when the film is in the reduced state, and the cationic MB enters the PPy film to balance out the excess of negative charge of the polymer backbone. In addition, the adsorption of MB in the PPy without the application of the reduction potential was investigated.

The electrochemically controlled release of MB from the PPy film was performed by applying a constant potential of + 0.6 V *vs.* SCE, as described previously in Section 5.3. A significant increase in MB release was noted when MB was loaded using a reduction potential compared with the incorporation of MB without applying a potential. The accumulative release profile of MB from the PPy films indicated that the release rate increases when the potential was applied to incorporate the MB in the PPy films was more negative, as depicted in Figure 5.14.

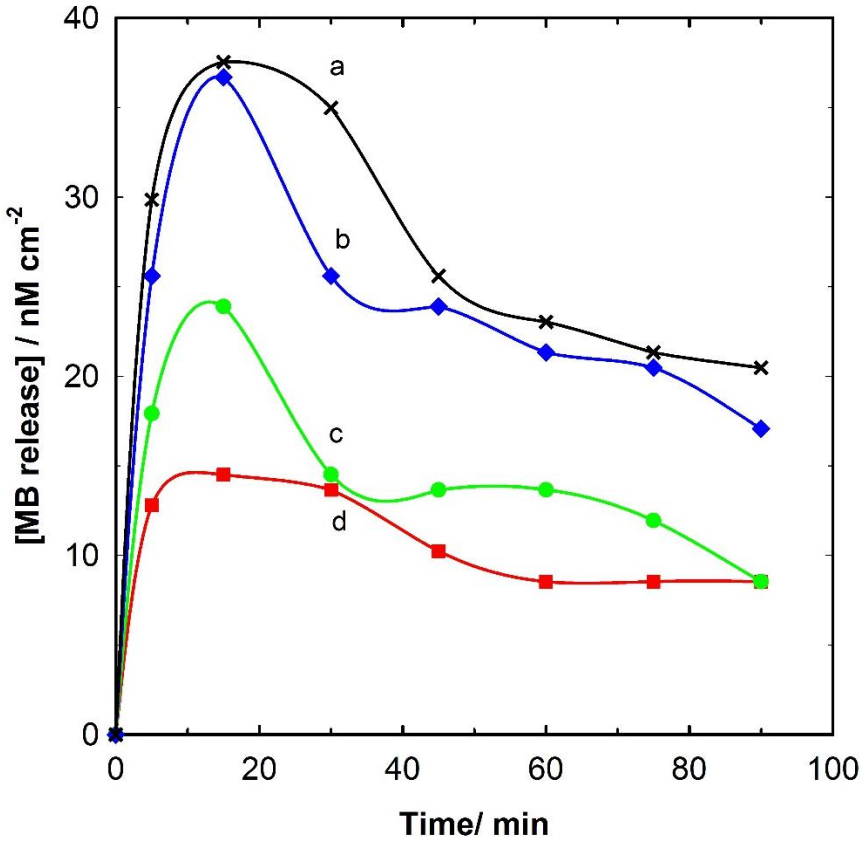

Figure 5-14: Release of MB from PPy films stimulated using + 0.6 V *vs.* SCE. The PPy films were grown for 1600 s at 0.3 mA cm^{-2} from a solution of 0.1 mol dm^{-3} Py and 0.025 mol dm^{-3} oxalic acid. The MB was incorporated in the PPy films after the polymerisation process from a solution of 0.5 x 10^{-3} mol dm^{-3} MB and 0.025 mol dm^{-3} oxalic acid by applying a reduction potential of (a) - 0.6 V *vs.* SCE, (b) - 0.4V *vs.* SCE, (c) - 0.2V *vs.* SCE and (d) without applying a potential for 1600 s.

The concentration of released MB reached 14.5 x 10^{-9} mol dm^{-3} cm^{-2} within 15 minutes when no incorporation potential was applied. The amount of MB released was similar to that released from the PPy-MB when the film was unstimulated. This suggests that a considerable amount of MB was adsorbed in the polymer surface and released when the film was oxidised. Further, the amount of MB significantly increased to 24 x 10^{-9} mol dm^{-3} cm^{-2} during the same period of time, as the incorporation potential of -0.2 *vs.* SCE was applied. The amount released of MB increased further to 36.5 x 10^{-9} mol dm^{-3} cm^{-2} when a potential of -0.4 V *vs.* SCE for 15 min was used to incorporate the MB. When the incorporation potential decreased further to -0.6 V

vs. SCE, the concentration of released MB reached 38 x 10^{-9} mol dm^{-3} cm^{-2} after 15 min. The use of more negative potential is more efficient in reducing the PPy films. This led to an increase in the amount of MB incorporated in the PPy films and, subsequently, the amount of released MB. However, this amount is lower than the amount released when the MB was incorporated during the polymerisation process. This indicates that the MB was unable to penetrate into the polymer bulk due to its large structure, and a considerable amount of MB was loaded on the film surface. This finding is consistent with that in previous studies, which reported that the polymer surface is more active to absorbed molecules compared to the polymer bulk [306].

5.8 The effect of initial methylene blue concentration on its release

The effect of the initial MB concentration was investigated. The PPy films were prepared without MB, as described in Section 5.7. Thereafter, the polymer-film-covered working electrode was moved to the same electrochemical cell arrangement, containing 0.025 mol dm^{-3} oxalic acid and 0.3, 0.5, 1.0 or 2.0 x 10^{-3} mol dm^{-3} of MB, and a reduction potential of -0.6 V *vs.* SCE was applied to the PPy film for 1600 s to incorporate the cationic dye MB in the PPy films. The electrochemically controlled release of MB from PPy film was performed by applying a constant potential of + 0.6 V *vs.* SCE, as described previously in section 5.3.

Figure 5.15 illustrates the effect of varying the initial concentration of MB on the release of MB from the PPy film. The amount of MB released increased as the initial concentration of MB increased in the polymerisation solution. The concentration of MB in the release medium reached 20 x 10^{-9} mol dm^{-3} cm^{-2} within 15 minutes after the preparation of the PPy film using

0.3 x 10^{-3} mol dm^{-3} of MB. The concentration of the released MB increased by approximately 90% (38 x 10^{-9} mol dm^{-3} approximately) when the initial concentration of MB in the polymerisation solution increased to 0.5 x 10^{-3} mol dm^{-3}.

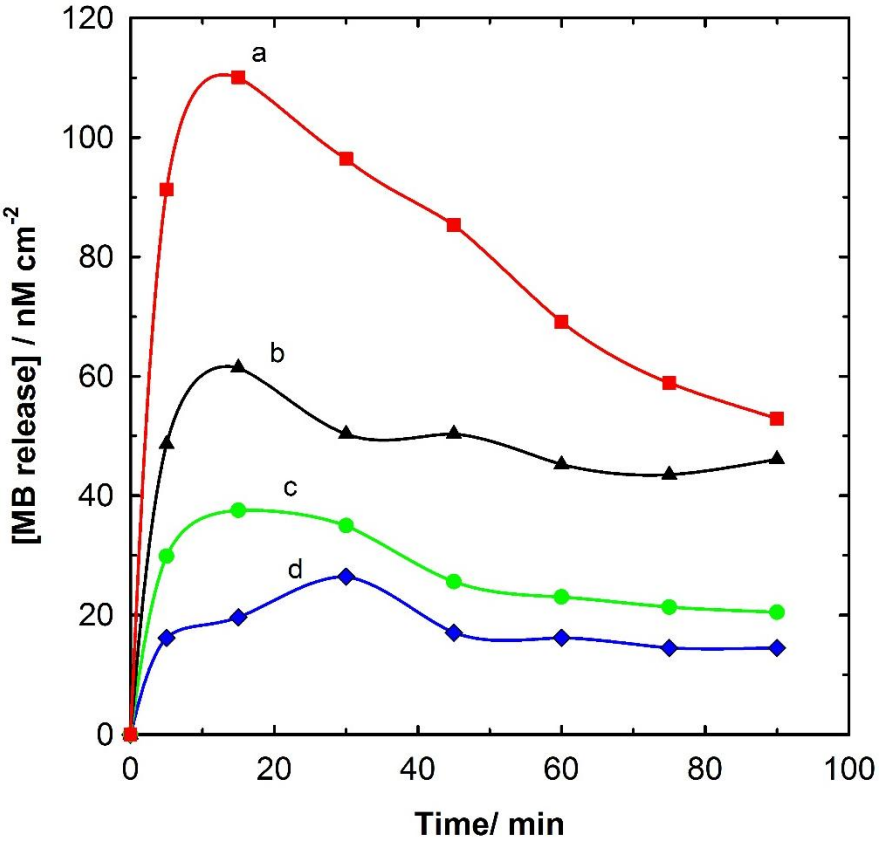

Figure 5-15: Release of MB from PPy films stimulated using + 0.6 V *vs.* SCE. The PPy films were grown for 1600 s at 0.3 mA cm^{-2} from a solution of 0.1 mol dm^{-3} Py, and 0.025 mol dm^{-3} oxalic acid. The MB was incorporated in the PPy films after the polymerisation process by applying a reduction potential of - 0.6 V *vs.* SCE for 1600 s from a solution containing 0.025 mol dm^{-3} oxalic acid and (a) 2 x 10^{-3} mol dm^{-3} MB, (b) 1 x 10^{-3} mol dm^{-3} MB, (c) 0.5 x 10^{-3} mol dm^{-3} MB and (d) 0.3 x 10^{-3} mol dm^{-3} MB.

The released amount of MB increased to 60 x 10^{-9} mol dm^{-3} cm^{-2} when the initial concentration of MB doubled to 1 x 10^{-3} mol dm^{-3}. When the initial concentration of MB increased from 1 to 2 x 10^{-3} mol dm^{-3}, the release rate of MB increased by approximately 85% (110 x 10^{-9} mol dm^{-}

^{3} cm^{-2}). The increase in the initial concentration of MB led to an increase in the diffusion of MB into the PPy films down their concentration gradient and the reduction potential, which resulted in increasing the amount of incorporated MB in the PPy films and, subsequently, increased the release rate of MB.

5.9 The release of MB from PPy/pTS-MB film

5.9.1 Polymer synthesis

PPy/pTS-MB films were synthesised using the two-layer approach; first, a thin layer was electrodeposited without MB. This film functions as a pre-layer which may improve polymer growth by shielding the electrode surface from organic molecules and improve polymer adherence to the electrode. In addition, this layer may increase the surface roughness, and therefore the surface area, of the electrode area. pTS ion is widley used as a doping ion and has proved that it increases the amount of the incorporated and released cationic drugs [88].Thompson et al. [88] that the use of the two-layer approach lead to a slight increase in the incorporation of a neurotrophic factor in the PPy films. Figure 5.15 shows a schematic diagram of a bilayer PPy drug delivery system.

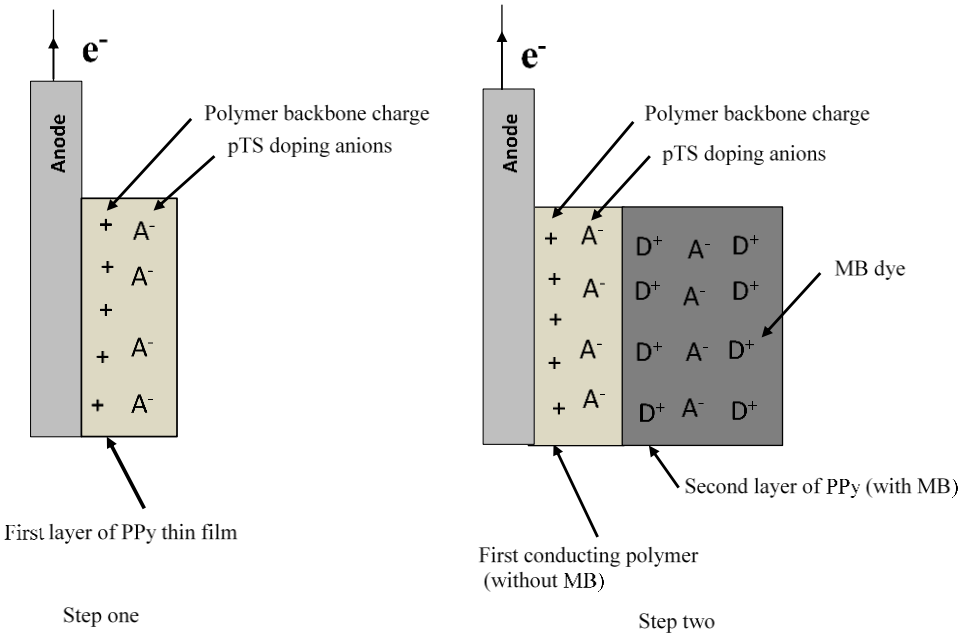

Figure 5-16: Bilayer PPy film for MB dye release system

The first thin layer was grown for 90 s from an electrolyte containing 0.2 mol dm^{-3} Py, 0.05 mol dm^{-3} *para*-Toluene sulphonic acid sodium salt (pTS), in the absence of MB at a current density of 0.3 mA cm^{-2}. Thereafter, the PPy-pTS polymer-covered working electrode was moved to an identical electrochemical cell arrangement containing 0.2 mol dm^{-3} Py, 0.05 mol dm^{-3} pTS and 0.5 x 10^{-3} mol dm^{-3} MB to prepare a second thick PPy layer containing MB on top of the previously prepared thin layer. The second layer was deposited by either employing the galvanostatic method by applying 0.3 mA cm^{-2} for 1600 s, or using CV at a linear potential sweep rate of 50 mV s^{-1} between 0 and 1.1 V *vs*. SCE for 10 cycles.

Figure 5.16 depicts the potential-time curves during the electrodeposition of the first and second layers of the PPy and PPy/pTS-MB films. Curve a in Figure 5.16 shows the evolved potential during the synthesis of the first layer. The potential quickly peaked at 0.7 V *vs.* SCE due to PPy nucleation and declined to 0.58 V *vs.* SCE approximately after 90 s.

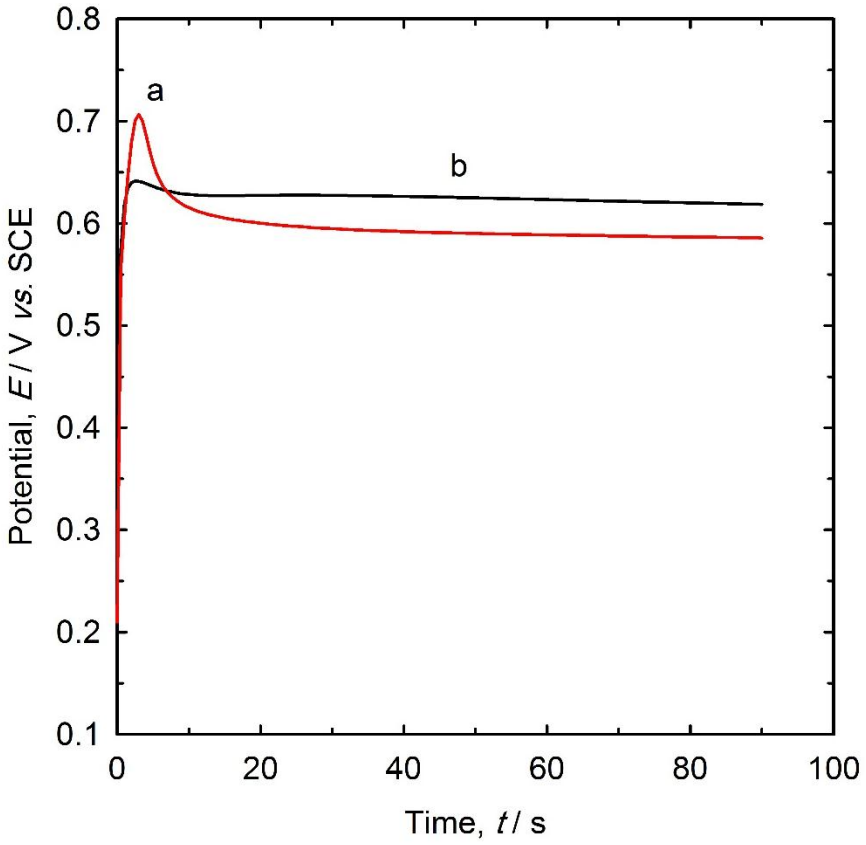

Figure 5-17: Chronopotentiogram for the galvanostatic polymerisation of PPy/pTS-MB films at current densities of 0.3 mA cm^{-2} from a solution comprising 0.2 mol dm^{-3} Py in 0.05 mol dm^{-3} pTS, and 0.5 x 10^{-3} mol dm^{-3} MB, for (a) first layer grown for 90 s and (b) second layer grown for 1600 s. For better clarity, only the first 90 s is shown here.

During the polymerisation of the second layer, the polymerisation potential immediately stabilised at 0.62 V *vs.* SCE and the nucleation initiated peaks did not appear, as shown by curve b. This was because the presence of the first PPy layer modified the electrode surface and catalysed the Py polymerisation process. This phenomenon also occurs during the polymerisation of Py using CV methods, where the Py oxidation process was begun at an earlier potential and the potential oxidation of Py monomers decreased relative to the increase of sweeping cycles, as shown in Figure 5.6.

5.9.2 Release of MB from the PPy/pTS-MB film

The release of MB from PPy/pTS-MB film was performed by applying a constant potential of + 0.6 V *vs.* SCE and unstimulated release, as described previously in Section 5.3. Figure 5.17 displays the cumulative release trends of MB from the PPy/pTS-MB film synthesis using galvanostatic and CV methods.

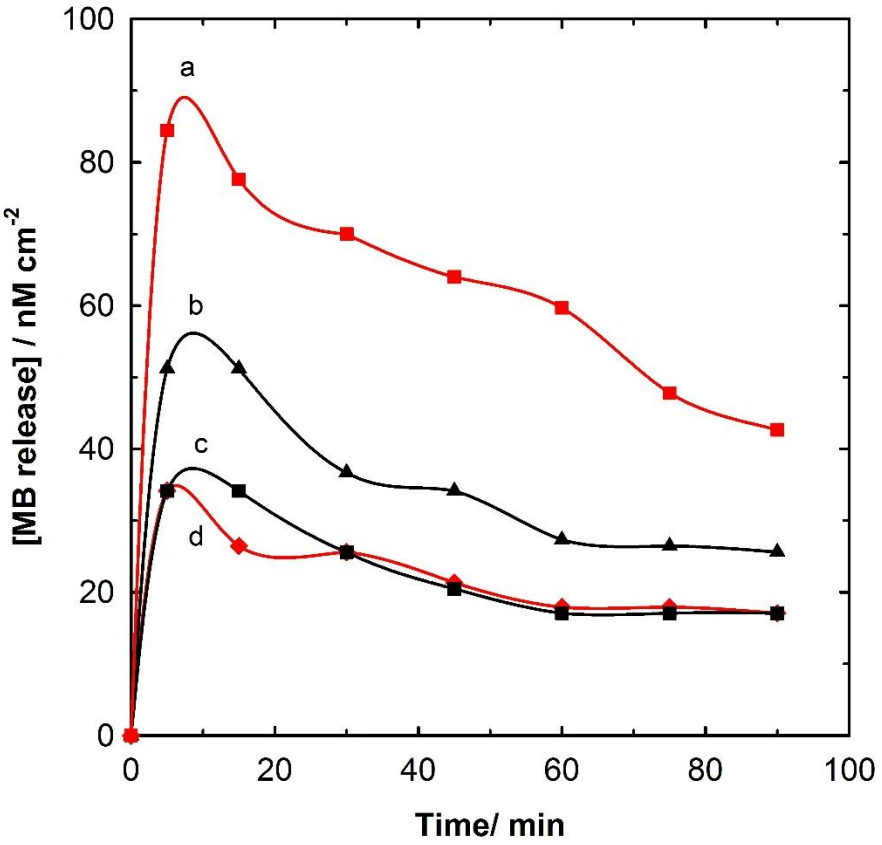

Figure 5-18: Release of MB from PPy/pTS-MB films that were grown for 1600 s at 0.3 mA cm^{-2} (red), and films grown using CV during 10 cycles from a solution of 0.2 mol dm^{-3} Py, 0.5 x 10^{-3} mol dm^{-3} MB and 0.05 mol dm^{-3} pTS. The films were stimulated with (a) + 0.6 V *vs.* SCE constant potential, (b) +0.6 V *vs.* SCE constant potential, (c) no stimulation and (d) no stimulation over 90 min.

It is clear that a larger amount of MB was released using electrical stimulation in all experiments. The trends related to the release of MB were characterised by a high burst of

release in the first 5 min, followed by a much lower amount of release over the remaining time. This was because the film's efficiency in releasing MB from its surface was higher than that from the polymer matrix. The MB may become entrapped in the film matrix, which would make its release difficult from the film. For the PPy/pTS-MB film synthesised using the galvanostatic method (Figure 5.17a), the stimulated polymer films released 84.5 x 10^{-9} mol dm^{-3} cm^{-2} in 5 minutes in contrast to the unstimulated films (Figure 4.17d) which released 34 x 10^{-9} mol dm^{-3} cm^{-2}. There was a significant increase in the MB released from the films' synthesis using the galvanostatic method compared with the films' synthesis using the CV method, when the films were stimulated using + 0.6 V *vs.* SCE. The concentration of MB released from the prepared films' use of the galvanostatic method reached 84 x 10^{-9} mol dm^{-3} cm^{-2} within 5 min, which was significantly higher than that released from the films that were synthesised using the CV method 51.2 x 10^{-9} mol dm^{-3} cm^{-2} during the same period of time. This occurs because some of the incorporated MB during the reduction CV cycles may have been expelled out of the film during the oxidation cycles. Therefore, a low amount of MB was loaded and released from the polymer film. The concentration of MB released from the films that were synthesised using the CV method reached approximately 34 x 10^{-9} mol dm^{-3} cm^{-2} after 5 minutes, which is close to the amount released from the films, and was formed galvanostatically when both films were unstimulated. According to this phenomenon, most of the MB is released due to desorption of MB from the polymer surface rather than from the polymer bulk as observed earlier in Sections 5.3 and 5.4.2.

The use of pTS as a doping anion led to an increased amount of MB being released from the electrochemically stimulated PPy films in comparison with the release from PPy doped with the oxalic acid anion. For example, 84.5 x 10^{-9} mol dm^{-3} cm^{-2} MB was released from PPy/pTS-MB films, compared with approximately 60 x 10^{-9} mol dm^{-3} cm^{-2} released from PPy film doped with oxalic acid, when both films were synthesised using the galvanostatic method and

stimulated under +0.6 V *vs.* SCE. One possible explanation for the decrease in MB being released is that the mobility of oxalate anion ($C_2O_4^{2-}$) is higher than the immobile anion pTS; therefore, the entrapped pTS create a negative net charge in the polymer, which is attracted to positively charged MB molecules.

5.10 Polymer synthesis for release of fluorescein sodium salt

A PPy film containing a model anionic drug FSS, was electrochemically deposited on a stainless steel electrode using a three-electrode cell where the auxiliary electrode was also a stainless steel sheet and SCE electrode was used as the reference. A polished rectangular stainless steel plate with a surface area of 1 cm^2 was used as a working electrode and immersed in an electrolytic solution of 0.1mol dm^{-3} Py monomer with 0.5 x 10^{-3}mol dm^{-3} FSS to conduct the electrochemical polymerisation. The working electrode potential was cycled between a potential range of 0 to 2.5 V *vs.* SCE at a scan rate 50 mV s^{-1} for 40 cycles.

The presence of FSS in the polymerisation solution seemed to inhibit the electropolymerisation of the Py monomer on the stainless steel substrate (Fig 5.18). The PPy did not cover the electrode surface, and only non-uniform polymer films grew in a discontinuous and random manner. Therefore, some drops of 0.05 x 10^{-3} mol dm^{-3} H_2SO_4 solution were added to lower the pH of the polymerisation solution from approximately 7.2 to 5. The decrease of the solution pH to 4 caused a change in the solution colour from yellow to light yellow; therefore, a solution with a pH of 5 was used.

Under these conditions (pH 5) the polymerisation experiments were conducted by sweeping the electrode potential from 0 V to 2.5 V *vs.* SCE at a potential sweep rate of 0.05 V s^{-1}, as shown in Figure 5.18. This led to the formation of a coherent and uniform PPy film. In addition, the galvanostatic polymerisation of PPy was conducted in the presence of different concentrations of oxalic acid 0.01, 0.025, 0.05 and 0.1 mol dm^{-3} in the experiments, and a platinum electrode was used as a counter electrode and SCE as a reference. A non-uniform and discontinuous spot was seen in a random manner when a low concentration of oxalic acid was used (0.01 mol dm^{-3}). The increase in oxalic acid concentration to 0.025 mol dm^{-3} lead to the formation of a uniform PPy film over the electrode surface.

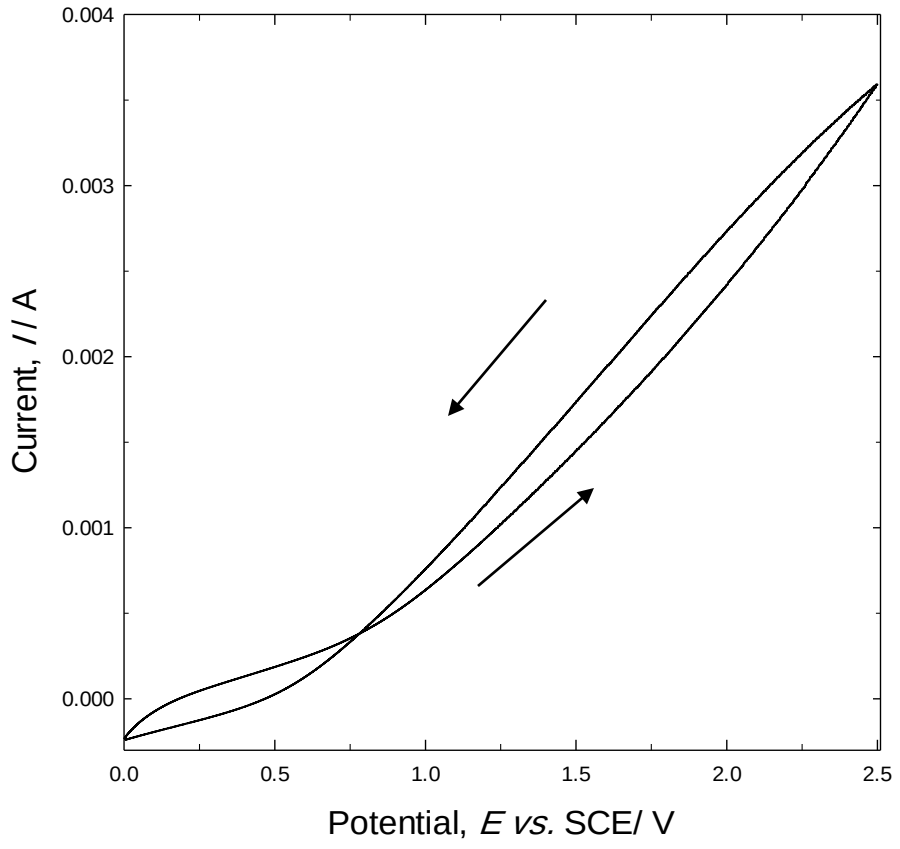

Figure 5-19: Cyclic voltammogram of 0.1 mol dm^{-3} Py in aqueous 0.5 x 10^{-3} mol dm^{-3} FSS at a potential sweep rate of 0.5 V s^{-1} at a SS electrode (1 cm^2 area). The 40^{th} cycle is shown here.

The increase in the oxalic concentration to 0.05 and 0.1 mol dm^{-3} seems to be because of the solubility of the FSS, since a dark orange powder precipitate formed on the bottom of the flask. In addition, since it seems that the colour of the solution changed when a higher concentration of oxalic acid was used and the solution pH also changed, the effect of the use of oxalic acid on FSS absorption was examined. The use of a low concentration of oxalic acid 0.01 mol dm^{-3} caused a reduction of the λ_{max} of FSS absorption and shifted the absorption from 1.717 a.u at λ_{max} 485 nm when no oxalic acid was used to λ_{max} 435nm when 0.01 mol dm^{-3} oxalic acid was used.

5.11 Release of fluorescein sodium salt

The PPy that contained FSS, was electrochemically deposited on a stainless steel electrode (PPy-SS), and was washed with 0.01 mol dm^{-3} NaCl for 5 min. The film was placed in an electrochemical cell containing 20 ml of 0.9% NaCl and a constant negative potential of - 0.75 V *vs.* Ag/ AgCl was applied for 1 hour to release the incorporated FSS model drug. At this potential, the polymer reduces and acquires a negative charge which repels the model drug. Samples of 5 cm^3 were taken at regular intervals of time from the release medium and replaced it with an equal volume from the original NaCl solution. The electrochemical release rate of FSS from the PPy-FSS electrode was higher than the release rate of FSS from unstimulated film. After 1 hour, maximum concentration of FSS released from the PPy-FSS electrode was 0.54 µmol dm^{-3} cm^{-2}, which is double the concentration of the FSS released from unstimulated film, as shown in Figure 5.19. The negative potential applied to release FSS from the PPy-SS electrode led to a reduction of the PPy film, which led to the expulsion of the incorporated FSS into the release medium.

Further, the release of anionic FSS from the stimulated and unstimulated PPy films is higher than the release of cationic MB. For example, the release concentration of MB from the PPy-pTS film when the film was stimulated using +0.6 V *vs.* SCE reached 0.084 μmol dm^{-3} after 5 minutes, which is significantly lower than the release of FSS from stimulated PPy film, which is 0.23 μmol dm^{-3}. Similarly, the release of FSS from unstimulated film within 5 minutes is 0.1 μmol dm^{-3}, which is significantly higher than the release of MB from the unstimulated PPy-pTS film 0.034 μmol dm^{-3}. This may occur because the uptake of the anionic FSS in the PPy film is higher than the uptake of the cationic MB, since the anionic FSS is incorporated into the PPy film during the polymerisation process to compensate the cationic charge of the PPy backbone; the similarity of the charge of the cationic MB and the cationic backbone of the oxidised PPy film diminishes the amount of MB that incorporated in the PPy film.

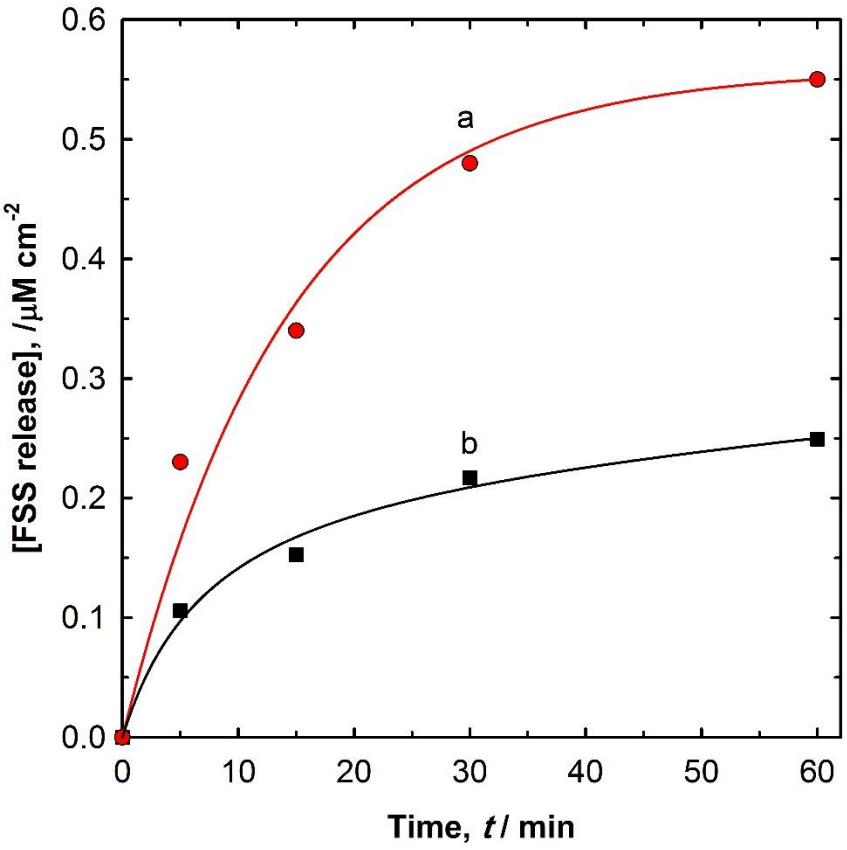

Figure 5-20: The concentration of FSS released from PPy films grown using the CV method during 40 cycles from a solution containing 0.1 mol dm^{-3} Py, 0.5 x 10^{-3} mol dm^{-3} FSS and adjusted to pH 5 with 0.05 x 10^{-3} mol dm^{-3} H_2SO_4. The films were stimulated with a) -0.75 V *vs.* Ag/AgCl constant potential and (b) no stimulation.

The MB may be absorbed on the PPy surface and physically entrapped in the PPy backbone, while the anionic FSS is incorporated in the PPy backbone owing to the presence of electrostatic interaction between the oxidised polymer bulk and the anionic nature of FSS.

Since the absorption of FSS is sensitive to the solution pH and this significantly affects the FSS release measurements, no further electrochemical experiments are conducted with FSS in this project.

5.12 Summary and Conclusions

The PPy films are able to release the cationic dye MB in a controlled manner using an electrical potential. The released concentration reached 60 nM after approximately 30 min when the PPy films were stimulated using + 0.6 V *vs.* SCE. The release decreased when the potential increased to 0.95 V *vs.* SCE. This occurred because the higher potential led to overoxidation of the films and a corresponding decrease in film electroactivity. However, the lowest amount of MB release was observed when the films were exposed to ± 0.6 V *vs.* SCE at 0.05 Hz. This may be because there was not sufficient time for the MB to diffuse outside the polymer matrix during the short oxidation periods; thus, it was attracted to the polymer matrix during the reduction period. The synthesis method of the polymer films did not appear to affect the MB release rate. There was no significant difference in the concentration of released MB when the polymer film was synthesised using either the CV or the galvanostatic method. The incorporation of TiNT in the PPy film slightly reduced the MB release rate. The decrease in the amount of MB released from PPy-TiNT-MB film may be because the adsorption of Py in TiNT is 240 mg g^{-1}, which is higher than the adsorption of MB in TiNT (133 mg g^{-1}) [90]. Therefore, the surface of TiNT is occupied by positively charged Py monomers, which may lead to reduced adsorption of MB. In addition, the incorporation of TiNT in the polymer matrix may change the film's morphology, thereby reducing the amount of MB released.

The efficiency of the conducting polymer films in releasing the drug from its surface is higher than from the polymer bulk. Increasing the film thickness increases the amount of drug released, but this increase does not cope with the amount of increase of film thickness and does not affect the release profile. This might have resulted from the fact that the thicker films are less electroactive and have a lower diffusion rate. The increase in the PPy film's thickness from 2 to 4 μm does not appear to significantly influence the amount of MB released. This is due to the fact that most of the MB was released from the film's surface. The concentration of MB in

the release medium increased by approximately 30% when the film increased by a factor of 4 from 2 to 8 μm .The increase in the amount of MB released can be attributed to the contribution of the MB from the polymer bulk, in addition to that released from the polymer surface due to the change in film structure and morphology. When the film thickness increased from 8 to 12 μm, the release rate of MB only increased by 10%. The release rate of MB from the PPy films is highly variable, because the MB is physically entrapped in the polymer film during the polymerization process instead of interacting electrostatically due to the charge similarity between the oxidised film and cationic MB.

The MB can be incorporated in the PPy film after the polymerisation process using a negative potential. The use of more negative potential is more efficient for reducing PPy films. This led to an increase in the amount of MB incorporated in the PPy films and, subsequently, on the amount of released MB. However, this amount is lower than the amount released when the MB was incorporated during the polymerisation process. This indicates that MB was unable to penetrate into the polymer bulk due to its large structure, and a considerable amount of MB was loaded on the film surface. In addition, the amount of MB released increased as the initial concentration of the MB in the solution increased. The increase of the initial MB concentration led to an increase in the diffusion of MB into the PPy films, lowering their concentration gradient and the reduction potential, which resulted in increasing the amount of incorporated MB in the PPy films and, subsequently, increased the MB release rate.

Chapter 6: Release of DA and IP Drugs from PPy Films

This chapter investigates the use of PPy films as a delivery system for cationic dopamine (DA) and anionic ibuprofen (IP) drugs. The two drugs have been particularly chosen to study the effect of the molecule charge on the drug release rate. CV and galvanostatic methods are used to synthesise the PPy films. In addition, the influence of the presence of the titanate nanotubes (TiNT) on the polymerisation solution on the uptake and release of the molecules from the polymer films as well as the effect of the variations of the doping anions is investigated. The effect of the use of stimulation potentials on the molecule's release rate is also examined.

6.1 Polymer synthesis using the CV and galvanostatic methods of DA release

PPy containing dopamine hydrochloride (DA) was synthesised from a solution composed of 0.1 mol dm^{-3} Py in 0.025 mol dm^{-3} oxalic acid and 0.5 x 10^{-3} mol dm^{-3} DA in both, the presence and absence of 1 mg mol^{-1} TiNT. The solutions were stirred at approximately 500 rpm with a magnetic stirring bar (2 cm) to disperse the TiNT. The PPy-DA film was deposited by two techniques. Firstly, the PPy containing DA was electrodeposited at a constant current of 0.3 mA cm^{-2} for 1600 s. The theoretical thickness of the obtained film was 2 μm. Secondly, the PPy-DA film was electrodeposited by CV at a linear sweep rate of 50 mV s^{-1} between -0.25 and 1 V *vs.* SCE over 10 cycles.

Figure 6.1 illustrates the chronopotentiogram for the polymerisation of Py in the presence and absence of dispersed TiNT. The curve a in the figure shows the evolved potential during the synthesis of PPy-TiNT-DA film. The potential rapidly peaked at 0.633 V *vs.* SCE, which

indicates the initial nucleation of the Py monomers to begin the polymerisation process. The potential then quickly dropped to 0.57 V *vs*. SCE within approximately four minutes. Thereafter, it reduced slightly until it reached 0.53 V *vs*. SCE toward the end of the polymerisation process. Curve b shows the evolved potential during the Py polymerisation in the absence of TiNT. During the early stage of the polymerisation, there was a slight decrease of 0.01 V with respect to curve a in the potential; the voltage tends to be a close match to the polymerisation voltage of PPy-TiNT-DA. The increase of the Py polymerisation voltage in the presence of TiNT may be because the catalysing effect of TiNT is high at the initial stage of the polymerisation process [90].

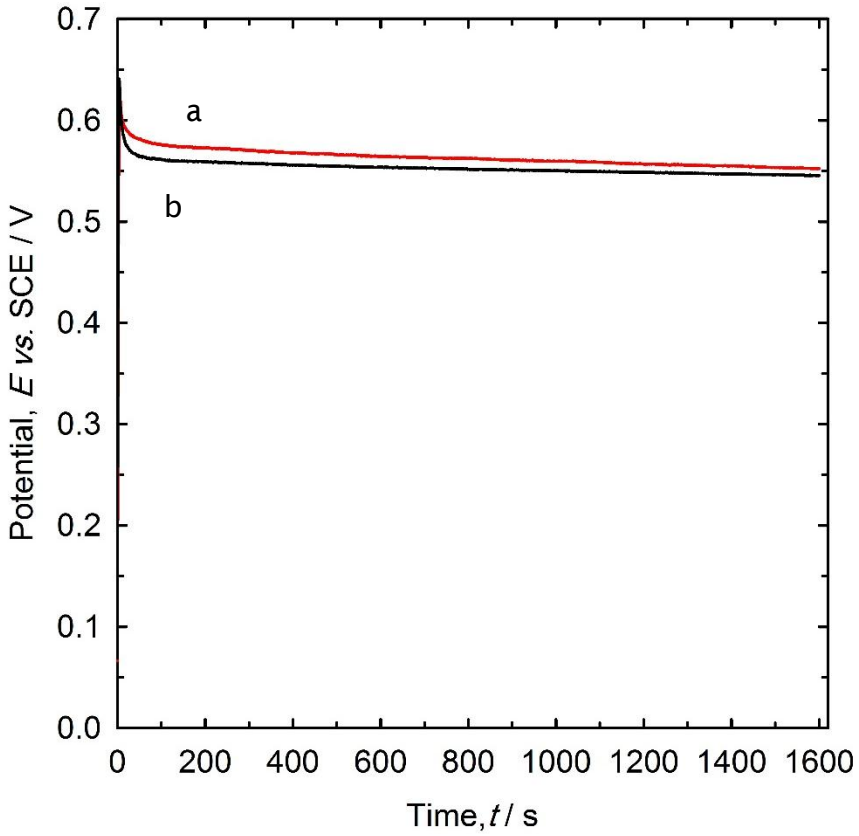

Figure 6-1: Chronopotentiogram for the galvanostatic polymerisation of PPy-DA films at current densities of 0.3 mA cm^{-2} for 1600 s from a solution composed of 0.1 mol dm^{-3} Py in 0.025 mol dm^{-3} oxalic acid, and 0.5 x 10^{-3} mol dm^{-3} DA in the presence (red), and absence (black), of 1 mg mol^{-1} TiNT.

Figure 6.2 depicts the 10th CV cycles during the synthesis of PPy-TiNT-DA (a) and PPy-DA films (b). Curve a in the figure represents the polymerisation current density of Py, which is approximately 7.29 mA cm^{-2} at 1.1 V *vs.* SCE, while the polymerisation current density for Py in the presence of TiNT (curve b) is 6.31 mA cm^{-2} at 1.1 V *vs.* SCE. The slight increase in the oxidation current observed in the presence of TiNT indicates that the TiNT catalysed the Py polymerisation process. This occurred because the Py monomer was adsorbed on the surface of the negatively charged TiNT. This, in turn, may lead to an increased concentration of Py monomers near the electrode surface, hence causing an increased polymerisation rate. However, the increased amount of TiNT in the solution (less than 10%) could have lead to an increased amount of adsorbed Py monomers, which might further increase in the polymerisation rate. It may also lead to a decrease in the conductivity of the PPy film due to the low conductivity of TiNT. A homogenous black PPy film was formed over the working electrode in both methods.

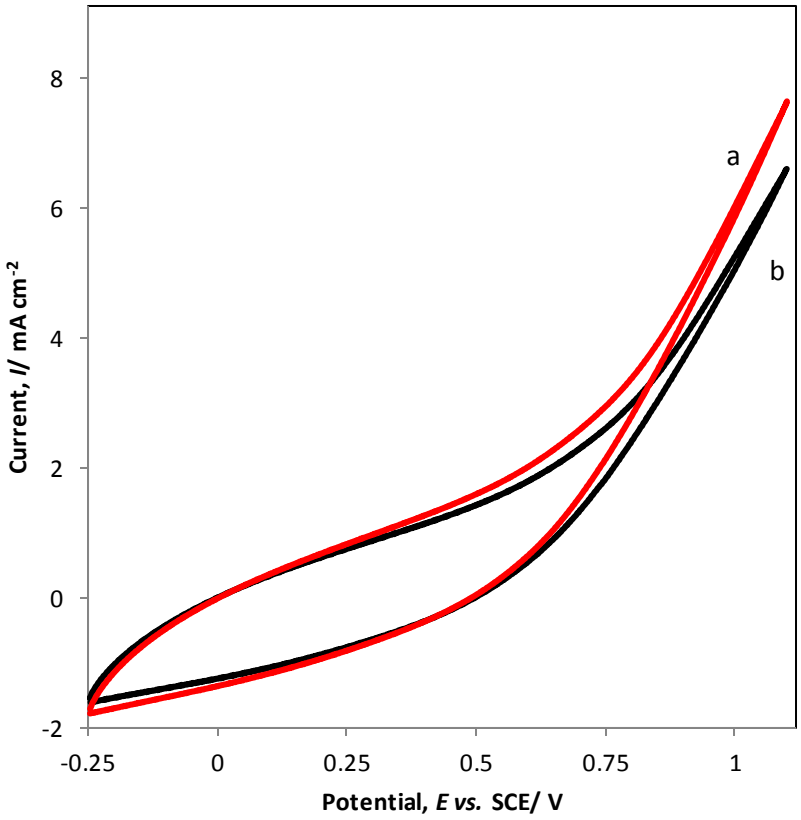

Figure 6-2: CV at a stainless steel electrode (1 cm^2) in 0.1 mol dm^{-3}, 0.025 mol dm^{-3} oxalic acid, and 0.5 x 10^{-3} mol dm^{-3} DA in the presence (a) and in the absence (b) of 1 mg mol^{-1} TiNT at a potential sweep rate of 50 mV s^{-1}. The solutions were stirred at approximately 500 rpm.

The CV analysis of the PPy-MB films which were synthesised from a solution composed of 0.1 mol dm^{-3} Py in 0.025 mol dm^{-3} oxalic acid and 0.5 x 10^{-3} mol dm^{-3} DA was carried out. The galvanostatic and CV methods described in Sections 5.1 and 5.4 were used. The CV analysis was carried out in a 0.9% NaCl aqueous solution to observe the effect of the synthesis method on the polymer films' electroactivity in the medium that would be used for the DA release. Figure 6.3 shows the CV curves for the PPy-DA sythetised using CV and the galvanostatic method in 0.9% NaCl aqueous solution. Curve a in Figure 6.3 shows wide oxidation and reduction waves with no clear oxidation or reduction peaks for the PPy-DA film which was synthesised using CV. The oxidation current of the film reached 9.8 mA cm^{-2} at 1.2 V *vs.* SCE;

the reduction peak current was approximately -2.39 mA cm^{-2} at 0 V *vs.* SCE. Curve b in the figure indicates a wide oxidation wave with no clear oxidation peak for the PPy-DA film synthesis using the galvanostatic method.

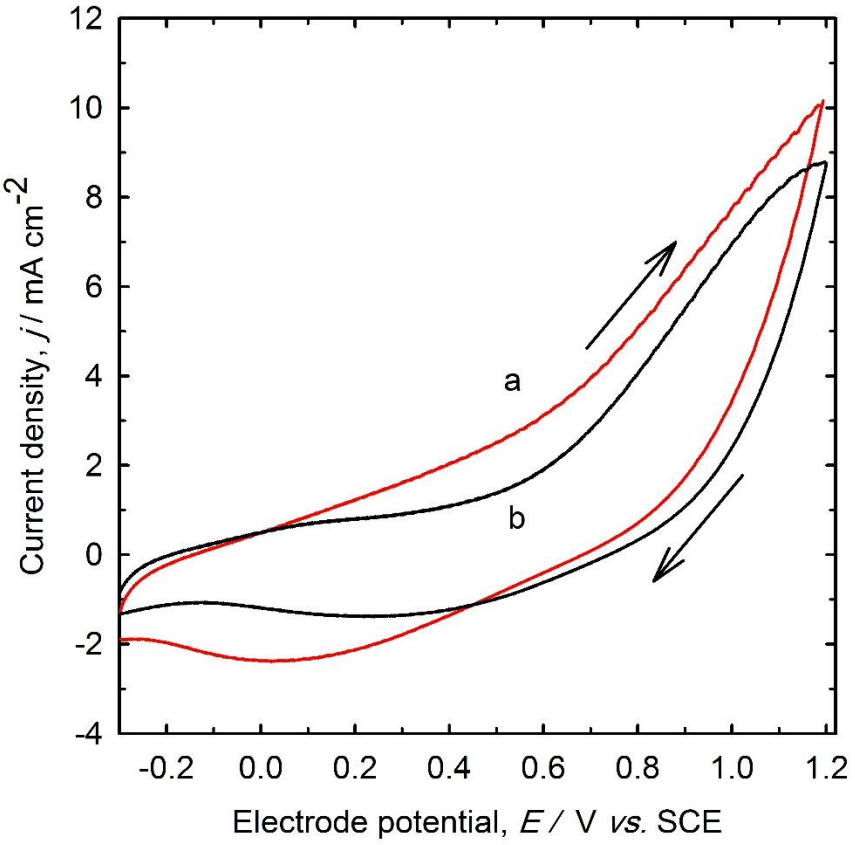

Figure 6-3: CV of PPy-DA films in 0.9% NaCl at a potential sweep rate of 50 mV s^{-1} a) PPy-DA film synthesis using CV at a potential sweep rate of 50 mV s^{-1} for 10 cycles and b) PPy-DA film grown galvanostatically for 1600 s at 0.3 mA .

The oxidation current reached 8.7 mA cm^{-2} at 1.2 V *vs.* SCE. The CV curves indicated an insignificant increase in the electroactivity of the PPy-DA synthesis using CV. It is clear from the CV analysis that the PPy-DA films' synthesis using CV is more active than the films' synthesis using the galvanostatic method. The anodic current began rising at a potential of 0.55 V *vs.* SCE, which indicated the oxidation of the PPy-DA film. The cathode current start declined

at a potential of approximately 0.48 V *vs*. SCE during the backward scan, which was an indication of the beginning of dedoping of the polymer film.

6.1.1 Open circuit potential measurements of PPy-dopamine films

The open circuit potential (OCP) of dopamine film in the release solution began at 0.11 V *vs.* SCE and decreased rapidly over the initial 30 min to 0.094 V *vs.* SCE. Then, the potential increased over the next 120 min to approximately 0.1 V *vs.* SCE and continued to increase at a slower rate until it reached 0.103 V *vs.* SCE, after 300 min before stabilising at approximately 0.102 V *vs.* SCE (Figure 6.4). The initial decrease in potential may be a result of the cation release that took place immediately after the film was immersed in the release solution. The diffusion of the cations from the film may have lead to changes in the polymer backbone charges, compensated by ion uptake from the solution to the polymer film. Comparing the OCP with corresponding CV analysis of the film shows that the OCP of the film is approximately 0.1 V *vs.* SCE. This finding indicates that the polymer film would be in a reduced state without the application of a stimulus potential.

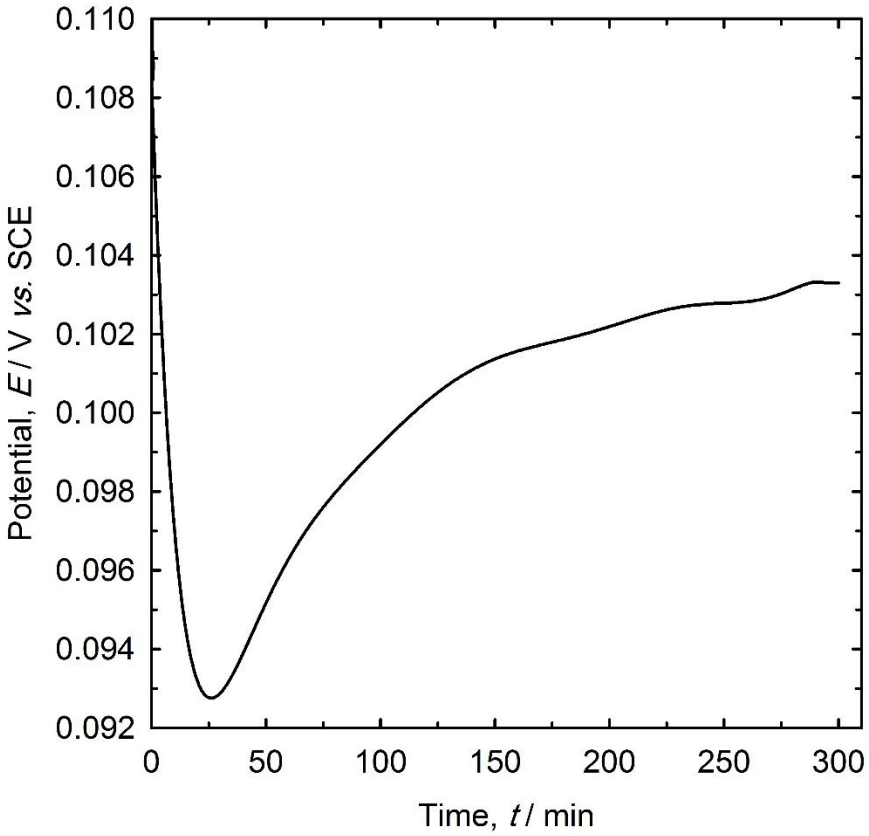

Figure 6-4: Open circuit potential for PPy-DA films deposited on a stainless steel electrode at 0.3 mA cm^{-2}. The potential was observed in 0.9% NaCl aqueous solution *vs.* SCE reference electrode, over 5 h.

6.1.2 Dopamine release from PPy-DA films

The dopamine release from the PPy films was carried out in a 0.9% NaCl solution. The DA release was performed using a constant potential of +0.6 V *vs.* SCE, a pulsed potential of ±0.6 V at 0.05 Hz *vs.* SCE and unstimulated release.

The application of electrical stimulation to the PPy-DA films resulted in a significantly higher release rate of DA compared to unstimulated films, as illustrated in Figure 6.5. A large initial burst release of DA was detected under all the applied stimulation protocols. Most of the DA was released during the initial 30 min of the film stimulation. The highest amount of DA

released from the PPy-DA films was observed when the polymer films were stimulated by pulsed potential (±0.6 V at 0.05 Hz *vs.* SCE). The maximum concentration of DA in the release medium extended to 7 μmol dm^{-3} during 30 min. Thereafter, the DA release rate linearly declined over the remaining stimulation period. The films spent the same amount of time in the oxidized and reduced states. The actuation of the film under pulsed potential may result in the increase and decrease of the film volume associated with the movement of mobile ions and associated solvent molecules in and out of the film matrix. These movements may pump the DA out of the polymer films. The DA release rate decreases when a constant oxidation potential of +0.6 V *vs.* SCE is applied to the PPy-DA film. The amount of DA cations released increased initially before reaching an almost stable plateau after 30 min. The maximum concentration of DA in the release solution was approximately 4.2 μmol dm^{-3}, which is 60% lower than that released using pulsed potential. A lower DA release rate was observed in unstimulated films. The concentration of DA reached 0.8 μmol dm^{-3} cm^{-2} within 15 min and decreased to 0.1 μmol dm^{-3} cm^{-2} after 75 minutes. This decrease occurred because the PPy film is in its reduced state, as has been proven from OCP and CV. Therefore, the cationic DA is entrapped in the polymer matrix due to the electrostatic attractive forces between the negatively charged polymer matrix and the positively charged DA molecules.

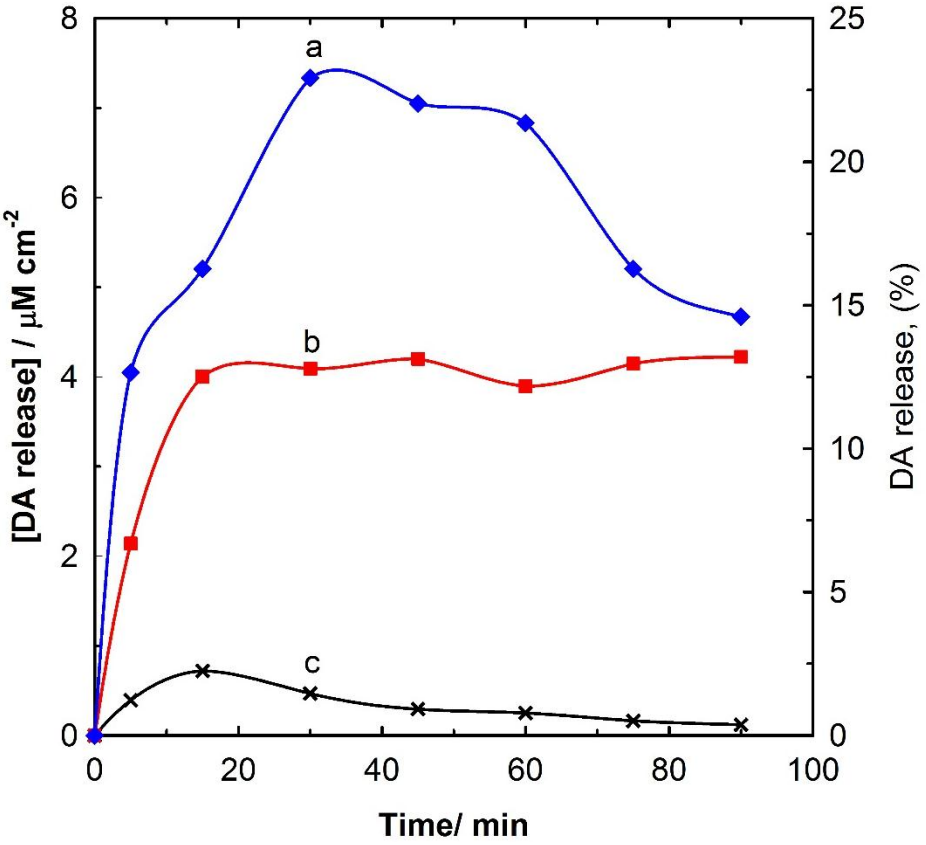

Figure 6-5: DA releases from PPy films grown for 1600 s at 0.3 mA cm^{-2} from a solution of 0.1 mol dm^{-3} Py, 0.5 x 10^{-3} mol dm^{-3} DA, and 0.025 mol dm^{-3} oxalic acid. The films were stimulated with (a) pulsed potential of ±0.6 V at a frequency of 0.05 Hz *vs.* SCE, (b) +0.6 V *vs.* SCE constant potential and (c) no stimulation over 90 min.

6.1.3 CV methods for increasing dopamine release

The dopamine released from PPy-DA films prepared by CV is displayed in Figure 6.6. The release pattern of DA is similar to that observed for the PPy-DA films formed galvanostatically, but there is an increase in DA release from the PPy-DA films prepared by CV compared to the films' synthesis by the galvanostatic method. The increase in the release amount of DA may have occurred because a higher quantity of DA was incorporated into the PPy films during the reduction cycle of the PPy film. The positive charge of the PPy backbone is neutralised during the film reduction and the incorporated oxalate anions ($C_2O_4^{2-}$) generate a net negative charge within the polymer matrix.

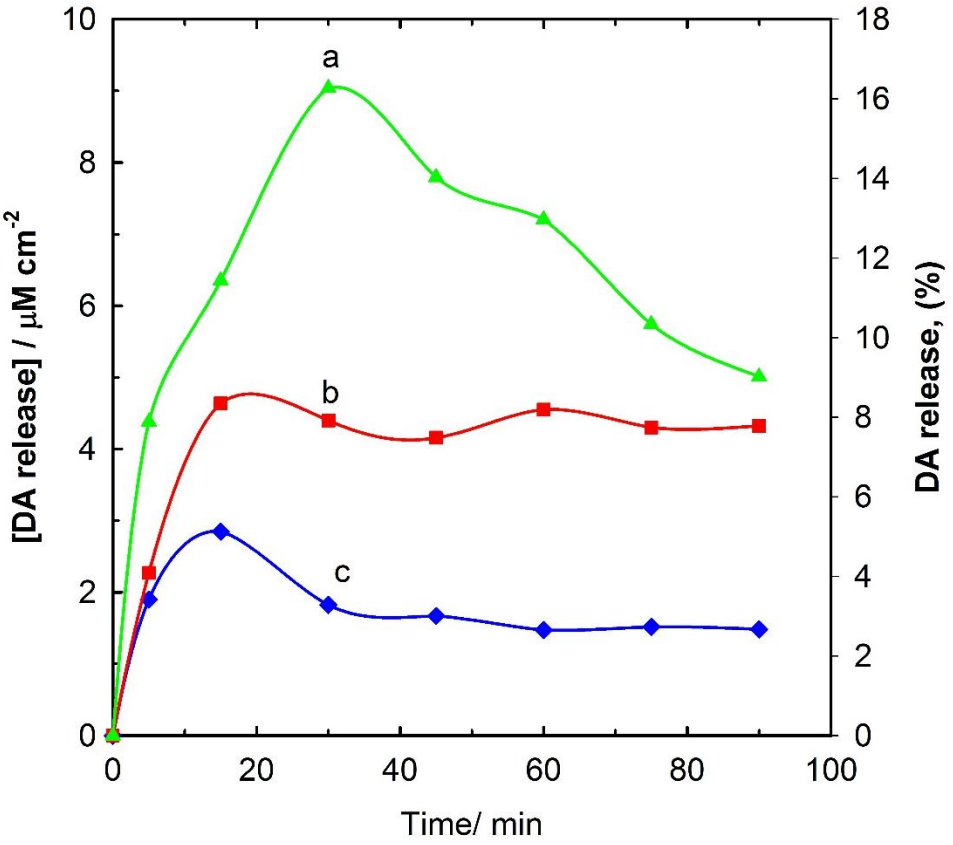

Figure 6-6: DA release from PPy films grown using CV for the 10th cycle from a solution of 0.1 mol dm^{-3} Py, 0.5 x 10^{-3} mol dm^{-3} DA and 0.025 mol dm^{-3} oxalic acid. The films were stimulated with (a) pulsed potential of ±0.6 V at a frequency of 0.05 Hz *vs.* SCE, (b) +0.6 V *vs.* SCE constant potential and (c) no stimulation over 90 min.

The DA cations will diffuse due to a concentration gradient and electrostatic attraction between opposite charges and are then incorporated into the PPy film to compensate for the polymer matrix's negative charge. In the same behaviour of the PPy-DA film synthesised galvanostatically, the highest amount of DA released from PPy-DA obtained using CV occurred when the film was stimulated using the pulsed potential ±0.6 V *vs.* SCE. The maximum concentration of DA in the release solution reached 9 μmol dm^{-3} cm^{-2}, which is slightly higher than the released amount from PPy-DA films synthesised using the galvanostatic method. The release rate of DA from the unstimulated film was significantly lower than that observed with

electrically stimulated films. This release was almost certainly due to the diffusion of the DA through the polymer backbone.

6.1.4 The influence of using TiNT on the DA release

The PPy-DA film was electrodeposited by CV and by the galvanostatic technique using an aqueous solution containing 0.1 mol dm^{-3} Py in 0.025 mol dm^{-3} oxalic acid and 0.5 x 10^{-3} mol dm^{-3} dopamine hydrochloride (DA) in the presence of 1 mg mol^{-1} TiNT, as outlined in Section 6.1. To disperse the TiNT, the solutions were stirred with a magnetic stirring bar at approximately 500 rpm.

6.1.4.1 DA release from PPy-TiNT-DA films

The DA release was performed by applying a constant potential of +0.6 V *vs.* SCE, a pulsed potential of ±0.6 V at 0.05 Hz *vs.* SCE and unstimulated release, as described previously in Section 2.10. Figure 6.7 displays the DA release profile from the PPy-TiNT-DA films' synthesis using galvanostatic and CV methods, when the films were exposed to different stimulation protocols. The release profile of DA from the PPy-TiNT-DA films is similar to that observed from the PPy-DA films. The amount of DA released from PPy-TiNT-DA is significantly higher than that released from the film without TiNT. In addition, the concentration of DA released from the PPy-TiNT-DA films' synthesis using CV is higher than that released from the films' synthesis using the galvanostatic method when both films were stimulated using a pulsed potential of ±0.6 V at 0.05 Hz *vs.* SCE. However, the DA release is very low, when the films are stimulated using a constant potential of +0.6 V *vs.* SCE or unstimulated. The concentration of DA released from the films that were synthesised using CV reached 4.3 μmol dm^{-3} cm^{-2} after

15 min, which is slightly higher than that released from the films, which is formed galvanostatically (1µmol dm^{-3} cm^{-2} approximately) when both films are unstimulated. When the films were stimulated using +0.6 V *vs.* SCE, the concentration of DA release from the prepared films' use of the galvanostatic method reached 5.8 µmol dm^{-3} cm^{-2} within 30 min. Further, the concentration of DA reduced to 4 µmol dm^{-3} cm^{-2} after 60 min probably due to the low amount of incorporated DA during the polymerisation. There was a slight increase in the DA release from the films' synthesis using the CV method compared to the films' synthesis using the galvanostatic method, when the films were stimulated under the same conditions. In addition, the concentration of DA in the release medium reached 6 µmol dm^{-3} cm^{-2} after 30 min and remained sustained at the same concentration for the remaining releasing time. When the films were stimulated using ±0.6 V at a frequency of 0.05 Hz *vs.* SCE, the release concentration of DA from the polymer films, which was formed using CV, increased to 18 µmol dm^{-3} cm^{-2} within 45 min. This result is higher by approximately 38% in comparison to the release concentration of DA from the polymer films, which were synthesised using the galvanostatic method.

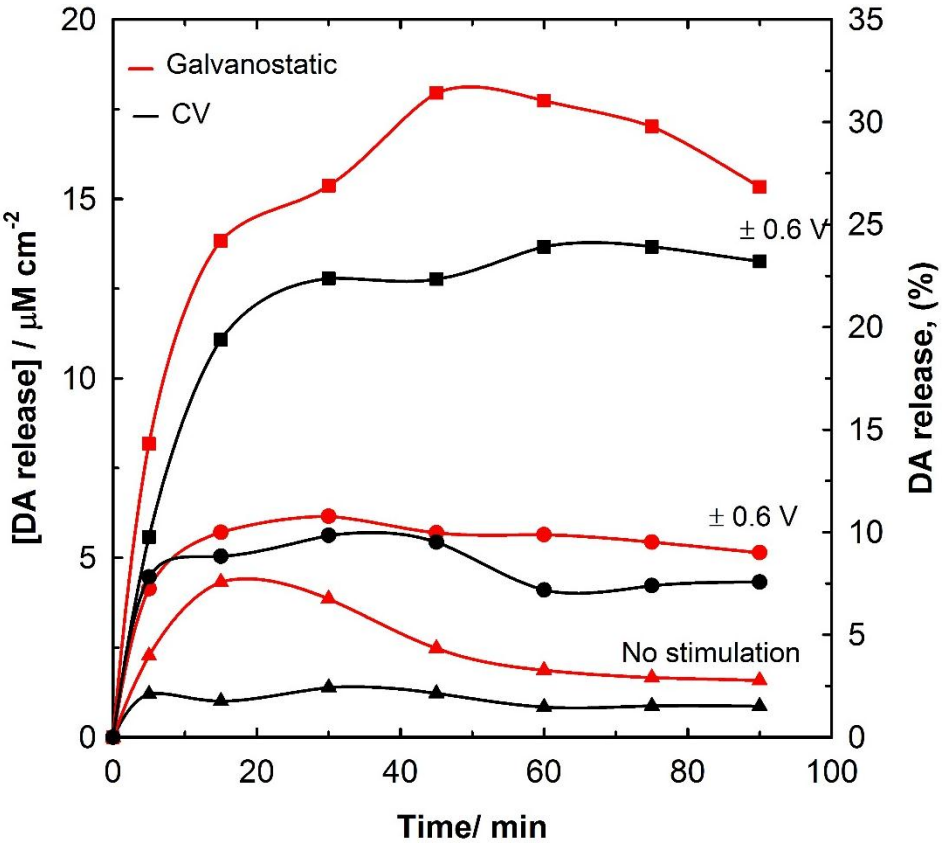

Figure 6-7: DA releases from PPy films grown for 1600 s at 0.3 mA cm^{-2} (red), and films grown using CV during 10 cycles from a solution of 0.1 mol dm^{-3} Py, 0.5 x 10^{-3} mol dm^{-3} DA and 0.025 mol dm^{-3} oxalic acid with 1 mg mol^{-1} TiNT. The films were stimulated with (■) a pulsed potential of ±0.6 V at a frequency of 0.05 Hz *vs.* SCE, (●) +0.6 V *vs.* SCE constant potential, and (▲) no stimulation over 90 min.

6.1.5 Release of DA from the PPy/pTS-DA film

The release of DA from the PPy/pTS-DA film was performed by applying a constant potential of +0.6 V *vs.* SCE and unstimulated release, as described previously in Section 5.3.

Figure 6.8 displays the cumulative release pattern of DA from the PPy/pTS-DA films' synthesis using galvanostatic and CV methods. The release profile of DA from PPy/pTS-DA film is similar to the release of DA from the PPy doped with oxalic acid, where greater amounts of DA

released from PPy films' synthesis using the CV method, when the films were stimulated using ± 0.6 V at a frequency of 0.05 Hz *vs.* However, there was a significant increase in the DA released from the PPy films doped with pTS compared with the films doped with oxalic acid on both released protocols. The amount of released DA from the PPy/pTS-DA films prepared using the CV method reached 19 µmol dm^{-3} cm^{-2} within 15 min, which was higher than that released from the films' synthesis using the galvanostatic method, 16.5 µmol dm^{-3} cm^{-2} during the same period of time. The amount of released DA was higher than that released from the PPy doped with oxalic acid, where 6.3 and 4.2 µmol dm^{-3} cm^{-2} were released from the films' synthesis using the CV and galvanostatic methods under identical release conditions. Similarly, 12.5 µmol dm^{-3} cm^{-2} DA was released from the PPy/pTS-DA film, compared with approximately 2.8 µmol dm^{-3} cm^{-2} released from PPy film doped with oxalic acid, when both films were synthesised using the CV method and unstimulated for a duration of 15 min. Similarly, the concentration of DA released from PPy/pTS-DA film which was synthesised using the galvanostatic method 10 µmol dm^{-3} cm^{-2} was significantly higher than that released from PPy doped with oxalic acid 0.8 µmol dm^{-3} cm^{-2}.

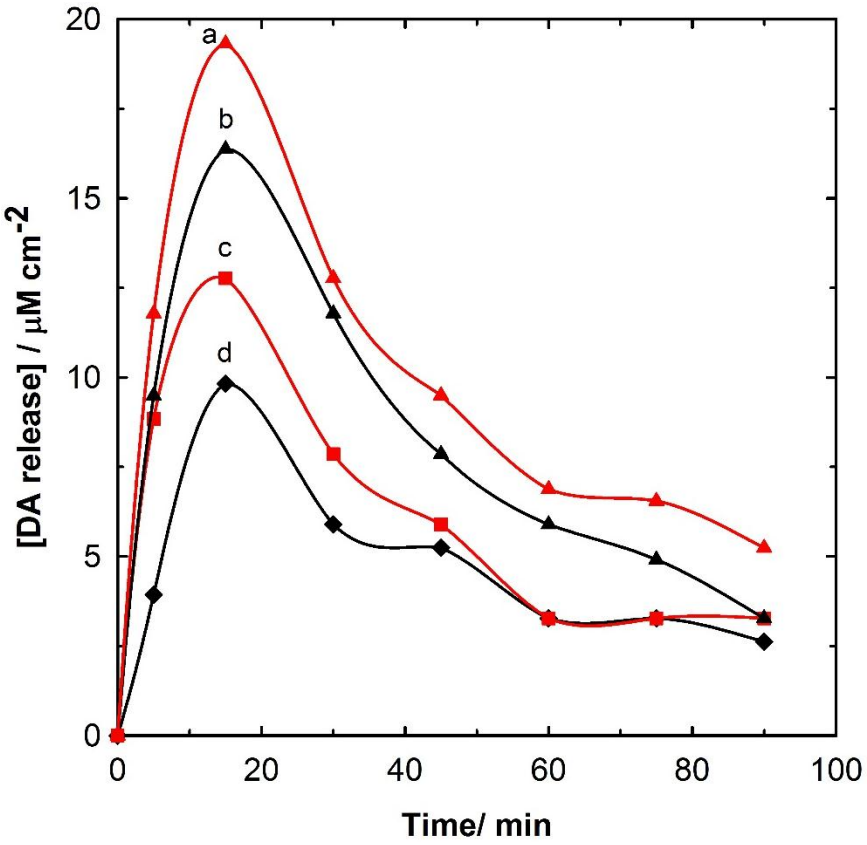

Figure 6-8: Dopamine release from PPy/pTS-DA films that were grown using CV during 10 cycles (red), the films were stimulated with (a) +0.6 V *vs.* SCE constant potential, (c) no stimulation and films grown for 1600 s at 0.3 mA cm^{-2} from a solution of 0.2 mol dm^{-3} Py, 0.5 x 10^{-3} mol dm^{-3} DA and 0.05 mol dm^{-3} pTS. The films were stimulated with (b) +0.6 V *vs.* SCE constant potential, and (d) no stimulation over 90 min.

6.2 Polymer synthesis for ibuprofen release

PPy containing IP was synthesised from a solution composed of 0.1 mol dm^{-3} Py in 0.025 mol dm^{-3} oxalic acid and of 0.5 x 10^{-3} mol dm^{-3} ibuprofen sodium salt (IP) in both the presence and absence of 1 mg mol^{-1} TiNT. The solutions were stirred at approximately 500 rpm with a magnetic stirring bar (2 cm) to disperse the TiNT. The PPy-IP film was deposited using two techniques. The PPy containing IP was electrodeposited galvanostatically at a constant current density of 0.3 mA cm^{-2} for 1600 s. The theoretical thickness of the obtained film is 2 μm [251]. In

addition, the PPy-IP film was electrodeposited by CV at a linear sweep rate of 50 mV s^{-1} between -0.25 and 1 V *vs.* SCE over 10 cycles.

Figure 6.9 illustrates the chronopotentiogram for the polymerisation of Py in the presence and absence of dispersed TiNT. Curve a in the figure represents the evolved potential during the synthesis of the PPy-TiNT-IP film. The potential rapidly peaked at 0.633 V *vs.* SCE, which indicates the initial nucleation of the Py monomers to begin the polymerisation process. Within approximately four minutes, the potential quickly reduced to 0.57 V *vs*. SCE. Thereafter, it reduced slightly until it reached 0.53 V *vs*. SCE toward the end of the polymerisation process. Curve b represents the evolved potential during the Py polymerisation in the absence of TiNT. During the early stage of the polymerisation, there was a slight decrease of 0.01 V *vs.* SCE in the potential; the voltage tended to be a close match to the polymerisation voltage of PPy-TiNT-IP. The increase in the Py polymerisation voltage in the presence of TiNT may be because the catalysing effect of TiNT is high in the early stage of the polymerisation process.

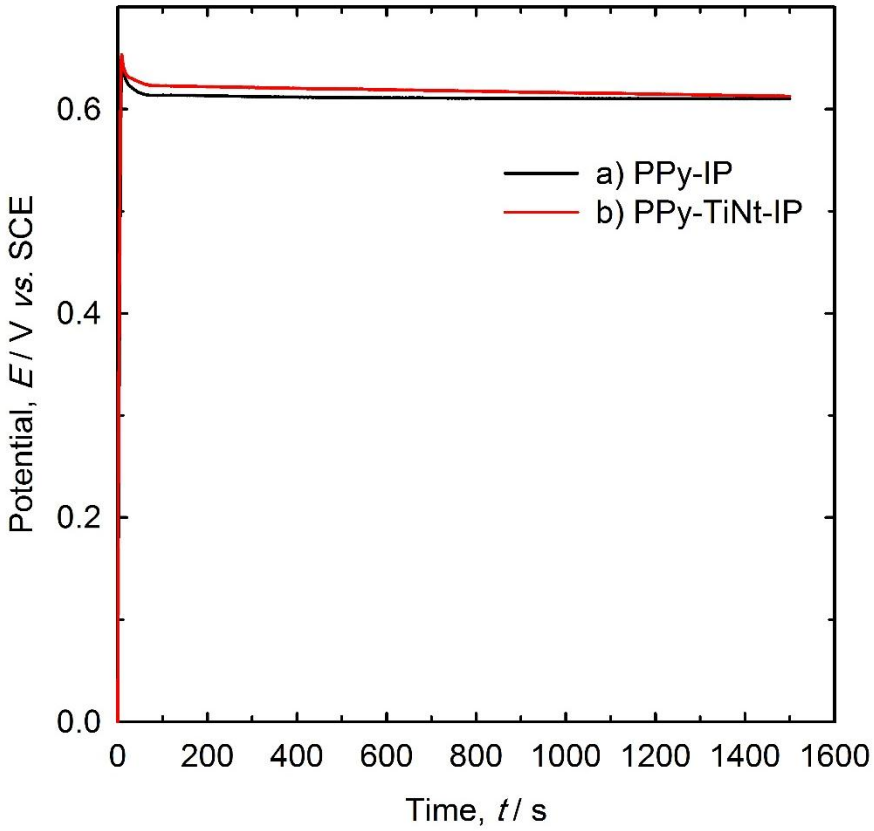

Figure 6-9: Chronopotentiogram for the galvanostatic polymerisation of PPy-IP films at current densities of 0.3 mA cm^{-2} for 1600 s from a solution that contains 0.1 mol dm^{-3} Py in 0.025 mol dm^{-3} oxalic acid and 0.5 x 10^{-3} mol dm^{-3} IP in the presence (red), and absence (black), of 1 mg mol^{-1} TiNT.

The OCP potential decreased quite rapidly over the first 100 min and then stabilised at 0.086 V *vs.* SCE due to the solvation effect after the film was immersed in the solution, as shown in Figure 6.10. A comparison of the OCP with a corresponding CV analysis of the film Figure 6.11 reveals that the potentials were lower than V *vs.* SCE. Therefore, the film is partially oxidised in nature without the application of a stimulus potential

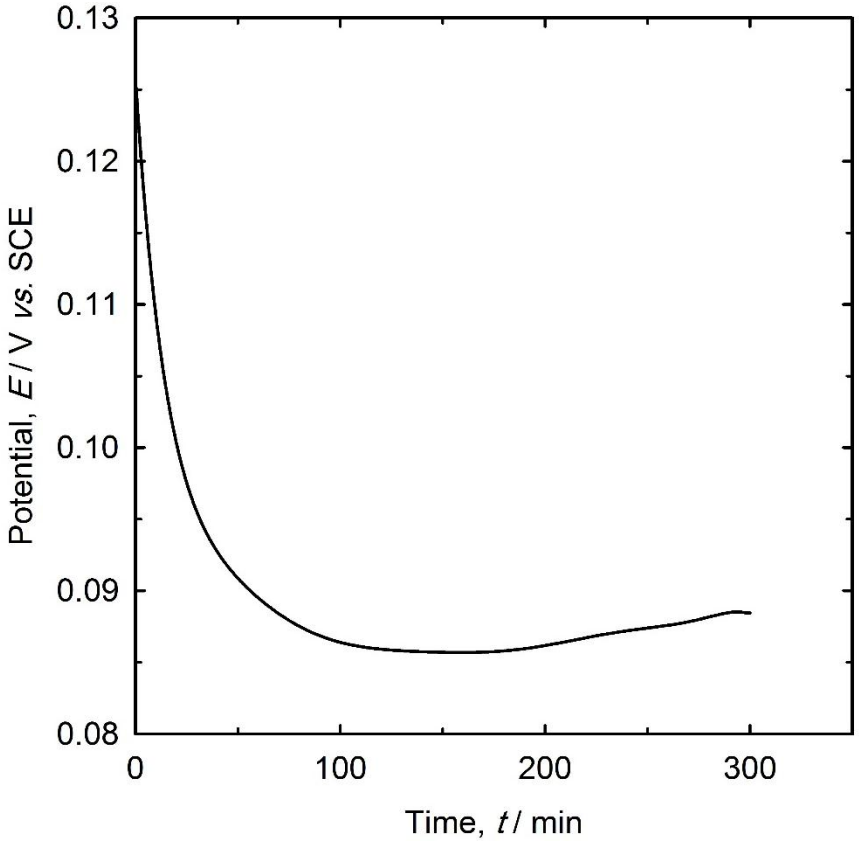

Figure 6-10: Open circuit potential for the PPy-IP film deposited on a stainless steel electrode at 0.3 mA cm^{-2}.The potential was observed in 0.9% NaCl aqueous solution *vs.* SCE reference electrode, over 5 h.

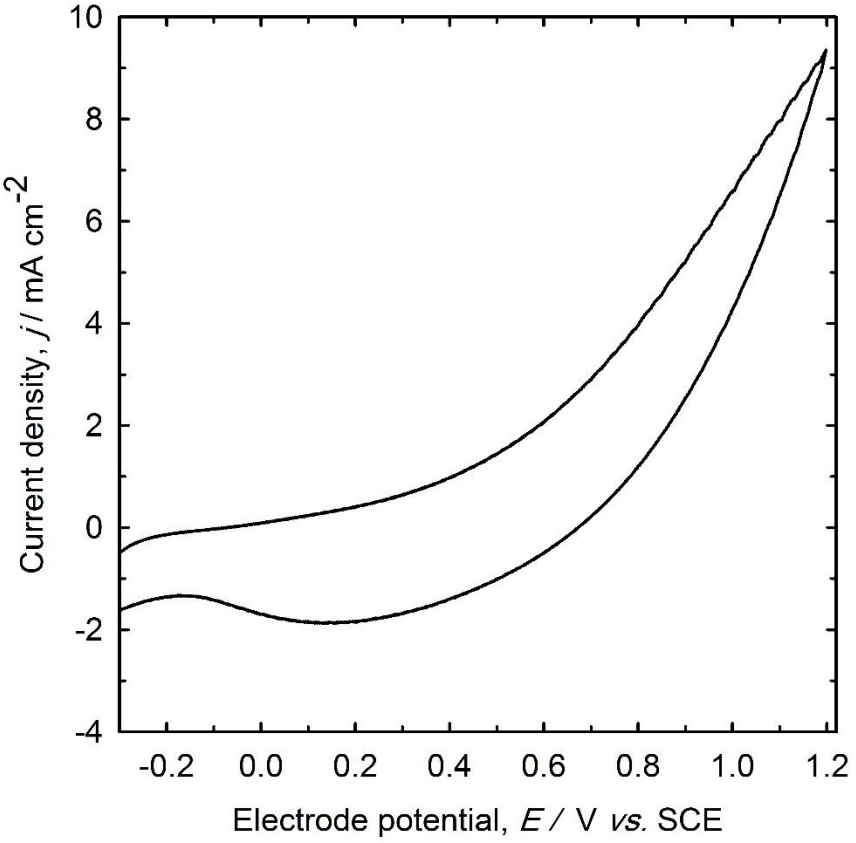

Figure 6-11: CV of PPy-IP films in 0.9% NaCl at a potential sweep rate of 50 mV s^{-1} grown galvanostatically for 1600 s at 0.3 mA.

6.2.1 Ibuprofen release from PPy-IP films doped with oxalic acid

PPy-ibuprofen films were electrodeposited during 10 cycles CV and by galvanostatic method at a constant current density of 0.3 mA cm^{-2} for 1600 s from a solution composed of 0.1 mol dm^{-3} Py in 0.025 mol dm^{-3} oxalic acid and of 0.5 x 10^{-3} mol dm^{-3} IP in both the presence and absence of 1 mg mol^{-1} TiNT the release of IP was carried out by applying a constant potential of - 0.6 V *vs.* SCE, and unstimulated release, as described previously in Section 5.3. Figure 6.12 displays the IP release profile from the PPy films', when the films were exposed to the mentioned stimulation protocol. The lowest released amount of IP was released when the films were unstimulated. This confirmed that the release of IP from PPy exhibit a potential controlled manner. The decline of the amount of IP released from unstimulated films was (the films were

not sufficiently reduced) expected because the unstimulated PPy films are in their oxidised state, which is confirmed from the open circuit potential and CV (Figures 6.10 and 6.11). It is evident that the amount of released IP from the synthesis of PPy films using the galvanostatic method is higher than the release from the synthesis of films using the CV method. For example, the amount of released IP from the PPy films' synthesis using the galvanostatic method for 30 min was 24 μmol dm^{-3} cm^{-2}, while that released from the synthesis of PPy films using the CV method when both films were unstimulated was 20 μmol dm^{-3} cm^{-2}. This reduction in the amount of IP released may have occurred because some of the incorporated IP during the oxidation of the PPy films was released during the reduction cycle. The use of TiNT led to a reduction in the amount of IP released from PPy films which were synthesised using both the CV and galvanostatic methods, when both stimulation and passive released were used. For example, the concentration of released IP decreased from 51 to 39 μmol dm^{-3} cm^{-2}, which was released from the PPy films synthesised using the CV method in the absence and presence of TiNT, respectively. Similarly, the concentration of released IP within 30 min decreased from 63 to 45 μmol dm^{-3} cm^{-2} in the synthesis of PPy films using the galvanostatic method in the absence and presence of TiNT, respectively, when both films were stimulated using -0.6 V *vs.* SCE. The decrease in the amount of IP released may have occurred because the absorption of IP in the TiNT is low due to the charge repulsion between the negatively charged IP anion and TiNT [90].

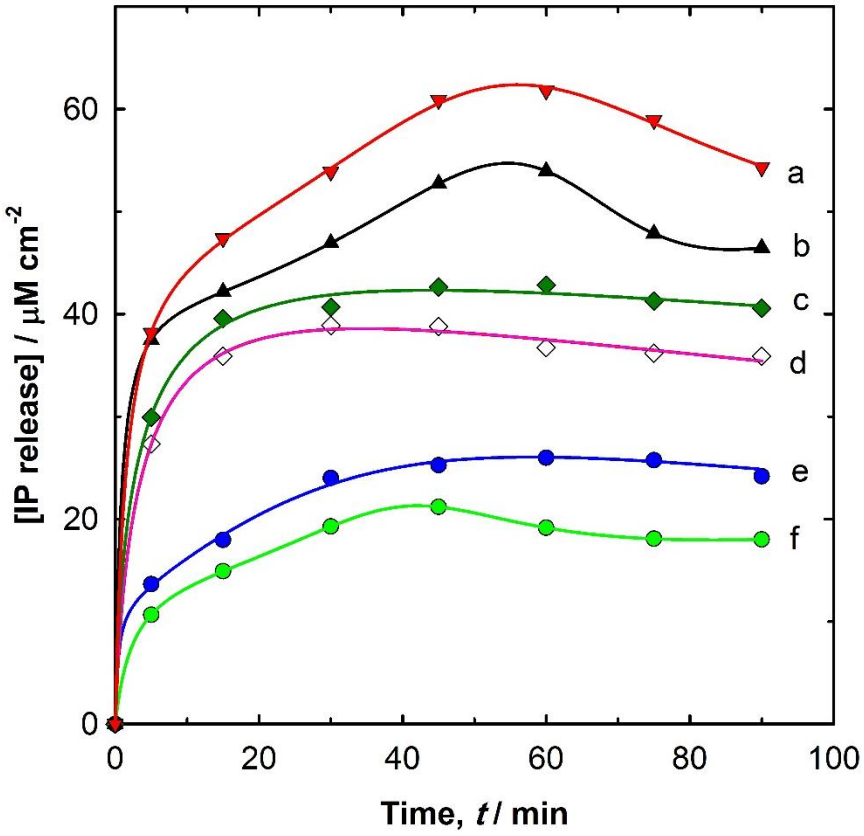

Figure 6-12: IP released from PPy films grown for 1600 s at 0.3 mA cm^{-2} from a solution of 0.1 mol dm^{-3} Py, 0.5 x 10^{-3} mol dm^{-3} IP and 0.025 mol dm^{-3} oxalic acid in the absence of TiNT. a) Film stimulated with -0.6 V *vs.* SCE, b) film stimulated with -0.6 V, and the film were grown using CV during 10 cycles in the absence of TiNT, c) films were stimulated with - 0.6 V *vs.* SCE, d) stimulated with - 0.6 V *vs.* SCE were the films synthesis using galvanostatic and CV method respectively, e) unstimulated film, and with 1 mg mol^{-1} TiNT and f) unstimulated film, and with 1 mg mol^{-1} TiNT.

6.3 The release of IP from PPy/pTS-IP films

PPy/pTS-IP films were synthesised using both the CV and galvanostatic methods, as described in Section 5.9.1, from an electrolyte containing 0.2 mol dm^{-3} Py, 0.05 mol dm^{-3} pTS and 0.5 x 10^{-3} mol dm^{-3} IP. The release was performed by applying a constant potential of –0.6 V *vs.* SCE, and unstimulated release, as described previously in section 5.3.

Figure 6.13 depicts the aggregate release pattern of IP from the PPy/pTS-IP films which were synthesised using galvanostatic and CV methods. The profile of IP released from the PPy/pTS-IP film is identical to the release pattern of IP from the PPy doped with oxalic acid, where greater amounts of IP were released from the PPy films that were synthesised using the galvanostatic method, when the films were stimulated using - 0.6 V *vs.* SCE. The use of pTS as a doping anion led to a significant increase in the amount of IP released from the PPy films as compared to the films doped with oxalic acid on both release protocols. Further, the amount of released IP from the PPy/pTS-IP films prepared using the CV method reached 275 μmol dm^{-3} cm^{-2} within 30 min; this was lower than that released from films that were synthesised using the galvanostatic method 523 μmol dm^{-3} cm^{-2} during the same period of time when both films were stimulated using -0.6 V *vs.* SCE. The concentration of these releases was higher than that released from the PPy films which were doped with oxalic acid, where 63 and 51 μmol dm^{-3} cm^{-2} were released from films synthesised using the CV and galvanostatic methods, respectively, when the films were stimulated under identical released conditions. Similarly, the amount of IP released from PPy/pTS-IP films which were synthesised using the galvanostatic and CV methods were 258 and 120 μmol dm^{-3} cm^{-2}, respectively, when both films were unstimulated during 30 min. Similarly, these amount of IP released were significantly higher than that released from PPy films doped with oxalic acid synthesis using the galvanostatic and CV methods, which were 24 and 20 μmol dm^{-3} cm^{-2}, respectively. This increase in the IP release rate may occur because the mobility of the IP anion is higher than the mobility of the pTS anion; therefore, the positively charged PPy backbone is compensated by the IP anion.

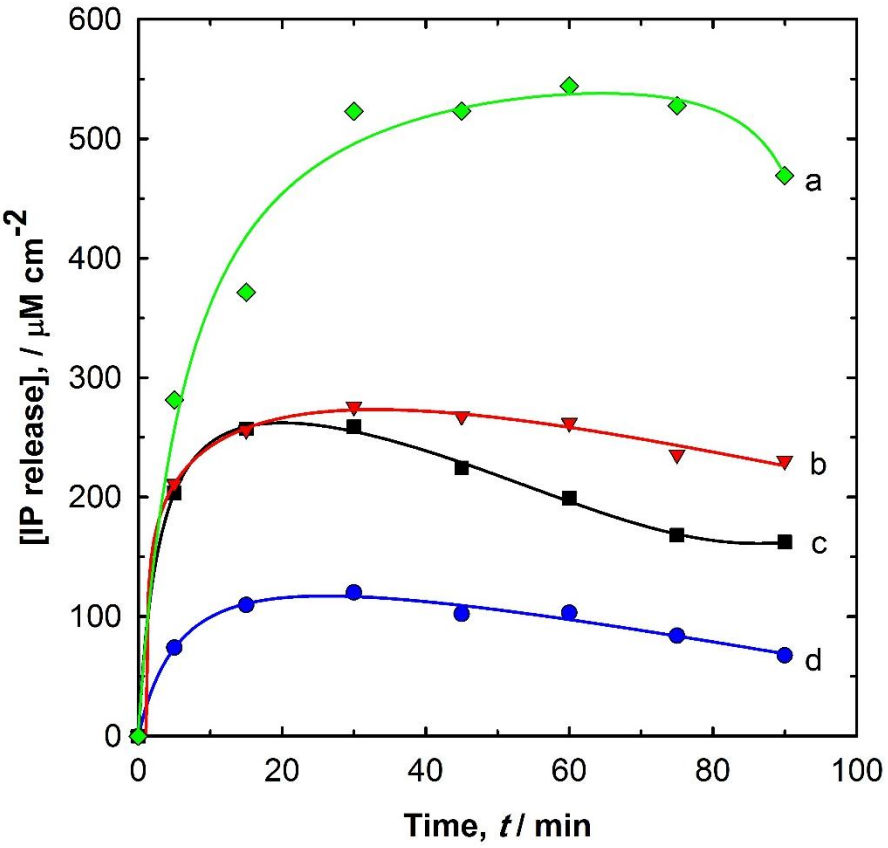

Figure 6-13: IP released from PPy/pTS-IP films grown for 1600 s at 0.3 mA cm^{-2} from a solution of 0.1 mol dm^{-3} Py, 0.5 x 10^{-3} mol dm^{-3} IP and 0.05 mol dm^{-3} pTS, a) film stimulated with -0.6 V *vs.* SCE, and film grown using CV during 10 cycles b) films stimulated with - 0.6 V *vs.* SCE, c) and d) unstimulated films were grown using galvanostatic and CV method respectively.

The amount of IP released from PPy-TiNT-IP films is lower than that released from the film without TiNT. In addition, the concentration of IP released from the PPy-TiNT-IP films synthesised using CV is higher than that released from films synthesised using the galvanostatic method, when both films were stimulated using a pulsed potential of ±0.6 V at 0.05 Hz *vs.* SCE. However, the IP release is very low, when the films are stimulated using a constant potential of +0.6 V *vs.* SCE or unstimulated. The concentration of DA released from the films that were synthesised using CV reached 4.3 μmol dm^{-3} cm^{-2} after 15 min, which is slightly higher than that released from films which were formed galvanostatically (1 μmol dm^{-3} cm^{-2}

approximately), when both films are unstimulated. When the films were stimulated using +0.6 V *vs.* SCE, the concentration of DA release from the films synthesised using the galvanostatic method reached 5.8 μmol dm^{-3} cm^{-2} within 30 min. The concentration of DA reduced to 4 μmol dm^{-3} cm^{-2} after 60 min and this was probably due to the low amount of incorporated DA during polymerisation. There was a slight increase in the DA released from films synthesised using the CV method, as compared to films synthesised using the galvanostatic method, when the films were stimulated under the same conditions. In addition, the concentration of DA in the release medium reached 6 μmol dm^{-3} cm^{-2} after 30 min and remained at the same concentration for the remaining release time. When the films were stimulated using ±0.6 V at a frequency of 0.05 Hz *vs.* SCE, the release concentration of DA from the polymer films, which was formed using CV, increased to 18 μmol dm^{-3} cm^{-2} within 45 min. This result is higher by approximately 38% in comparison to the release concentration of DA from the polymer films, which were synthesised using the galvanostatic method.

6.4 Summary and Conclusions

The use of pTS as a doping anion led to an increased in the amount of MB, DA and IP being released from the electrochemically stimulated PPy films in comparison with the release from PPy doped with oxalic acid anion. One possible explanation for the decrease in the amount of MB being released is that the mobility of oxalate anion ($C_2O_4^{2-}$) is higher than the immobile anions pTS. Therefore, the entrapped pTS created a negative net charge in the polymer, which is attracted to the positively charged MB and DA molecules.

The highest amount of DA released from the PPy-DA films was observed when the polymer films were stimulated using pulsed potential (± 0.6 V at 0.05 Hz *vs.* SCE). The actuation of the film under pulsed potential may result in an increase or decrease in the film volume associated with the movement of mobile ions and associated solvent molecules in and out of the film matrix. These movements may pump the DA out of the polymer films. Moreover, CV increases dopamine release.

There is an increase in the amount of DA released from the PPy-DA films synthesised using CV, as compared to the films synthesised using the galvanostatic method. The increase in the amount of DA released may have occurred because a higher quantity of DA was incorporated into the PPy films during the reduction cycle of the PPy film. The positive charge of the PPy backbone is neutralised during film reduction, and the incorporated oxalate anions ($C_2O_4^{2-}$) generate a net negative charge within the polymer matrix. Thus, the DA cations diffuse due to a concentration gradient and electrostatic attraction between opposite charges and are then incorporated into the PPy film to compensate for the polymer matrix's negative charge.

The release of anionic drug IP from the PPy films is significantly higher than the release of cationic molecules, DA and MB. This occurs because during the oxidation of the PPy, a high amount of IP is incorporated in the PPy films to compensate the positively charged PPy backbone. The IP anion is electrostatically attracted to the cationic oxidised PPy backbone unlike the cations which may be physically entrapped in the polymer bulk and absorbed in the polymer surface.

The use of TiNT led to a decrease in the amount of released IP, because the absorption of IP in the TiNT is low due to the charge repulsion between the negatively charged IP anion and TiNT.

Chapter 7: Pyrrole chemical polymerisation in a two compartment cell

The aim of the work described in this chapter is to prepare a self-powered drug delivery system based on galvanic coupling of PPy composite film and a thin layer of a reactive metal coating such as Mg. Since it is difficult to electrodeposit the PPy film on active metals, the PPy films were chemically polymerised on CC and DM membranes using a two-compartment cell. A thin layer of Mg was sputtered on one side of the obtained film and the release of the incorporated model drugs were measured using a UV-VIS spectrophotometer.

7.1 Synthesis of the drug delivery system

The PPy-containing drug was chemically deposited using a two-compartment cell, which were separated by a CC or a DM membrane, where a PPy-containing a model drug was formed. One of the cell compartments contained 14 x 10^{-3} mol dm^{-3} Py monomers with different concentrations at the time of polymerisation (0.01, 0.05, 0.5 and 0.7 x 10^{-3} mol dm^{-3}) of rhodamine (Rh-6G), FSS, MB, DA or IP to study the effect of the molecules types on the adsorption and drug release. The other compartment contains the oxidant solution, ammonium persulfate. The cell was filled with the two solutions and kept at room temperature (295 K) for four hours. The two solutions diffused through the membrane and the Py monomer gradually oxidised, thereby forming the PPy composite film doped with the model drug on the outer and inner surfaces of the membrane pores. Figure 7.1 depicts the two-compartment cell after it was filled with the solutions, and Figure 7.2 presents an image of the CC membrane from the ammonium persulfate side immediately after the compartments were filled with the solution and 15 min after the growth of the PPy in the CC film was seen.

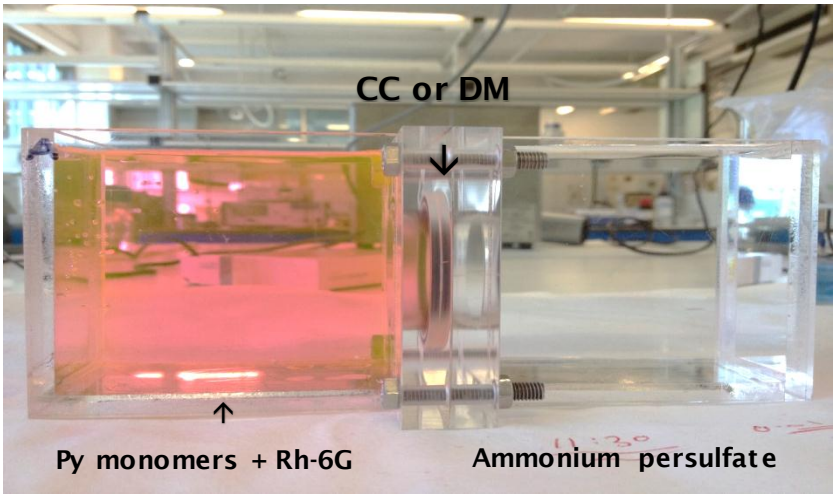

Figure 7-1: Two-compartment cell containing oxidised solution ammonium persulfate and Py monomers with Rh-6G separated by CC or DM films.

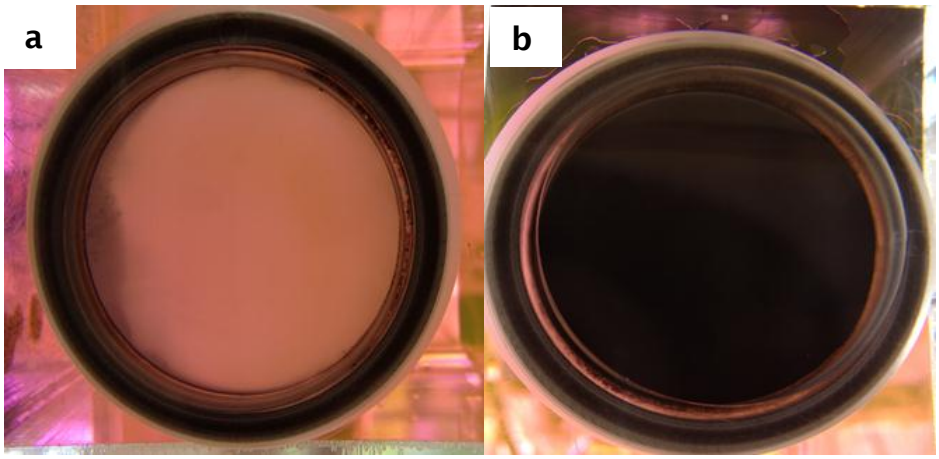

Figure 7-2: Celluose acetate membrane (CC) a) immediately after the cell was filled with solution b) after 15 minutes. The images show the formation of the PPy-CC-Rh-6G composite film, D 34 mm.

The cell was dismantled and the membrane containing the doped polymer was cleaned thoroughly with an aqueous solution of 0.01 mol dm^{-3} NaCl for 5 minutes and the film dried under vacuum at 40 ^{o}C for 3 hours A thin layer of Mg (2 μm) was sputtered in one side of the film using a magnetron sputtering machine.

7.2 Characterisation of the system

To examine the membrane absorption without the PPy, two types of membrane CC and DM were fitted in the cell. The cell compartments were filled with oxidant solution and 0.7 x 10^{-3} mol dm^{-3} Rh-6G in the absence of Py monomers for four hours. The films were cleaned with NaCl aqueous solution for five minutes. The results show that the DM films absorbed Rh-6G to a large extent and could not be cleaned easily. Therefore, this may significantly affect the volume of the released Rh-6G since a large proportion of Rh-6G may be released from the DM membrane itself. Therefore, the DM membrane was excluded from the release experiments.

Figure 7.3 presents a digital photo of the chemically prepared PPy-CC composite films. The films were highly flexible and could be bent easily when wet, which makes it useful for drug delivery in a curved surface. In addition, the CC membrane was lightweight and biodegradable, which made it suitable for use in implant drug delivery systems. However, when the composite film dried, it became brittle and fractured easily when bent.

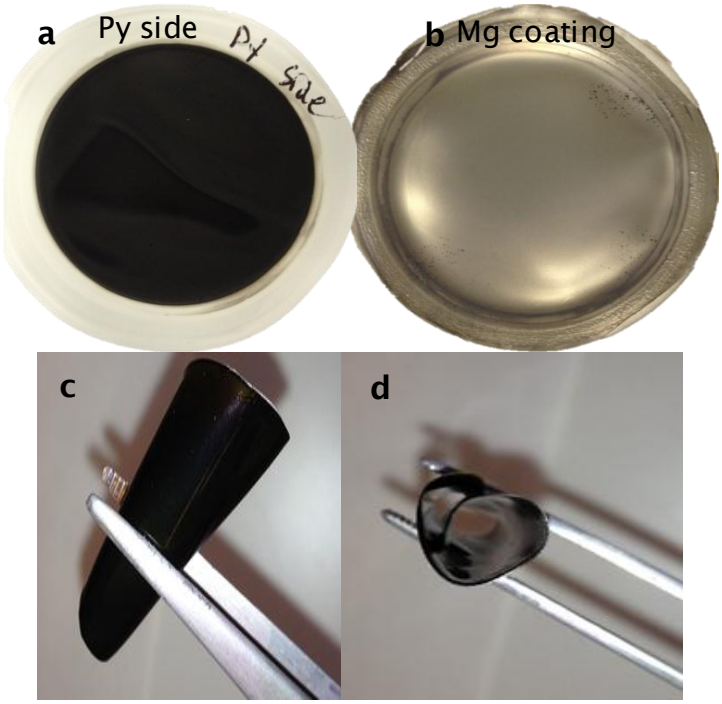

Figure 7-3: Images of the CC-PPy composite films. a) PPy composite film, b) coating with a thin magnesium layer on one side, c and d) bent film. The diameter and thickness of the film are 30 mm and 130 μm approximately, respectively.

7.3 Scanning electron microscopy

Figure 7.4 depicts the scanning electron microscopy (SEM) of the CC membrane after being immersed in 0.05 x 10^{-3} mol dm^{-3} Rh-6G in the absence of Py monomer at two magnifications. The CC membrane appears to retain its original porous structure. The diameter of the pores are irregular and range between 1.2 to 3.7 μm. Figure 7.5 depicts the SEM images of DM film immersed in 0.5 mmol dm^{-3} Rh-6G. The image shows the formation of Rh-6G microtubes of size ranging between 2.78 μm and 8.31 μm. These tubes are probably formed due to the adsorption of water by the membrane and the precipitation of Rh-6G. In addition, the density of the tubes decreases with the decrease in Rh-6G concentration. Moreover, these tubes were not observed in the DM membrane in the presence of Py monomers, as shown in Figure 7.6 and on the CC membrane, as shown in Figure 7.7. In the presence of the Py monomer, the

growth of PPy within the porous membrane may lead to a reduction in the diffusion of Rh-6G across the membrane and therefore eliminate the formation of the tubes.

a

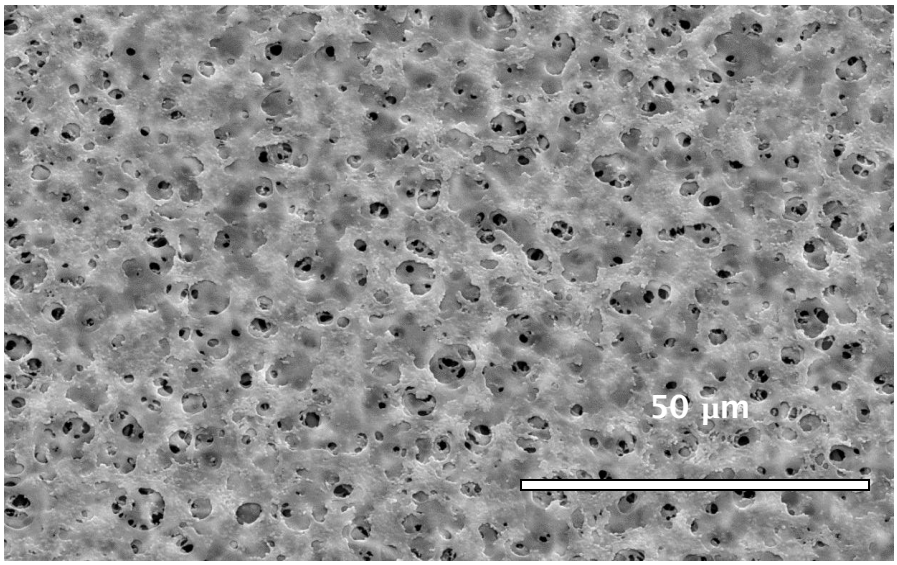

b

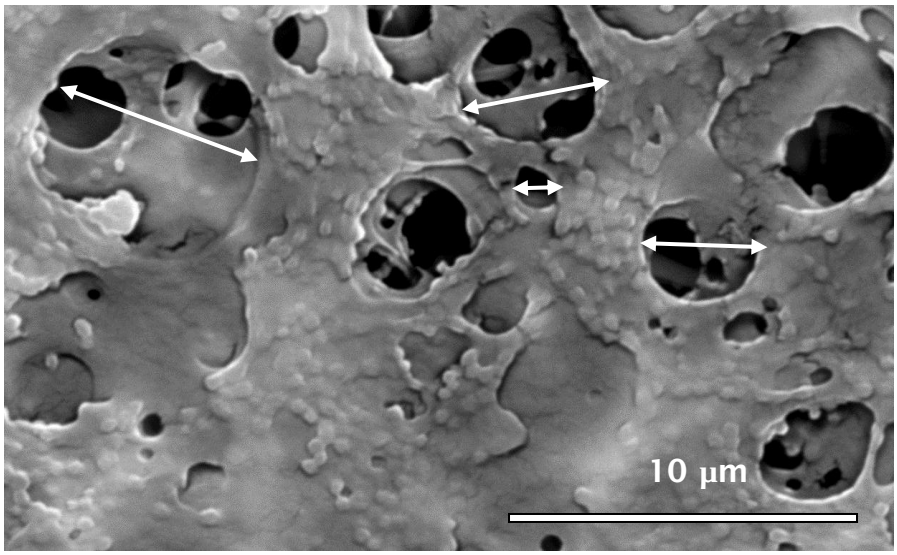

Figure 7-4: a and b are SEM images of CC-Rh-6G composite film prepared from 0.05 x 10^{-3} mol dm^{-3} rhodamine on cellulose acetate filter in the absence of Py monomer at different magnifications.

a

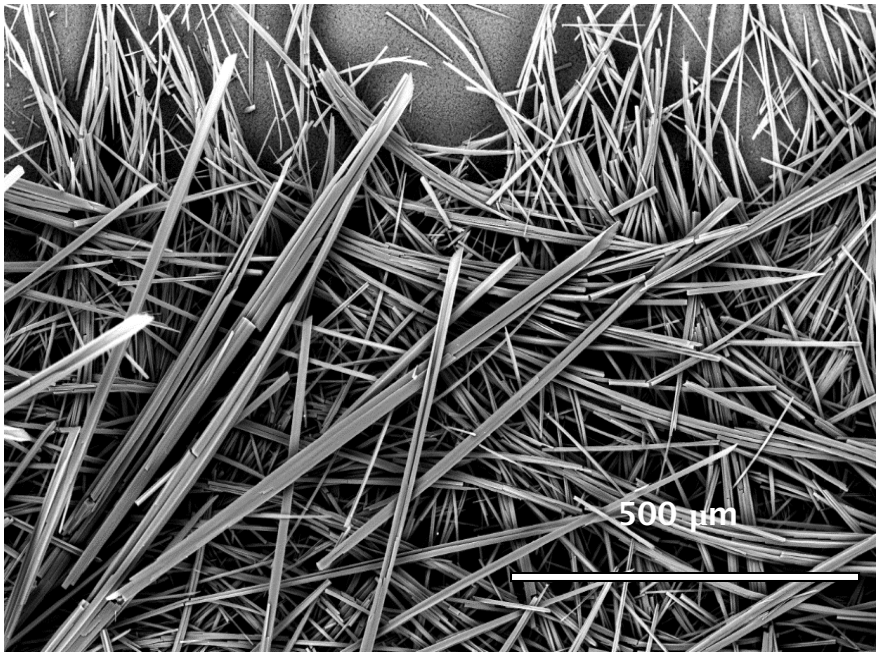

b

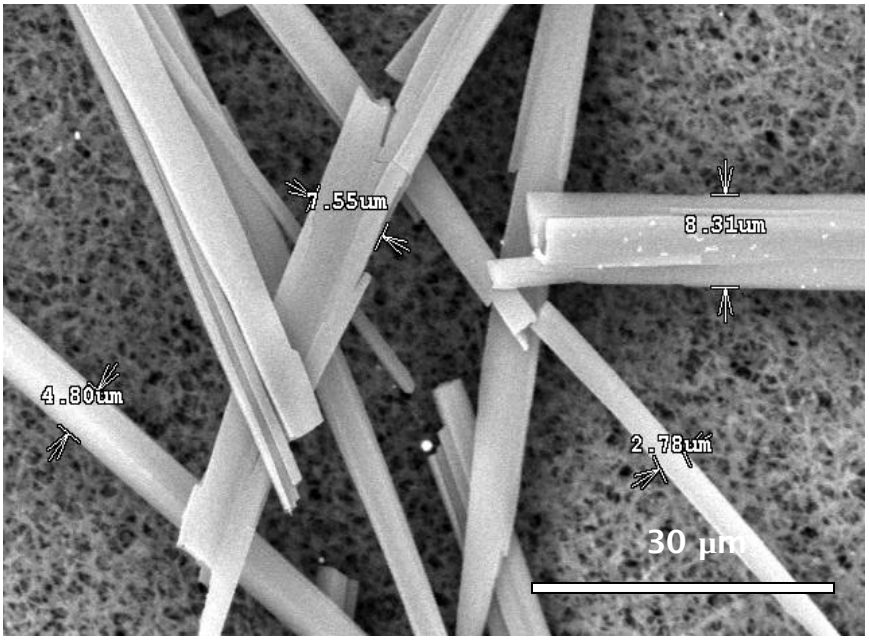

Figure 7-5: a) and b) are SEM images of Rh-6G on DM film prepared from 0.05 x 10^{-3} mol dm^{-3} Rh-6G in the absence of Py monomer at different magnifications.

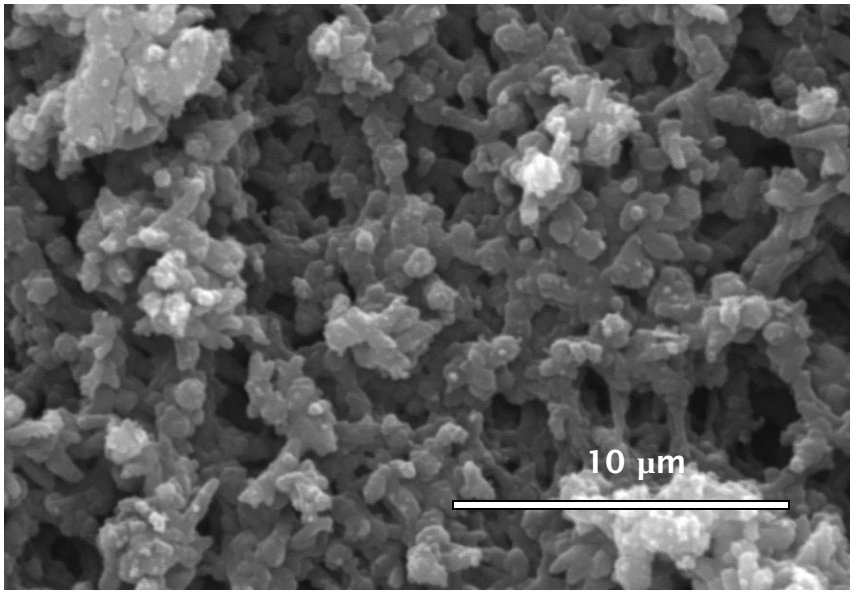

Figure 7-6: SEM image of PPy-DM-Rh-6G composite film prepared with 0.5 x 10^{-3} mol dm^{-3} rhodamine and 14 x 10^{-3} mol dm^{-3} of Py monomer on DM film.

Figure 7.7 depicts the SEM images of PPy-CC-Rh-6G composite films synthesis using 0.01 x 10^{-3} mol dm^{-3} Rh-6G with 14 x 10^{-3} mol dm^{-3} of Py monomer. The CC membrane is completely covered with the PPy doped with Rh-6G. The PPy exhibits a spherical shape with a uniform distribution. The PPy microstructure exhibits a compact porous structure replicating the original CC membrane structure. Further, the PPy-DM-Rh-6G composite film has a higher porosity than the PPy-CC-Rh-6G, as is evident from Figure 7.8.

a

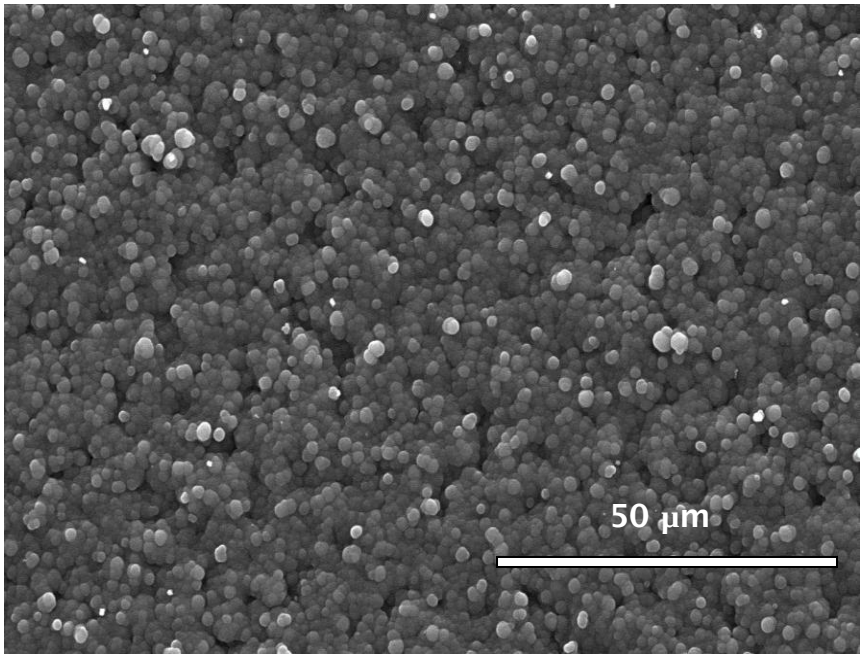

b

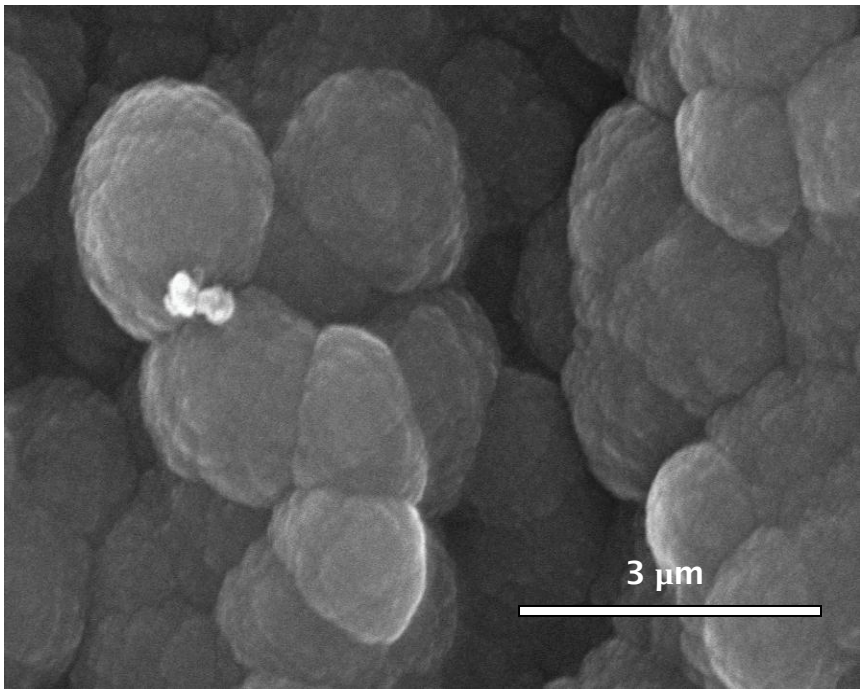

Figure 7-7: a) and b) are SEM images of PPy-CC-Rh-6G composite film prepared with 0.1 x 10^{-3} mol dm^{-3} rhodamine and 14 x 10^{-3} mol dm^{-3} of Py monomer at different magnifications.

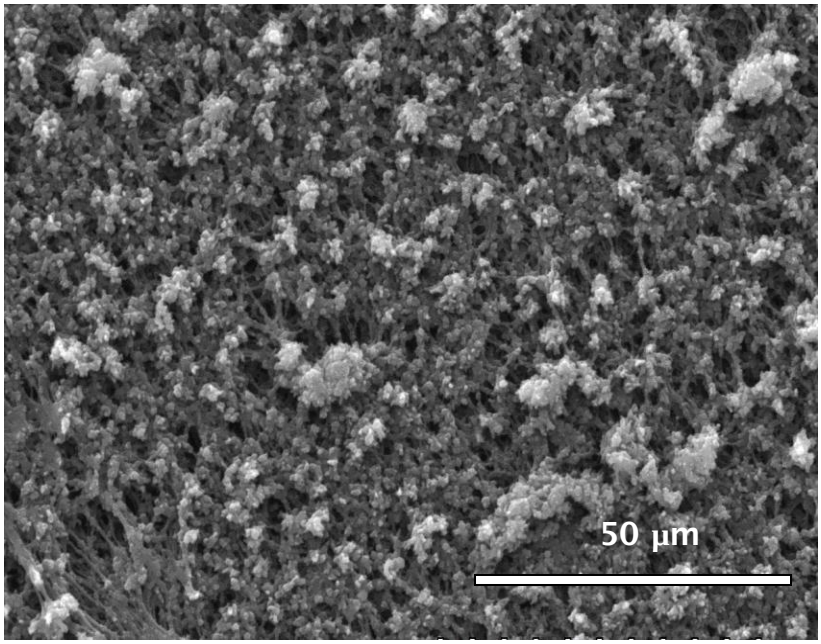

Figure 7-8: PPy-DM-Rh-6G composite film prepared from 0.05 x 10^{-3} mol dm^{-3} rhodamine and 14 x 10^{-3} mol dm^{-3} Py monomers on a DM filter.

a

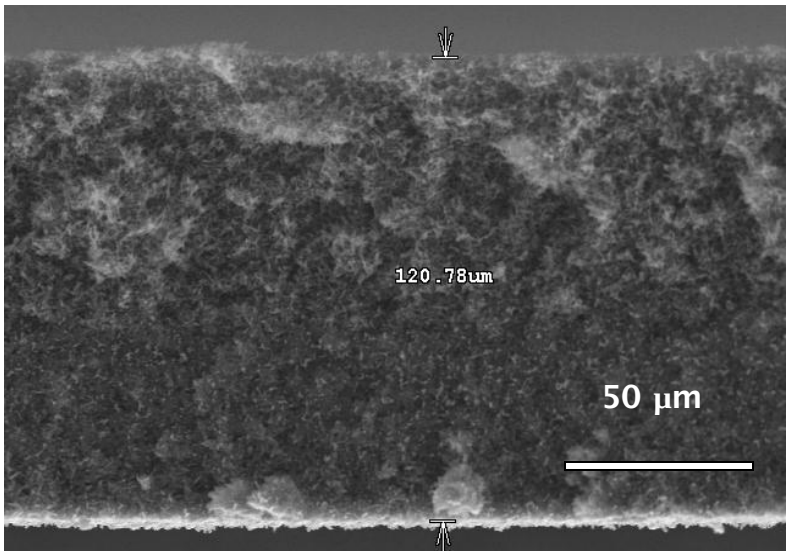

b

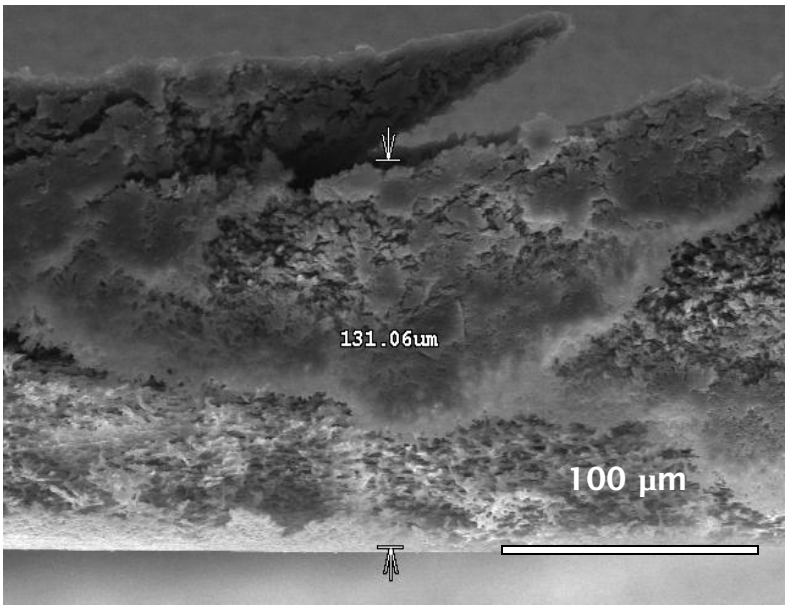

Figure 7-9: SEM images of a cross-section of a) PPy-DM-Rh-6G composite film and b) PPy-CC-Rh-6G composite film.

7.4 Rhodamine release from PPy-membrane films

Four concentrations of Rh-6G, 0.01, 0.05, 0.5 and 0.7 x 10^{-3} mol dm^{-3} were used to test the effect of the initial Rh-6G concentration on the Rh-6G released from the composite membrane. It was noticed that after cleaning the films and rinsing thoroughly with NaCl solution 0.01 x 10^{-3} mol dm^{-3} for 5 minutes, the film prepared with a high rhodamine concentration 0.7 x 10^{-3} mol dm^{-3} still releases the dye in the cleaning solution. Therefore, the film prepared in 0.7 x 10^{-3} mol dm^{-3} was excluded from the experiments because the film contained a large amount of Rh-6G on its surface. In addition, a thick layer of cationic red colour molecules Rh-6G and blue MB was seen on the composite film surface; this was not found on the other film prepared with anionic molecule FSS. However, the other anionic molecule IP is colourless and cannot be seen. The formation of this layer of cationic molecules may have occurred due to the absorption of the cation on the composite film surface and the difficulty of incorporating into the polymer bulk due to the charge repulsion between the cationic polymer backbone and the cationic model drugs. The release of the incorporated Rh-6G was conducted as described previously in Section 2.10, where the obtained films were immersed in 20 ml of (0.9%) NaCl aqueous solution at room temperature and stirred using a magnetic bar. Samples of 5 ml were taken at selected times from the solution and replaced with an equal volume of 0.9% NaCl solution. The samples were analysed using UV-VIS spectrometer to determine the concentration of the Rh-6G that was released. Figure 7.10 shows the concentration profiles of the released Rh-6G *vs.* time from PPy-CC-Rh-6G composite film prepared with different initial concentration of Rh-6G with and without the Mg layer coating.

The release rate of Rh-6G increased with the increase in the initial concentration of Rh-6G used to prepare the composite films. This was expected because the increase in the Rh-6G initial concentration tended to increase the diffusion of Rh-6G into the composite film; hence, more Rh-6G became available to be absorbed and incorporated in the film. The concentration of Rh-6G released from the film prepared with a high concentration of Rh-6G (0.5×10^{-3} mol dm^{-3}) without Mg coating increased with time, reaching a max of 0.002×10^{-3} mol dm^{-3} after 2 hours. When the film coated with a thin layer (2μm) of Mg was tested, the concentration of Rh-6G released decreased by approximately 40% after 2 hours. This finding also applied to other films prepared with lower initial concentration of Rh-6G. The rate of release declined by approximately 25% when the initial concentration of Rh-6G was 0.01 and 0.05 when the films were coated with Mg compared to that without the Mg coating. The release rate of Rh-6G may have decreased due to two reasons: (1) The formation of a magnesium oxide layer on the surface of the Mg between the metal and the PPy-CC composite film. The oxide layer may serve as an insulator and prevents the flow of electrons between the PPy-CC composite film and the Mg layer. The presence of the Mg and the Mg oxide layer decreases the surface available for desorption and prevents the Rh-6G from being released. (2) The cationic nature of Rh-6G might cause the Rh-6G to become only physically entrapped in the composite film and sorption on the film surface due to the charge similarity between the cationic Rh-6G and the positively charged oxidised PPy. Therefore, the reduction of the polymer as a result of Mg corrosion leads to the reincorporation of the cationic Rh-6G on the polymer bulk, and only the Rh-6G that was absorbed on the polymer surface diffuses into the release medium. The release of other cationic molecules MB and DA will be tested in the following section to confirm this finding.

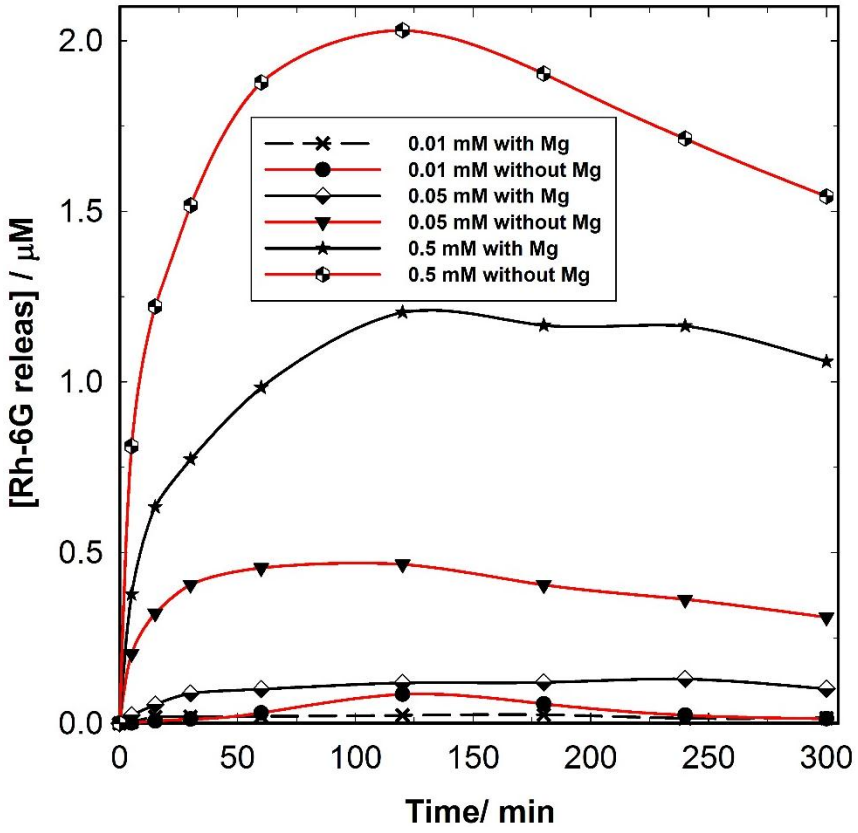

Figure 7-10: Release of Rh-6G from PPy CC-Rh-6G composite films chemically grown for 4 hours from a solution containing different concentrations of Rh-6G in the presence and absence of Mg coating.

7.5 Release of methylene blue (MB)

PPy-CC-MB films were chemically synthesised, as described in the experimental section, from a solution containing 0.1 mol dm^{-3} Py and 0.5 x 10^{-3} mol dm^{-3} MB in both, the presence and absence of 1 mg mol^{-1} TiNT. The release of the incorporated MB was performed in 0.9% NaCl solution. Figure 7.11 depicts the concentration profiles of released MB *vs.* time synthesis in the presence and absence of TiNT, with and without the Mg layer coating. After 30 min, the maximum concentration of MB released from the PPy-CC-MB film, which was prepared in the absence of TiNT and without the Mg coating, was 0.4 μmol dm^{-3}. The concentration of MB released decreased by approximately 60% when the film was coated with a thin layer of Mg.

The release rate of MB may decline due to the reduction of the polymer as a result of the Mg corrosion, which leads to the reincorporation of the cationic MB on the polymer bulk and minimises the diffusion of MB into the release medium. This result complies with the release of cationic Rh-6G, where the presence of the Mg coating significantly reduced the release rate of the incorporated molecules.

Similarly, this finding can also be applied to other films prepared with TiNT. The use of TiNT leads to a decrease in the release rate of MB from the composite film. This corresponds with the release of MB from the PPy films which are synthesised using electrochemical methods, where the presence of TiNT leads to a decrease in the amount of MB released, because the adsorption of MB in TiNT is lower than the adsorption of Py in TiNT.

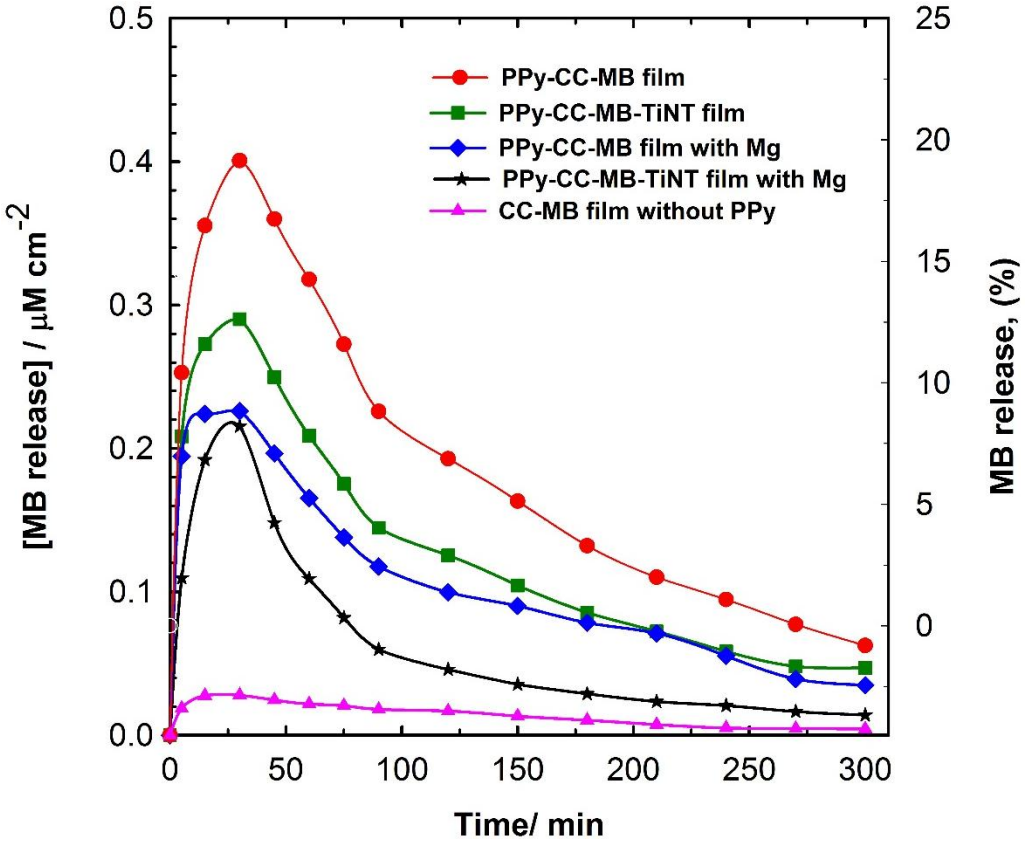

Figure 7-11: Evolution of the released concentration of MB *vs.* time from the PPy-CC composite films.

7.6 Release of ibuprofen

The effect of the drug type on the adsorption and drug release was examined using an anionic model drug IP, PPy-CC-IP films were synthesised using a two-compartment cell, as described in Section 2.6, from a solution containing 0.1 mol dm^{-3} Py and 0.5 x 10^{-3} mol dm^{-3} IP in both the presence and absence of 1 mg mol^{-1} TiNT. The release of the incorporated IP was performed in 0.9% NaCl solution, as described in Section 2.10.

Unlike the MB, the concentration of IP in the release medium increased when the PPy composite films were coated with a thin layer of Mg, as shown in Figure 6.12. The concentration of IP released from the PPy-CC-IP film, which was prepared in the absence of TiNT and without the Mg coating, reached 20 μmol dm^{-3} after 30 min. The concentration of IP released increased by approximately 100 % when the film was coated with a thin layer of Mg. Further, the release rate of IP increased due to the reduction of the polymer as a result of the Mg corrosion, which lead to the removal of the electrostatic attractive force between the cationic polymer backbone and the incorporated IP anions. This permits the IP to diffuse into the release solution. This finding can also be applied to other films prepared with TiNT. Similar to MB release, the use of TiNT leads to a decrease in the release rate of IP from the composite film.

The amount of released IP is greater than the amount of released cationic molecules MB and DA; the reason for this may be that a low amount of the cationic MB was incorporated into the polymer matrix during the polymerisation process, thereby indicating the physical entrapment of the cationic molecules MB and DA into the polymer film during the polymerisation process, rather than electrostatic interactions which occur between the anionic IP and the cationic

polymer backbone. This finding is identical to that of electrochemical experiments where the release of anionic IP is higher than the release of cationic molecules such as MD and DA.

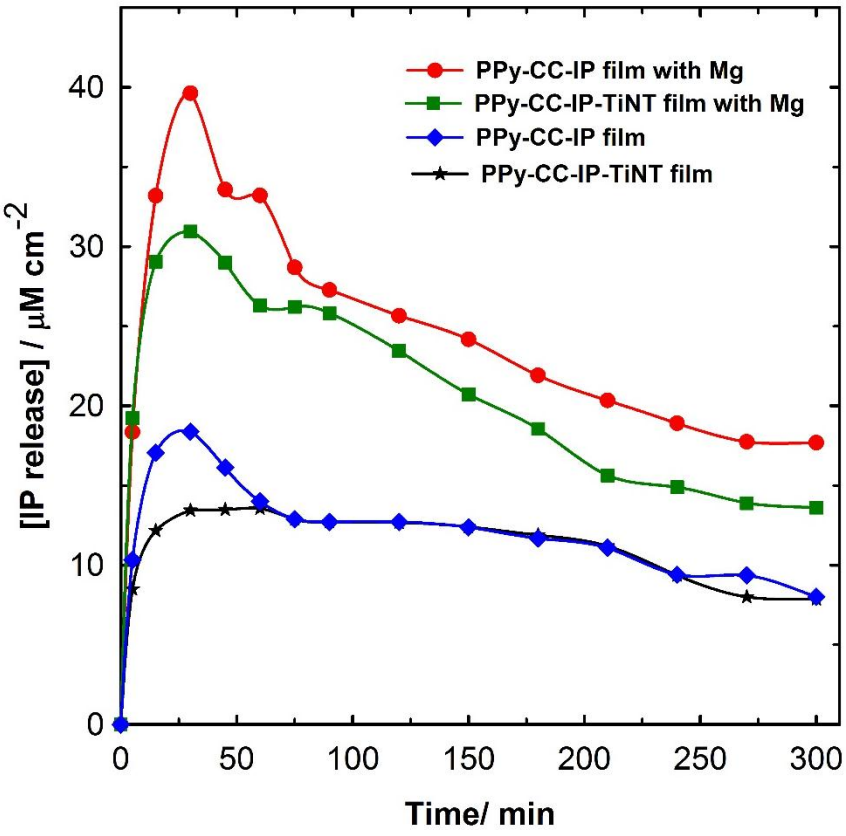

Figure 7-12: Evolution of the released concentration of IP vs. time from the PPy-CC composite films.

7.7 Summary and Conclusions

The galvanic coupling between the Mg thin layer coating and the PPy composite films led to a decrease in cationic MB, DA and Rh-6G release rate, because the oxidation of Mg reduced the PPy composite films, which led to reincorporation of the cationic molecules MB, DA and Rh-6G on the polymer bulk and minimised the diffusion of MB, DA and Rh-6G into the release medium. This could be used as an autonomous self-powered source and controller for a long-term implant drug delivery system by galvanic coupling between the Mg thin layer (anode) and PPy composite film (cathode) in the presence of NaCl electrolyte.

The concentration of IP in the release medium increased when the PPy composite films were coated with a thin layer of Mg due to the reduction of the polymer as a result of Mg corrosion, which led to the removal of the electrostatic attractive force between the cationic polymer backbone and the incorporated IP anions. This permitted the IP to diffuse into the release solution.

Chapter 8: Conclusions and Suggestions for Further Work

8.1 Summary and Conclusions

This chapter presents the summary and the main conclusion of this work. For the first time, the self-powered ibuprofen drug release system based on direct electrodeposition of PPy film on AZ31 Mg alloy had been synthesised. The incorporation and the release of the ibuprofen drug from the PPy film was investigated. The effect of the present of ibuprofen drug on PPy polymerisation and PPy film structure was evaluated using electrochemical methods, optical microscope, SEM and DSI techniques. Additionally, the chemical polymerisation of PPy on CC film and coated with a thin Mg film has been presented and characterised as alternative choice for the self-powered drug delivery system. The following points are summarise the main conclusion of the thesis.

- Polymerisation conditions such as electrolyte type, temperature, pH, monomer concentration and nature of the uploaded doping molecules, significantly affect the formation and film properties of the conducting polymers. The polymerisation conditions also affect the delivery of molecules added to the structure. These are critical issues for the development of drug delivery systems for medical applications.

- PPy films are capable of releasing different cationic molecules such as MB. The cationic dye MB was uploaded into the PPy structure and delivered in an aqueous system in a controlled manner using an electrical potential stimulus. The released concentration reached 60 x 10^{-9} mol dm^{-3} after approximately 30 min when the PPy films were stimulated at + 0.6 V *vs.* SCE. The release

decreased when the potential increased to + 0.95 V *vs.* SCE. There was no significant difference in the concentration of released MB when the polymer film was synthesised using either the CV or the galvanostatic method.

In addition, an increase in the PPy film's thickness from 2 to 4 μm does not appear to affect significantly the amount of MB released. Since most of the MB was released from the film's surface. The concentration of MB in the release medium increased by approximately 30% when the film thickness increased by a factor of 4, from 2 to 8 μm. This increase was attributed to the contribution of the MB from the polymer bulk, in addition to the MB molecules released from the polymer surface. At an increase of 8 to 12 μm, the release rate of MB increased only by 10%. The release rate of MB from the PPy films is highly variable, possibly because the MB is physically entrapped within the polymer film during the polymerization process instead of interacting electrostatically due to the charge similarity between the oxidised film and cationic nature of MB.

The amount of drug that can be uploaded in a polymer film tends to be small and the initial spontaneous drug release from the conducting polymer can be high. Thus, the development of nanoporous and nanostructured conducting polymers may provide electrode structure materials with good electrical conductivity, low operation potential and a high surface area relative to size.

However it was observed that the incorporation of TiNT in the PPy film slightly reduced the MB release rate. The decrease in the amount of MB released from PPy-TiNT-MB film was due to the adsorption of Py in TiNT (240 mg g^{-1}), which is higher than the adsorption of MB in TiNT (133 mg g^{-1}) [90]. This is possibly due to the fact that the surface of TiNT is occupied by positively charged Py monomers, which lead to reduced adsorption of MB. In addition, the incorporation of TiNT in the polymer matrix changes the film's morphology, thereby reducing the amount of MB released.

- The use of pTS as a doping anion led to an increase in the amount of MB, DA and IP being released from the electrochemically stimulated PPy films in comparison with the release from PPy doped with oxalic acid anion. One possible explanation for the decrease in the amount of MB being released is that the mobility of oxalate anion ($C_2O_4^{2-}$) is higher than the immobile anion pTS. Therefore, the entrapped pTS created a negative net charge in the polymer, which is attracted to the positively charged MB and DA molecules.

There is an increase in the amount of DA released from the PPy-DA films synthesised using CV, as compared to the films synthesised using the galvanostatic method. An increase in the amount of DA released take place because a higher quantity of DA is incorporated into the PPy films during the reduction cycle of the PPy film. The positive charge of the PPy backbone is neutralised during the film reduction, and the incorporated oxalate anions ($C_2O_4^{2-}$) generate a net negative charge within the polymer matrix. Thus, the DA cations diffuse due to a concentration gradient and electrostatic attraction

between opposite charges, then they are incorporated into the PPy film to compensate for the polymer matrix's negative charge.

The release of anionic drugs such as IP from the PPy films is significantly higher than the release of cationic molecules. This is because during the oxidation of the PPy, a high amount of IP is incorporated in the PPy films to compensate for the positively charged PPy backbone. The IP anion is electrostatically attracted to the cationic oxidised PPy backbone unlike the cations, which are physically entrapped in the polymer bulk and absorbed in the polymer surface.

- The galvanic coupling between biocompatible reactive anodes, such as Mg, and a conducting polymer film cathode can be used as autonomous release systems. However, according to the findings, the galvanic coupling between the Mg thin layer coating and the PPy composite films led to a decrease in cationic MB, DA and Rh-6G release rate, because the oxidation of Mg reduced the PPy composite films, which led to reincorporation of the cationic molecules MB, DA and Rh-6G on the polymer bulk and minimised the diffusion of MB, DA and Rh-6G into the release medium.

- The use of salicylate as a doping anion during the electroploymerisation of PPy films on the surface of an AZ31 Mg alloy substrate inhibited the rapid dissolution of the substrate. An oxidation peak denotes the formation of an intermedia layer of hydroxide that serves as a support for the film and passivating the surface. Therefore, a compact globular-like structure PPy film has been obtained. The structure of the films modified to a needle like structure when ibuprofen added to the polymerisation solutions. The addition of drugs into polymer chains may affect the structure, morphology and mechanical

properties of the film. For instance, the incorporation of ibuprofen into the film increases the number of cracks and inhibits the formation of the protective salicylate magnesium film. Samples scanned at high potentials with high concentration of IP show a pitted area with the existence of volcano-like pits on the surface. The releasing of the drug *in-situ* experiments denotes the liberation of the ibuprofen from the uploaded film. The mechanical properties determined by nanoindentations show a film with a lower strength and more elasticity after the addition of ibuprofen. The results showed a decrrase in the film hardness and reduced modulus by 54 and 40% respectively, indicating a more plastic film with ibuprofen. The addition of the large molecule ibuprofen into the PPy matrix, the ibuprofen acts as an additional ion dopant along with the salicylate ions results in an increase in the gap between the polymer chains, reducing the strength of the attractive forces between them making polymer chain motion and deformation easier than IP free polymer films.

8.2 Suggestions for Further Work

Although extensive work has been carried out to improve the use of conducting polymer in biomedical applications, considerable challenges prevent their use in *in vivo* release systems. Several obstacles need to be resolved in order to expand the use of conducting polymer drug delivery systems.

- Intrinsic conducting polymers are not biodegradable materials, thus they may need to be expelled from the body using surgery, thereby increasing the risk of infection and reducing the patient's healing and comfort. This problem can be overcome by grafting the monomers to a side group biodegradable material such as glycine ethyl

ester, or using conducting polymers with controlled biodegradable characteristics, and a matrix with nanoparticles attached to non-conducting biodegradable polymers.

- There have been attempts to overcome the shortcomings of controlling the drug release and to take advantage of the influence of conducting polymers through physical and chemical factors, such as changes in temperature and pH causing the conducting polymers to function as a sensor, and to combine them with an electric stimulus to control drug release. Theoretically, the conducting polymer can selectively sense the redox reagent in the solution; simultaneously, the redox reagent triggers the drug release from the conducting polymers and the drug will be released as a function of the concentration of the detected redox reagent where ionic exchange has occurred.

- In order to use Mg alloys as a power source for a self-powered drug delivery systems, the corrosion mechanism must be understood for the sake of precisely controlling the rate of Mg corrosion *in vivo*. The corrosion of Mg *in vivo* is a complicated process influenced by the composition and temperature of the surrounding environment. Therefore, the corrosion behaviour of Mg implants should be examined in an appropriate physiological solution depending on the place where the implant will be fitted into. The Mg should biodegrade at a rate so as to provide the required power to release the drug from the conducting polymer and expel it from the body once the treatment period has ended. A detailed understanding of the toxicity, corrosion process and amount of ion dissolution is required before Mg can be used in an implant system.

- Theoretical study and modelling of the self-powered drug delivery system are required to predict the effects of incorporated drugs on conducting polymer structure using density functional theory and multiphysics software in order to understand the system behaviour.

References

[1] J. Unsworth, B.A. Lunn, P.C. Innis, Z. Jin, A. Kaynak, N.G. Booth, Conducting polymer electronics, Journal of Intelligent Material Systems and Structures, 3 (1992) 380-395.

[2] J.-Z. Wang, S.-L. Chou, H. Liu, G.X. Wang, C. Zhong, S. Yen Chew, H. Kun Liu, Highly flexible and bendable free-standing thin film polymer for battery application, Materials Letters, 63 (2009) 2352-2354.

[3] E. Tekin, P.J. Smith, U.S. Schubert, Inkjet printing as a deposition and patterning tool for polymers and inorganic particles, Soft Matter, 4 (2008) 703-713.

[4] J. Ryu, J. Park, B. Kim, J.-O. Park, Design and fabrication of a largely deformable sensorized polymer actuator, Biosensors and Bioelectronics, 21 (2005) 822-826.

[5] J.Y. Kim, M.H. Kwon, Y.K. Min, S. Kwon, D.W. Ihm, Self-assembly and crystalline growth of poly(3,4-ethylenedioxythiophene) nanofilms, Advanced Materials, 19 (2007) 3501.

[6] L. Dou, J. You, J. Yang, C.-C. Chen, Y. He, S. Murase, T. Moriarty, K. Emery, G. Li, Y. Yang, Tandem polymer solar cells featuring a spectrally matched low-bandgap polymer, Nat Photon, 6 (2012) 180-185.

[7] L. Changzhi, Z. Borong, W. Baochen, Development of cylindrical secondary lithium/polyaniline batteries, Journal of Power Sources, 44 (1993) 669-672.

[8] J.J. Langer, M. Filipiak, J. Ke¸cińska, J. Jasnowska, J. Włodarczak, B. Buładowski, Polyaniline biosensor for choline determination, Surface Science, 573 (2004) 140-145.

[9] C. Pozo-Gonzalo, D. Mecerreyes, J.A. Pomposo, M. Salsamendi, R. Marcilla, H. Grande, R. Vergaz, D. Barrios, J.M. Sanchez-Pena, All-plastic electrochromic devices based on PEDOT as switchable optical attenuator in the near IR, Solar Energy Materials and Solar Cells, 92 (2008) 101-106.

[10] R.J. Mortimer, Electrochromic Materials, Annual Review of Materials Research, 41 (2011) null.

[11] M.C. Chen, D.J. Liaw, Y.C. Huang, H.Y. Wu, Y. Tai, Improving the efficiency of organic solar cell with a novel ambipolar polymer to form ternary cascade structure, (2011).

[12] Y. Galagan, I.G. de Vries, A.P. Langen, R. Andriessen, W.J.H. Verhees, S.C. Veenstra, J.M. Kroon, Technology development for roll-to-roll production of organic photovoltaics, Chemical Engineering and Processing: Process Intensification, 50 (2011) 454-461.

[13] P.K. Singh, K.W. Kim, H.-W. Rhee, Quantum dot doped solid polymer electrolyte for device application, Electrochemistry Communications, 11 (2009) 1247-1250.

[14] G.A. Snook, P. Kao, A.S. Best, Conducting-polymer-based supercapacitor devices and electrodes, Journal of Power Sources, 196 (2011) 1-12.

[15] H. Nishide, K. Oyaizu, Toward flexible batteries, Science, 319 (2008) 737-738.

[16] J. Z. Wang, S. L. Chou, J. Chen, S. Y. Chew, G. X. Wang, K. Konstantinov, J. Wu, S.-X. Dou, H.K. Liu, Paper-like free-standing polypyrrole and polypyrrole-LiFePO4 composite films for flexible and bendable rechargeable battery, Electrochemistry Communications, 10 (2008) 1781-1784.

[17] J.-Z. Wang, S.-L. Chou, H. Liu, G.X. Wang, C. Zhong, S. Yen Chew, H. Kun Liu, Highly flexible and bendable free-standing thin film polymer for battery application, Materials Letters, 63 (2009) 2352-2354.

[18] L. Oropeza-Ramos, A. Maci as, S. Jua rez, A. Falco n, A. Torres, M. Hautefeuille, H. Gonza lez, Low cost micro-platform for culturing and stimulation of cardiomyocyte tissue, 2011 IEEE 24th International Conference on Micro Electro Mechanical Systems, (2011), 912-915.

[19] S. De Koker, L.J. De Cock, P. Rivera-Gil, W.J. Parak, R. Auzely Velty, C. Vervaet, J.P. Remon, J. Grooten, B.G. De Geest, Polymeric multilayer capsules delivering biotherapeutics, DOI (2011).

[20] D. Ge, X. Ru, S. Hong, S. Jiang, J. Tu, J. Wang, A. Zhang, S. Ji, V. Linkov, B. Ren, W. Shi, Coating metals on cellulose-polypyrrole composites: A new route to self-powered drug delivery system, Electrochemistry Communications, 12 (2010) 1367-1370.

[21] S. Geetha, C.R.K. Rao, M. Vijayan, D.C. Trivedi, Biosensing and drug delivery by polypyrrole, Analytica Chimica Acta, 568 (2006) 119-125.

[22] P.M. George, D.A. Lavan, J.A. Burdick, C.-Y. Chen, E. Liang, R. Langer, Electrically controlled drug delivery from biotin-doped conductive polypyrrole, Advanced Materials, 18 (2006) 577-581.

[23] K. Kontturi, P. Pentti, G. Sundholm, Polypyrrole as a model membrane for drug delivery, Journal of Electroanalytical Chemistry, 453 (1998) 231-238.

[24] C. Wang, H. Xu, C. Wang, J. Zoval, M. Madou, Artificial muscle valves for responsive drug delivery systems, MEM, MOEMS, and Micromachining, April 29-30, 2004, SPIE, Strasbourg, France, 2004, pp. 109-115.

[25] B. Adhikari, S. Majumdar, Polymers in sensor applications, Progress in Polymer Science, 29 (2004) 699-766.

[26] X.J. Xu, L.D. Li, B. Liu, Y.P. Zou, Organic semiconductor memory devices based on a low-band gap polyfluorene derivative with isoindigo as electron-trapping moieties, Applied Physics Letters, 98 (2011).

[27] W.L. Leong, N. Mathews, B. Tan, S. Vaidyanathan, F. Dotz, S. Mhaisalkar, Towards printable organic thin film transistor based flash memory devices, Journal of Materials Chemistry, 21 (2011) 5203-5214.

[28] S.K. Bhattacharya, M.M. Tentzeris, L. Yang, S. Basat, A. Rida, Flexible LCP and paper-based substrates with embedded actives, passives, and RFIDs, Polytronic 2007 - 6th International IEEE Conference on Polymers and Adhesives in Microelectronics and Photonics, January 15, 2007 - January 18, 2007, Inst. of Elec. and Elec. Eng. Computer Society, Tokyo, Japan, 2007, pp. 159-166.

[29] M. Knoll, A self-writing smart label based on doping front migration, Electrochimica Acta, 54 (2008) 216-219.

[30] M.J. Moser, H. Zangl, Temperature and pressure monitoring of a whipped cream device, IEEE Sensors 2009 Conference - SENSORS 2009, October 25, 2009 - October 28, 2009, Institute of Electrical and Electronics Engineers Inc., Christchurch, New zealand, 2009, pp. 683-686.

[31] L.W.F. Chaves, C. Decker, A survey on organic smart labels for the Internet-of-Things, 7th International Conference on Networked Sensing Systems, INSS, IEEE Computer Society, Kassel, Germany, 2010, pp. 161-164.

[32] S.Y.Y. Leung, D.C.C. Lam, Performance of Printed Polymer-Based RFID Antenna on Curvilinear Surface, Electronics Packaging Manufacturing, IEEE Transactions on, 30 (2007) 200-205.

[33] N.J. Kirsch, N.A. Vacirca, E.E. Plowman, T.P. Kurzweg, A.K. Fontecchio, K.R. Dandekar, Optically transparent conductive polymer RFID meandering dipole antenna, RFID, 2009 IEEE International Conference on, 2009, pp. 278-282.

[34] T. Xuyuan, V. Koncar, C. Dufour, Geometry Pattern for the Wire Organic Electrochemical Textile Transistor, Journal of the Electrochemical Society, DOI 10.1149/1.3562962(2011) H572-577.

[35] E. Smela, Conjugated Polymer Actuators for Biomedical Applications, Advanced Materials, 6 (2003) 14.

[36] T.F. Otero, Soft, wet, and reactive polymers. Sensing artificial muscles and conformational energy, Journal of Materials Chemistry, 19 (2009) 681-689.

[37] V.S. Saji, A Review on Recent Patents in Corrosion Inhibitors, Recent Patents on Corrosion Science, 2 (2010) 7.

[38] S.A. Umoren, Polymers as Corrosion Inhibitors for Metals in Different Media - A Review, The Open Corrosion Journal, 2 (2009) 14.

[39] A. Malinauskas, Electrocatalysis at conducting polymers, Synthetic Metals, 107 (1999) 75-83.

[40] Organic and Printed Electronics Organic Electronic Association, 2009.

[41] G. Dennler, S. Bereznev, D. Fichou, K. Holl, D. Ilic, R. Koeppe, M. Krebs, A. Labouret, C. Lungenschmied, A. Marchenko, D. Meissner, E. Mellikov, J. Méot, A. Meyer, T. Meyer, H. Neugebauer, A. Öpik, N.S. Sariciftci, S. Taillemite, T. Wöhrle, A self-rechargeable and flexible polymer solar battery, Solar Energy, 81 (2007) 947-957.

[42] R. Koeppe, P. Bartu, S. Bauer, N.S. Sariciftci, Light- and Touch-Point Localization using Flexible Large Area Organic Photodiodes and Elastomer Waveguides, Advanced Materials, 21 (2009) 3510-3514.

[43] R.D. Henderson, R.M. Guijt, P.R. Haddad, E.F. Hilder, T.W. Lewis, M.C. Breadmore, Manufacturing and application of a fully polymeric electrophoresis chip with integrated polyaniline electrodes, Lab on a Chip, 10 (2010) 1869-1872.

[44] E. Holder, B.M.W. Langeveld, U.S. Schubert, New Trends in the Use of Transition Metal–Ligand Complexes for Applications in Electroluminescent Devices, Advanced Materials, 17 (2005) 1109-1121.

[45] I. Bidd, Polymer OLED Technology –A peek at the development for Display and Lighting Applications, Cambridge display technology, 2010.

[46] J. Cho, K.-H. Shin, J. Jang, Micropatterning of conducting polymer tracks on plasma treated flexible substrate using vapor phase polymerization-mediated inkjet printing, Synthetic Metals, 160 (2010) 1119-1125.

[47] L. Gonzalez-Macia, A. Morrin, M.R. Smyth, A.J. Killard, Advanced printing and deposition methodologies for the fabrication of biosensors and biodevices, Analyst, 135 (2010) 845-867.

[48] J.J. S. Ummartyotin, C. Wu, M. Sain, and H. Manuspiya, Deposition of PEDOT: PSS Nanoparticles as a Conductive Microlayer Anode in OLEDs Device by Desktop Inkjet Printer, Journal of Nanomaterials, 2011 7.

[49] Y. Yoshioka, G.E. Jabbour, Desktop inkjet printer as a tool to print conducting polymers, Synthetic Metals, 156 (2006) 779-783.

[50] J. Swingler, Degradation Characteristics of Desktop Inkjet Printed Conducting PEDOT/PSS Polymer on Cellulose Substrates, 2010.

[51] B. Weng, R. Shepherd, J. Chen, G.G. Wallace, Gemini surfactant doped polypyrrole nanodispersions: An inkjet printable formulation, Journal of Materials Chemistry, 21 (2011) 1918-1924.

[52] A.J. Heeger, Semiconducting polymers: the Third Generation, Chemical Society Reviews, 39 (2010).

[53] A.J. Heeger, Nobel Lecture: Semiconducting and metallic polymers:The fourth generation of polymeric materials, Reviews of Modern Physics, 73 (2001) 681-700.

[54] N. Bengt, The nobel prize in chemistry, 2000: Conductive polymers, The Royal Swedish Academy of Sciences, (2000).

[55] N.C. Greenham, S.C. Moratti, D.D.C. Bradley, R.H. Friend, A.B. Holmes, Efficient light-emitting diodes based on polymers with high electron affinities, Nature, 365 (1993) 628-630.

[56] C. Dhand, M. Das, M. Datta, B.D. Malhotra, Recent advances in polyaniline based biosensors, Biosensors and Bioelectronics, 26 (2011) 2811-2821.

[57] Y.S. Negi, P.V. Adhyapak, Development in Polyaniline Conducting Polymers Journal of Macromolecular Science, Part C: Polymer Reviews, 42 (2002) 35-53.

[58] J. Huang, Syntheses and applications of conducting polymer polyaniline nanofibers, Pure Appl. Chem, 78 (2006) 13.

[59] M. Li, Y. Guo, Y. Wei, A.G. MacDiarmid, P.I. Lelkes, Electrospinning polyaniline-contained gelatin nanofibers for tissue engineering applications, Biomaterials, 27 (2006) 2705-2715.

[60] S. Li, G. Zhang, G. Jing, J. Kan, Aqueous zinc–polyaniline secondary battery, Synthetic Metals, 158 (2008) 242-245.

[61] H. Zhong, R. Yuan, Y. Chai, W. Li, X. Zhong, Y. Zhang, In situ chemo-synthesized multi-wall carbon nanotube-conductive polyaniline nanocomposites: Characterization and application for a glucose amperometric biosensor, Talanta, 85 (2011) 104-111.

[62] H. Chang, Y. Yuan, N. Shi, Y. Guan, Electrochemical DNA Biosensor Based on Conducting Polyaniline Nanotube Array, Analytical Chemistry, 79 (2007) 5111-5115.

[63] V.T. Ivanova, G.S. Katrukha, A.V. Timofeeva, M.V. Ilyna, Y.E. Kurochkina, L.A. Baratova, I.Y. Sapurina, V.F. Ivanov, The sorption of influenza viruses and antibiotics on carbon nanotubes and polyaniline nanocomposites, Journal of Physics: Conference Series, 291 (2011) 012004.

[64] R.A. Green, N.H. Lovell, G.G. Wallace, L.A. Poole-Warren, Conducting polymers for neural interfaces: Challenges in developing an effective long-term implant, Biomaterials, 29 (2008) 3393-3399.

[65] S.A. Chen, C.C. Tsai, Structure/properties of conjugated conductive polymers. 2. 3-Ether-substituted polythiophenes and poly(4-methylthiophenes), Macromolecules, 26 (1993) 2234-2239.

[66] S.H. Ahn, M. z. Czae, E. R. Kim, H. Lee, S. H. Han, J. Noh, M. Hara, Synthesis and Characterization of Soluble Polythiophene Derivatives Containing Electron-Transporting Moiety, Macromolecules, 34 (2001) 2522-2527.

[67] M.R. Karim, C.J. Lee, M.S. Lee, Synthesis and characterization of conducting polythiophene/carbon nanotubes composites, Journal of Polymer Science Part A: Polymer Chemistry, 44 (2006) 5283-5290.

[68] N. Rozlosnik, New directions in medical biosensors employing poly(3,4-ethylenedioxy thiophene) derivative-based electrodes, Analytical and Bioanalytical Chemistry, 395 (2009) 637-645.

[69] O. Bertran, E. Armelin, F. Estrany, A. Gomes, J. Torras, C. Alemán, Poly(2-thiophen-3-yl-malonic acid), a Polythiophene with Two Carboxylic Acids Per Repeating Unit, The Journal of Physical Chemistry B, 114 (2010) 6281-6290.

[70] A.O. Patil, Y. Ikenoue, F. Wudl, A.J. Heeger, Water soluble conducting polymers, Journal of the American Chemical Society, 109 (1987) 1858-1859.

[71] P. Saville, Polypyrrole, formation and use, Defence Research and Development Atlantic Dartmouth Canada, 2005.

[72] E. Garfias-García, M. Romero-Romo, M.T. Ramírez-Silva, J. Morales, M. Palomar-Pardavé, Mechanism and kinetics of the electrochemical formation of polypyrrole under forced convection conditions, Journal of Electroanalytical Chemistry, 613 (2008) 67-79.

[73] R. ANSARI, Polypyrrole Conducting Electroactive Polymers: Synthesis and Stability Studies, E-Journal of Chemistry, 3 (2006) 16.

[74] S. Sadki, P. Schottland, N. Brodie, G. Sabouraud, The mechanisms of pyrrole electropolymerization, Chemical Society Reviews, 29 (2000).

[75] E.M. Genies, G. Bidan, A.F. Diaz, Spectroelectrochemical study of polypyrrole films, Journal of Electroanalytical Chemistry and Interfacial Electrochemistry, 149 (1983) 101-113.

[76] C. Della Pina, E. Falletta, M. Rossi, Conductive materials by metal catalyzed polymerization, Catalysis Today, 160 (2011) 11-27.

[77] J. Fink, B. Scheerer, W. Wernet, M. Monkenbusch, G. Wegner, H.J. Freund, H. Gonska, Electronic structure of pyrrole-based conducting polymers: An electron-energy-loss-spectroscopy study, Physical Review B, 34 (1986) 1101-1115.

[78] R.H. Geiss, G.B. Street, W. Volksen, J. Economy, Polymer structure determination using electron diffraction techniques, IBM J. Res. Dev., 27 (1983) 321-329.

[79] K. Teshima, K. Yamada, N. Kobayashi, R. Hirohashi, Effect of electropolymerization temperature on structural, morphological and conductive properties of poly (aniline) deposits prepared in 1, 2-dichloroethane without a proton donor, Journal of Electroanalytical Chemistry, 426 (1997) 97-102.

[80] C.O. Yoon, H.K. Sung, J.H. Kim, E. Barsoukov, J.H. Kim, H. Lee, The effect of low-temperature conditions on the electrochemical polymerization of polypyrrole films with high density, high electrical conductivity and high stability, Synthetic metals, 99 (1999) 201-212.

[81] S. Shimoda, E. Smela, The effect of pH on polymerization and volume change in PPy(DBS), Electrochimica Acta, 44 (1998) 219-238.

[82] A. Bhattacharya, A. De, S. Das, Electrochemical preparation and study of transport properties of polypyrrole doped with unsaturated organic sulfonates, Polymer, 37 (1996) 4375-4382.

[83] S.B. Saidman, J.B. Bessone, Electrochemical preparation and characterisation of polypyrrole on aluminium in aqueous solution, Journal of Electroanalytical Chemistry, 521 (2002) 87-94.

[84] D.R. Owens, B. Zinman, G. Bolli, Alternative routes of insulin delivery, Diabetic Medicine, 20 (2003) 886-898.

[85] S. Zafar Razzacki, P.K. Thwar, M. Yang, V.M. Ugaz, M.A. Burns, Integrated microsystems for controlled drug delivery, Advanced Drug Delivery Reviews, 56 (2004) 185-198.

[86] R. Wadhwa, C.F. Lagenaur, X.T. Cui, Electrochemically controlled release of dexamethasone from conducting polymer polypyrrole coated electrode, Journal of Controlled Release, 110 (2006) 531-541.

[87] S. Geetha, C.R.K. Rao, M. Vijayan, D.C. Trivedi, Biosensing and drug delivery by polypyrrole, Analytica Chimica Acta, 568 (2006) 119-125.

[88] B.C. Thompson, S.E. Moulton, J. Ding, R. Richardson, A. Cameron, S. O'Leary, G.G. Wallace, G.M. Clark, Optimising the incorporation and release of a neurotrophic factor using conducting polypyrrole, Journal of Controlled Release, 116 (2006) 285-294.

[89] X. Luo, C. Matranga, S. Tan, N. Alba, X.T. Cui, Carbon nanotube nanoreservior for controlled release of anti-inflammatory dexamethasone, Biomaterials, 32 (2011) 6316-6323.

[90] P. Herrasti, A.N. Kulak, D.V. Bavykin, C.P. de Léon, J. Zekonyte, F.C. Walsh, Electrodeposition of polypyrrole–titanate nanotube composites coatings and their corrosion resistance, Electrochimica Acta, 56 (2011) 1323-1328.

[91] E. Smela, Conjugated Polymer Actuators for Biomedical Applications, Advanced Materials, 15 (2003) 481-494.

[92] D. Ateh, H.A. Navsaria, P. Vadgama, Polypyrrole-based conducting polymers and interactions with biological tissues, The Royal Society, 22 (2006) 741–752.

[93] K. Kontturi, P. Pentti, G. Sundholm, Polypyrrole as a model membrane for drug delivery, Journal of Electroanalytical Chemistry, 453 (1998) 231-238.

[94] D. Svirskis, J. Travas-Sejdic, A. Rodgers, S. Garg, Electrochemically controlled drug delivery based on intrinsically conducting polymers, Journal of Controlled Release, 146 (2010) 6-15.

[95] L.L. Miller, A.N.K. Lau, E.K. Miller, Electrically stimulated release of neurotransmitters from a surface. An analog of the presynaptic terminal, Journal of the American Chemical Society, 104 (1982) 5242-5244.

[96] B. Zinger, L.L. Miller, Timed release of chemicals from polypyrrole films, Journal of the American Chemical Society, 106 (1984) 6861-6863.

[97] R. Ravichandran, S. Sundarrajan, J.R. Venugopal, S. Mukherjee, S. Ramakrishna, Applications of conducting polymers and their issues in biomedical engineering, Journal of The Royal Society Interface, 7 (2010) S559-S579.

[98] N.K. Guimard, N. Gomez, C.E. Schmidt, Conducting polymers in biomedical engineering, Progress in Polymer Science, 32 (2007) 876-921.

[99] C. Vallejo-Giraldo, A. Kelly, M.J.P. Biggs, Biofunctionalisation of electrically conducting polymers, Drug Discovery Today, 19 (2014) 88-94.

[100] T.F. Otero, J.G. Martinez, J. Arias-Pardilla, Biomimetic electrochemistry from conducting polymers. A review: Artificial muscles, smart membranes, smart drug delivery and computer/neuron interfaces, Electrochimica Acta, 84 (2012) 112-128.

[101] B. Guo, L. Glavas, A.-C. Albertsson, Biodegradable and electrically conducting polymers for biomedical applications, Progress in Polymer Science, 38 (2013) 1263-1286.

[102] E. Llorens, E. Armelin, M. del Mar Pérez-Madrigal, L. del Valle, C. Alemán, J. Puiggalí, Nanomembranes and Nanofibers from Biodegradable Conducting Polymers, Polymers, 5 (2013) 1115-1157.

[103] J.R. Smith, D.A. Lamprou, Polymer coatings for biomedical applications: a review, Transactions of the IMF, 92 (2014) 9-19.

[104] Y. Z. Long, M. M. Li, C. Gu, M. Wan, J. L. Duvail, Z. Liu, Z. Fan, Recent advances in synthesis, physical properties and applications of conducting polymer nanotubes and nanofibers, Progress in Polymer Science, 36 (2011) 1415-1442.

[105] V. Pillay, T.-S. Tsai, Y.E. Choonara, L.C. du Toit, P. Kumar, G. Modi, D. Naidoo, L.K. Tomar, C. Tyagi, V.M.K. Ndesendo, A review of integrating electroactive polymers as responsive systems for specialized drug delivery applications, Journal of Biomedical Materials Research Part A, 102 (2014) 2039-2054.

[106] Z. Yue, S.E. Moulton, M. Cook, S. O'Leary, G.G. Wallace, Controlled delivery for neuro-bionic devices, Advanced Drug Delivery Reviews, 65 (2013) 559-569.

[107] M. Asplund, C. Boehler, T. Stieglitz, Anti-inflammatory polymer electrodes for glial scar treatment, Frontiers in Neuroengineering, 7 (2014).

[108] D. Svirskis, B.E. Wright, J. Travas-Sejdic, A. Rodgers, S. Garg, Evaluation of physical properties and performance over time of an actuating polypyrrole based drug delivery system, Sensors and Actuators B: Chemical, 151 (2010) 97-102.

[109] M.R. Gandhi, P. Murray, G.M. Spinks, G.G. Wallace, Mechanism of electromechanical actuation in polypyrrole, Synthetic Metals, 73 (1995) 247-256.

[110] L. Leprince, A. Dogimont, D. Magnin, S. Demoustier-Champagne, Dexamethasone electrically controlled release from polypyrrole-coated nanostructured electrodes, Journal of Materials Science: Materials in Medicine, 21 (2010) 925-930.

[111] J. M. Pernaut, J.R. Reynolds, Use of Conducting Electroactive Polymers for Drug Delivery and Sensing of Bioactive Molecules. A Redox Chemistry Approach, The Journal of Physical Chemistry B, 104 (2000) 4080-4090.

[112] D. Ge, R. Qi, J. Mu, X. Ru, S. Hong, S. Ji, V. Linkov, W. Shi, A self-powered and thermally-responsive drug delivery system based on conducting polymers, Electrochemistry Communications, 12 (2010) 1087-1090.

[113] S.E. Moulton, M.D. Imisides, R.L. Shepherd, G.G. Wallace, Galvanic coupling conducting polymers to biodegradable Mg initiates autonomously powered drug release, Journal of Materials Chemistry, 18 (2008) 3608-3613.

[114] Y. Song, D. Shan, R. Chen, F. Zhang, E.-H. Han, Biodegradable behaviors of AZ31 magnesium alloy in simulated body fluid, Materials Science and Engineering: C, 29 (2009) 1039-1045.

[115] B. Winther-Jensen, N.B. Clark, Controlled release of dyes from chemically polymerised conducting polymers, Reactive and Functional Polymers, 68 (2008) 742-750.

[116] C.Y. Wang, S. Ashraf, C.O. Too, G.G. Wallace, Ionic liquid as electrolyte in a self-powered controlled release system, Sensors and Actuators B: Chemical, 141 (2009) 452-457.

[117] C.M. Boutry, S. Wei, T. Strunz, H. Chandrahalim, C. Hierold, Development and characterization of biodegradable conductive polymers for the next generation of RF bio-resonators, Frequency Control Symposium (FCS), IEEE International, 2010, pp. 258-261.

[118] Q. S. Zhang, Y. H. Yan, S. P. Li, T. Feng, Synthesis of a novel biodegradable and electroactive polyphosphazene for biomedical application, Biomedical Materials, 4 (2009) 035008.

[119] S. Kehoe, X.F. Zhang, D. Boyd, FDA approved guidance conduits and wraps for peripheral nerve injury: A review of materials and efficacy, Injury, 43 (2012) 553-572.

[120] M.C.O. Rodrigues, A.A. Rodrigues, L.E. Glover, J. Voltarelli, C.V. Borlongan, Peripheral Nerve Repair with Cultured Schwann Cells: Getting Closer to the Clinics, The Scientific World Journal, 2012 (2012) 10.

[121] L. Li, C. Huang, Electrochemical/Electrospray Mass Spectrometric Studies of Electrochemically Stimulated ATP Release from PP/ATP Films, Journal of the American Society for Mass Spectrometry, 18 (2007) 919-926.

[122] K. Kontturi, P. Pentti, G. Sundholm, Polypyrrole as a model membrane for drug delivery, Journal of Electroanalytical Chemistry, 453 (1998) 231-238.

[123] X. Luo, X.T. Cui, Electrochemically controlled release based on nanoporous conducting polymers, Electrochemistry Communications, 11 (2009) 402-404.

[124] S. Jiang, Y. Sun, X. Cui, X. Huang, Y. He, S. Ji, W. Shi, D. Ge, Enhanced drug loading capacity of polypyrrole nanowire network for controlled drug release, Synthetic Metals, 163 (2013) 19-23.

[125] Z. Liu, J. Ya, Y. Xin, J. Ma, C. Zhou, Assembly of polystyrene colloidal crystal templates by a dip-drawing method, Journal of Crystal Growth, 297 (2006) 223-227.

[126] S. Li, J. Zheng, Y. Zhao, Y. Liu, Preparation of a three-dimensional ordered macroporous titanium dioxide material with polystyrene colloid crystal as a template, Journal of Applied Polymer Science, 107 (2008) 3903-3908.

[127] F. Zeng, Z. Sun, C. Wang, B. Ren, X. Liu, Z. Tong, Fabrication of Inverse Opal via Ordered Highly Charged Colloidal Spheres, Langmuir, 18 (2002) 9116-9120.

[128] Y. Cho, R.B. Borgens, Biotin-Doped Porous Polypyrrole Films for Electrically Controlled Nanoparticle Release, Langmuir, 27 (2011) 6316-6322.

[129] M. Sharma, G.I.N. Waterhouse, S.W.C. Loader, S. Garg, D. Svirskis, High surface area polypyrrole scaffolds for tunable drug delivery, International Journal of Pharmaceutics, 443 (2013) 163-168.

[130] S.J. Cho, H.J. Kim, J.H. Lee, H.W. Choi, H.G. Kim, H.M. Chung, J.T. Do, Silica coated titania nanotubes for drug delivery system, Materials Letters, 64 (2010) 1664-1667.

[131] N. Yang, X. Chen, T. Ren, P. Zhang, D. Yang, Carbon nanotube based biosensors, Sensors and Actuators B: Chemical, 207, Part A (2015) 690-715.

[132] M.A. Barik, J.C. Dutta, Fabrication and characterization of junctionless carbon nanotube field effect transistor for cholesterol detection, Applied Physics Letters, 105 (2014) 053509.

[133] Z. Wu, W.-q. Sun, T. Feng, S.W. Tang, G. Li, K.-l. Jiang, S.-y. Xu, C.K. Ong, Imaging of soft material with carbon nanotube tip using near-field scanning microwave microscopy, Ultramicroscopy, 148 (2015) 75-80.

[134] P. Knittel, M.J. Higgins, C. Kranz, Nanoscopic polypyrrole AFM-SECM probes enabling force measurements under potential control, Nanoscale, 6 (2014) 2255-2260.

[135] S.H. Barghi, T.T. Tsotsis, M. Sahimi, Chemisorption, physisorption and hysteresis during hydrogen storage in carbon nanotubes, International Journal of Hydrogen Energy, 39 (2014) 1390-1397.

[136] S.G. Hashmi, T. Moehl, J. Halme, Y. Ma, T. Saukkonen, A. Yella, F. Giordano, J.D. Decoppet, S.M. Zakeeruddin, P. Lund, M. Gratzel, A durable SWCNT/PET polymer foil based metal free counter electrode for flexible dye-sensitized solar cells, Journal of Materials Chemistry A, 2 (2014) 19609-19615.

[137] H. Ren, S. Pyo, J.-I. Lee, T.-J. Park, F.S. Gittleson, F.C.C. Leung, J. Kim, A.D. Taylor, H.-S. Lee, J. Chae, A high power density miniaturized microbial fuel cell having carbon nanotube anodes, Journal of Power Sources, 273 (2015) 823-830.

[138] X. Luo, C. Matranga, S. Tan, N. Alba, X.T. Cui, Carbon nanotube nanoreservior for controlled release of anti-inflammatory dexamethasone, Biomaterials, (2011). 05-20.

[139] A. Shvedova, V. Castranova, E. Kisin, D. Schwegler-Berry, A. Murray, V. Gandelsman, A. Maynard, P. Baron, Exposure to Carbon Nanotube Material: Assessment of Nanotube Cytotoxicity using Human Keratinocyte Cells, Journal of Toxicology and Environmental Health, Part A, 66 (2003) 1909-1926.

[140] S.K. Manna, S. Sarkar, J. Barr, K. Wise, E.V. Barrera, O. Jejelowo, A.C. Rice-Ficht, G.T. Ramesh, Single-Walled Carbon Nanotube Induces Oxidative Stress and Activates Nuclear Transcription Factor-κB in Human Keratinocytes, Nano Letters, 5 (2005) 1676-1684.

[141] J. Muller, F. Huaux, N. Moreau, P. Misson, J.-F. Heilier, M. Delos, M. Arras, A. Fonseca, J.B. Nagy, D. Lison, Respiratory toxicity of multi-wall carbon nanotubes, Toxicology and Applied Pharmacology, 207 (2005) 221-231.

[142] D. Cui, F. Tian, C.S. Ozkan, M. Wang, H. Gao, Effect of single wall carbon nanotubes on human HEK293 cells, Toxicology Letters, 155 (2005) 73-85.

[143] V. Zwilling, E. Darque-Ceretti, A. Boutry-Forveille, D. David, M.Y. Perrin, M. Aucouturier, Structure and physicochemistry of anodic oxide films on titanium and TA6V alloy, Surface and Interface Analysis, 27 (1999) 629-637.

[144] D. Gong, C.A. Grimes, O.K. Varghese, W. Hu, R.S. Singh, Z. Chen, E.C. Dickey, Titanium oxide nanotube arrays prepared by anodic oxidation, Journal of Materials Research, 16 (2001) 4.

[145] G. Liu, K. Wang, N. Hoivik, H. Jakobsen, Progress on free-standing and flow-through TiO2 nanotube membranes, Solar Energy Materials and Solar Cells, 98 (2012) 24-38.

[146] X. Xiao, L. Yang, M. Guo, C. Pan, Q. Cai, S. Yao, Biocompatibility and in vitro antineoplastic drug-loaded trial of titania nanotubes prepared by anodic oxidation of a pure titanium, Science in China Series B: Chemistry, 52 (2009) 2161-2165.

[147] M.P. Neupane, I.S. Park, T.S. Bae, H.K. Yi, M. Uo, F. Watari, M.H. Lee, Titania nanotubes supported gelatin stabilized gold nanoparticles for medical implants, Journal of Materials Chemistry, 21 (2011) 12078-12082.

[148] K.C. Popat, M. Eltgroth, T.J. LaTempa, C.A. Grimes, T.A. Desai, Titania Nanotubes: A Novel Platform for Drug-Eluting Coatings for Medical Implants?, Small, 3 (2007) 1878-1881.

[149] C. von Wilmowsky, S. Bauer, R. Lutz, M. Meisel, F.W. Neukam, T. Toyoshima, P. Schmuki, E. Nkenke, K.A. Schlegel, In vivo evaluation of anodic TiO2 nanotubes: An experimental study in the pig, Journal of Biomedical Materials Research Part B: Applied Biomaterials, 89B (2009) 165-171.

[150] D. Baowan, W. Sukchom, K. Chayantrakom, P. Satiracoo, Three possible encapsulation mechanics of TiO2 nanoparticles into single-walled carbon nanotubes, Journal of Nanomaterials, 2011 (2011).

[151] E. Balaur, J.M. Macak, H. Tsuchiya, P. Schmuki, Wetting behaviour of layers of TiO2 nanotubes with different diameters, Journal of Materials Chemistry, 15 (2005).

[152] N. Swami, Z. Cui, L.S. Nair, Titania Nanotubes: Novel Nanostructures for Improved Osseointegration, Journal of Heat Transfer, 133 (2011) 034002.

[153] K. Noh, K.S. Brammer, S.H. Kim, C. Choi, C.J. Frandsen, S. Jin, A New Nano-Platform for Drug Release via Nanotubular Aluminum Oxide Journal of Biomaterials and Nanobiotechnology, 2 (2011) 8.

[154] Y. Kong, H. Ge, J. Xiong, S. Zuo, Y. Wei, C. Yao, L. Deng, Palygorskite polypyrrole nanocomposite: A new platform for electrically tunable drug delivery, Applied Clay Science, 99 (2014) 119-124.

[155] D. Patra, S. Sengupta, W. Duan, H. Zhang, R. Pavlick, A. Sen, Intelligent, self-powered, drug delivery systems, Nanoscale, 5 (2013) 1273-1283.

[156] M. Pumera, Electrochemically powered self-propelled electrophoretic nanosubmarines, Nanoscale, 2 (2010) 1643-1649.

[157] H. Zhang, W. Duan, L. Liu, A. Sen, Depolymerization-powered autonomous motors using biocompatible fuel, Journal of the American Chemical Society, 135 (2013) 15734-15737.

[158] W. Wang, W. Duan, A. Sen, T.E. Mallouk, Catalytically powered dynamic assembly of rod-shaped nanomotors and passive tracer particles, Proceedings of the National Academy of Sciences, 110 (2013) 17744-17749.

[159] W.F. Paxton, K.C. Kistler, C.C. Olmeda, A. Sen, S.K. St. Angelo, Y. Cao, T.E. Mallouk, P.E. Lammert, V.H. Crespi, Catalytic Nanomotors: Autonomous Movement of Striped Nanorods, Journal of the American Chemical Society, 126 (2004) 13424-13431.

[160] R. Golestanian, T.B. Liverpool, A. Ajdari, Propulsion of a molecular machine by asymmetric distribution of reaction products, Physical review letters, 94 (2005) 220801.

[161] A.A. Solovev, Y. Mei, E. Bermúdez Ureña, G. Huang, O.G. Schmidt, Catalytic Microtubular Jet Engines Self-Propelled by Accumulated Gas Bubbles, Small, 5 (2009) 1688-1692.

[162] A. Ghosh, P. Fischer, Controlled propulsion of artificial magnetic nanostructured propellers, Nano letters, 9 (2009) 2243-2245.

[163] W. Gao, S. Sattayasamitsathit, K.M. Manesh, D. Weihs, J. Wang, Magnetically powered flexible metal nanowire motors, Journal of the American Chemical Society, 132 (2010) 14403-14405.

[164] G. Loget, A. Kuhn, Propulsion of microobjects by dynamic bipolar self-regeneration, Journal of the American Chemical Society, 132 (2010) 15918-15919.

[165] A.A. Solovev, E.J. Smith, C.C. Bof'Bufon, S. Sanchez, O.G. Schmidt, Light-Controlled Propulsion of Catalytic Microengines, Angewandte Chemie International Edition, 50 (2011) 10875-10878.

[166] Y. Hong, M. Diaz, U.M. Córdova-Figueroa, A. Sen, Light-Driven Titanium-Dioxide-Based Reversible Microfireworks and Micromotor/Micropump Systems, Advanced Functional Materials, 20 (2010) 1568-1576.

[167] W. Wang, L.A. Castro, M. Hoyos, T.E. Mallouk, Autonomous motion of metallic microrods propelled by ultrasound, ACS nano, 6 (2012) 6122-6132.

[168] V. Garcia-Gradilla, J. Orozco, S. Sattayasamitsathit, F. Soto, F. Kuralay, A. Pourazary, A. Katzenberg, W. Gao, Y. Shen, J. Wang, Functionalized ultrasound-propelled magnetically guided nanomotors: Toward practical biomedical applications, ACS nano, 7 (2013) 9232-9240.

[169] M. Pumera, Nanomaterials meet microfluidics, Chemical Communications, 47 (2011) 5671-5680.

[170] K.K. Dey, S. Bhandari, D. Bandyopadhyay, S. Basu, A. Chattopadhyay, The pH taxis of an intelligent catalytic microbot, Small, 9 (2013) 1916-1920.

[171] Y. Hong, N.M. Blackman, N.D. Kopp, A. Sen, D. Velegol, Chemotaxis of nonbiological colloidal rods, Physical review letters, 99 (2007) 178103.

[172] Y. Wang, S.-t. Fei, Y.-M. Byun, P.E. Lammert, V.H. Crespi, A. Sen, T.E. Mallouk, Dynamic interactions between fast microscale rotors, Journal of the American Chemical Society, 131 (2009) 9926-9927.

[173] K.K. Dey, B.R. Panda, A. Paul, S. Basu, A. Chattopadhyay, Catalytic gold nanoparticle driven pH specific chemical locomotion, Journal of colloid and interface science, 348 (2010) 335-341.

[174] S. Sundararajan, P.E. Lammert, A.W. Zudans, V.H. Crespi, A. Sen, Catalytic motors for transport of colloidal cargo, Nano letters, 8 (2008) 1271-1276.

[175] J. Orozco, S. Campuzano, D. Kagan, M. Zhou, W. Gao, J. Wang, Dynamic isolation and unloading of target proteins by aptamer-modified microtransporters, Analytical chemistry, 83 (2011) 7962-7969.

[176] S. Sundararajan, S. Sengupta, M.E. Ibele, A. Sen, Drop-Off of Colloidal Cargo Transported by Catalytic Pt–Au Nanomotors via Photochemical Stimuli, Small, 6 (2010) 1479-1482.

[177] J. Burdick, R. Laocharoensuk, P.M. Wheat, J.D. Posner, J. Wang, Synthetic nanomotors in microchannel networks: Directional microchip motion and controlled manipulation of cargo, Journal of the American Chemical Society, 130 (2008) 8164-8165.

[178] J. Wang, K.M. Manesh, Motion control at the nanoscale, Small, 6 (2010) 338- 345.

[179] T. Mirkovic, N.S. Zacharia, G.D. Scholes, G.A. Ozin, Nanolocomotion—catalytic nanomotors and nanorotors, Small, 6 (2010) 159-167.

[180] N. Mano, A. Heller, Bioelectrochemical propulsion, Journal of the American Chemical Society, 127 (2005) 11574-11575.

[181] L. Zhang, J.J. Abbott, L. Dong, B.E. Kratochvil, D. Bell, B.J. Nelson, Artificial bacterial flagella: Fabrication and magnetic control, Applied Physics Letters, 94 (2009) 64107.

[182] W. Gao, D. Kagan, O.S. Pak, C. Clawson, S. Campuzano, E. Chuluun-Erdene, E. Shipton, E.E. Fullerton, L. Zhang, E. Lauga, Cargo-Towing Fuel-Free Magnetic Nanoswimmers for Targeted Drug Delivery, small, 8 (2012) 460-467.

[183] G.T.R. Palmore, G.M. Whitesides, Microbial and enzymatic biofuel cells, ACS Symp Ser, 566 20.

[184] M.H. Osman, A.A. Shah, F.C. Walsh, Recent progress and continuing challenges in bio-fuel cells. Part II: Microbial, Biosensors and Bioelectronics, 26 (2010) 953-963.

[185] S. Aquino Neto, A.R. De Andrade, New energy sources: the enzymatic biofuel cell, Journal of the Brazilian Chemical Society, 24 (2013) 1891-1912.

[186] R.A. Bullen, T.C. Arnot, J.B. Lakeman, F.C. Walsh, Biofuel cells and their development, Biosensors and Bioelectronics, 21 (2006) 2015-2045.

[187] M.H. Osman, A.A. Shah, F.C. Walsh, Recent progress and continuing challenges in bio-fuel cells. Part I: Enzymatic cells, Biosensors and Bioelectronics, 26 (2011) 3087-3102.

[188] J.A. Cracknell, K.A. Vincent, F.A. Armstrong, Enzymes as Working or Inspirational Electrocatalysts for Fuel Cells and Electrolysis, Chemical Reviews, 108 (2008) 2439-2461.

[189] B.I. Rapoport, J.T. Kedzierski, R. Sarpeshkar, A glucose fuel cell for implantable brain–machine interfaces, PLoS One, 7 (2012) e38436.

[190] A. Heller, Potentially implantable miniature batteries, Analytical and Bioanalytical Chemistry, 385 (2006) 469-473.

[191] N.S. Oliver, C. Toumazou, A.E.G. Cass, D.G. Johnston, Glucose sensors: a review of current and emerging technology, Diabetic Medicine, 26 (2009) 197-210.

[192] M. Zhou, Y. Du, C. Chen, B. Li, D. Wen, S. Dong, E. Wang, Aptamer-Controlled Biofuel Cells in Logic Systems and Used as Self-Powered and Intelligent Logic Aptasensors, Journal of the American Chemical Society, 132 (2010) 2172-2174.

[193] M. Zhou, N. Zhou, F. Kuralay, J.R. Windmiller, S. Parkhomovsky, G. Valdés-Ramírez, E. Katz, J. Wang, A Self-Powered "Sense-Act-Treat" System that is Based on a Biofuel Cell and Controlled by Boolean Logic, Angewandte Chemie International Edition, 51 (2012) 2686-2689.

[194] S. Pirsa, N. Alizadeh, A selective DMSO gas sensor based on nanostructured conducting polypyrrole doped with sulfonate anion, Sensors and Actuators B: Chemical, 168 (2012) 303-309.

[195] G.M. Spinks, G.G. Wallace, L. Liu, D. Zhou, Conducting polymers electromechanical actuators and strain sensors, Macromolecular Symposia, 192 (2003) 161-170.

[196] A.P. Tjahyono, K.C. Aw, J. Travas-Sejdic, A novel polypyrrole and natural rubber based flexible large strain sensor, Sensors and Actuators B: Chemical, 166–167 (2012) 426-437.

[197] L. Pan, A. Chortos, G. Yu, Y. Wang, S. Isaacson, R. Allen, Y. Shi, R. Dauskardt, Z. Bao, An ultra-sensitive resistive pressure sensor based on hollow-sphere microstructure induced elasticity in conducting polymer film, Nat Commun, 5 (2014).

[198] S.T. McGovern, G.M. Spinks, G.G. Wallace, Micro-humidity sensors based on a processable polyaniline blend, Sensors and Actuators B: Chemical, 107 (2005) 657-665.

[199] C. Steffens, A. Manzoli, F.L. Leite, O. Fatibello, P.S.P. Herrmann, Atomic force microscope microcantilevers used as sensors for monitoring humidity, Microelectronic Engineering, 113 (2014) 80-85.

[200] E. Song, J. W. Choi, Self-calibration of a polyaniline nanowire-based chemiresistive pH sensor, Microelectronic Engineering, 116 (2014) 26-32.

[201] R. Stella, J.N. Barisci, G. Serra, G.G. Wallace, D. De Rossi, Characterisation of olive oil by an electronic nose based on conducting polymer sensors, Sensors and Actuators B: Chemical, 63 (2000) 1-9.

[202] T.E. Campbell, B.J. Munro, G.G. Wallace, J.R. Steele, Can fabric sensors monitor breast motion?, Journal of Biomechanics, 40 (2007) 3056-3059.

[203] T. Galán, B. Prieto-Simón, M. Alvira, R. Eritja, G. Götz, P. Bäuerle, J. Samitier, Label-free electrochemical DNA sensor using "click"-functionalized PEDOT electrodes, Biosensors and Bioelectronics, 74 (2015) 751-756.

[204] S. Nambiar, J.T.W. Yeow, Conductive polymer-based sensors for biomedical applications, Biosensors and Bioelectronics, 26 (2011) 1825-1832.

[205] H. Peng, L. Zhang, C. Soeller, J. Travas-Sejdic, Conducting polymers for electrochemical DNA sensing, Biomaterials, 30 (2009) 2132-2148.

[206] E.-S. Park, D. H. Jang, Y. I. Lee, C.W. Jung, D. woo Lim, B.S. Kim, Y. K. Jeong, N.V. Myung, Y. H. Choa, Fabrication and sensing property for conducting polymer nanowire-based biosensor for detection of immunoglobulin G, Research on Chemical Intermediates, 40 (2014) 2565-2570.

[207] R.E. Ionescu, N. Jaffrezic-Renault, L. Bouffier, C. Gondran, S. Cosnier, D.G. Pinacho, M.P. Marco, F.J. Sánchez-Baeza, T. Healy, C. Martelet, Impedimetric immunosensor for the specific label free detection of ciprofloxacin antibiotic, Biosensors and Bioelectronics, 23 (2007) 549-555.

[208] S. Tokonami, Y. Nakadoi, H. Nakata, S. Takami, T. Kadoma, H. Shiigi, T. Nagaoka, Recognition of gram-negative and gram-positive bacteria with a functionalized conducting polymer film, Research on Chemical Intermediates, 40 (2014) 2327-2335.

[209] R. Chaudhari, A. Joshi, R. Srivastava, Oxygen sensing glucose biosensors based on alginate nano-micro systems, SPIE Smart Structures and Materials+ Nondestructive Evaluation and Health Monitoring, International Society for Optics and Photonics, 2014, pp. 906005-906006.

[210] A. Joshi, R. Chaudhari, R. Srivastava, FITC-tagged macromolecule-based alginate microspheres for urea sensoring, SPIE Smart Structures and Materials+ Nondestructive Evaluation and Health Monitoring, International Society for Optics and Photonics, (2014) 90600P-90606P.

[211] L. Xia, Z. Wei, M. Wan, Conducting polymer nanostructures and their application in biosensors, Journal of Colloid and Interface Science, 341 (2010) 1-11.

[212] U. Lange, N.V. Roznyatovskaya, V.M. Mirsky, Conducting polymers in chemical sensors and arrays, Analytica Chimica Acta, 614 (2008) 1-26.

[213] M. Gerard, A. Chaubey, B.D. Malhotra, Application of conducting polymers to biosensors, Biosensors and Bioelectronics, 17 (2002) 345-359.

[214] P. Wang, Q. Liu, Biomedical sensors and measurement, Springer2011.

[215] G. Danaei, M.M. Finucane, Y. Lu, G.M. Singh, M.J. Cowan, C.J. Paciorek, J.K. Lin, F. Farzadfar, Y.-H. Khang, G.A. Stevens, M. Rao, M.K. Ali, L.M. Riley, C.A. Robinson, M. Ezzati, National, regional, and global trends in fasting plasma glucose and diabetes prevalence since 1980: systematic analysis of health examination surveys and epidemiological studies with 370 country-years and 2·7 million participants, The Lancet, 378 (2011) 31-40.

[216] WHO, Global health risk: mortality and burden of disease attribrtable to selected major risk 2009.

[217] A.D. Association, Economic Costs of Diabetes in the U.S. in 2007, Diabetes Care, 31 (2008) 596-615.

[218] A.D. Association, Economic costs of diabetes in the US in 2012, Diabetes Care, 36 (2013) 1033-1046.

[219] WHO, Diabetes Fact Sheet, 2008.

[220] A. Heller, Implanted Electrochemical Glucose Sensors for the Management of Diabetes, Annual Review of Biomedical Engineering, 1 (1999) 153-175.

[221] X. Li, Y. Zhou, Z. Zheng, X. Yue, Z. Dai, S. Liu, Z. Tang, Glucose Biosensor Based on Nanocomposite Films of CdTe Quantum Dots and Glucose Oxidase, Langmuir, 25 (2009) 6580-6586.

[222] J.V. Veetil, S. Jin, K. Ye, A glucose sensor protein for continuous glucose monitoring, Biosensors and Bioelectronics, 26 (2010) 1650-1655.

[223] H.D. Park, K.J. Lee, H.R. Yoon, H.H. Nam, Design of a portable urine glucose monitoring system for health care, Computers in Biology and Medicine, 35 (2005) 275-286.

[224] K.S. K., A.H. T., A. Mangilal., J. FANG, D.M. A, A simple enzyme based biosensor on flexible plastic substrate, Society of Photo-Optical Instrumentation Engineers, 7759 (2010).

[225] G.G. Guilbault, G. Palleschi, G. Lubrano, Non-invasive biosensors in clinical analysis, Biosensors and Bioelectronics, 10 (1995) 379-392.

[226] M. Yamaguchi, M. Mitsumori, Y. Kano, Noninvasively measuring blood glucose using saliva, Engineering in Medicine and Biology Magazine, IEEE, 17 (1998) 59-63.

[227] E.-H. Yoo, S.-Y. Lee, Glucose Biosensors: An Overview of Use in Clinical Practice, Sensors, 10 (2010) 4558-4576.

[228] M. Singh, P.K. Kathuroju, N. Jampana, Polypyrrole based amperometric glucose biosensors, Sensors and Actuators B: Chemical, 143 (2009) 430-443.

[229] M. Trojanowicz, M.L. Hitchman, A potentiometric polypyrrole-based glucose biosensor, Electroanalysis, 8 (1996) 263-266.

[230] C.G.J. Koopal, B. Eijsma, R.J.M. Nolte, Chronoamperometric detection of glucose by a 3RD-generation biosensor constructed from conducting microotubules of polypyrrole, Synthetic Metals, 57 (1993) 3689-3695.

[231] M.M. Rahman, A.J.S. Ahammad, J.-H. Jin, S.J. Ahn, J.-J. Lee, A Comprehensive Review of Glucose Biosensors Based on Nanostructured Metal-Oxides, Sensors, 10 (2010) 4855-4886.

[232] K. Toghill , R. Compton, Electrochemical Non-enzymatic Glucose Sensors: A Perspective and an EvaluationInt. J. Electrochem. Sci., 5 (2010) 55.

[233] G. Harsanyi, Sensors in Biomedical Applications: Fundamentals, Technology and Applications, CRC Press LLC, Florida., 2000.

[234] B. Eggins, Chemical sensors and biosensors, John Willey & Sons,Ltd.2002.

[235] E. Tamiya, I. Karube, S. Hattori, M. Suzuki, K. Yokoyama, Micro glucose using electron mediators immobilized on a polypyrrole-modified electrode, Sensors and Actuators, 18 (1989) 297-307.

[236] T. Kwok-Siong, L. Liwei, A polypyrrole-carbon-nanotube (PPy-MWNT) nanocomposite glucose sensor, Micro Electro Mechanical Systems. 17th IEEE International Conference on. (MEMS), 2004, pp. 395-398.

[237] G. Ozyilmaz, A. Ozyilmaz, F. Can, Glucose oxidase-polypyrrole electrodes synthesized in p-toluenesulfonic acid and sodium p-toluenesulfonate, Applied Biochemistry and Microbiology, 47 (2011) 196-205.

[238] P. Palod, S. Pandey, S. Hayase, V. Singh, Template-Assisted Electrochemical Growth of Polypyrrole Nanotubes for Development of High Sensitivity Glucose Biosensor, Appl Biochem Biotechnol, 174 (2014) 1059-1072.

[239] M. Medina-Sánchez, C. Martínez-Domingo, E. Ramon, A. Merkoçi, An Inkjet-Printed Field-Effect Transistor for Label-Free Biosensing, Advanced Functional Materials, 24 (2014) 6291-6302.

[240] N.Y. Shim, D.A. Bernards, D.J. Macaya, J.A. DeFranco, M. Nikolou, R.M. Owens, G.G. Malliaras, All-plastic electrochemical transistor for glucose sensing using a ferrocene mediator, Sensors, 9 (2009) 9896-9902.

[241] S.K. Kanakamedala, H.T. Alshakhouri, M. Agarwal, M.A. DeCoster, A simple polymer based electrochemical transistor for micromolar glucose sensing, Sensors and Actuators B: Chemical, 157 (2011) 92-97.

[242] J. Shi, P. Ci, F. Wang, H. Peng, P. Yang, L. Wang, S. Ge, Q. Wang, P.K. Chu, Nonenzymatic glucose sensor based on over-oxidized polypyrrole modified Pd/Si microchannel plate electrode, Biosensors & Bioelectronics, 26 (2011) 2579-2584.

[243] P.P. Wang, J. Frazier, H. Brem, Local drug delivery to the brain, Advanced Drug Delivery Reviews, 54 (2002) 987-1013.

[244] M.S. Shoichet, S.R. Winn, Cell delivery to the central nervous system, Advanced Drug Delivery Reviews, 42 (2000) 81-102.

[245] Y.-C. HUANG, Y.-Y. HUANG, Tissue engineering for nerve repair, Biomed. Eng. Appl. Basis. Comm., 18 (2006) 100-110.

[246] C. Hassler, T. Boretius, T. Stieglitz, Polymers for neural implants, Journal of Polymer Science Part B: Polymer Physics, 49 (2011) 18-33.

[247] M.R. Abidian, K.A. Ludwig, T.C. Marzullo, D.C. Martin, D.R. Kipke, Interfacing Conducting Polymer Nanotubes with the Central Nervous System: Chronic Neural Recording using Poly(3,4-ethylenedioxythiophene) Nanotubes, Advanced Materials, 21 (2009) 3764-3770.

[248] S.Y. Yang, B.N. Kim, A.A. Zakhidov, P.G. Taylor, J.-K. Lee, C.K. Ober, M. Lindau, G.G. Malliaras, Detection of Transmitter Release from Single Living Cells Using Conducting Polymer Microelectrodes, Advanced Materials, 23 (2011) H184-H188.

[249] A.F. Quigley, J.M. Razal, B.C. Thompson, S.E. Moulton, M. Kita, E.L. Kennedy, G.M. Clark, G.G. Wallace, R.M.I. Kapsa, A Conducting-Polymer Platform with Biodegradable Fibers for Stimulation and Guidance of Axonal Growth, Advanced Materials, 21 (2009) 4393-4397.

[250] Y. Wan, J. Gao, J. Zhang, W. Peng, G. Qiu, Biodegradability of conducting chitosan-g-polycaprolactone/polypyrrole conduits, Polymer Degradation and Stability, 95 (2010) 1994-2002.

[251] J. Tietje-Girault, C. Ponce de León, F.C. Walsh, Electrochemically deposited polypyrrole films and their characterization, Surface and Coatings Technology, 201 (2007) 6025-6034.

[252] Basinc, Instruction manual for basi epsilon for electrochemistry, 2009.

[253] T. Tüken, B. Yazıcı, M. Erbil, The corrosion behaviour of polypyrrole coating synthesized in phenylphosphonic acid solution, Applied Surface Science, 252 (2006) 2311-2318.

[254] J.I. Martins, M. Bazzaoui, T.C. Reis, E.A. Bazzaoui, L. Martins, Electrosynthesis of homogeneous and adherent polypyrrole coatings on iron and steel electrodes by using a new electrochemical procedure, Synthetic Metals, 129 (2002) 221-228.

[255] L.M. Martins dos Santos, J.C. Lacroix, K.I. Chane-Ching, A. Adenier, L.M. Abrantes, P.C. Lacaze, Electrochemical synthesis of polypyrrole films on copper electrodes in acidic and neutral aqueous media, Journal of Electroanalytical Chemistry, 587 (2006) 67-78.

[256] M. Bazzaoui, J.I. Martins, S.C. Costa, E.A. Bazzaoui, T.C. Reis, L. Martins, Sweet aqueous solution for electrochemical synthesis of polypyrrole: Part 2. On ferrous metals, Electrochimica Acta, 51 (2006) 4516-4527.

[257] A.J. Downard, D. Pletcher, The influence of water on the electrodeposition of polypyrrole in acetonitrile, Journal of Electroanalytical Chemistry and Interfacial Electrochemistry, 206 (1986) 139-145.

[258] M.E.P. Pardavé, MES 24: Electrochemical Applications to Biology, Nanotechnology, and Environmental Engineering and Materials, The Electrochemical Society, 2009.

[259] J.O. Iroh, W. Su, Characterization of the passive inorganic interphase and polypyrrole coatings formed on steel by the aqueous electrochemical process, Journal of Applied Polymer Science, 71 (1999) 2075-2086.

[260] T. Otero, J. Martinez, Activation energy for polypyrrole oxidation: film thickness influence, J Solid State Electrochem, 15 (2011) 1169-1178.

[261] B. Alshammary, F.C. Walsh, P. Herrasti, C.P. de Leon, Electrodeposited conductive polymers for controlled drug release: polypyrrole, J Solid State Electrochem, DOI (2015) 1-21.

[262] X. Luo, X.T. Cui, Electrochemical deposition of conducting polymer coatings on magnesium surfaces in ionic liquid, Acta Biomaterialia, 7 (2011) 441-446.

[263] D. Ge, X. Ru, S. Hong, S. Jiang, J. Tu, J. Wang, A. Zhang, S. Ji, V. Linkov, B. Ren, W. Shi, Coating metals on cellulose–polypyrrole composites: A new route to self-powered drug delivery system, Electrochemistry Communications, 12 (2010) 1367-1370.

[264] X. Ru, W. Shi, X. Huang, X. Cui, B. Ren, D. Ge, Synthesis of polypyrrole nanowire network with high adenosine triphosphate release efficiency, Electrochimica Acta, 56 (2011) 9887-9892.

[265] M.C. Turhan, M. Weiser, M.S. Killian, B. Leitner, S. Virtanen, Electrochemical polymerization and characterization of polypyrrole on Mg–Al alloy (AZ91D), Synthetic Metals, 161 (2011) 360-364.

[266] A. Srinivasan, P. Ranjani, N. Rajendran, Electrochemical polymerization of pyrrole over AZ31 Mg alloy for biomedical applications, Electrochimica Acta, 88 (2013) 310-321.

[267] M.P. Staiger, A.M. Pietak, J. Huadmai, G. Dias, Magnesium and its alloys as orthopedic biomaterials: A review, Biomaterials, 27 (2006) 1728-1734.

[268] S.C. Bondy, Review: Low levels of aluminum can lead to behavioral and morphological changes associated with Alzheimer's disease and age-related neurodegeneration, Neurotoxicology, 52 (2016) 222-229.

[269] P. Herrasti, A.N. Kulak, D.V. Bavykin, C.P. de Léon, J. Zekonyte, F.C. Walsh, Electrodeposition of polypyrrole–titanate nanotube composites coatings and their corrosion resistance, Electrochim. Acta, 56 (2011) 1323-1328.

[270] M. Asplund, C. Boehler, T. Stieglitz, Anti-inflammatory polymer electrodes for glial scar treatment: bringing the conceptual idea to future results, Front. Neuroeng., 7 (2014).

[271] D. Svirskis, J. Travas-Sejdic, A. Rodgers, S. Garg, Electrochemically controlled drug delivery based on intrinsically conducting polymers, J. Controlled Release, 146 (2010) 6-15.

[272] O. Uzun, N. Başman, C. Alkan, U. Kölemen, F. Yılmaz, Investigation of mechanical and creep properties of polypyrrole by depth-sensing indentation, Polym. Bull., 66 (2011) 649-660.

[273] M. Gandhi, G. Spinks, R. Burford, G. Wallace, Film substructure and mechanical properties of electrochemically prepared polypyrrole, Polymer, 36 (1995) 4761-4765.

[274] P. Herrasti, L. Dıaz, P. Ocón, A. Ibáñez, E. Fatas, Electrochemical and mechanical properties of polypyrrole coatings on steel, Electrochim. Acta, 49 (2004) 3693-3699.

[275] S. Yang, Y.-W. Zhang, K. Zeng, Analysis of nanoindentation creep for polymeric materials, Journal of applied physics, 95 (2004) 3655-3666.

[276] K. Cysewska, S. Virtanen, P. Jasiński, Electrochemical activity and electrical properties of optimized polypyrrole coatings on Iron, J. Electrochem. Soc., 162 (2015) E307-E313.

[277] J.R. Smith, Y. Li, P.A. Cox, S.A. Campbell, S. Breakspear, D.C. Whitley, F.C. Walsh, Electrochemical and computational studies of electrically conducting polymer coatings, Trans. Inst. Met. Finish., 89 (2011) 244-248.

[278] B.C. Thompson, S.E. Moulton, J. Ding, R. Richardson, A. Cameron, S. O'Leary, G.G. Wallace, G.M. Clark, Optimising the incorporation and release of a neurotrophic factor using conducting polypyrrole, J. Controlled Release, 116 (2006) 285-294.

[279] A.C. Cascalheira, L.M. Abrantes, The electrochemical behaviour of copper in sodium salicylate aqueous solutions, Electrochim. Acta, 49 (2004) 5023-5028.

[280] N. Alizadeh, E. Shamaeli, Electrochemically controlled release of anticancer drug methotrexate using nanostructured polypyrrole modified with cetylpyridinium: Release kinetics investigation, Electrochim. Acta, 130 (2014) 488-496.

[281] M.C. Turhan, M. Weiser, M.S. Killian, B. Leitner, S. Virtanen, Electrochemical polymerization and characterization of polypyrrole on Mg–Al alloy (AZ91D), Synth. Met., 161 (2011) 360-364.

[282] Z. Grubač, I.Š. Rončević, M. Metikoš-Huković, Corrosion properties of the Mg alloy coated with polypyrrole films, Corros. Sci., 102 (2016) 310-316.

[283] M.C. Alvarez-Ros, S. Sánchez-Cortés, J.V. García-Ramos, Vibrational study of the salicylate interaction with metallic ions and surfaces, Spectrochim. Acta, Part A, 56 (2000) 2471-2477.

[284] A. Srinivasan, P. Ranjani, N. Rajendran, Electrochemical polymerization of pyrrole over AZ31 Mg alloy for biomedical applications, Electrochim. Acta, 88 (2013) 310-321.

[285] A.J. Bard, L.R. Faulkner, Electrochemical methods: fundamentals and applications, 2nd ed., John Wiley & Sons, Inc, New York, 2001.

[286] J. Zhang, W. Zhang, C. Yan, K. Du, F. Wang, Corrosion behaviors of Zn/Al–Mn alloy composite coatings deposited on magnesium alloy AZ31B (Mg–Al–Zn), Electrochim. Acta, 55 (2009) 560-571.

[287] M.C. Alvarez-Ros, S. Sánchez-Cortés, J.V. García-Ramos, Vibrational study of the salicylate interaction with metallic ions and surfaces, Spectrochimica Acta Part A: Molecular and Biomolecular Spectroscopy, 56 (2000) 2471-2477.

[288] A.T. Lorenzo, M.L. Arnal, J. Albuerne, A.J. Müller, DSC isothermal polymer crystallization kinetics measurements and the use of the Avrami equation to fit the data: Guidelines to avoid common problems, Polym. Test., 26 (2007) 222-231.

[289] E. Shamaeli, N. Alizadeh, Kinetic studies of electrochemically controlled release of salicylate from nanostructure conducting molecularly imprinted polymer, Electrochim. Acta, 114 (2013) 409-415.

[290] R. Colle, A. Curioni, Density-functional theory study of electronic and structural properties of doped polypyrroles, J. Am. Chem. Soc., 120 (1998) 4832-4839.

[291] P. Montoya, T. Marín, J.A. Calderón, F. Jaramillo, Electrodeposition of Polypyrrole Films: Influence of Fe3O4 Nanoparticles and Platinum Co-Deposition, Aspects on Fundaments and Applications of Conducting Polymers (2012) 137-158.

[292] S.U. Rahman, M.S. Ba-Shammakh, Thermal effects on the process of electropolymerization of pyrrole on mild steel, Synthetic Metals, 140 (2004) 207-223.

[293] T. Uyar, L. Toppare, J. Hacaloğlu, Spectroscopic investigation of oxidation of p-toluene sulfonic acid doped polypyrrole, Synthetic Metals, 123 (2001) 335-342.

[294] S.P. Ozkorucuklu, Y. Sahin, G. Alsancak, Voltammetric Behaviour of Sulfamethoxazole on Electropolymerized-Molecularly Imprinted Overoxidized Polypyrrole, Sensors, 8 (2008) 8463-8478.

[295] U. Páramo-García, J. Ibanez, N. Batina, Electrochemical Modulation of the Thickness of Polypyrrole Films by Using Different Anionic Dopants, Int. J. Electrochem. Sci, 6 (2011) 5172-5188.

[296] A.S. Liu, M.C. Bezerra, L.Y. Cho, Electrodeposition of Polypyrrole Films on Aluminum Surfaces from a para-Toluene Sulfonic Acid Medium, Materials Research, 12 (2009) 503-507.

[297] A.F. Diaz, J.I. Castillo, A polymer electrode with variable conductivity: polypyrrole, Journal of the Chemical Society, Chemical Communications, 0 (1980) 397-398.

[298] B.C. Thompson, S.E. Moulton, R.T. Richardson, G.G. Wallace, Effect of the dopant anion in polypyrrole on nerve growth and release of a neurotrophic protein, Biomaterials, 32 (2011) 3822-3831.

[299] J.O. Iroh, W. Su, Formation of Corrosion Resistant Organic Polymer Coatings by an Electrochemical Process, DTIC Document, 1999.

[300] S.B. Saidman, Influence of anion and pH on the electrochemical behaviour of polypyrrole synthesised in alkaline media, Electrochimica Acta, 48 (2003) 1719-1726.

[301] H. Yang, J. Kwak, Mass Transport Investigated with the Electrochemical and Electrogravimetric Impedance Techniques. 2. Anion and Water Transport in PMPy and PPy Films, The Journal of Physical Chemistry B, 101 (1997) 4656-4661.

[302] Y.J. Yuan, S.B. Adeloju, G.G. Wallace, In-situ electrochemical studies on the redox properties of polypyrrole in aqueous solutions, European Polymer Journal, 35 (1999) 1761-1772.

[303] S. Bruckenstein, J. Chen, I. Jureviciute, A.R. Hillman, Ion and solvent transfers accompanying redox switching of polypyrrole films immersed in divalent anion solutions, Electrochimica Acta, 54 (2009) 3516-3525.

[304] D. Svirskis, B.E. Wright, J. Travas-Sejdic, A. Rodgers, S. Garg, Development of a Controlled Release System for Risperidone Using Polypyrrole: Mechanistic Studies, Electroanalysis, 22 (2010) 439-444.

[305] D.V. Bavykin, L. Passoni, F.C. Walsh, Hierarchical Tube-in-tube Structures Prepared by Electrophoretic Deposition of Nanostructured Titanates into TiO2 Nanotubes Array, Chem. Commun., DOI (2013).

[306] G. Liljegren, J. Pettersson, K.E. Markides, L. Nyholm, Electrochemical solid- phase microextraction of anions and cations using polypyrrole coatings and an integrated three-electrode device, Analyst, 127 (2002) 591-597.